MOLECULAR MECHANISMS AND BIOLOGY OF TRANSGLUTAMINASE-2 IN CORNEAL EPITHELIUM

EVELYN PNG YEN SOO
(B.SC. (HONS.), NUS)

A THESIS SUBMITTED

FOR THE DOCTORAL DEGREE OF PHILOSOPHY
DEPARTMENT OF OPHTHALMOLOGY
NATIONAL UNIVERSITY OF SINGAPORE

2015

DECLARATION

I hereby declare that this thesis is my original work and it has been written by me in its entirety. I have duly acknowledged all the sources of information which have been used in the thesis.

This thesis has also not been submitted for any degree in any university previously.

Evelyn Png Yen Soo

24 July 2015

ACKNOWLEDGEMENTS

I would like to express my sincere gratitude to my supervisors Assoc Prof Louis Tong, Prof Aung Tin and Assoc Prof Tina Wong for their patience, guidance and supervision throughout my study. I am grateful for their constant support and advice. I sincerely thank past and present staffs of SERI, particularly members in ocular surface research team: Ms Melissa Lazaroo, Ms Yong Siew Sian, Ms Chen Silin, Mr Poon Kip Hoe, Dr Hou Aihua, Ms Tin Min Qi, Ms Yeo Shel Hwa and Dr Shyam Chaurasia. I would like to thank Mr Andri Riau and Ms Yeo Huiling for their help in animal work. My work in Singapore was supported by CSA R707 and CSA R980 and SNEC HREF Learning Award.

I would also like to thank Dr. Sia Kian Chuan and Dr. Paula Lam from Humphrey Oei Institute of Cancer Research, Singapore National Cancer Centre for providing technical support on construction of the stable shRNA control and shTG cell lines, Dr Kaoru Araki-Sasaki from Kinki Central Hospital, Hyogo, Japan for providing the immortalised human corneal epithelial cell line, Dr Peter J Davies from University of Texas Health Science Center, Houston for providing plasmids expressing full length TG-2, Dr Zhou Lei from Singapore Eye Research Institute, Singapore for the collaboration in liquid chromatography and mass spectrometry, Dr Earnest Mendoz and Prof Lim Chwee Teck from National University of Singapore for the collaboration in cell migration microscopy experiment, Dr Siiri Iismaa from Victor Chang Cardiac Research Institute, Australia for

her advice and comments on the wound healing project and Mr Benjamin Kang for proof reading my thesis.

Special thanks go to my family, especially my parents, who have always been supportive and encouraging from the beginning of my studies.

TABLE OF CONTENTS

SUMMARY **9**

LIST OF FIGURES **12**

LIST OF METHODOLOGY FLOW CHARTS **15**

LIST OF TABLES **16**

CHAPTER 1. INTRODUCTION **17**

1.1 THE OCULAR SURFACE 17
1.1.1 Structure and Functions of Corneal Epithelium and Tear Film *17*
1.1.2 Ocular Surface Diseases *19*
1.1.3 Current Treatment Options for Ocular Surface Diseases *20*
1.2 TRANSGLUTAMINASE-2 22
1.2.1 TG-2 Expression and Its Regulation of Activities *22*
1.2.2 TG-2 Plasmids *24*
1.2.3 Animal Models *25*
1.3 TRANSGLUTAMINASE-2 AND CORNEA 27
1.3.1 TG-2 Localisation in Cornea *27*
1.3.2 The Role of TG-2 in Ocular Surface Diseases *27*
1.4 TRANSGLUTAMINASE-2 AND WOUND HEALING 29
1.4.1 TG-2 Binding Partners and Adhesion Signalling *29*
1.4.2 TG-2 in Wound Healing *33*
1.5 FOCAL ADHESION PROTEINS AND TG-2 36
1.5.1 TG-2 and Paxillin *36*
1.5.2 TG-2 and Other Focal Adhesion Proteins *40*
1.6 UNANSWERED QUESTIONS AND SPECIFIC AIMS 41

CHAPTER 2. HYPEROSMOLARITY-MEDIATED MITOCHONDRIAL DYSFUNCTION REQUIRES TRANSGLUTAMINASE-2 IN HUMAN CORNEAL EPITHELIAL CELLS **46**

2.1 TEAR OSMOLARITY AND DRY EYE DISEASES 46
2.2 TG-2 AND CELLULAR STRESS 47
2.3 TG-2 AND MITOCHONDRIA 48
2.4 HYPOTHESIS AND SPECIFIC AIMS 50
2.5 METHODOLOGY 52
2.5.1 Immortalised Human Corneal Epithelial Cells *53*
2.6 HYPEROSMOLAR STIMULATION INDUCED MITOCHONDRIAL DEPOLARISATION 56
2.7 EFFECTS OF TG-2 OVEREXPRESSION 59

2.8 Hyperosmolarity Induced Mitochondrial Depolarisation is TG-2 Dependent 66
2.9 Discussion 73
2.10 Conclusion 76

CHAPTER 3. TRANSGLUTAMINASE-2 AND BINDING PARTNERS 76

3.1 Subcellular Compartmentalisation of Proteins 77
3.2 Subcellular Trafficking and Corneal Wound Healing 79
3.3 High-speed Cellular Protein Separation 80
3.4 Hypothesis and Specific Aims 81
3.5 Methodology 83
3.5.1 Protein-protein Interactions 83
3.5.2 Characterisation and Grouping of TG-2 Ligands/ Organelles 84
3.6 Identification of Potential TG-2 Binding Partners 85
3.7 Grouping of TG-2 Binding Partners 92
3.8 Characterisation of Organelles in Different Sucrose Fractions 97
3.9 Discussion 99
3.9.1 Possible Roles of TG-2 Binding Proteins 101
3.9.2 Proposed Hypothesis 105
3.10 Conclusion 107

CHAPTER 4. TRANSGLUTAMINASE-2 IN CORNEAL EPITHELIAL MIGRATION AND ADHESION 108

4.1 TG-2 in Cell Adhesion and Migration 108
4.2 Hypothesis and Specific Aims 111
4.3 Methodology 113
4.4 Delayed Wound Closure in TG-2 Deficient Cells 114
4.5 *In vitro* Study of TG-2 Deficiency in Cell Migration and Adhesion 117
4.5.1 TG-2 Deficiency Reduced Cell Migration Speed 117
4.5.2 TG-2 Deficiency Reduced Cell Adhesion/Spreading 124
4.6 TG-2 Deficiency Disrupts Actin Cytoskeleton 129
4.7 Interaction and Effects of TG-2 with Focal Adhesion Proteins 131
4.7.1 TG-2 Deficiency Reduced Phosphorylation of Ser178 Paxillin 131
4.7.2 TG-2 Interacts with Paxillin in In vitro 135
4.7.3 TG-2 Cannot Phosphorylate Paxillin Directly 142
4.7.4 Interaction of TG-2 and JNK 146
4.8 Discussion 150
4.9 Conclusion 157

CHAPTER 5. CONCLUSION AND FUTURE DIRECTIONS 159

5.1 Summary and Discussion 161
5.2 Strengths 165
5.3 Limitations 167
5.4 Clinical Significance and Future Studies 170
5.5 Conclusion 174

BIBLIOGRAPHY 175

APPENDICES 201

APPENDIX A. LIST OF LABORATORY TECHNIQUES 201

A1. Cell Culture 201
A1.1. Immortalised Human Corneal Epithelial Cells 201
A1.2. Scrambled shRNA and shTG Cells 201
A1.3. Trypsinizing, Counting and Passaging Cells 202
A1.4. Freezing and Thawing cells 203
A2. Preparation of Plasmids and Transfection 204
A2.1. Preparation of Luria-Bertani (LB) Broth and Agar Plate 204
A2.2. Propagation of Plasmid DNA Expressing TG-2 Fragments 204
A2.3. Plasmid DNA Over-Expressing TG-2 207
A2.4. Plasmid Propagation, DNA Extraction, Purification and Quantification 208
A2.5. Plasmid Transfection 210
A2.6. SiRNA Transfection 215
A3. Use of Chemical Inhibitors, Hyperosmolar Stimulation and Fibronectin Coating 216
A3.1. Caspase Inhibitor 216
A3.2. Hyperosmolar stimulation 216
A3.3. Fibronectin Coating on Polystyrene Surface 216
A4. Cell Lysis 217
A4.1. Extraction of RNA and Quantification 217
A4.2. Total Proteins Extraction 218
A4.3. Mitochondrial Protein Extraction 218
A4.4. Bicinchoninic Acid (BCA) Protein Assay 219
A5. Western Blotting 221
A5.1. Preparation of Buffers 221
A5.2. Gel Electrophoresis 221
A5.3. Transfer and Blotting 221
A5.4. Densitometry 223
A6. Centricollation 225
A6.1. Cell Lysis for Centricollation 225
A6.2. Centricollation 226

A7. IMMUNOPRECIPITATION 228
A7.1. Co-Immunoprecipitation to Pull Down TG-2 Binding Partners 228
A7.2. Co-Immunoprecipitation to Pull Down Paxillin Interacting Partners 230
A7.3. Cell Free In Vitro Immunoprecipitation 230
A8. LIQUID CHROMATOGRAPHY-TANDEM MASS SPECTROMETRY (LC-MS/MS) 232
A9. MAPPING OF PROTEIN LIGANDS TO TG DOMAINS 235
A10. IMMUNOSTAINING 237
A10.1. Immunocytochemistry and Immunohistochemistry 237
A10.2. Immunofluorescence Staining with Phalloidin 238
A11. POLYMERASE CHAIN REACTION (PCR) 240
A11.1. Reverse Transcription 240
A11.2. Quantitative Real Time PCR (qPCR) 242
A12. FUNCTIONAL ASSAYS 244
A12.1. Caspase Assay 244
A12.2. Mitochondrial Depolarisation Assay 245
A12.3. Transglutaminase Colorimetric Microassay Kit 246
A12.4. G-LISA Kit 247
A12.4.1. RhoA and Rac1/2/3 G-LISA Activation Assay 248
A12.4.2. Cdc42 G-LISA Activation Assay 251
A13. CELL VIABILITY/PROLIFERATION ASSAY 254
A13.1. Crystal Violet 254
A13.2. MTS Cell Proliferation Assay 254
A13.3 Ki-67 Assay 255
A13.4 Cell Cycle Analysis 257
A14. CELL ADHESION AND MIGRATION ASSAY 258
A14.1. Cell Impedance 258
A14.2. Trypsinisation Assay 259
A14.3. Real Time Cell Migration Assay 259
A14.4. Scratched Wound Assay 260
A14.5. Cell Area Measurement 260
A15. ANIMAL WORK 262
A15.1. Mouse Model 262
A15.2. Assessing Corneal Wound Healing in Mouse 262
A16. *IN VITRO* LABEL FREE PROTEIN INTERACTION ASSAY 264
A17. *IN VITRO* KINASE ASSAY 266
A17.1. TG-2 Intrinsic Kinase Activity Assay 266
A17.2. In vitro Autoradiographic Kinase Assay 267
A18. ANALYSIS 269
A18.1. Statistical Analysis 269
A18.2. ImageJ Analysis 269

A18.3. Cell Oscillation Analysis..... 273

APPENDIX B. ANTIBODIES LIST..... 274

APPENDIX C. LIST OF REAGENTS AND CHEMICALS..... 275

APPENDIX D. SUPPLEMENTARY INFORMATION..... 276

APPENDIX E. LIST OF PUBLICATIONS..... 281

SUMMARY

The cornea is the front part of the eye and its clarity depends on both ocular surface health and tear film integrity. In many common ocular diseases such as dry eye and recurrent corneal erosion, wound healing is deranged. Transglutaminase (TG)-2 is a ubiquitous multi-functional protein known to affect skin wound healing but has not been evaluated on cornea surface. This work aims to evaluate the functions of TG-2 in mitochondrial mediated apoptosis, protein interactions and trafficking, as well as corneal epithelial wound closure.

Increase in tear osmolarity has been associated with dry eye and ocular surface disorders. Hyperosmolar stimulation in cultured human corneal epithelial (HCE-T) cells induced a significant increase in mitochondrial potential, accompanied by reduced proliferation. Transient overexpression of TG-2 increased cellular transamidase activity and reduced viability. Importantly, in contrast to vector alone transfection, TG-2 overexpression has a higher proportion of mitochondrial depolarisation, accompanied by increased caspase 3/7 and 9 activity. About 48% of hyperosmolar-induced mitochondrial depolarisation is TG-2 dependent in HCE-T cells.

Several TG-2 binding proteins with known wound healing functions were identified and their distribution was evaluated using novel centricollation technology. The binding partners' concentrations were studied in human corneal epithelial cells expressing short hairpin RNA against TG-2 (shTG) and scrambled sequence shRNA (control shRNA). TG-2 deficiency decreased the expression levels of specific organelle markers, such as

late endosomes (RAB7), recycling endosomes (RAB11A) and secretory vesicles (RAB27A), as well as the expression of some binding proteins such as Golgi-associated protein (GOLGA2), which may cause preferential accumulation in other subcellular compartments. TG-2 levels may indirectly regulate cell adhesion and migration via the trafficking of these proteins and alteration of organelle functions.

Cell migration, proliferation and adhesion are crucial components of epithelial wound closure. shTG cells have reduced impedance compared to control cells. There was no significant difference between shTG and control cells in spreading areas on non-fibronectin substrate, the proportion of proliferating cells and cell cycles. shTG cells detached faster, showed decreased Rho protein activities and migrated significantly slower compared to control cells. Consistent with *in vivo* findings, TG-2 deficiency delayed the closure of the scratched wound. ShTG showed reduced phosphorylation of adhesion proteins at specific residues; the reduction of phosphorylation at S178 paxillin was the most notable since it was previously discovered to be crucial for adhesion and migration in human corneal epithelial cells. TG-2 cannot directly phosphorylate paxillin, and JNK1 was found to be the possible kinase candidate. However, TG-2 cannot directly recruit JNK1, and contrary to previous reports on human neuroblastoma cells, TG-2 cannot indirectly recuit JNK1 through DLK in human corneal epithelial cells. Hence, JNK1 may mediate serine phosphorylation of paxillin through an unknown kinase in a TG-2 dependent manner.

In conclusion, these studies suggest that TG-2 is important in the modulation of cell stress, protein trafficking, cell adhesion and migration in corneal epithelial cells. Strategies targeting TG-2 may protect corneal epithelium from wound healing disorders.

(483 words)

LIST OF FIGURES

Figure 1.1. Diagram showing functions of transglutaminase (TG)-2 in cell matrix adhesion. 32
Figure 1.2. Representative immunofluorescence images of TG-$2^{+/+}$ and TG-$2^{-/-}$ mouse cornea 4 hours and 120 hours after scratching. 39
Figure 1.3. Schematic showing TG-2 as the focus of this work. 41
Figure 2.1. Schematic showing the focus of this chapter, as depicted by the blue square. 51
Figure 2.2. Results from different experiments to determine the amount of TG-2 in control shRNA and shTG cells. 54
Figure 2.3. Flow cytometry result showing differential expression of cell surface TG-2 in shTG and control shRNA cells. 55
Figure 2.4. Table showing reverse transcription real-time PCR result of transglutaminase (TG)-2 transcript levels, normalised to GAPDH 55
Figure 2.5. Figures showing the effects of basal osmolarity and hyperosmolarity on cell proliferation/viability. 58
Figure 2.6. Figures showing semi-quantitative reverse transcription-polymerase chain reaction (RT-PCR) against different exons of TG-2 and western blot images of transfected cells against TG-2 primary antibody 60
Figure 2.7. Microscopy images showing HCE-T cells 24 hours after various electroporation conditions in serum free condition. 61
Figure 2.8. Figures showing effects of transfecting cells with pSG or pSG5 TG-2 plasmids on transamidase activity, cell proliferation and caspases activities. 64
Figure 2.9. Figures showing crystal violet cell proliferation assay of cells 65
Figure 2.10. Flow cytometry analysis showing percentages of cells with mitochondrial depolarisation 68
Figure 2.11. Flow cytometry analysis showing percentages of cells with mitochondrial depolarisation in normal (300mOsM) and hyperosmolar (460mOsm) conditions 70
Figure 2.12. Schematic showing that basal cells exposed to hyperosmolar condition can induce mitochondrial depolarisation through transglutaminase-2 dependent or non-transglutaminase-2- dependent mechanisms 72
Figure 3.1. Schematic showing the focus of this chapter, as depicted by the blue square. 82
Figure 3.2. Western blots showing the TG-2 ligands identified using commercially available antibodies. 86
Figure 3.3. Schematic showing proteins interacting with different domains of TG-2 87
Figure 3.4. Molecular network showing the interactions of TG-2 and its potential binding partners. 88

Figure 3.5. Figure showing the approximate distribution of organelles 90
Figure 3.6. Western blotting images showing TG-2 ligands expression levels in centricollated control shRNA and shTG cell lysates 91
Figure 3.7. Representative western blot images showing TG-2 ligands expression levels in centricollated cell lysates. 96
Figure 3.8. Western blots showing expression levels of organelle markers according to various densities of sucrose fractions in centricollated control and shTG cells 98
Figure 4.1. The corneal epithelial layers and the basement membrane of homozygous transglutaminase (TG)-2 deleted (TG-$2^{-/-}$) mice showed delayed corneal wound closure compared to wild type (TG-$2^{+/+}$) mice. 110
Figure 4.2. Schematic showing the focus of this chapter, as depicted by the blue square. 112
Figure 4.3. TG-2 knockdown in human corneal epithelial cells caused delayed wound closure 116
Figure 4.4. Figures showed results of non-traumatic cell migration assay. 122
Figure 4.5. Histograms showing the distribution of numbers of cells (y-aixs) against the oscillation of cells in micrometre (x-axis) over time 123
Figure 4.6. The reduced cell impedance in TG-2 knockdown corneal epithelial cells was due to the decrease in cell adhesion and spreading, but not cell proliferation..... 128
Figure 4.7. Figures showing FITC-conjugated phalloidin staining and 130
Figure 4.8. Figures showing western blot images of shTG and control shRNA cell lysate on primary antibodies against various adhesion proteins. 133
Figure 4.9. Human corneal epithelial cells with TG-2 deficiency reduced the phosphorylation of several focal adhesion proteins 134
Figure 4.10. Co-immunoprecipitation of shTG and control cell lysate against anti-paxillin. 138
Figure 4.11. Graphs showing Enspire Label-free biochemical assay which showed a spectral shift after the addition of recombinant proteins to immobilised paxillin 141
Figure 4.12. Figures showing autoradiogram of in vitro kinase activities as well as a library of Serine/Threonine kinases to identify the protein kinase that phosphorylates paxillin. 144
Figure 4.13. Barchart showing activity value (in counts per minute, cpm) of JNK1 with paxillin substrate. 145
Figure 4.14. Cell free *in vitro* immunoprecipitation and western blotting. 149
Figure A1. Circular map and features of pIRES-hrGFP II expression vector 205
Figure A2. Nucleotide sequences of human TG-2 four fragments: N terminal, catalytic core, N-Terminal 1 and N-Terminal 2 206
Figure A3. Circular map and features of pSG5 vector 207
Figure A4. (A) Pictures showing optimization of electroporation conditions on immortalised human corneal epithelial (HCET) cells 214

Figure A5. Diagram showing the process of centricollation 227
Figure A6. Mass spectrogram showing the ion fragment with peptide sequence..... 234
Figure A7. Diagram showing a summary of reverse transcription to obtain cDNA from RNA 241
Figure A8. Diagram showing the electrode impedance in the Xcelligence system..... 258
Figure A9. Diagram illustrates the theory behind the cell oscillation analysis software273
Figure A10. β3 integrin is expressed in cultured human corneal epithelial cell (HCE-T) and primary human limbal epithelial cells..... 276
Figure A11. 190 Ser/Thr kinase assays showing activity values (in cpm) with 5µg of paxillin. 280

LIST OF METHODOLOGY FLOW CHARTS

Methodology Flow Chart 1. Flow chart showing general methodology to study the effects of hyperosmolarity induced mitochondrial depolarisation in cultured human corneal epithelial cells..... 52
Methodology Flow Chart 2. Flow chart shows general methodology to study the protein-protein interactions in cultured human corneal epithelial cells..... 83
Methodology Flow Chart 3. Flow chart showing general methodology to study the protein trafficking in cultured human corneal epithelial cells 84
Methodology Flow Chart 4. Flow chart showing general methodology to study the role of TG-2 on cornea epithelial wound healing and relevant wound healing processes consist of cell adhesion, spreading and migration 113

LIST OF TABLES

Table 1. Table showing reverse transcription real-time PCR result of transglutaminase (TG)-2 transcript levels, normalised to GAPDH. 71
Table 2. Examples of TG-2 binding partners identified by mass spectrometry and MASCOT protein database search..... 87

CHAPTER 1. INTRODUCTION

1.1 The Ocular Surface

1.1.1 Structure and Functions of Corneal Epithelium and Tear Film

The cornea is the transparent front part of the eye and its clarity is important for vision. A healthy cornea and an overlaying tear film form the major anterior refractive surface of the eye, accounting for 75% of the total refractive power [1, 2]. The outermost surface of the cornea consists of 4 to 5 layers of stratified, non-keratinising squamous epithelium, which functions as a protective barrier to the external environment [1]. This corneal epithelium is around 50μm in thickness and is morphologically divided into three layers: bottom basal cell layer, middle wing layer, and outermost superficial or squamous cell layer [3]. Basal cells are the germinative layer of the epithelium which migrate anteriorly and differentiate into wing cells and superficial cells [3, 4]. The outermost superficial cells have microscopic projections which can increase the contact area and adherence between the overlaying tear film and the cells [5]. Like the rest of the epithelial cells in the body, the corneal epithelium is in a constant state of turnover, which is approximately every 7 days [4]. Superficial epithelial cells are continually shed into the tear pool, with the deeper cells slowly replenishing the desquamating superficial cells [1, 3]. This rapid turnover of cells is crucial to maintain a healthy and intact corneal epithelium structure, so that worn, injured or infected epithelial cells can be discarded within a short period of time [3].

The tight junction between laterally adjacent superficial cells contributes to the corneal epithelium's barrier function, preventing potentially harmful substances from entering the eye [6]. Corneal epithelial barrier function is disrupted in majority of the ocular surface disorders which affect vision, such as dry eye [3], corneal infection [7], corneal ulceration [8], and scarring or melting of the corneal stroma [9]. Untreated dry eye patients showed 2.7-3 times more corneal epithelial permeability compared to patients with normal tear function [10]. The integrity of the barrier function in dry eye patients can be clinically measured by the increased permeability of the corneal epithelial to fluorescein dye [10]. Besides tight junction, corneal epithelial barrier function is also dependent on the integrity of the ocular surface tear film [1].

Ocular surface and tear secreting glands work together as a functional unit to maintain the clarity of the cornea [10]. The surface of the cornea must be kept lubricated to prevent damage to the underlying epithelium. This is achieved by the spreading of a thin layer (7μm thick) of tear film over the epithelium through blinking to smoothen and lubricate the cornea [4]. The tear film, composed of lipid, aqueous and mucin layers, functions as a mechanical and antimicrobial barrier [11, 12]. Lipid layer secreted by the meibumian gland stabilises and retards evaporation of the aqueous layer, thus prevents drying of the corneal epithelium between blinks [11]. The mucin in the tear film lubricates the ocular surface, hence minimising the friction exerted by the eye lid during blinking as well as ocular rotational movements [11, 12]. Tear film supplies nutrients, oxygen, immunological and growth factors essential for the growth, proliferation and repair of the

epithelial cells. It also helps to maintain a smooth anterior surface for light refraction [2, 11].

1.1.2 Ocular Surface Diseases

The clarity of the cornea depends on both the health of the ocular surface and the integrity of the tear film [10]. Ocular surface diseases are disorders affecting the surface of the cornea. The ocular surface is densely innervated with sensory nerves; patients suffering from ocular surface diseases often display a variety of symptoms, such as dryness, discomfort, infection, erosion, ulceration and scarring [6]. In severe cases, vision can be affected. Common ocular surface diseases include dry eye, blepharitis, pterygium, recurrent corneal erosion, chemical and thermal injuries, scarring and immunological conditions such as Sjogren's Syndrome. In many of these ocular diseases, wound healing is deranged.

Altered tear production associated with dysfunction of the lacrimal functional unit can show an unstable, proinflammatory tear film, and may promote ocular surface inflammation and apoptosis [10]. This can lead to a common ocular surface epithelial disease known as lacrimal keratoconjunctivitis (LKC), or commonly known as dry eye disease. Dry eye is a multi-factorial disease affecting tear film and ocular surface through increased osmolarity of tear film and inflammation of the ocular surface [13]. Evaporative dry eyes and aqueous deficient dry eyes are two major classes of dry eye disease; with evaporative dry eye being the more prevalent form of dry eye in Asia [13]. Dry eye disease affects millions of people with an estimated prevalence as high as 11–

22% in the population [14]. It is characterised by symptoms ranging from mild discomfort to dryness, grittiness, foreign body sensation and visual disturbance [15]. Dry eye disease also lowers the patients' quality of life by adversely affecting their daily activities.

Patients who suffer from dry eye syndromes are more likely to develop recurrent corneal erosions (RCE) in the corneal epithelium [16]. RCE is a condition characterised by repeated epithelium breakdown due to defective adhesion of epithelial cells to the underlying membrane [17]. This kind of corneal epithelial defect must be rapidly restored to avoid infection and further damage to the corneal tissue. The migration of the corneal epithelial cells underpins the early phase of corneal wound healing as well as other ocular diseases [18, 19].

1.1.3 Current Treatment Options for Ocular Surface Diseases

Ocular surface disorders such as dry eye, persistent epithelial defects, recurrent corneal errosions *et cetera* can cause great discomfort to the patients. If these conditions are left untreated, patients usually develop corneal opacification caused by fibrosis, which eventually lead to irreversible loss of vision. Corneal transplantation would have to be performed as a last resort to restore vision. Vision corrective surgeries such as LASIK (laser *in situ* keratomileusis) are very popular nowadays. Hence, the importance of corneal wound healing has also gained attention. Due to the unique requirement for transparency in the cornea, the understanding of wound healing responses to restore

visual acuity without causing scarring continues to remain a key challenge. This summarises why the studies described in this thesis are important.

1.2 Transglutaminase-2

1.2.1 TG-2 Expression and Its Regulation of Activities

Transglutaminase (TG)-2, also known as tissue TG, is a 76-85kDa monomeric protein with distinct and reciprocally regulated transamidation function [20]. TG-2 is a ubiquitous protein, with almost all mammalian cells expressing this enzyme to varying extent [21]. This wide spread occurrence is due to its constitutive expression in ubiquitous cell types: endothelial cells, smooth muscle cells and other organ specific cells such as mesangial, colonic pericryptal fibroblasts and renomedullary interstitial cells [21, 22]; whereas in other cell types such as human peripheral blood monocytes, TG-2 expression can be induced by a variety of stimuli such as treatment with retinoic acid [23, 24].

Human TG-2 has four distinct domains, which are evolutionary conserved among all the other TGs: an N-terminal β-sandwich, an α/β catalytic core and two C-terminal β-barrel domains [25]. In the presence of Ca^{2+}, TG-2 catalyses post-translational modification of protein by forming isopeptide bond between the γ-carboxyamide group of protein bound glutamine residues and the primary amine group of either protein-bound lysine residue or a polyamine [26]. The resulting cross-linked proteins form stable complexes thus increasing their resistance to degradation [23]. The presence of Ca^{2+} is essential for the TG-2 transamidase activity as its binding changes the TG-2 conformation and exposes key residue in the active site, thus allowing substrate to access the binding site [27].

Human TG-2 gene (designated as *TGM-2*) is mapped on chromosome 20q12. *TGM-2* comprises of 13 exons and 12 introns spanning across 32.5 kilobases [28]. TG-2 is perhaps the most intriguing member in the mammalian TG superfamily which consists of TG-1 to 7, factor XIII and band 4.2. What distinguishes TG-2 from other family members are its non-transamidation functions. These include intracellular G-protein signalling, protein kinase activity, integrin binding co-receptor for fibronectin, extracellular protein disulphide isomerase (PDI) activity and other non-enzymatic functions [29]. TG-2 has been reported to participate in important biological processes such as wound healing [30], apoptosis [31], inflammation [32], cancer progression and metastasis [33, 34].

TG-2 is predominantly a cytosolic protein with 70-80% of its cellular pool present in the cytoplasm, while a small fraction is localised in the nucleus and mitochondria; no TG-2 is detected in endoplasmic reticulum (ER) and golgi apparatus [35]. Depending on cell types, around 10-20% of TG-2 is secreted extracellularly and localised to plasma membrane and extracellular matrix (ECM) [36]. Interestingly, TG-2 lacks an amino-terminal hydrophobic leader sequence and therefore cannot be externalised through the classical ER/golgi dependent secretory pathway [23]. The exact mechanism by which TG-2 is secreted remains elusive, however a recent study suggested that cytosolic TG-2 is recruited into perinuclear recycling endosomes prior to externalisation [37]. Another study reported that in renal tubular epithelial cells, a specific sequence in the TG-2 N-terminal β-sandwich domain is crucial for its externalisation [38].

TG-2 is the only member among the TG family that can bind and hydrolyse guanosine-5'-triphosphate (GTP), acting as a classic G-protein which regulates signal transduction [39]. The enzymatic activity of TG-2 is reciprocally regulated by the binding of Ca^{2+} and GTP, which causes conformational changes in TG-2 and inhibits its GTPase or transamidation functions respectively [23, 40]. Inside the cells, the Ca^{2+} concentration is low in the cytoplasm, hence TG-2's transamidating activity remains dormant and it functions as a GTPase [40]. However, this latent form of cytosolic TG-2 activity can be activated by increasing the intracellular Ca^{2+} concentration, either from intracellular stores or influx of extracellular Ca^{2+} [27, 41].

1.2.2 TG-2 Plasmids

Obtaining cDNA clone for a particular protein is vital for the expression of this specific desired protein in genetic engineering. The physiological functions of TG-2 can be studied through introduction of a constitutively expressed TG-2 plasmid in cultured cells. Ikura *et al* had first cloned TG-2 from guinea pig liver, followed by the successful isolation of full-length cDNA clones for human TG-2 by Gentile's group [42, 43]. They reported that the isolated human TG-2 cDNA clone consisted of 5'untranslated sequence, coding domain, 1058 nucleotides of 3'untranslated sequence, but lacked a consensus polyadenylation sequence [42]. This clone was 3.3kb and had a molecular weight of 77,253. Gentile *et al* then constructed an expression vector of human TG-2 by inserting the TG-2 cDNA into pSG5 eukaryotic expression vector containing a SV-40 early gene promoter and polyadenylation signal sequence (Appendix A, Figure A3) [44]. The

successful isolation and characterisation of human TG-2 cDNA clone opened the pathway to study the physiological functions of human TG-2.

1.2.3 Animal Models

To study the *in vivo* functions of TG-2, two different strains of *TGM-2* knockout mouse models had been established by independent groups. Melino group replaced part of exon 5 and all of exon 6 in the catalytic core domain of *TGM-2* with a neomycin resistance gene [45]. The other mouse model generated by Graham's laboratory inserted loxP sites into introns 5 and 8, flanking exons 6-8, which would inactivate both *TGM2* alleles after cross-breeding with animals expressing Cre-recombinase [46]. The homozygote progenies of both mouse models showed no expression of TG-2 protein. Since TG-2 is ubiquitously expressed with diverse functions, it was surprising that the homozygous knockout of *TGM-2* gene did not produce an embryonic-lethal phenotype [45]. The homozygous null animals of TG-2 were phenotypically normal at birth and born with expected Mendelian ratios. This lack of serious phenotypes may be explained by the compensation of other TGs present in the mammalian tissue [47]. However, alterations were expected in these TG-$2^{-/-}$ mice since the other mammalian TGs did not bind GDP/GTP and they were absent on the cell surface (except FXIIIa). Preliminary evidences reported that these TG-2 null mice, especially under certain pathological conditions and stresses, showed altered fibroblast function in attachment and motility, impaired wound healing, defective phogocytosis clearance of apoptotic cells, as well as mild glucose intolerance and hyperglycaemia, consistent with the suggested functions of

TG-2 [44, 48, 49]. To date, no confirmed TG-2 deficiency has been reported in humans, hence the TG-2 null animals study provided a possible direction for future clinical studies.

1.3 Transglutaminase-2 and Cornea

1.3.1 TG-2 Localisation *in Cornea*

TG-2 activities are present in almost all human ocular tissues with different degree of expression [30]. Immunohistochemistry has shown that in the human cornea, TG-2 is expressed in the corneal epithelium, keratocytes and the corneal endothelium [30]. In the corneal epithelium, biotin-labelled cadaverine incorporation and immunohistochemistry has shown that TG-2 is predominantly found along the basement membranes, and also within the intercellular spaces and in the cytoplasm of the epithelial cells [50, 51]. *In vitro*, western blotting also showed that TG-2 was present in immortalised human corneal epithelial cells [52].

1.3.2 The Role of TG-2 in Ocular Surface Diseases

TG-2 has been reported to play an important role in various ocular surface inflammation and wound healing diseases such as allergic conjunctivitis [53], glaucoma [54] and pterygium [55]. These eye conditions not only cause morbidity such as pain and discomfort, but also affects the transparency of the cornea, leading to permanent loss of sight thus affecting the quality of life [56]. The involvement of TG-2 in ocular surface inflammation has been demonstrated by the success of using TG-2 inhibitor in the treatment of allergic conjunctivitis in guinea pigs [53]. In glaucoma, the role of TG-2 is supported by both *in vitro* and *in vivo* studies. Wordinger's group reported that there were more TG-2 proteins and enzyme activity detected in cultured human glaucomatous cells compared to the normal control cells [57]. This was further supported by another study

which showed the presence of functionally active TG-2 in the scarring bleb of failed glaucoma filtration surgery patients [54]. Moreover, our group showed that there are aberrant DNA methylations on TG-2 promoter of excised pterygium tissues, compared to uninvolved conjunctiva tissue from the same patients [58].

1.4 Transglutaminase-2 and Wound Healing

1.4.1 TG-2 Binding Partners and Adhesion Signalling

Extracellular TG-2 is known to interact with the ubiquitous and abundant ECM proteins, including fibronectin, collagen, vitronectin, osteopontin, *et cetera*. Among these ECM substrates, the binding of TG-2 to fibronectin (Fn) is characterised best. During wound repair, Fn provides a provisional matrix prior to collagen deposition for cell adhesion, migration and proliferation [18]. It has been reported that in normal rabbit cornea, fibronectin was only detected at decemet's membrane, but soon after wounding, fibronectin was detected on the denuded corneal surface. This deposited fibronectin helped the migration of the epithelium to cover the denuded area [59]. Most of the extracellular roles of TG-2 that affect early wound repair involves its interaction with Fn [60]. TG-2 binds to the 42-kD gelatin-binding domain of Fn which lacks both the integrin-binding sites and RGD motif (Arginine-glycine-aspartate) [61, 62]. This binding occurs in a stochiometric ratio of 2:1 with high affinity (Kd 8-10nM) and does not require its transamidase crosslinking activity [63, 64]. The high affinity interaction between extracellular TG-2 and Fn mediates cell-matrix adhesions and enhances other adhesion-related phenomena such as cell migration, ECM assembly and remodelling [65, 66]. Studies have showed that Fn protects cell surface TG-2 from proteolytic degradation, hence supporting cell adhesion and migration [67]. On the contrary, there are numerous studies which suggest that the crosslinking and polymerisation of Fn with cell surface TG-2 is linked to cell adhesion. In osteoblasts and human umbilical vein endothelial

cells, it has been demonstrated that the crosslinking of Fn by extracellular TG-2 significantly promotes cell adhesion and increases β1 integrin clustering [68, 69].

Besides binding to Fn, extracellular TG-2 non-covalently interacts with β_1, β_3 and β_5-subunits of the integrin family [70-72]. It is estimated that up to 40% of β_1 integrins on the cell surface are associated with TG-2 and all extracellular TG-2 are complexed with integrins in a 1:1 ratio [29]. The precise mapping of the interaction site of TG-2 and integrin remains elusive. TG-2-integrins interaction is a direct interaction not mediated by Fn and is independent from the TG-2 transamidase activity [40]. It is well known that Fn can interact with integrin α5β1 through its 29-kD Fn domain containing RGD motif [73]. However, integrins have low affinity for ECM proteins, even for the ubiquitous Fn [29]. This relatively weak affinity of integrin-Fn association together with the stable interaction of TG-2-integrins and TG-2-Fn suggest that extracellular TG-2 may act as an integrin-associated adhesion co-receptor for Fn [29, 74]. All the three proteins in this ternary complex are able to interact with each other thus contributing to increased cell adhesion and spreading. Since both extracellular TG-2 and integrin can independently bind to different domains of Fn (42-kD and 29-kD respectively), therefore they are more collaborating in cell adhesion rather than acting as competitors.

Apart from strengthening the cell-ECM adhesion, cell surface TG-2 can potentiate outside-in signalling by promoting integrin clustering on the cell surface, even in the absence of Fn [75]. The TG-2-integrin complexes have been shown to activate multiple downstream intracellular pathways and signalling targets, such as focal adhesion kinase

(FAK) and PI3K/Akt survival pathway, RhoA GTPase and its downstream target Rho-associated coiled-coil containing serine/threonine protein kinase (ROCK), leading to the formation of focal adhesions, actin stress fibers and increased actomyosin contractility [35, 75].

Heparan sulphate proteoglycan (HSPG) syndecan-4 is a recently discovered binding partner of extracellular TG-2. Among the four mammalian syndecans, only syndecan-4 is ubiquitously expressed and present in focal adhesions [76]. Syndecan-4 interacts with the heparin binding domains of Fn and supports the formation of actin cytoskeleton [77]. A report by Telci *et al* in 2008 revealed that the interaction between syndecan-4 and extracellular TG-2 could be important during tissue injury or wound healing [77]. They found that syndecan-4 interacted with Fn-associated TG-2 and activated protein kinase Cα (PKCα), followed by the binding of β1 integrin [77]. These initiated a cascade of signalling events leading to the formation of focal adhesion, actin cytoskeleton reorganisation and the activation of survival kinase pathway. This TG-2-mediated RGD-independent cell adhesion may be significant in wound healing, where the presence of RGD peptides due to ECM breakdown may act as a competitive inhibitor, causing loss of cell adhesion and anoikis [76, 77]. Under these circumstances, Fn bound TG-2 would be able to rescue cell adhesion and facilitate wound repair by binding to cell surface heparin sulphate chain of syndecan-4.

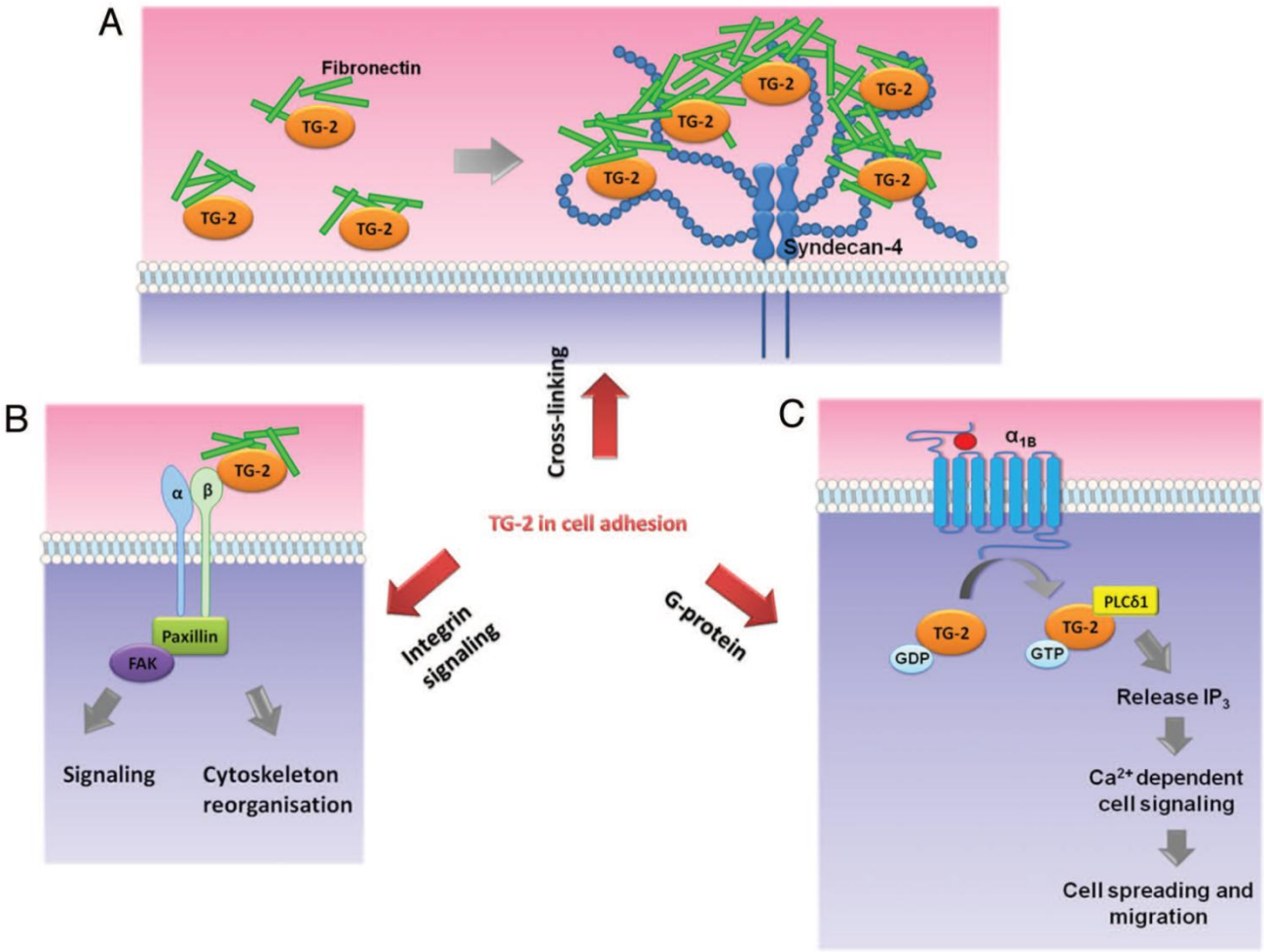

Figure 1.1. Diagram showing functions of transglutaminase (TG)-2 in cell matrix adhesion. (A) In the extracellular matrix environment, TG-2 non-covalently binds to fibronectin (green bars). Using its heparin sulfate chain, syndecan-4 helps to bring TG-2-bound fibronectin close together, thus TG-2 is able to cross-link with more neighboring fibronectin molecules, increasing the matrix stiffness. (B) There are multiple domains on fibronectin (not shown) which can interact with either TG-2 or integrin. As a co-receptor of β1 or β3 integrins, TG-2 can bind non-covalently to fibronectin, recruiting downstream focal adhesion proteins, leading to cytoskeleton reorganization and/or downstream signaling. (C) TG-2 functions as a G protein. GDP bound TG-2 is inactive. The binding of agonist (red sphere) activates the transmembrane α1B-adrenergic receptor (α1B), which then regulates the activation of phospholipase Cδ1 (PLCδ1), which can hydrolyse phosphatidylinositol diphosphate (PIP2) to produce inositol-1,4,5- trisphosphate (IP3) and diacylglycerol (DAG), which have important role in cell signalling pathway through elevation of intracellular calcium which can affect cell spreading and migration.

1.4.2 TG-2 in Wound Healing

The significance of extracellular TG-2 goes beyond cell adhesion and spreading; TG-2 is involved in wound healing. Wound healing is an intricate and dynamic process that aims to restore the function and integrity of the damaged tissues after injury [78]. Wound healing processes involve 3 major components: cell migration, cell proliferation and cell adhesion [18]. It includes continuous interaction of multiple cell types and an array of signalling peptides, proceeding in overlapping stages which consist of inflammation, proliferation and remodelling [78]. However, wound healing is never perfect. TG-2 activities are found to increase with the formation of scar tissue [79]. The formation of non-functional scar tissue may have functional or aesthetic consequences [80].

Accumulating evidences have reported the involvement and importance of TG-2 in wound healing processes, particularly in dermal wound healing [81, 82]. An early dermal wound repair study in rats by Bowness *et al* reported the increase in transglutaminase activity at the wound healing sites [81]. Another study reported that TG-$2^{-/-}$ mice showed delayed skin wound healing compared to their wild type counterparts [82]. At cellular level, Upchurch *et al* reported that TG-2 was found to localise in ECM after the wounding of embryonic human lung fibroblast cells, and these TG-2 persisted around the wound site for many hours [83]. TG-2 has been implicated in different phases of dermal wound repair. Haroon *et al* reported that early in the skin wound healing process, TG-2 was elevated in migrating keratinocytes, infiltrating macrophages and skeletal muscles cells [84]. Raghunath *et al* discovered that TG-2 was expressed in dermo-epidermal junctions [85]. In this study, TG-2 was found to cross-link the anchoring fibrils and may

have a role in maintaining the stability of the dermo-epidermal junctions. They even suggested that TG-2 might play a role in attaching the epidermal layer to the dermo-epithelial junction [84, 85]. The migration of endothelial and inflammatory cells into fibrin is an indispensable part of the skin wound repair process. It has been demonstrated that the macrophages expressing TG-2 invade the fibrin clot to stabilise the fibrin network. This ability of TG-2 to stabilise the provisional fibrin and resist proteolytic degradation may play an important role in orchestrating the tissue repair. A definitive role of TG-2 in tissue repair has been shown by the impaired skin wound healing in TG-2 knockout mice. This delayed wound closure can be rescued by external application of TG-2 to the wound site [82].

In fact, the kinetics and distribution of TG-2 in ocular surfaces are not that dissimilar to those in the skin [51]. This similarity is crucial because the role of TG-2 in *in vivo* dermal wound healing has been extensively studied, and may provide insights to the role of TG-2 in corneal epithelial wound healing. Cornea, like skin and other tissues in the body, is susceptible to frequent insult and wounding encountered in daily life. Most corneal epithelial wounds are repaired promptly and healed within 2 days from an injury [30]. TG-2 helps to stabilise the ECM at the wound site to promote corneal epithelial wound healing.

Zhang *et al* reported that TG-2 was strongly up-regulated in the early wound healing process in rat cornea, especially in actively migrating corneal epithelial cells and stromal fibroblasts [30]. The ability of TG-2 to stabilise the fibrin network in skin inspired Zhang

et al to suggest that corneal keratocytes or inflammatory cells may produce TG-2 to create a provisional matrix in the stroma for the migration of cells [30]. Recently, this hypothesis has been confirmed by another study which showed that TG-2 was indeed required for the crosslinking of the fibrillar collagen in the stroma [86]. The common phenomenon of scarring, which is frequently present during tissue wound healing, is to be avoided in corneal wound healing. This is because scarring and edema can affect the clarity and transparency of the cornea, leading to loss of sight. Irreversible crosslinking by TG-2 has been shown to be present in cornea scar tissue which affects visual acuity [87].

1.5 Focal Adhesion Proteins and TG-2

Focal adhesions (FA) are multi-protein structures that provide the mechanical link between actin cytoskeleton and underlying extracellular matrix. This interaction enables cells to interact with their surrounding environment and to regulate various cell behaviours such as cell adhesion, proliferation, survival, differentiation and migration [88].

The initiation of FA formation occurs upon the binding of ECM ligands to integrin, followed by subsequent integrin clustering [89]. This leads to the sequential recruitment of various adaptor and signalling proteins such as talin, paxillin, vinculin, focal adhesion kinase (FAK) *et cetera*, forming large intracellular protein complexes at the integrin tails [90]. FA acts as a structural link between the ECM and the actin cytoskeleton which coordinates the transmission of downstream signals [91]. The assembly of FA is regulated by the Rho GTPase family of GTP-binding proteins such as RhoA, Rac1 and Cdc42 [91]. They regulate actin organization, cell contractility, lamellipodia and filopodia formation, membrane ruffling as well as cell polarity [92]. Several literatures have shown that TG-2 was involved either directly or indirectly in the regulation, activation or signalling of several adhesion proteins [29, 71, 75].

1.5.1 TG-2 and Paxillin

Paxillin is a 68 kDa adaptor protein containing several protein-binding sites important for the coordinated recruitment of a diverse range of adaptor and signalling molecules,

leading to the sequential activation of other proteins [89]. Paxillin is indispensable as research has shown that the deletion of paxillin gene in mice is lethal in early embryonic development stage [89]. This early termination in embryonic development might be due to defective cell migration and cell spreading, as demonstrated by the paxillin-deficient fibroblasts cells [93].

Paxillin has multiple phosphorylation sites at serine, threonine and tyrosine [94-96]. These phosphorylation sites are targeted by various kinases activated by wide array of stimuli such as growth factors and cell adhesion signalling. The phosphorylation of paxillin at specific amino acids has been associated with the recruitment of other signalling molecules into the complex, thus mediating the formation of focal adhesion and stress fibers, leading to cell adhesion and migration [95].

Paxillin consists of two main structural domains: the amino (N) terminus and the carboxyl (C) terminus. The paxillin's C-terminal contains four LIM (Lin-11, Isl-1, Mec-3) domains (LIM1–4), which are zinc-finger motifs that can mediate protein-protein interactions [89]. It has been reported that phosphorylation on serine and tyrosine residues in paxillin LIM2 and LIM3 domains localises paxillin to the focal adhesions, regulating maturation and turnover of the focal adhesions [94]. On the other hand, the N-terminus of paxillin consists of a leucine-rich motif with the consensus sequence LDXLLXXL, known as LD motifs (LD1-5) [93]. These LD motifs play an important role in the recruitment of signaling molecules as well as to function as binding sites for other proteins such as vinculin, FAK and E6 oncoprotein from papilomavirus [97, 98]. Hence,

it is not surprising that the phosphorylation of these LD motifs is related to the recruitment of downstream signalling molecules. For example, Nayal *et al* reported that the phosphorylation of paxillin on serine273, which lies within the LD4 domain, could regulate Rho GTPase signaling, thus controlling downstream signalling to the cytoskeletons [93, 99].

Although the phosphorylation of paxillin is commonly studied on its tyrosine residues; paxillin is also heavily phosphorylated on its serine residues during cell adhesion [100]. Serine178 is one of the key serine residues located within LD2 and LD3 motifs of paxillin [100], and may have an important role in signalling. Kimura *et al* reported that when Ser178 in paxillin was mutated to Ala178, an amino acid that could not be phosphorylated, they observed disrupted cytoskeletal remodeling, cell migration and adhesion in cultured human corneal epithelial cells [101]. This showed that the phosphorylation of Ser178 paxillin was important for cell adhesion and migration. Currently, there is no known interaction between TG-2 and paxillin. Furthermore, our laboratory reported a novel observation that lesser phosphorylated Ser178 paxillin were detected at the advancing edge of wounded corneal epithelium in TG-2 knockout mouse ($TG\text{-}2^{-/-}$) compared to the wild type mouse ($TG\text{-}2^{+/+}$). This *in vivo* data suggested that TG-2 may be involved in the phosphorylation of Ser178 paxillin in mouse corneal epithelial wound healing (Figure 1.2).

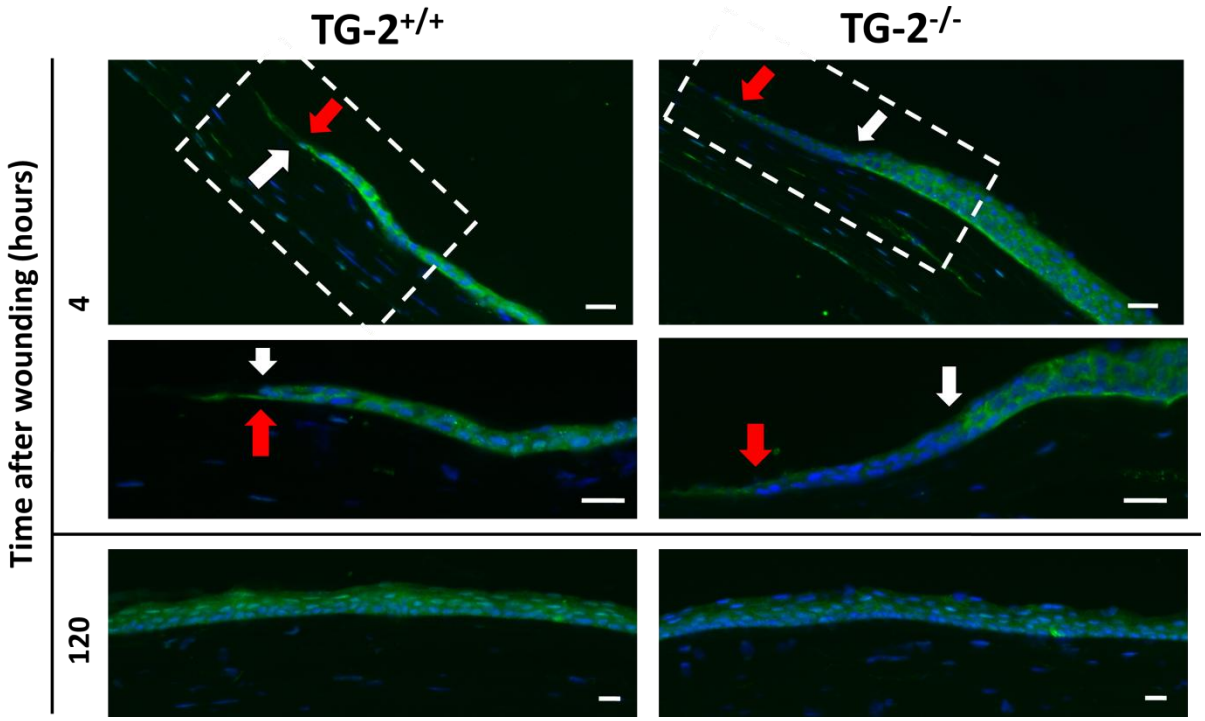

Figure 1.2. Representative immunofluorescence images of TG-$2^{+/+}$ and TG-$2^{-/-}$ mouse cornea 4 hours and 120 hours after scratching. Immunofluorescence staining was performed using antibody against phosphorylated Ser178 paxillin, followed by FITC-conjugated secondary antibody (green). Nuclei were stained with DAPI (blue). Red arrows indicate the corneal epithelium wound edge; white arrows indicate the margin where the staining of phosphorylated Ser178 paxillin started. Scale bar = 50 μm.

1.5.2 TG-2 and Other Focal Adhesion Proteins

As mentioned earlier in this introduction chapter, extracellular TG-2 can interact non-covalently with β-integrin which is important in cell-ECM adhesion [29]. The TG-2-integrin complexes were shown to activate multiple downstream intracellular pathways and signalling targets, leading to the formation of focal adhesions, actin stress fibers and increased actomyosin contractility [35, 75]. This functional collaboration between TG-2 and integrins was illustrated by a study, whereby the deficiency of TG-$2^{-/-}$ macrophages in phagocytosis was due to impaired signalling and the inability of integrin β_3 to accumulate in the phagocytic cup [102]. Also, Janiak *et al* showed that TG-2 promoted RhoA activation through β-1 integrin signaling and reduction of phosphorylation on src kinase [75]. In another study, Verma *et al* reported that TG-2 expression inhibited the phosphorylation of tumor suppressor phosphatase PTEN, causing its degradation and subsequently increased the phosphorylation of FAK at Tyr397 in pancreatic adenocarcinoma cell line [74]. Contradictory to this result, Stephens *et al* reported that human foreskin fibroblast cells transfected with TG-2-antisense showed an increase in phosphorylation of FAK at Tyr397 compared to mock transfected or TG-2 overexpressing cells [103]. These studies showed that TG-2 expression in the cells could affect the activation of some of the focal adhesion proteins. However, the effect of TG-2 in the phosphorylation of focal adhesion proteins in corneal epithelial cells have not been evaluated.

1.6 Unanswered Questions and Specific Aims

TG-2 is the protein of interest in this work. The focus of this work is on common biological processes such as apoptosis, cell adhesion and migration. TG-2 potentially links these biological processes to several *in vivo* human diseases such as evaporative dry eye, ocular surface damage and wound healing defects (Figure 1.3). Three chapters have been allocated to discuss the role of TG-2 in hyperosmolarity induced mitochondrial cell death (Chapter 2), the interacting proteins partners of TG-2 (Chapter 3) and the functional role of TG-2 in corneal epithelial wound healing (Chapter 4).

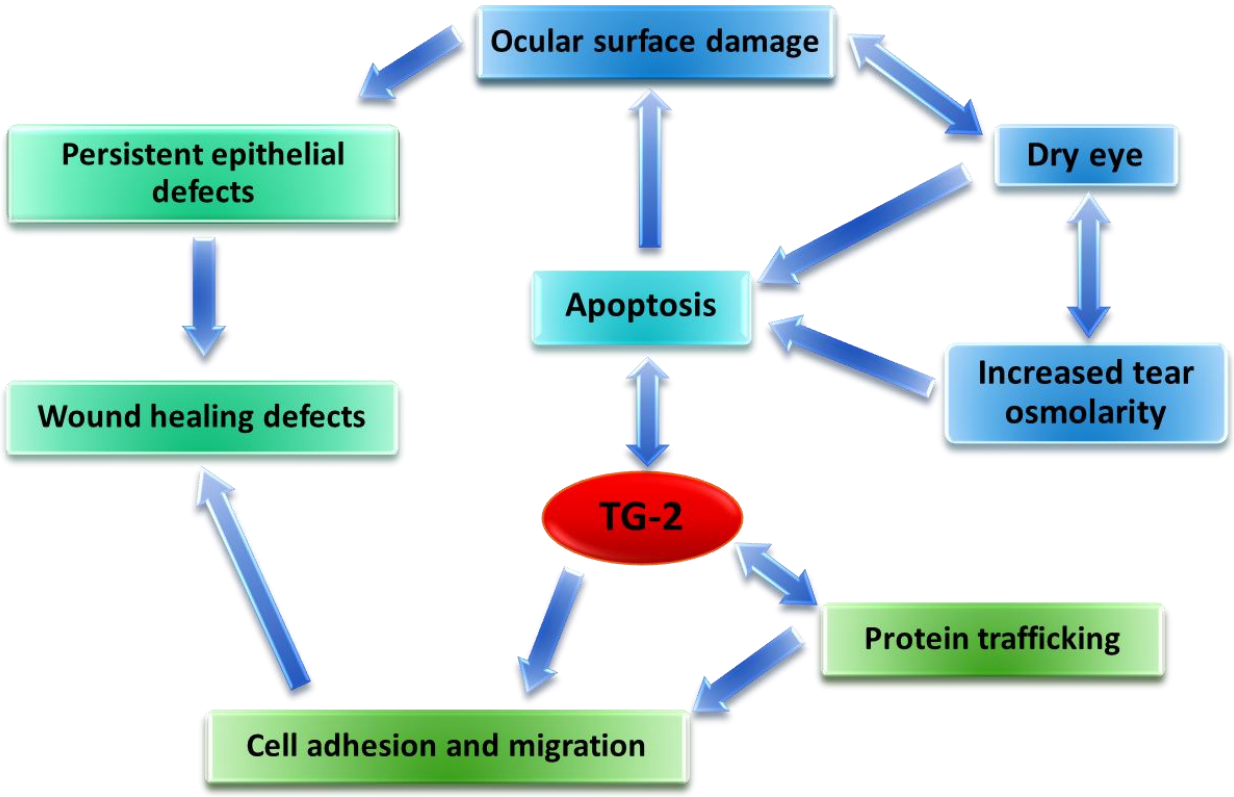

Figure 1.3. Schematic showing TG-2 as the focus of this work. TG-2 potentially links these biological processes to several *in vivo* human diseases such as evaporative dry eye, ocular surface damage and wound healing defects.

Evaporative dry eye is a more prevalent form of dry eye in Asia, including in Singapore [13]. One of the central mechanisms of dry eye is tear hyperosmolarity, which involves apoptotic cell death, causing ocular surface damage [13]. The damaged ocular surface can release inflammatory cytokines which will further aggravate dry eye and cause more apoptosis [10]. Although hyperosmolarity is known to activate the mitochondrial apoptotic pathway [104], it is not known if TG-2 is involved in this process in human corneal epithelial cells. Also, is TG-2 an inducer of mitochondrial damage in hyperosmolar stimulated cells? Chapter 2 investigates whether cell death induced by hyperosmolarity in human corneal epithelial cells is dependent on TG-2.

Cornea wound healing deserves to be evaluated as a unique scenario, as defective wound healing will reduce cornea transparency and affect visual function. Corneal epithelial wound healing consists of 3 major components: cell migration, proliferation and adhesion [18]. During the wound healing process, adhesion complex proteins and cytoskeletal proteins are transported/recycled continuously from one compartment to another. These transported proteins may contribute to crucial cell migration processes such as rearrangement of actin filaments, formation of lamellipodia and filopodia, as well as the assembly and disassembly of molecular motors. This study was thus extended to identify the interacting proteins partners of TG-2 and their protein transport which may affect cell adhesion and migration. In the cell, proteins that are involved in cell adhesion and migration are transported continuously from one compartment of the cells to another compartment. TG-2 which is present abundantly in the cells during this transport process is likely to interact with these transported proteins. What are the proteins that interact

with TG-2 that may affect cell adhesion and migration? How are these proteins transported? More specifically, which fragments of TG-2 are these proteins interacting with? These will be studied in Chapter 3 of this thesis.

In Chapter 4, I further extended my study to elucidate the functional role of TG-2 in wound healing which also involves epithelial cell adhesion and migration. Under normal circumstances, ocular surface damage usually heals within 2-3 days [67]. However, some of these wounds have defects in healing. They heal very slowly or do not heal at all. Cell adhesion and migration may be involved in this process since they are the main components of wound healing. Most literatures have chosen to use fibroblast or cancer cells to investigate the role of TG-2 in the wound healing process [68, 105, 106]. Little or no work has been done to study the role of TG-2 in corneal epithelial wound closure. Although cell surface TG-2 is known to activate downstream signalling pathways [75], it is not known how TG-2 affects other proteins in the cell-adhesion complex.

Specific Aims

1. To investigate the role of TG-2 in hyperosmolarity mediated mitochondrial cell death (Chapter 2).
    a. To elucidate whether hyperosmolar treatment can mediate cell death in cultured human corneal epithelial cells by checking cell proliferation, viability and cell death.
    b. To study whether mitochondria is involved in hyperomolar-induced cell death using flow cytometry analysis.
    c. To determine the presence of TG-2 in mitochondria; and whether TG-2 can induce mitochondrial damage in hyperosmolarity-stimulated cells.
    d. To study the effect of overexpressing TG-2 on cell proliferation and viability in cultured human corneal epithelial cells.
2. To discover and characterise cell adhesion or migration related proteins which interact with TG-2 (Chapter 3).
    a. To characterise the proteins that interact with different TG-2 fragments using immunoprecipitation, LC/MS and MASCOT database search.
    b. To understand how these proteins are trafficked between cell compartments using centricollation and immunoblotting of potential binding partners in cells in combination with RNA interference of TG-2.
    c. To determine whether TG-2 level can affect the relative concentration of cell-adhesion proteins in sub-cellular fractions using western blotting.
3. To study the functional significance of TG-2 on cell adhesion and migration in corneal epithelial wound closure (Chapter 4).

a. To investigate the role of TG-2 in cell migration, adhesion and proliferation using *in vitro* techniques such as cell scratching assay, cell migration assay, immunofluorescence staining and trypsinisation assay.

b. To evaluate the possible interaction of TG-2 and focal adhesion proteins in cultured human corneal epithelial cells by performing western blot against focal adhesion proteins.

c. To determine if TG-2 affects paxillin incorporation in adhesion complexes by checking its *in vitro* kinase activity.

d. To check the effects of TG-2 on JNK through co-immunoprecipitation and western blotting.

CHAPTER 2. HYPEROSMOLARITY-MEDIATED MITOCHONDRIAL DYSFUNCTION REQUIRES TRANSGLUTAMINASE-2 IN HUMAN CORNEAL EPITHELIAL CELLS

2.1 Tear Osmolarity and Dry Eye Diseases

The human corneal epithelium is covered by a layer of tear film which provides mechanical and antimicrobial barrier, lubrication and nutrients to the underlying conjunctiva and cornea, to ensure a smooth surface for light refraction [11]. The osmolarity of the tear film is important for normal functioning of the ocular surface and any changes to the tear osmolarity may cause cell death or induce inflammatory response in the cornea epithelial cells [104, 107]. Tear osmolarity in normal eyes has been reported to range from approximately 300 to 310 mOsm/L [108, 109]. The increase in tear osmolarity has been associated with dry eye and ocular surface disorders [110]. This rise in tear osmolarity has been correlated with pathological changes of the ocular surface, as well as increased epithelial cell death, leading to the loss of barrier function and reduced cornea transparency [59, 111]. Hence, the effect of hyperosmolarity on corneal epithelial cells, especially its effects in the downstream death signalling pathway, deserves evaluation. It is important to note that most of the *in vitro* and animal dry eye studies require long-term and high levels of hyperosmolar treatment (400-600 mOsM/L) in order to induce inflammatory response on the ocular surface [103, 108].

2.2 TG-2 and Cellular Stress

TG-2 can be regulated by cellular stress. It has been reported that oxidative stress promotes *in situ* activation of TG-2. For instance, Shin *et al* reported that human lens epithelial cells treated with hydrogen peroxide promoted oxidative stress, leading to increase in *in situ* TG-2 activity [112]. Similarly, an increase in TG-2 activity was observed when apoptotic cell death was induced in human peripheral blood mononuclear cells using a ROS (reactive oxygen species) generating enzyme xanthine oxidoreductase [113]. Also, TG-2 is involved in stimulating corneal epithelial cell death after UV irradiation [114]. It has been shown that hyperosmolarity and increased intracellular calcium levels can induce cell death in various cell types [115, 116]. In addition, previous studies also reported that osmotic stress such as increased concentration of sorbitol and sodium chloride (NaCl) can increase the *in situ* transamidase activity [111, 117].

2.3 TG-2 and Mitochondria

Mitochondria are known as the powerhouse of the cell as it plays a key role in adenosine triphosphate (ATP) synthesis for energy production [118]. Mitochondria are also important in regulating caspase activity and apoptosis [119]. In intrinsic or mitochondria-dependent apoptosis triggered by different types of intracellular stress, the permeabilisation of mitochondrial membrane leads to the release of crucial apoptotic molecules such as cytochrome c and caspases, thereby causing apoptosis [119, 120]. The integrity of the outer mitochondrial membrane depends on the interactions of both pro- and anti-apoptotic members of the Bcl-2 family proteins [119].

The involvement of mitochondria in human corneal epithelial cell death pathway has been implicated through the release of cytochrome c [104]. Although most of the TG-2 are cytosolic, TG-2 can also be found in mitochondria [121]. TG-2 has been associated to mitochondria-induced cell death in non-ocular context [122, 123]. For example, Piacentini *et al* reported that TG-2 overexpression increased mitochondrial membrane potential and sensitised the neuronal cells to apoptosis [122]. Another study reported that the impairment of mitochondrial function in neuroblastoma cells significantly promoted the *in situ* TG-2 activity [123]. It has been proposed that TG-2 is a novel member of a multifunctional BH3-only pro-apoptotic protein whereby it shares 70% similarity with the BH3 domain of Bcl-2 family [124]. Besides its involvement in mitochondria-dependent apoptosis, other evidences also showed that TG-2 may participate in other mitochondrial functions such as mitochondrial energy production and regulation of mitochondrial potential [125].

Currently, there are limited studies done to evaluate the role of TG-2 in hyperosmolar-induced cell death. Also, it is uncertain whether mitochondria are involved in TG-2-mediated cell death in human corneal epithelial cells.

2.4 Hypothesis and Specific Aims

It is hypothesised that osmotic stress induced cell death in human corneal epithelial cells is TG-2 dependent.

The aim of this study is to determine whether cell death induced by hyperosmolarity in human corneal epithelial (HCE-T) cells is dependent on TG-2. If this dependence exists, we aim to ascertain the role of the mitochondria in this death process.

Specific Aims

To investigate the role of TG-2 in hyperosmolarity mediated mitochondrial cell death.

a. To elucidate whether hyperosmolar treatment can mediate cell death in cultured human corneal epithelial cells by checking cell proliferation, viability and cell death.
b. To study whether mitochondria is involved in hyperomolar-induced cell death using flow cytometry analysis.
c. To determine the presence of TG-2 in mitochondria; and whether TG-2 can induce mitochondrial damage in hyperosmolarity-stimulated cells.
d. To study the effect of overexpressing TG-2 on cell proliferation and viability in cultured human corneal epithelial cells.

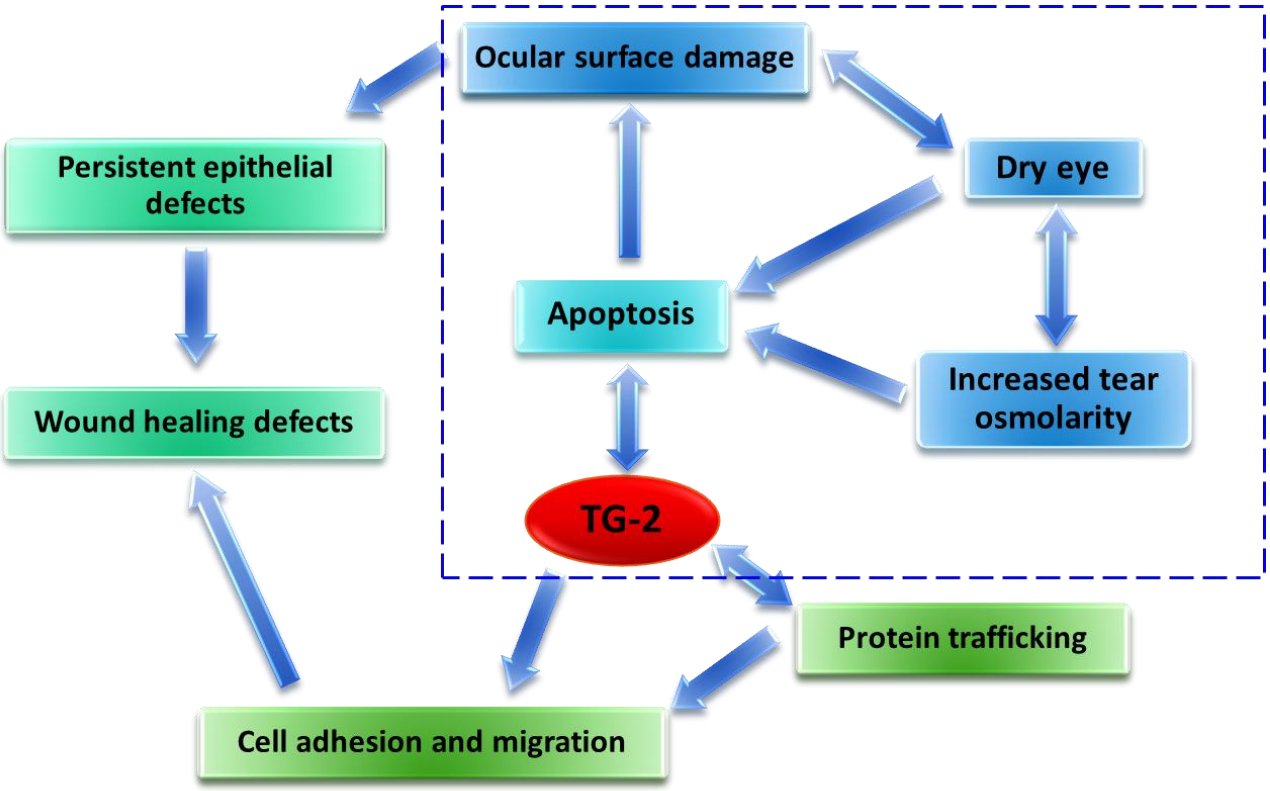

Figure 2.1. Schematic showing the focus of this chapter, as depicted by the blue square. The main objective of this chapter is to elucidate the role of TG-2 in hyperosmolar induced mitochondrial depolarisation.

2.5 Methodology

The materials and methods will be presented in flow chart in every chapter. The overall methodology of this chapter is presented as Methodology Flow Chart 1. Due to space constrains, the details of the materials and methods are presented in the Appendix.

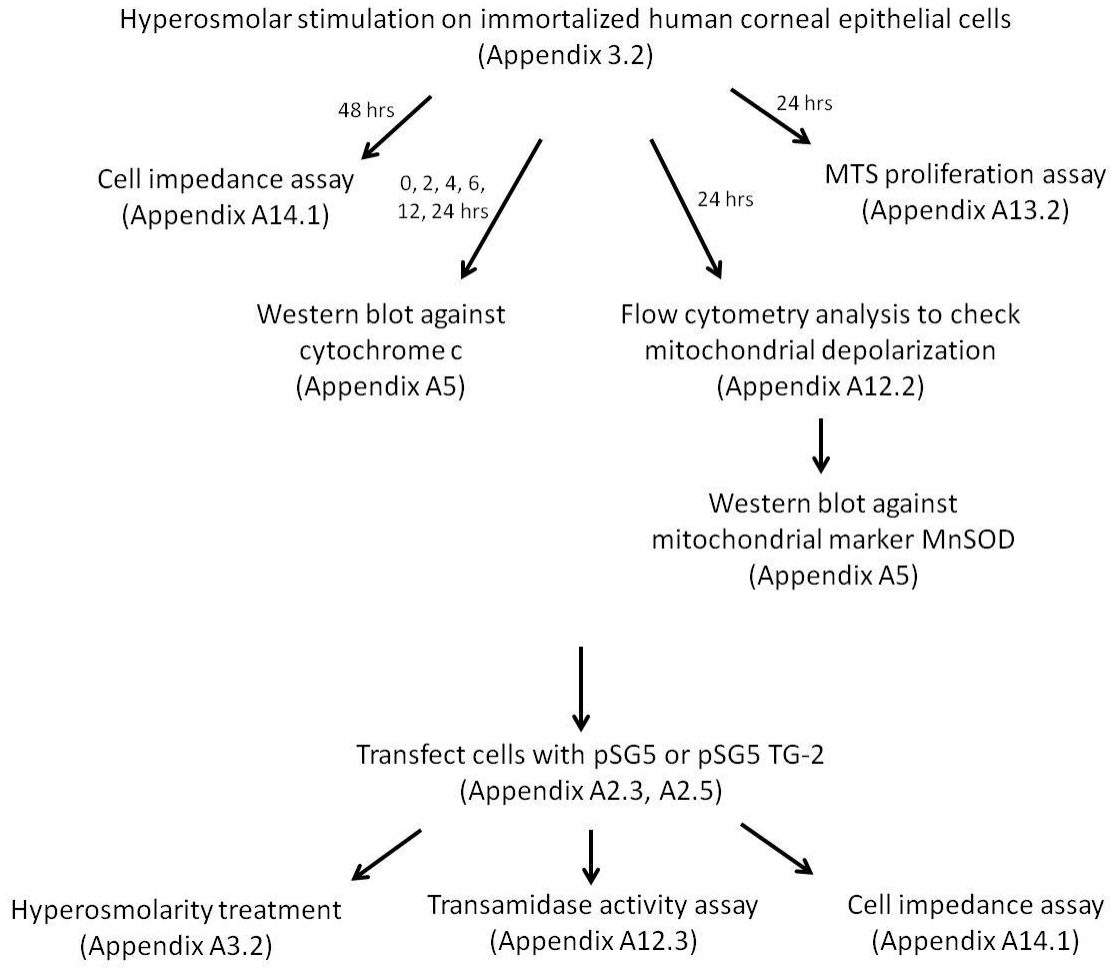

Methodology Flow Chart 1. Flow chart showing general methodology to study the effects of hyperosmolarity induced mitochondrial depolarisation in cultured human corneal epithelial cells. The detailed protocol for each technique was described in Appendix A.

2.5.1 Immortalised Human Corneal Epithelial Cells

In vitro experiments in my projects were performed using immortalised human corneal epithelial (HCE-T) cells due to various factors such as high requirement of cells numbers in various experiments, changes of phenotypes in primary cells upon passaging, high cost of primary cell culture medium and the translational medical implications of using human cells.

To study the effects of TG-2 deprivation in human corneal epithelial cells, HCE-T cells were stably transfected with shRNA targeting TG-2 to generate TG-2 knock-down cells, known as shTG cells in this thesis; or with scrambled shRNA to produce a control cell line, known as control shRNA cells (See methods at Appendix A1.2). The specificity of this shRNA targeting TG-2 sequence was confirmed by the following experiments: firstly, the reduction of TG-2 transcript and protein in HCE-T cells (Figure 2.2), secondly, the reduction of TG-2 expression on cell surface (Figure 2.3), and thirdly, the overexpression of wild type TG-2 overcoming the functional effect of TG-2 deficiency (Figure 2.4).

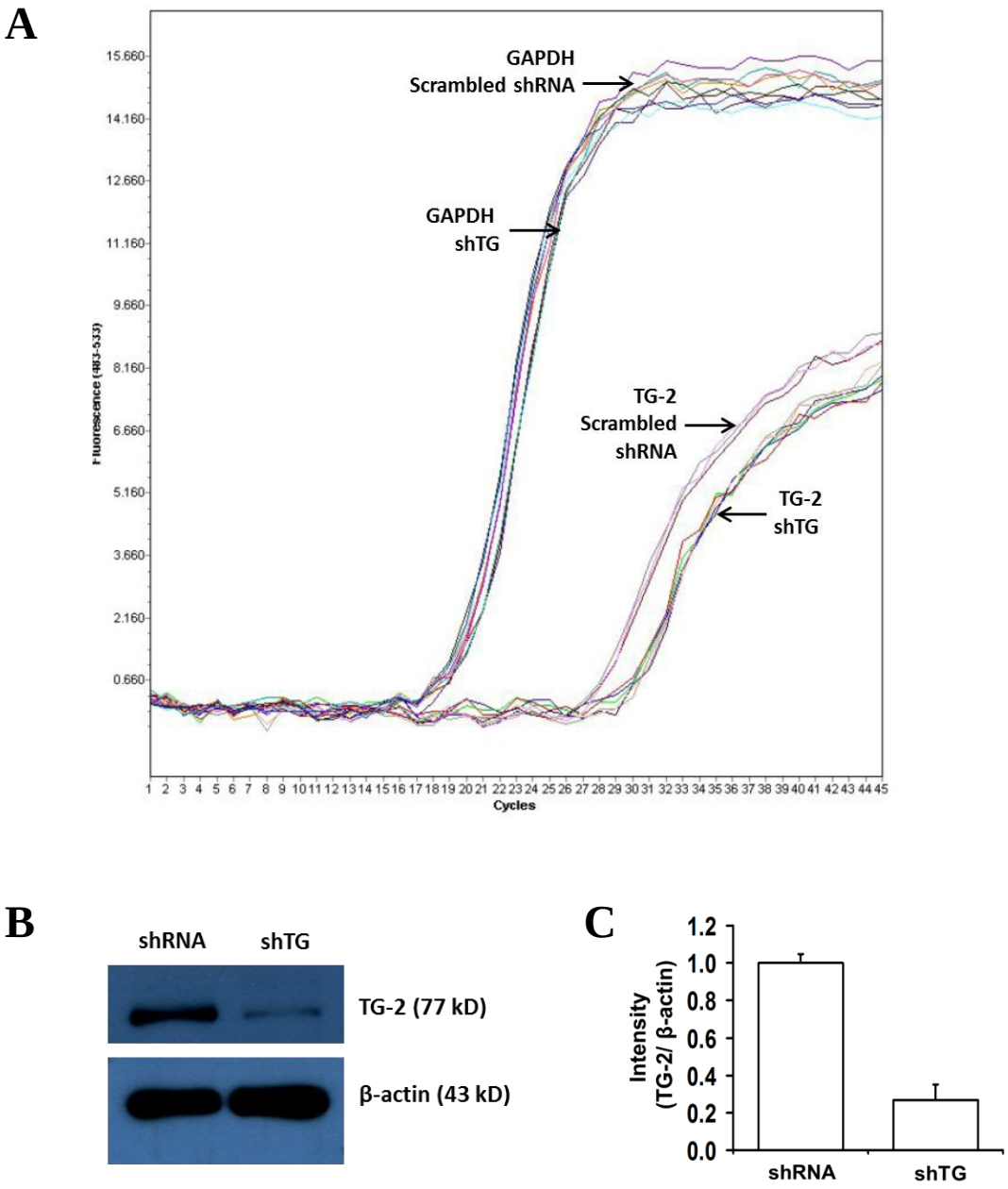

Figure 2.2. Results from different experiments to determine the amount of TG-2 in control shRNA and shTG cells. (A) Real-time Quantitative RT-PCR result of shRNA and shTG cells. GAPDH was used as a control. (B) Western blot showed the expression of TG-2 protein in shRNA and shTG cells. (C) Bar chart showing densitometry for the western blot. The intensity of TG-2 was normalised to that of the β actin.

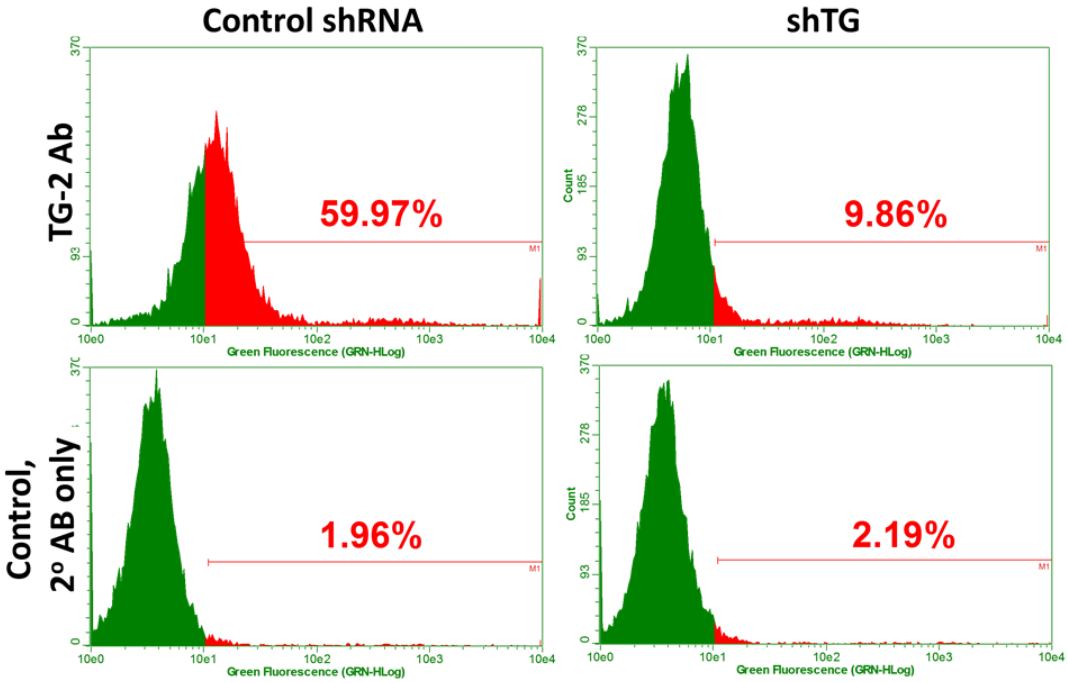

Figure 2.3. Flow cytometry result showing differential expression of cell surface TG-2 in shTG and control shRNA cells. Scrambled shRNA (control) and shTG cells were trypsinised and incubated with primary antibody against transglutaminase (TG)-2 and Alexa Fluor 488 secondary antibody. The proportion (%) of cells stained positive for TG-2 was calculated and shown for each of the cell types. Bottom row: Graph shows the background signal obtained by the addition of secondary antibody only.

Treatment	TG-2 fold change normalised to GAPDH	SEM
shRNA pSG5	1	0.01
shTG pSG5	0.45	0.06
shRNA pSG5 TG-2	444.69	0.02
shTG pSG5 TG-2	533.74	0.04

Figure 2.4. Table showing reverse transcription real-time PCR result of transglutaminase (TG)-2 transcript levels, normalised to GAPDH. Cultured human corneal epithelial cells (HCE-T) stably expressing scrambled shRNA (shRNA) and shRNA targeting transglutaminase (TG)-2 (shTG) were used. These cells were transiently transfected with either pSG5 plasmid (control) or pSG5 TG-2 plasmid (over-expression of TG-2). Total RNA was then extracted from these transfected cells. The fluorescence of amplified products was measured at 483-533nm.

2.6 Hyperosmolar Stimulation Induced Mitochondrial Depolarisation

A series of sodium chloride concentration with different osmolarity was tested on cultured human corneal epithelial (HCE-T) cells over a period of 24 hours (Figure 2.5A). Based on the amount of mitochondrial depolarisation as well as references from previous literature [103], 460mOsM was chosen as a suitable hyperosmolar treatment for the experiment. This osmolarity of 460mOsm is applicable to clinical situation as a keratoconjunctivitis sicca patient has recorded a hyperosmotic tear film of approximately 450 mOsm [109].

Consistent to the 24 hour MTS cell proliferation assay (Figure 2.5A), cell impedance assay also showed that HCE-T cells treated in hyperosmolar condition at 460mOsM has reduced proliferation/ viability compared to those grown in normal osmolarity (Figure 2.5B). When the cells were incubated for extended hours (12 and 24 hours) in hyperosmolar medium with (Top, Figure 2.5C) or without serum (Bottom, Figure 2.5C), there was a gradual increase in cytochrome c protein level in the cell cytosol/total protein lysate. Flow cytometry results showed that after the cells were treated with hyperosmolar medium at 460mOsM for 24 hour, 14.5% more cells (27.3% minus 12.8%) showed mitochondrial depolarisation, compared to the control untreated cells at 300mOsM. As a positive control, cells treated with Carbonyl Cyanide m-Chlorophenylhydrazone (CCCP), a known mitochondrial oxidative phosphorylation uncoupler, caused 99.8% of the cells to undergo mitochondrial depolarisation compared to control (Figure 2.5D).

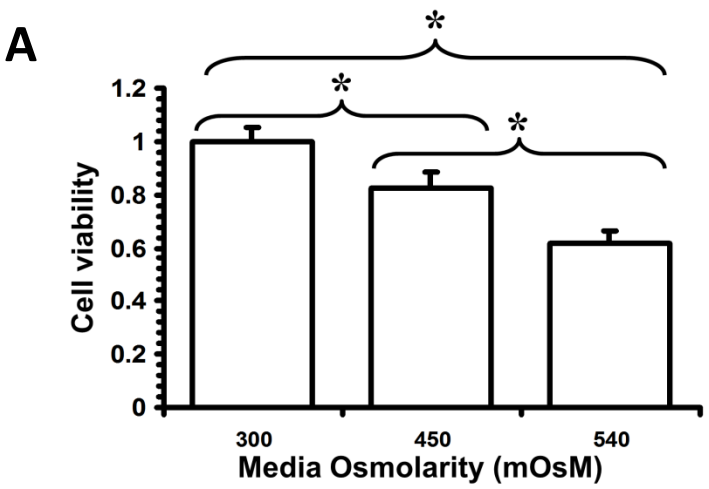
A
*
*
*
1.2
1
0.8
0.6
0.4
0.2
0
Cell viability
300
450
540
Media Osmolarity (mOsM)

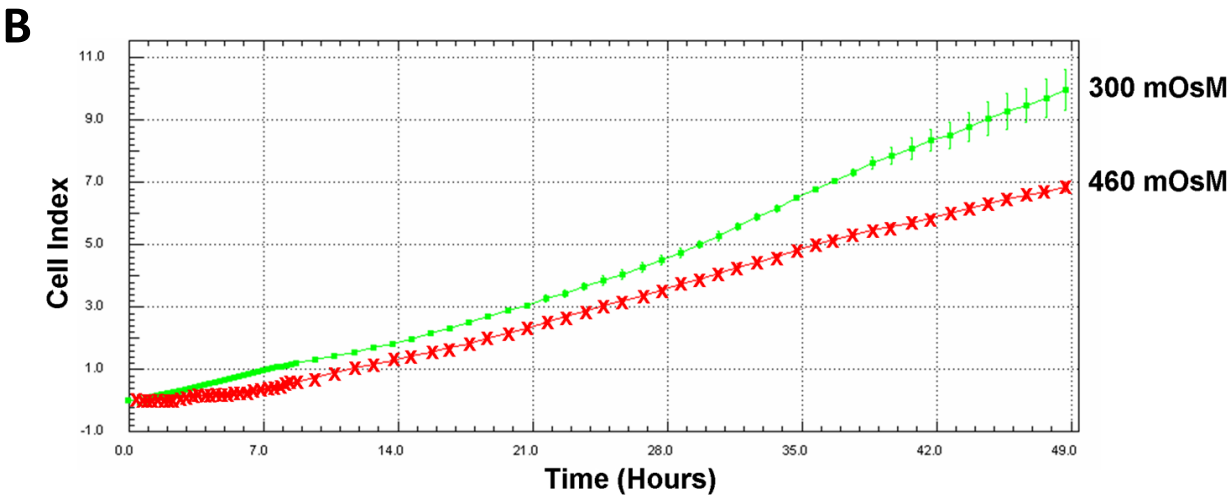
B
11.0
9.0
7.0
5.0
3.0
1.0
-1.0
Cell Index
0.0
7.0
14.0
21.0
28.0
35.0
42.0
49.0
Time (Hours)
300 mOsM
460 mOsM

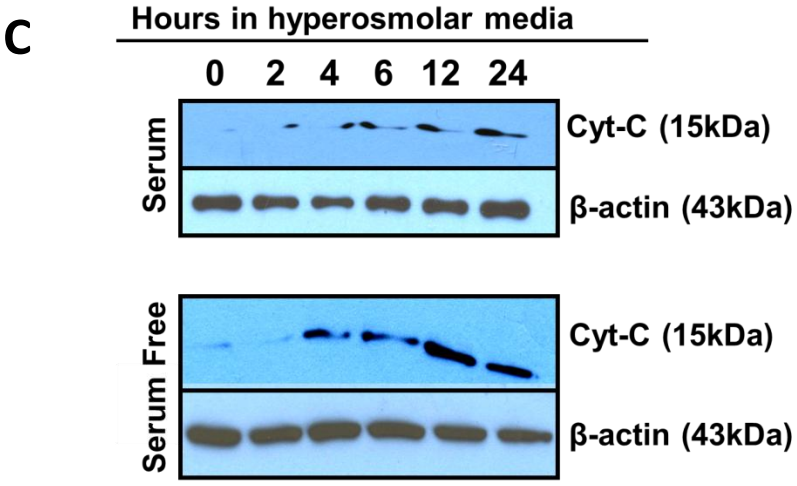
C
Hours in hyperosmolar media
0 2 4 6 12 24
Serum
Cyt-C (15kDa)
β-actin (43kDa)
Serum Free
Cyt-C (15kDa)
β-actin (43kDa)

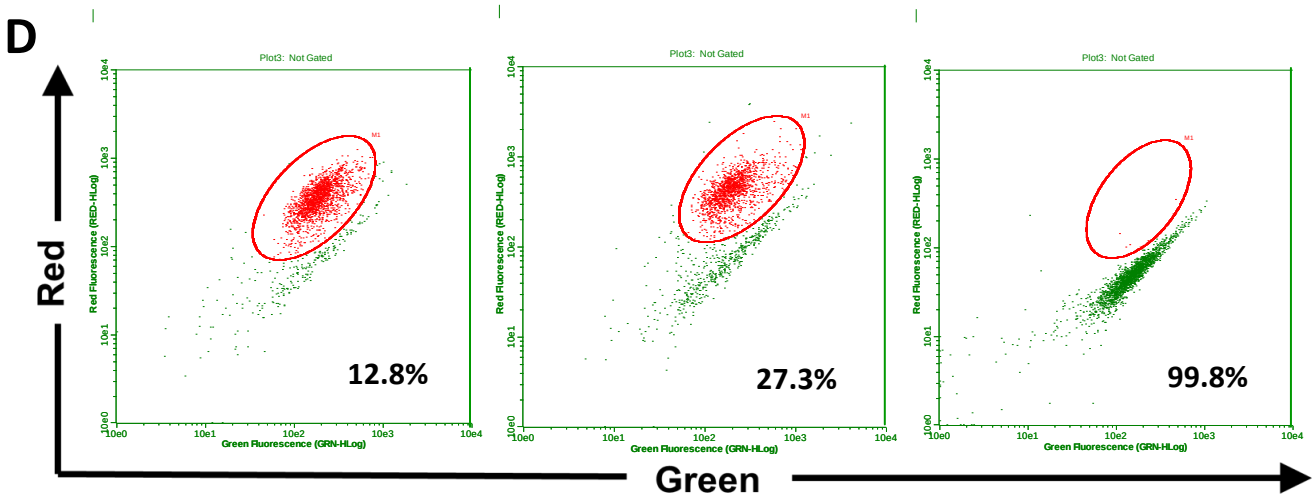

Figure 2.5. Figures showing the effects of basal osmolarity and hyperosmolarity on cell proliferation/viability. (A) MTS cell proliferation assay was performed to evaluate the proliferation/ viability of human corneal epithelial cell treated to media of various osmolarity (300, 450, 540mOsM) for 24 hour. Cell viability was calculated by normalising the absorbance values of the cells in various osmolarity to control (300mOsm). Three independent experiments were performed. P value was calculated with anova followed by the 3 post hoc multiple comparisons. *: $p < 0.05$. (B) A real-time cellular impedance based assay (Xcelligence) was performed to monitor the proliferation of cultured human corneal epithelial cells (HCE-T). Cell index provides information regarding cell viability, number, morphology, and adhesion degree. In this experiment, an equal number of cells was seeded in each well and the cells were treated with hyperosmolar medium (460mOsm) or control (300mOsm). Quadruplicates were done for each condition. (C) Sub-confluent HCE-T cells were exposed to either 5% fetal bovine serum-containing media (Top) or serum-free media (Bottom) for various time points. Western blots were then performed on the total cell lysates using primary antibodies against cytochrome (Cyt) c or β-actin. (D) Flow cytometry scatterplot shows the percentage of cells with mitochondrial depolarisation. Sub-confluent HCE-T cells were exposed to control medium (Left: 300mOsm) and hyperosmolar medium (Middle: 460mOsm) for 24 hours, prior to trypsin detachment and staining with JC-1, a membrane permeant dye which indicates mitochondrial membrane potential. JC-1 dye shows mitochondrial potential-dependent accumulation which is demonstrated by a green (~529 nm) to red (~590 nm) fluorescence emission shift. Hence, mitochondrial depolarisation is measured by a reduction in the red/green fluorescence intensity ratio. In this scatterplot, an ellipse was drawn around the cells with no mitochondrial depolarisation; the percentage of cells outside the delineated ellipse was shown. As a positive control, cells were incubated with carbonyl cyanide m-chlorophenylhydrazone (CCCP), a known mitochondrial depolariser (0.1M), 30 minutes before the flow cytometry (Right: CCCP).

2.7 Effects of TG-2 Overexpression

To study the effect of TG-2 overexpression, one can compare the effects of cells expressing control plasmid versus cells expressing TG-2 plasmid. TG-2 overexpression was achieved by electroporating cells with 1ug of pSG5 TG-2 plasmid, while control cells were generated by electroporation with same the amount of pSG5 plasmid (See Methods at Appendix A2.5). Reverse transcription real-time PCR was performed against different exons of TG-2 in order to confirm that the TG-2 sequence in the plasmid was expressed in full length (Figure 2.6). The electroporation conditions and the control vector used in the overexpression experiments were also checked in HCE-T cells to ensure that they did not cause significant cell loss (Figure 2.7).

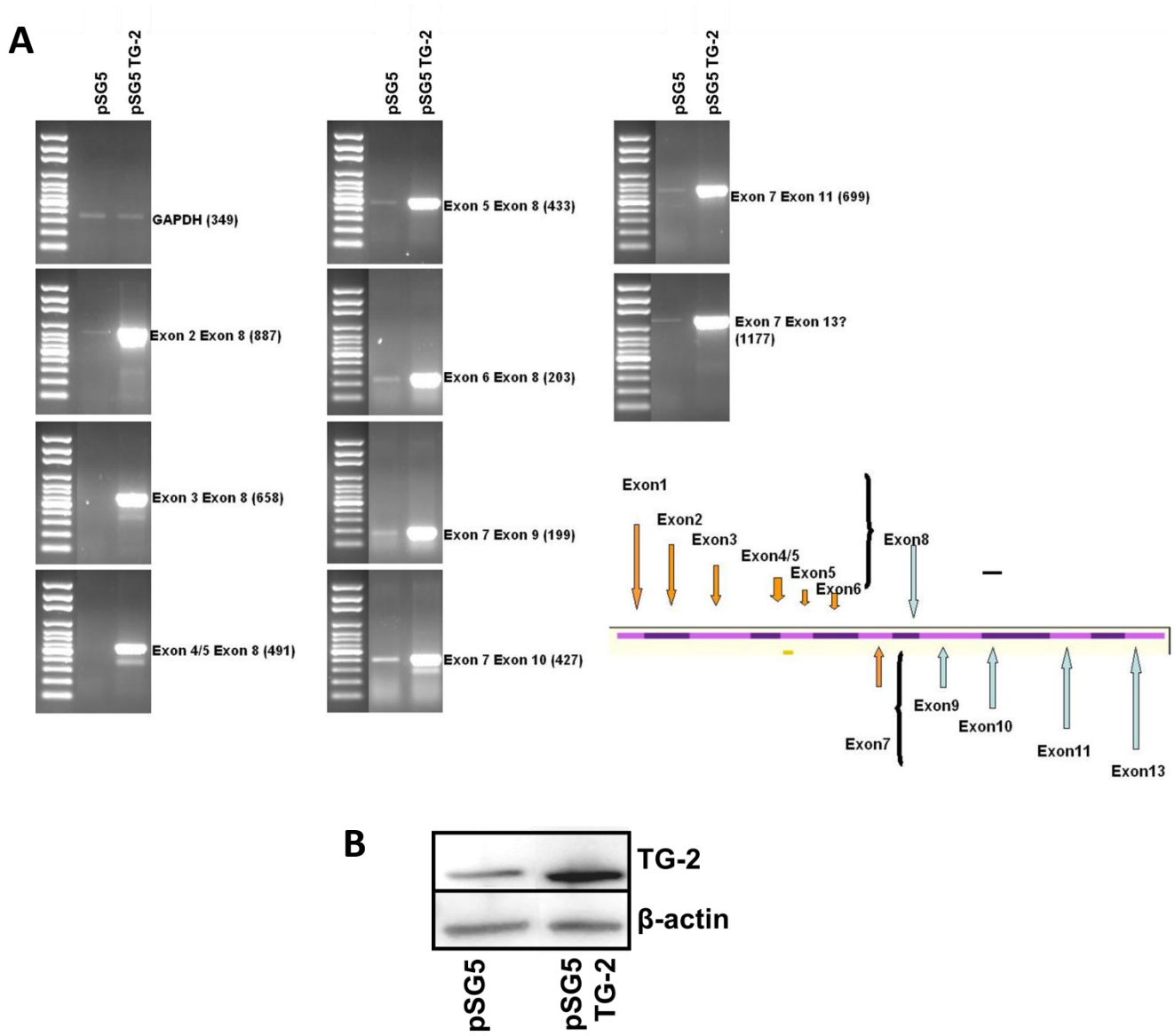

Figure 2.6. Figures showing semi-quantitative reverse transcription-polymerase chain reaction (RT-PCR) against different exons of TG-2 and western blot images of transfected cells against TG-2 primary antibody (A) Human corneal epithelial (HCE-T) cells were transfected with either pSG5 or pSG5 TG-2 plasmids, followed by 24 hours of incubation. Total RNA extraction and reverse transcription was then carried out to obtain cDNA. GAPDH was used as a housekeeping gene. Semi-quantitative reverse transcription-polymerase chain reaction (RT-PCR) against different exons of TG-2 was performed. Bottom right: Diagram showing position of primers on various TG-2 exons. Primers that are intron-spanning pairs were used. (B) Western blot showing cell lysate of pSG5 or pSG5 TG-2 transfected HCE-T cells blotting against TG-2 primary antibody. β-actin was used as loading control.

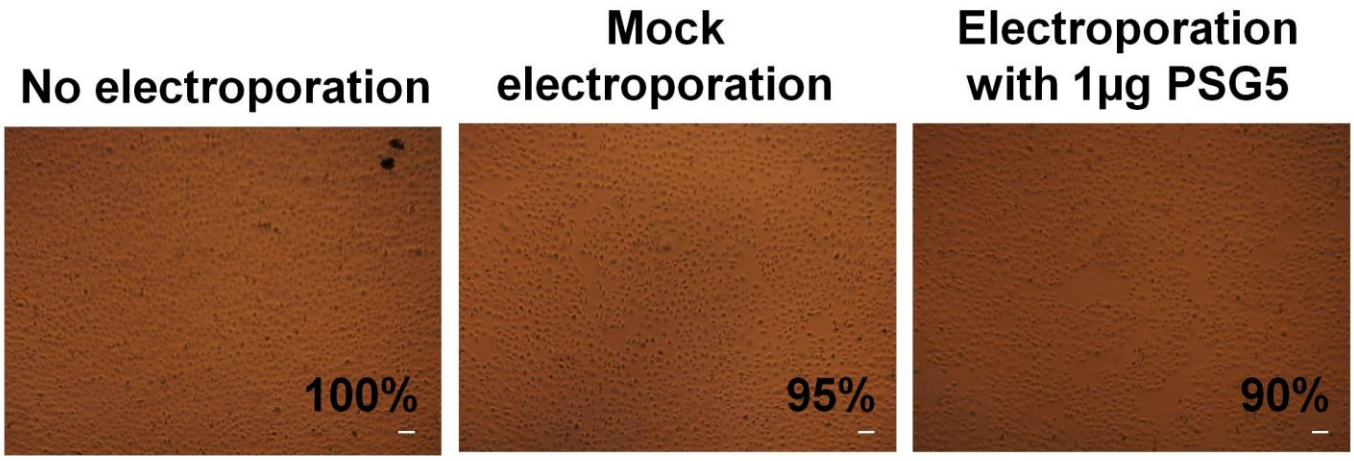

Figure 2.7. Microscopy images showing HCE-T cells 24 hours after various electroporation conditions in serum free condition. $1x10^6$ cells were seeded into each well of 6-well plate. Cell were electroporated with (Right) or without plasmid DNA (Middle). Cells without electroporation are shown on the Left. The percentages indicate cell confluency. Scale bar = 50 µm.

Compared to HCE-T cells expressing control plasmid (HCE-T pSG5), there was two-fold increase in transamidase activity in HCE-T cells overexpressing TG-2 (HCET pSG5 TG-2) (Figure 2.8A). To confirm that TG-2 could localise in the mitochondria of cultured HCE-T cells, western blot was performed and TG-2 was successfully detected in the mitochondrial extract (Figure 2.8B). The integrity of the mitochondrial extract was shown by immunoreactivity to mitochondrial antioxidant manganese superoxide dismutase (MnSOD). shRNA and shTG cells transfected with control plasmid pSG5 (shRNA pSG5 and shTG pSG5) showed similar cell index; however, the cell index dropped when they overexpressed TG-2 (shRNA pSG5 TG-2 and shTG pSG5 TG-2), suggesting a decrease in cell proliferation (Figure 2.8C). This reduction in proliferation due to overexpression of TG-2 was confirmed by crystal violet cell proliferation assay (Figure 2.8D). Also, the overexpression of TG-2 (pSG5 TG-2) in HCE-T cells increased caspase-3/7 and -9 activities (Figure 2.8E, F). As a negative control, ZVAD-FMK, a pan-caspase inhibitor, significantly reduced ($p < 0.05$) the caspase-3/7 and -9 activities in both TG-2 overexpressing cells (pSG5 TG-2) and control cells (pSG5). The concentration of Z-VAD-FMK used in these experiments did not affect cell proliferation (Figure 2.9).

A

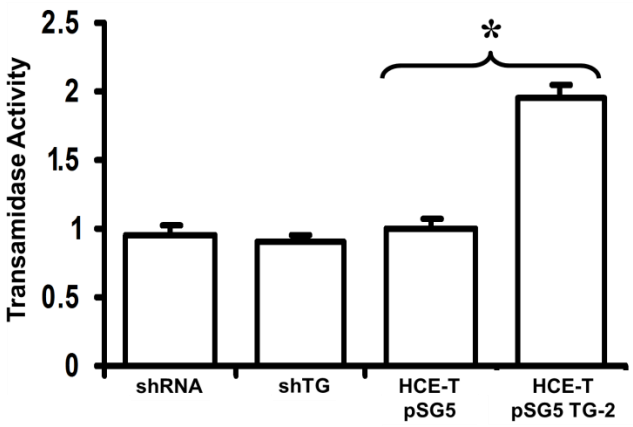
Transamidase Activity
2.5
2
1.5
1
0.5
0
*
shRNA
shTG
HCE-T pSG5
HCE-T pSG5 TG-2

B

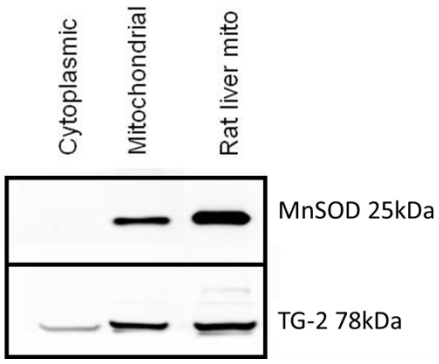
Cytoplasmic
Mitochondrial
Rat liver mito
MnSOD 25kDa
TG-2 78kDa

C

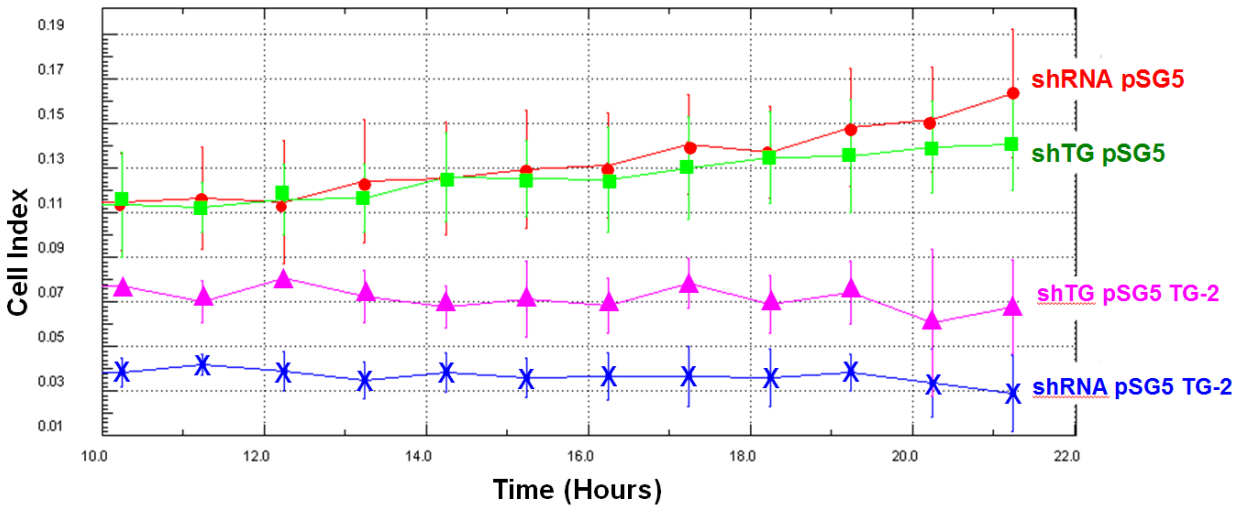
Cell Index
0.19
0.17
0.15
0.13
0.11
0.09
0.07
0.05
0.03
0.01
10.0
12.0
14.0
16.0
18.0
20.0
22.0
Time (Hours)
shRNA pSG5
shTG pSG5
shTG pSG5 TG-2
shRNA pSG5 TG-2

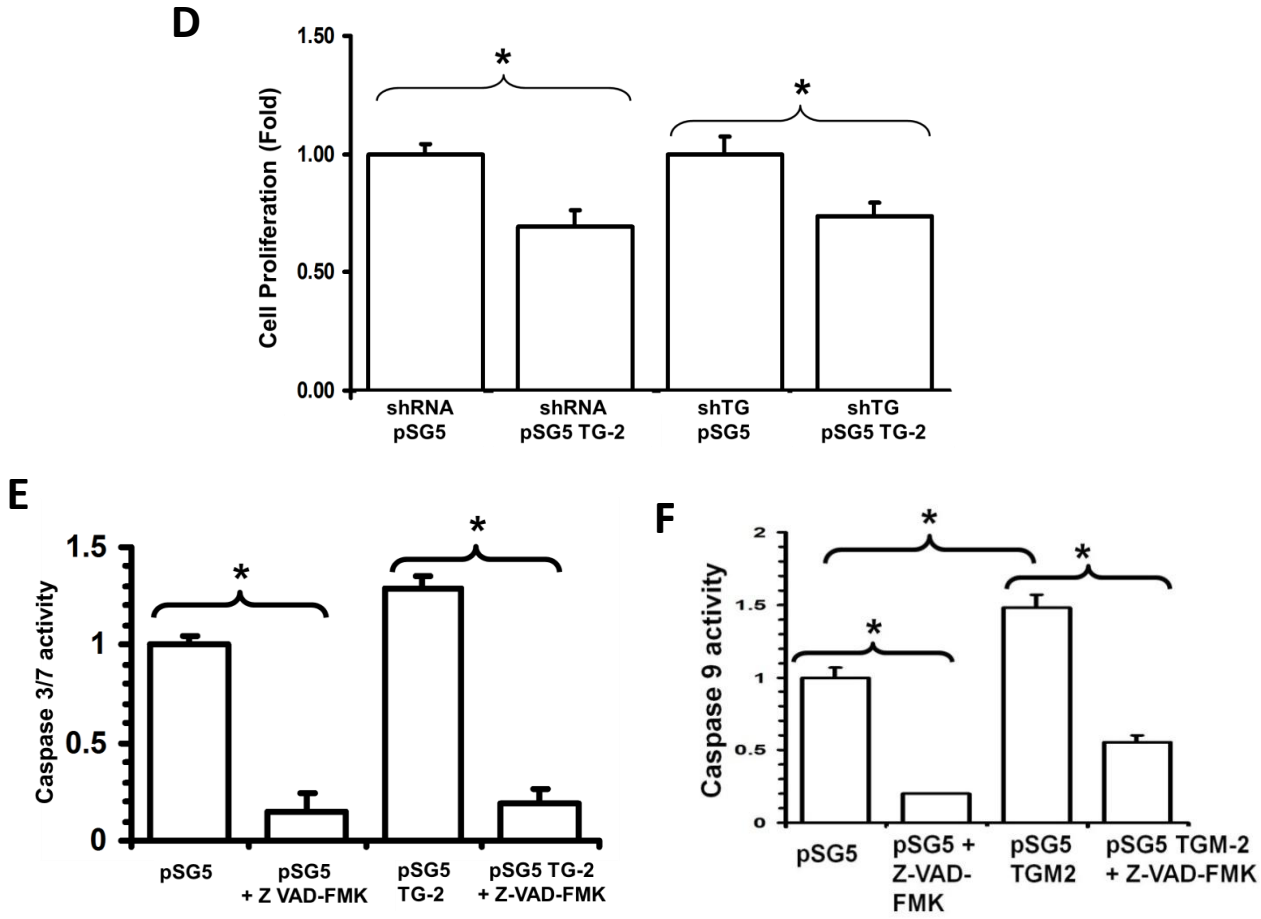

Figure 2.8. Figures showing effects of transfecting cells with pSG or pSG5 TG-2 plasmids on transamidase activity, cell proliferation and caspases activities. (A) In the transamidase activity assay, the transgluatminase crosslinking activity was calibrated to the commercially available purified guinea pig liver transglutaminase-2 activity. *: $p < 0.05$. Height of bars: mean, error bars: SD. (B) Western blot showing the presence of TG-2 protein in the cytoplasmic fraction and mitochondrial extract of HCE-T cells, as well as in rat liver mitochondrial extract. The integrity of mitochondria was determined by manganese superoxide dismutase (MnSOD). (C) Line graph showing result of cell impedance assay (see Appendix A14.1), whereby cell index was plotted against time for four types of cells. (D) Barchart showing the results of cell proliferation using crystal violet assay. The effect of TG-2 overexpression on cell densities was shown in cells transfected with pSG5 TG-2 plasmids. Three independent experiments were performed. *: $p < 0.05$. Height of bars: mean, error bars: SD. (E), (F) Barcharts showing the results of cell-based caspase 3/7 and 9 activity assays, 24 hours after transfection. Negative control, Z-VAD-FMK, a cell permeable pan-caspase inhibitor, was added at a concentration of 20mM. Three independent experiments were performed. *$p < 0.05$. Height of bars: mean; error bars: SD.

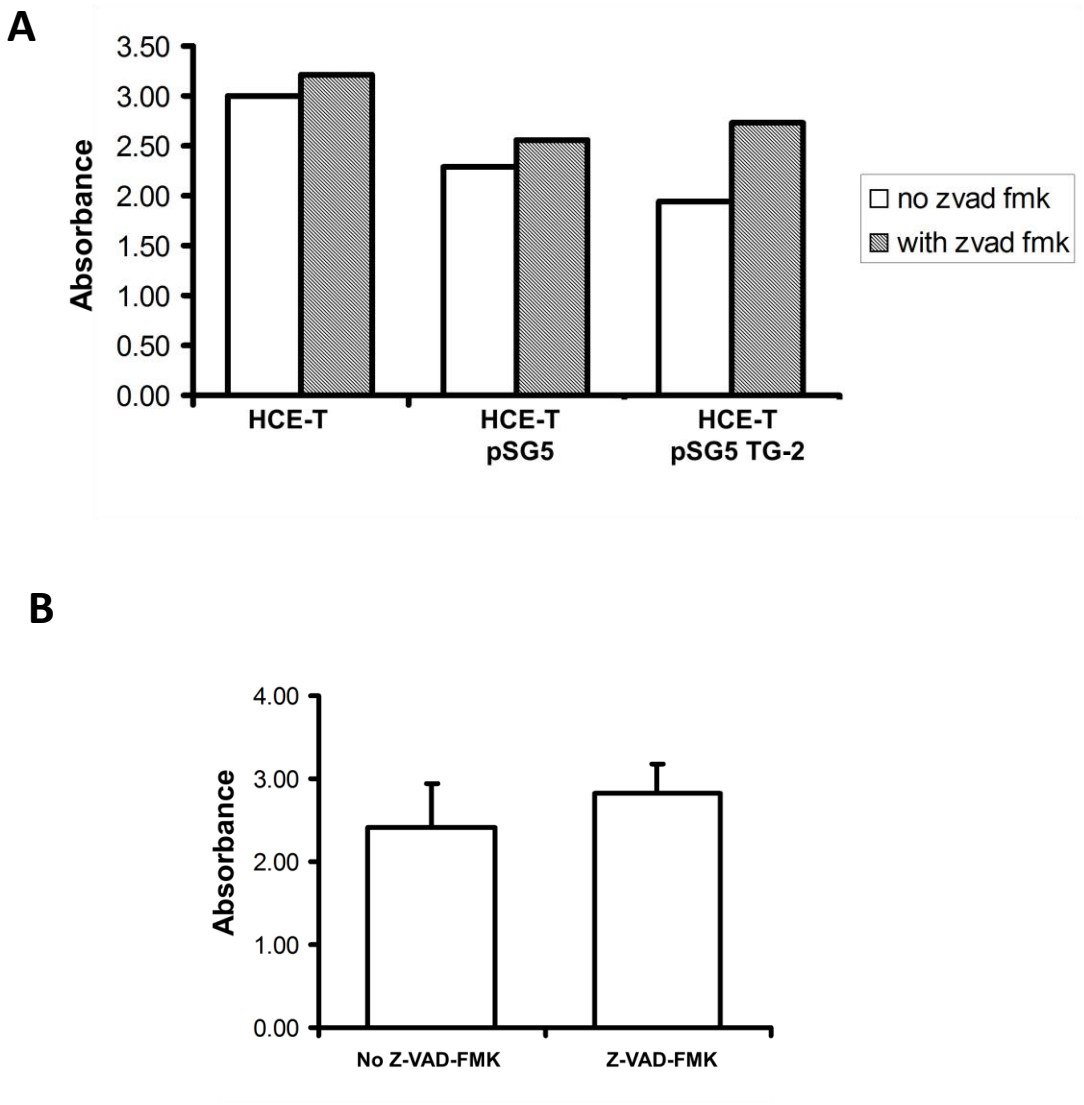

Figure 2.9. Figures showing crystal violet cell proliferation assay of cells incubated with or without Z-VAD-FMK (A) Human corneal epithelial (HCE-T) cells, HCE-T transfected with pSG5 or pSG5 TG-2 were treated with or without Z-VAD-FMK for 24 hours. Cell density was proportional to absorbance measured at 595nm. (B) Bar graph showing comparison between HCE-T cells treated with Z-VAD-FMK (mean of HCE-T, HCE-T pSG5 and HCE-T pSG5 TG-2) *versus* mean of untreated cells. Paired T test revealed that there was no significant difference between treatment and no treatment ($p = 0.15$).

2.8 Hyperosmolarity Induced Mitochondrial Depolarisation is TG-2 Dependent

Under basal osmolarity of 300mOsm, there was no significant mitochondrial depolarisation in untransfected cells, shRNA, shTG, mock transfected cells and cells transfected with pSG5 plasmids (Figure 2.10).

In 300mOsm medium, 14.6% of shRNA cells transfected with control plasmid pSG5 showed mitochondrial depolarisation; the percentage increased to 27.1% when the cells were exposed to hyperosmolar medium of 460mOsm (Figure 2.11A, top row). This 12.5% difference (27.1% minus 14.6%) represented a 1.86-fold change (27.1% / 14.6%) in mitochondrial depolarisation (Figure 2.11A, top row). Under the same condition, 6.2% (23.9% minus 17.7%) or 1.35-fold (23.9% / 17.7%) of shTG cells transfected with control plasmid pSG5 showed mitochondrial depolarisation (Figure 2.11A, bottom row). Hence, shRNA pSG5 cells showed that greater proportion of cells underwent hyperosmolar-induced mitochondrial depolarisation compared to shTG pSG5 cells (1.86 versus 1.35-fold change), suggesting that hyperosmolar-induced mitochondrial depolarisation was partly dependent on TG-2.

When cells were transfected with pSG5 TG-2 plasmids in 300mOsm, the proportion of cells undergoing mitochondrial depolarisation in shRNA pSG5 TG-2 cells were similar to that of shTG pSG5 TG-2, either under normal osmolarity (Figure 2.11B, left column: 23.5% / 23% = 1.02-fold change) or in 460mOsM (Figure 2.11B, right column: 33.5% / 33.3% = 1.0-fold change). This was probably because the overexpression of TG-2 by

transfection increased transcript levels over a few 100-fold (Table 1), suggesting that TG-2 was already saturated in the transfected cells. Hence, it was not surprising that cells overexpressing TG-2 responded in a similar fashion to hyperosmolar stimulation. Comparing hyperosmolar treated and untreated conditions, shRNA pSG5 TG-2 showed 1.45-fold change in mitochondrial depolarisation, similar to the 1.43-fold change in shTG pSG5 TG-2 (Figure 2.11B).

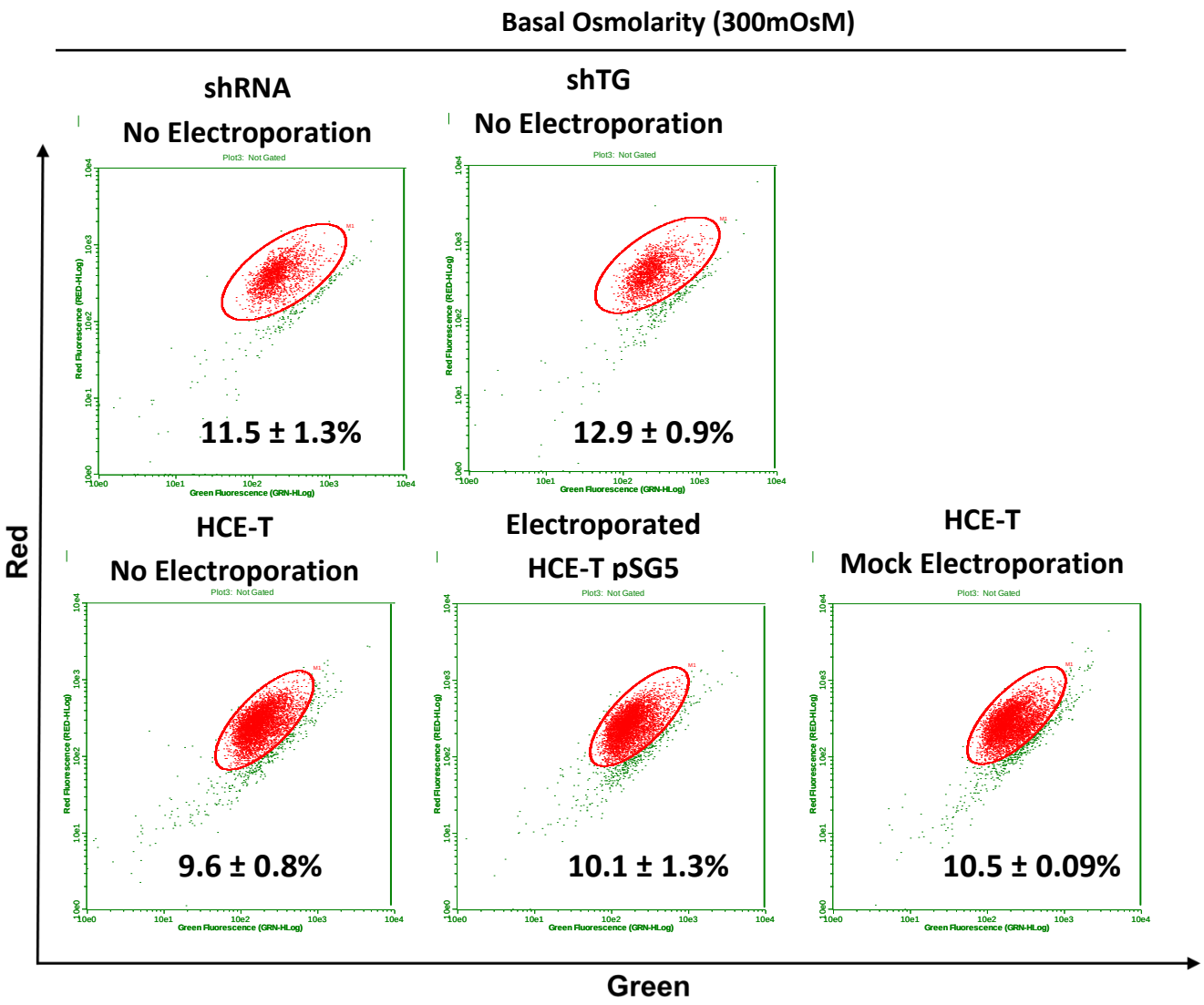

Figure 2.10. Flow cytometry analysis showing percentages of cells with mitochondrial depolarisation under basal osmolarity (300mOsM) condition. Human corneal epithelial cells (HCE-T no electroporation), HCE-T expressing scrambled RNA (shRNA no electroporation), HCE-T expressing shRNA targeting TG-2 (shTG no electroporation), HCE-T cells transfected without plasmid DNA (HCE-T mock electroporation) and HCE-T transfected with control plasmid pSG5 (Electroporated HCE-T: pSG5) were incubated for 24 hours. Sub-confluent adherent cells were trypsinised and non-adherent cells in the medium were collected. Both the trypsinised adherent cells and non-adherent cells were combined and stained with mitochondrial dye JC-1. Each point represents a single cell. An ellipse was drawn to delineate the population of cells with healthy mitochondria. The percentage of cells outside of the ellipse, which were cells with depolarised mitochondria, was calculated. Three independent experiments have been performed.

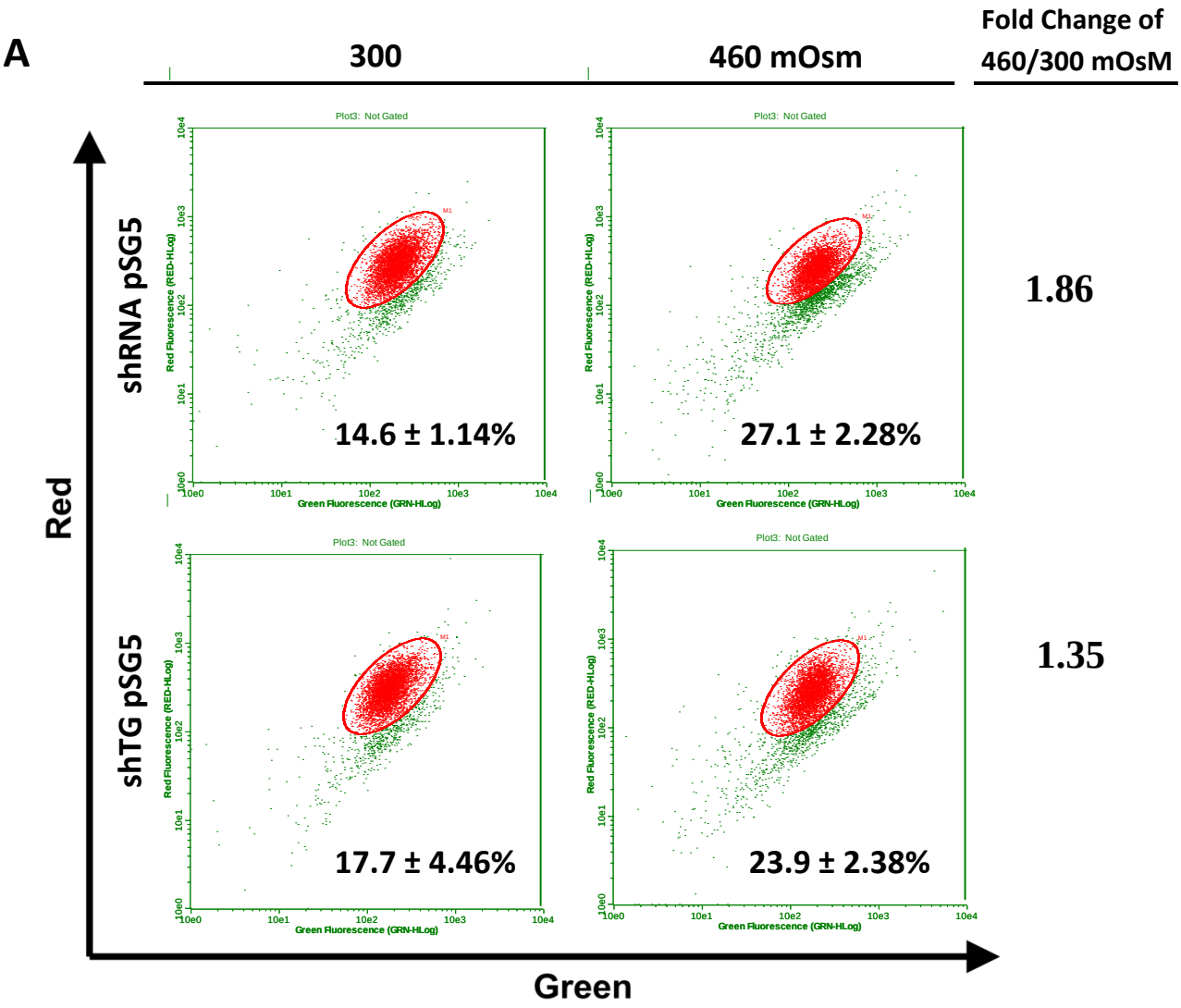
A
300
460 mOsm
Fold Change of 460/300 mOsM
shRNA pSG5
shTG pSG5
Red
Green
Plot3: Not Gated
Red Fluorescence (RED-HLog)
Green Fluorescence (GRN-HLog)
14.6 ± 1.14%
27.1 ± 2.28%
17.7 ± 4.46%
23.9 ± 2.38%
1.86
1.35

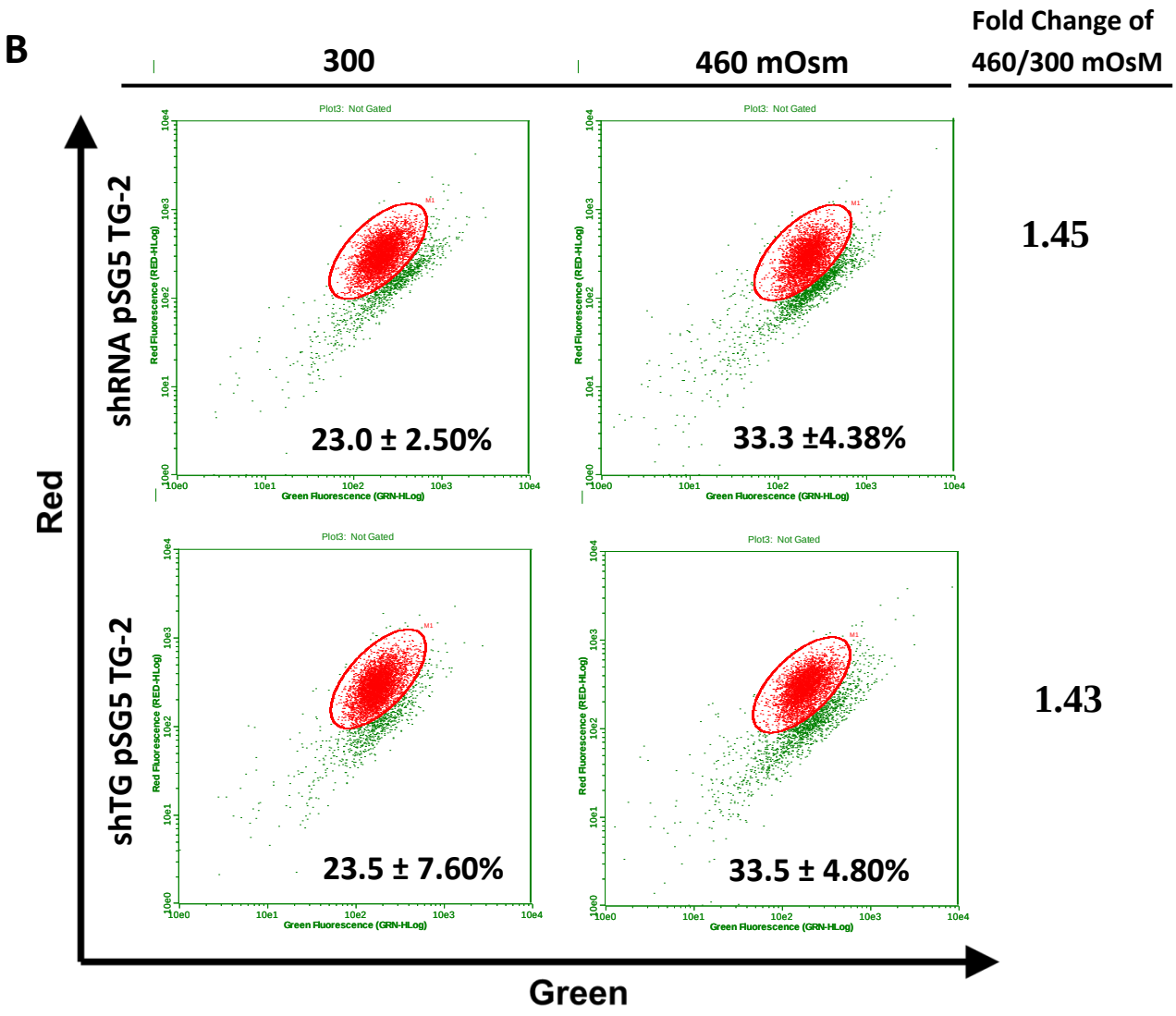

Figure 2.11. Flow cytometry analysis showing percentages of cells with mitochondrial depolarisation in normal (300mOsM) and hyperosmolar (460mOsm) conditions. Sub-confluent adherent cells were trypsinised and non-adherent cells in the medium were collected. Both the trypsinised adherent cells and non-adherent cells were combined and stained with mitochondrial dye JC-1 (Methods see Appendix D, A12.2). An ellipse was drawn to delineate the population of cells with healthy mitochondria. The percentage of cells outside of the ellipse, which were cells with depolarised mitochondria, was calculated (mean of three experiments). The fold change of hyperosmolar-induced mitochondrial depolarised cells for each cell type was shown on the right by dividing the percentage in the "460mOsM" by that in the "300 mOsM". Control shRNA and shTG cells under 360mOsM and 460mOsM were transfected with either (A) PSG5 plasmids or (B) PSG5 TG-2 plasmids. Three independent experiments have been performed.

Treatment	TG-2 fold change normalised to GAPDH	SEM
shRNA pSG5	1.00	0.01
shTG pSG5	0.45	0.06
shRNA pSG5 TG-2	444.69	0.02
shTG pSG5 TG-2	533.74	0.04

Table 1. Table showing reverse transcription real-time PCR result of transglutaminase (TG)-2 transcript levels, normalised to GAPDH. Cultured human corneal epithelial cells (HCE-T) stably expressing scrambled shRNA (shRNA) and shRNA targeting TG-2 (shTG) were used. These cells were transiently transfected with either pSG5 plasmid (control) or pSG5 TG-2 plasmid (over-expression of TG-2). Total RNA was then extracted from these transfected cells. The fluorescence of amplified products was measured at 483-533nm. SEM: standard error means

Why was the mitochondrial depolarisation in cells overexpressing TG-2 not as high as in the cells expressing the control plasmid (1.86-fold change)? One of the reasons was that at 300 mOsm, the pSG5 plasmid transfected cells had lower basal TG-2 compared to the saturated levels of TG-2 in pSG5 TG-2 expressing cells. The fold increase in pSG5 TG-2 cells in Figure 2.11B may not be due to TG-2 mechanisms. Hence, one could interpret that 1.45-fold (Figure 2.11B, top row) out of the 1.86-fold (Figure 2.11A, top row) increase in the hyperosmolar-induced mitochondrial depolarisation was due to non-TG-2 mechanism. Thus the hyperosmolar-induced mitochondrial depolarisation that was TG-2-dependent would be 1.41-fold (1.86-fold minus 1.45-fold). In terms of percentages, this meant that about 48% (41/86 x 100%) out of the total amount of hyperosmolar-induced mitochondrial depolarisation was TG-2 dependent (Figure 2.12).

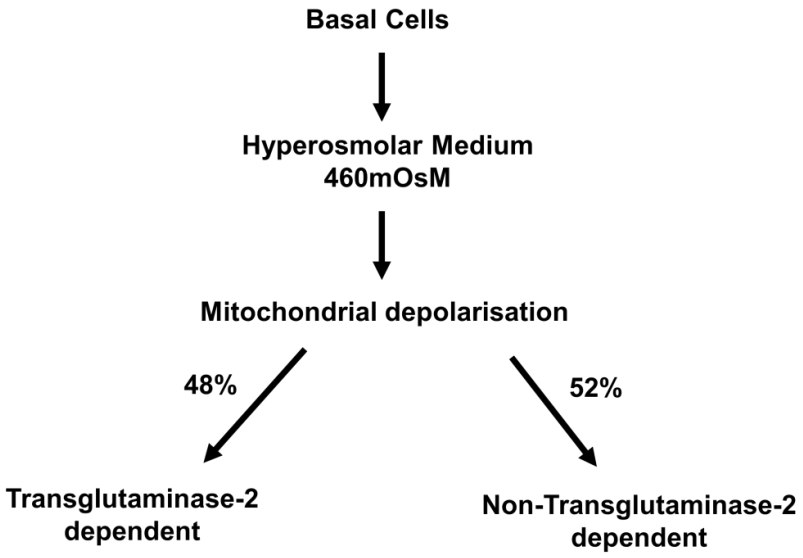

Figure 2.12. Schematic showing that basal cells exposed to hyperosmolar condition can induce mitochondrial depolarisation through transglutaminase-2 dependent or non-transglutaminase-2- dependent mechanisms.

2.9 Discussion

HCE-T cells exposed to hyperosmolar medium have reduced proliferation/viability through mitochondria and caspase-dependent mechanism which is partially dependent on TG-2 function. Dry eye is a multi-factorial disease that is accompanied by hyperosmolar tears and ocular surface inflammation [13]. This clinical condition was simulated by hyperosmolar culture medium in cultured HCE-T cells. The tear osmolarity in normal eyes is around 300 to 310mOsM [108, 109], while dry eye patients have an osmolarity of 343 ± 32 (306 to 441) mOsM [109]. A keratoconjunctivitis sicca patient has even recorded a hyperosmotic tear film of approximately 450 mOsm [109, 126]. The increase in extracellular osmolarity has been reported to affect cell functions in various tissues such as human bronchial epithelial cells [127], peripheral blood mononuclear cells [128], as well as the corneal epithelium [104]. Results in this study agree with previous literatures that hyperosmolarity induced apoptosis in primary corneal epithelial cells through cytochrome c-mediated pathway [104, 122].

Around 70% of TG-2 is localised to the cytosol; however, some of them are also localised to other organelles such as mitochondria [129]. In this study, TG-2 was found to be present in the mitochondria extract from both the cultured HCE-T cells and rat liver. It has been suggested that TG-2 may act as a protein disulphide isomerase (PDI) in mitochondria, contributing to the correct assembly and homeostasis of respiratory chain complexes [125]. TG-2 plays an important role in mitochondria physiology. Aberrant TG-2 has been reported to cause mitochondrial dysfunction both *in vitro* and *in vivo* [122]. For example TG-2 knockout mice showed mitochondrial energy production

impairment as evidenced by decreased ATP levels after physical stress, suggesting a role of TG-2 in regulating ATP synthesis [125, 130]. Also, after mitochondrial-mediated apoptosis by staurosporine, TG-2 overexpressed cells showed rapid loss of mitochondrial membrane potential compared to control cells [122]. However, the relationship between TG-2 and mitochondria in human cornea has not been evaluated.

The link between TG-2 and apoptotic cell death has been reported both *in vitro* [131] and *in vivo* [31]. Overexpression of TG-2 sensitises the cells to apoptosis or makes them more susceptible to apoptotic-inducing stimuli [44, 122]. For instance, Chen *et al* reported that the expression of TG-2 sensitised drug resistant breast carcinoma cells to apoptosis [132]. However, the direct link between TG-2 and apoptosis has not been established on the ocular surface. An earlier paper reported that the intracellular delivery of exogenous transglutaminase by a peptide delivery system into cornea epithelial cells significantly increased caspase-3 activity compared to vehicle control, suggesting that TG-2 may be linked to cell death in primary cultured HCE-T cells [114]. In addition, the expression of TG-2 in drug-resistant breast carcinoma cells rendered the cells more sensitive to apoptotic stimuli accompanied by activation of caspase-3 -7 and -9 [132]. Hence, the overexpression of TG-2 in HCE-T cells which induced higher caspase-3, -7, and -9 activity compared to the control cells in this project correlated well with the previously mentioned publications [114, 132]. Pan-caspase inhibitor Z-VAD-FMK was added as a negative control.

Compared to previous literatures, the current methodology is different whereby TG-2 was overexpressed in cultured HCE-T cells and the caspase activities were quantified [114, 132]. TG-2 has been reported to be involved in several types of stress-induced apoptosis. The differences in the experimental outcomes were likely due to the choices of different apoptotic stress, or different cell types. Chen *et al* reported that higher cell death was induced by staurosporine treatment to TG-2 overexpressed neuroblastoma cells as compared to similarly stressed cells with endogenous TG-2 [132]. Literatures also reported that TG-2 played a role in apoptosis due to oxidative stress in lens tissues [133] and alcohol-induced stress in hepatic cells [134]. On the contrary, hyperosmolar stimulation did not further increase the mitochondrial depolarisation in TG-2 overexpressing cells (Figure 2.11B, 1.45 and 1,43-fold) compared to cells with endogenous TG-2 (Figure 2.11A, top panel, 1.86-fold), suggesting that the endogenous TG-2 already saturated the requirement for TG-2. From Figure 2.12, around 48% of the hyperosmolar-induced cell death was TG-2 dependent.

2.10 Conclusion

This study concludes that hyperosmolar stimulation induced apoptosis in corneal epithelial cells via caspase-dependent mitochondrial dysfunction is dependent on TG-2. Protection against mitochondrial stress in the ocular surface through targeting TG-2 may have important implications in the treatment of inflammatory eye diseases.

Key Findings

a. Hyperosmolar treatment mediated cell death and reduced cell viability in cultured human corneal epithelial cells.

b. Hyperosmolar stimulation caused the release of cytochrome-c and mitochondrial depolarisation.

c. TG-2 was present in mitochondrial extract. Hyperosmolar stimulation did not further increase the mitochondrial depolarisation in TG-2 overexpressing cells compared to cells with endogenous TG-2; while in TG-2 deficient cells, hyperosmolar conditions induced less amount of mitochondrial depolarisation, indicating a partial dependence on TG-2 function.

d. TG-2 overexpression increased transamidase activity, reduced cornea epithelial cell proliferation and increased caspase-3/7 and 9 activity.

CHAPTER 3. TRANSGLUTAMINASE-2 AND BINDING PARTNERS

3.1 Subcellular Compartmentalisation of Proteins

TG-2 in subcellular compartments can affect physiological functions differently since its Ca^{2+} -dependent transglutaminase cross-linking activity and GTPase activity are known to be modulated by the local environment [23]. Previously Milakovic *et al* reported that cytosolic TG-2 was pro-apoptotic whereas nuclear TG-2 was anti-apoptotic [135]. Lesort *et al* also demonstrated that different subsets of proteins were modified by nuclear TG-2 compared to the cytosolic TG-2 [136]. It is important to understand the binding partners which interact with different domains of TG-2 in the cell, as it may impact the cell migration or adhesion signaling pathways. For example, the interaction of TG-2 with endocytic receptor LRP-1 (low-density lipoprotein receptor-related protein 1) at different locations, either *in vitro* and on the cell surface, may affect endocytosis and other physiological functions [35].

The protein-binding partners of TG-2, apart from integrins and ECM proteins such as fibronectin, have yet to be investigated. Also, proteins that interact with specific domains of TG-2 are not known. Moreover, the roles of TG-2 in cell trafficking and compartmental localisation have not been studied in cornea epithelial cells. The cellular proteins need to be separated efficiently in order to fully understand the function of TG-2. Previously, TG-2 binding partners, such as Bcl-2-associated X protein (Bax), were discovered by immunoprecipitation [124]. In this study, a mass spectrometry-based method was employed to elucidate the protein binding partners of TG-2. Fragments of

flag-tagged TG-2 were expressed and the complexes were then pulled down by anti-flag immunoglobulins.

3.2 Subcellular Trafficking and Corneal Wound Healing

Several literatures have examined the relationship between corneal wound healing and sub-cellular trafficking [137-139]. Kucerova *et al* found that heterozygous deficiency in Pax6, which was associated with congenital ocular surface diseases, disrupted glycoprotein trafficking, thus it affected wound healing response in corneal epithelial cells [137]. Meanwhile, McClintock and Ceresa studied the effects of two growth factors: transforming growth factor-α (TGF-α) and epidermal growth factor (EGF), on endocytic trafficking of growth factor receptor (EGFR) protein which could influence EGFR-mediated corneal wound healing [138]. Shankardas *et al* studied the expression and distribution of 14-3-3 proteins in human cornea and conjunctiva, and suggested that the proteins may be involved in epithelia specific signalling and trafficking pathways [139, 140]. These literatures evaluated the significance of protein trafficking in corneal wound healing. However, they did not study the sub-cellular localisation of the trafficked proteins through fractionation. Also, the mechanism by which proteins were trafficked between sub-cellular compartments was not elucidated. Moreover, the link between TG-2 and corneal epithelial wound healing was not evaluated in these studies.

3.3 High-speed Cellular Protein Separation

Ultracentrifugation is a pelleting process that has been used in several studies examining subcellular trafficking. However, conventional ultracentrifugation has drawbacks such as requiring long extraction times and not preserving the sample integrity very efficiently, as the sample remains at high centrifugal force for a longer time.

Centricollation is a novel method of protein separation based on a stepwise density extraction or flotation principle. It provides uniform and specific separations by applying equal centrifugal force to the entire sample. The hallmark of this technique is that the sample stays at high centrifugal force for only 2 to 3 min for each fraction. The centricollated samples can rapidly accelerate to 125,000g within a very short time of 45 seconds instead of multiple hours, allowing multiple extractions in a relatively short time. This technique uses sucrose solution with increasing density and produces sucrose fractions ranging from 8.5-40%. Other advantages of using centricollation technique include the possible usage of small samples with extraction volumes as low as 50μL up till 3mL, usage of predefined density extracting media with a range of increasing densities, non-denaturing separation conditions and high recovery yield of more than 90%. The fractionation conditions are also non-denaturing to the sample. Moreover, the sucrose fractions generated are compatible with all downstream analyses, including gel electrophoresis, HPLC, mass spectrometry, and microarrays.

3.4 Hypothesis and Specific Aims

It is hypothesised that specific TG-2-protein and protein-protein interactions in cell compartments are important in the understanding of corneal epithelium wound healing and may suggest new treatment options for ocular surface diseases.

Specific Aims

To discover and characterise cell adhesion or migration related proteins which interact with TG-2.

a. To characterise the proteins that interact with different TG-2 fragments using immunoprecipitation, LC/MS and MASCOT database search.
b. To understand how these proteins are trafficked between cell compartments using centricollation and immunoblotting of potential binding partners in cells in combination with RNA interference of TG-2.
c. To determine whether TG-2 level can affect the relative concentration of cell-adhesion proteins in sub-cellular fractions using western blotting.

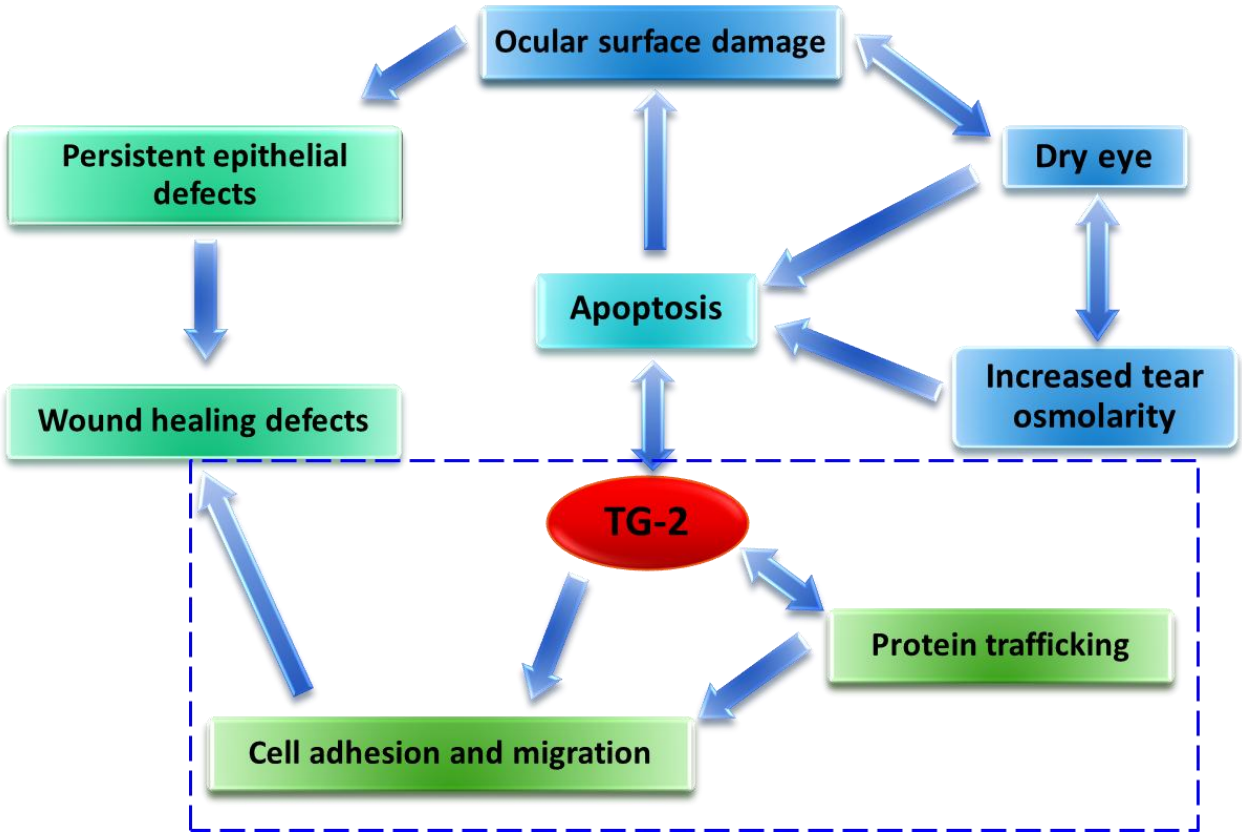

Figure 3.1. Schematic showing the focus of this chapter, as depicted by the blue square. The main objective of this chapter is to discover TG-2 interacting proteins and their trafficking.

3.5 Methodology

3.5.1 Protein-protein Interactions

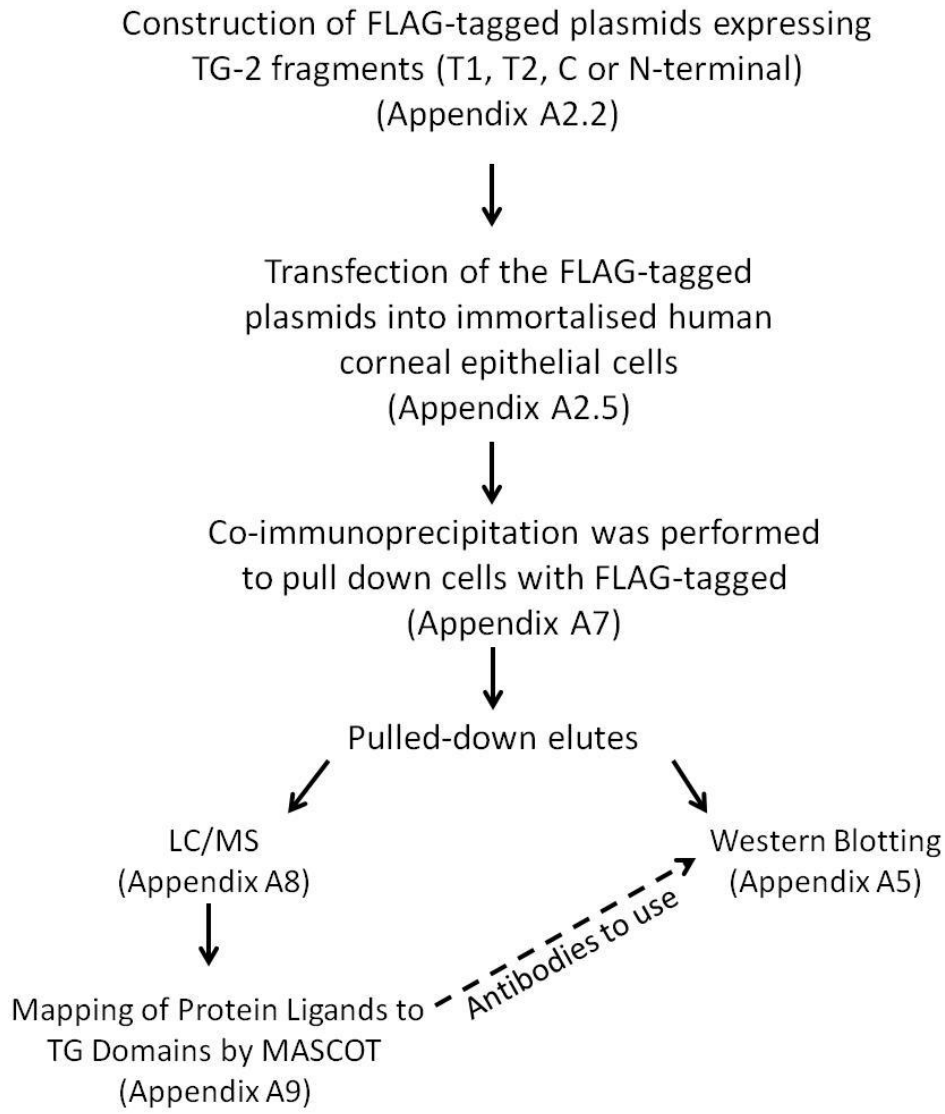

Methodology Flow Chart 2. Flow chart shows general methodology to study the protein-protein interactions in cultured human corneal epithelial cells. The detailed protocol for each technique is described in the Appendix.

3.5.2 Characterisation and Grouping of TG-2 Ligands/ Organelles

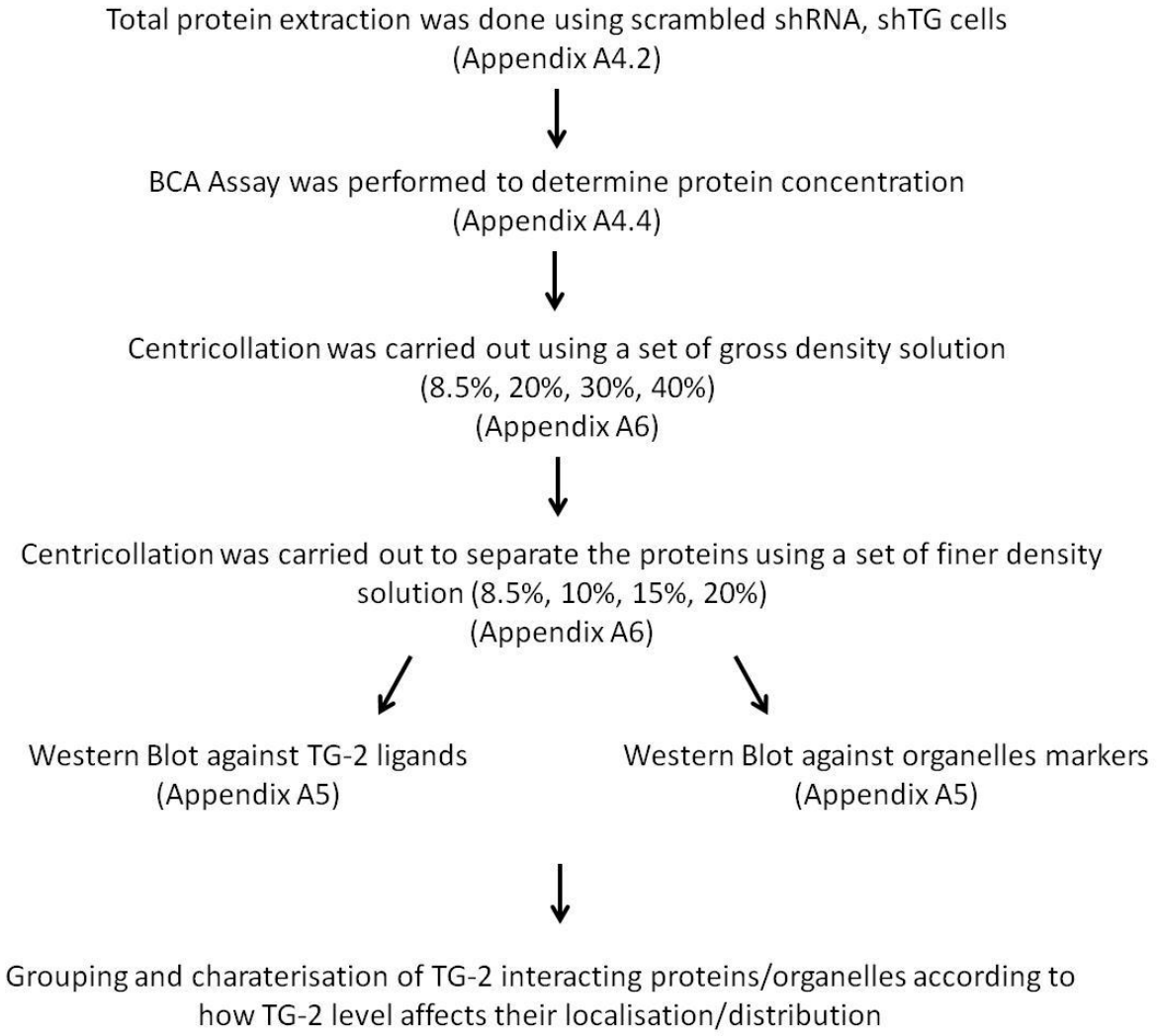

Methodology Flow Chart 3. Flow chart showing general methodology to study the protein trafficking in cultured human corneal epithelial cells. The detailed protocol for each technique is described in the Appendix.

3.6 Identification of Potential TG-2 Binding Partners

Fifteen TG-2 interacting proteins that bind to different TG-2 fragments (Figure 3.2, Figure 3.3) were identified using mass spectrometry and MASCOT protein database search (Appendix A8, A10). Table 2 shows examples of TG-2 binding partners identified by mass spectrometry and MASCOT protein database search. One example of potential binding peptide was shown for each TG-2 fragment (Table 2). Individual mass spectrometry experiments were done using independent and repeated co-immunoprecipitation experiments (Methods at Appendix A7.1) which successfully pulled down the same 15 TG-2 interacting proteins, thereby increasing the confidence of the interaction. In addition, the same co-immunoprecipitation elute that was used to run the mass spectrometry was used to perform immunoblotting. The same TG-2 ligands discovered in MASCOT were successfully identified using commercially available antibodies (Appendix B). Moreover, these proteins had been shown to be indirectly linked to TG-2 in publications (Figure 3.4).

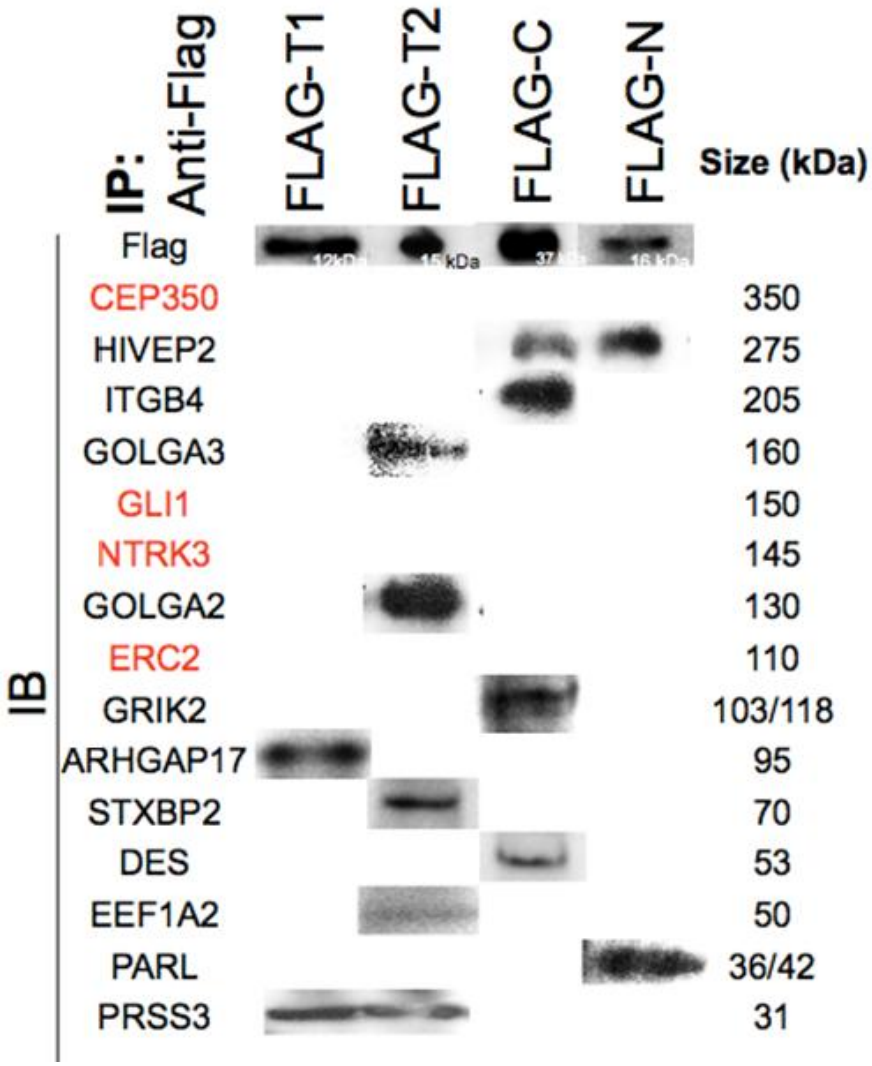

Figure 3.2. Western blots showing the TG-2 ligands identified using commercially available antibodies. Immortalised human corneal epithelial cells were transfected with FLAG-tagged plasmids expressing TG-2 fragments (denoted as FLAG-T1, FLAG-T2, FLAG-N, FLAG-C). Co-immunoprecipitation was performed to pull down proteins with FLAG-tagged. Western blotting successfully identified 11 out of 15 of the TG-2 ligands (in black font).

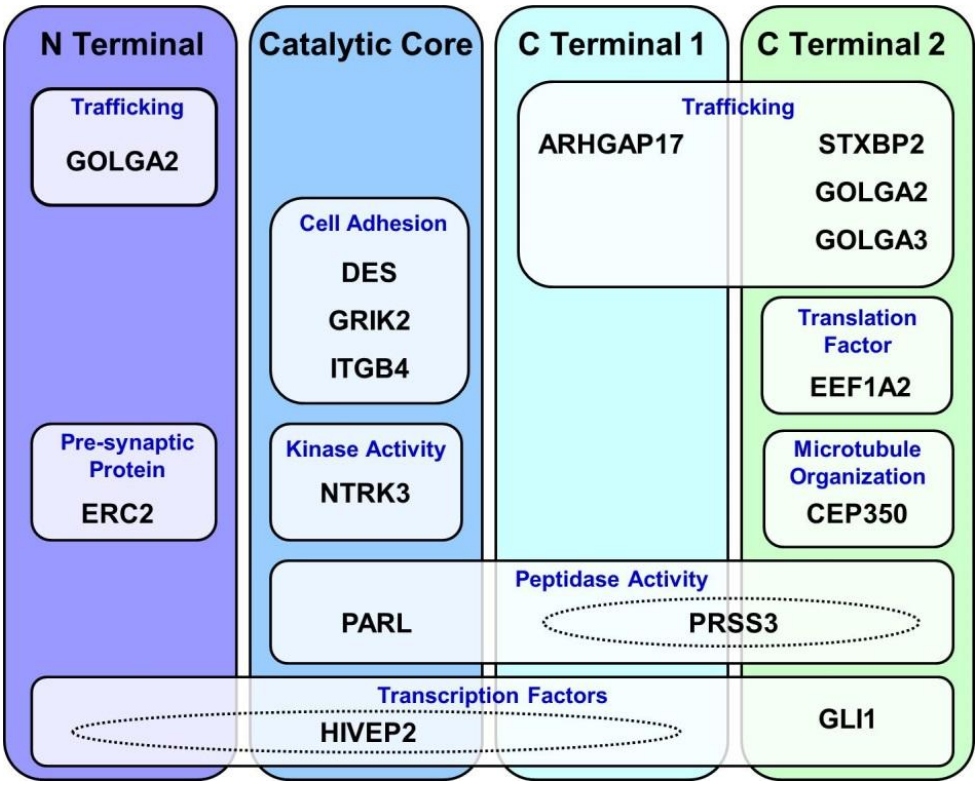

Figure 3.3. Schematic showing proteins interacting with different domains of TG-2 and the biological functions.

Examples of ion fragments pulled down by TG-2

TG-2 fragment	Peptide	Fragment	m/z
N	GOLGA2	K.SELEEKLR.V	502.25
T1	ARHGAP17	R.SIFPEMHSDSASK.D	718.29
T2	STXBP2	K.ILSGVIRSKV.K	536.27
C	ITGB4	R.LTAGVPDTPTR.L	564.29

Table 2. Examples of TG-2 binding partners identified by mass spectrometry and MASCOT protein database search. One example of potential binding peptide was shown for each TG-2 fragment.

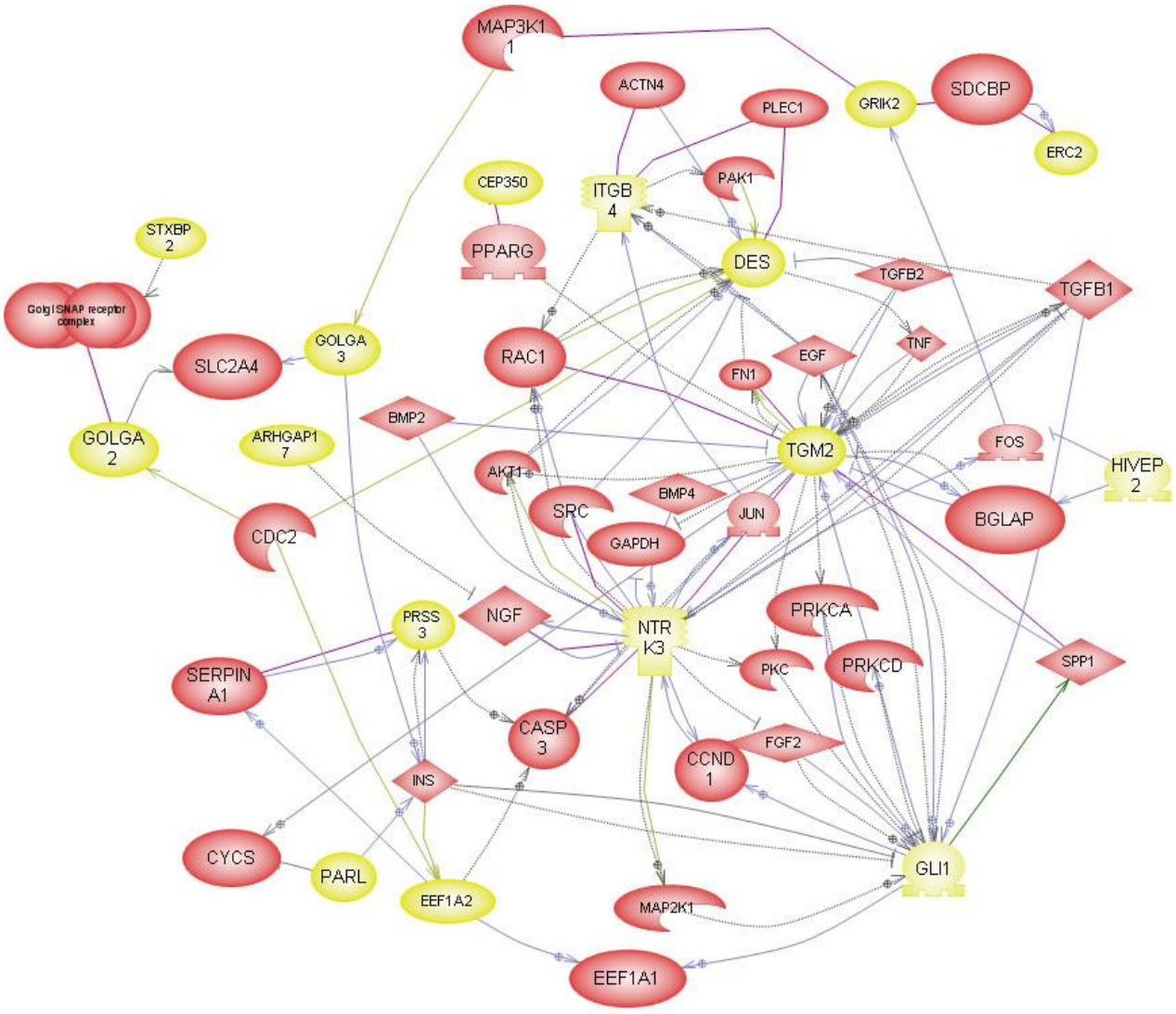

Figure 3.4. Molecular network showing the interactions of TG-2 and its potential binding partners. Yellow entities: Mass spectrometry and MASCOT database showed that these interacting proteins had some relationship with TG-2 through indirect pathways. Red entities: Existing scientific literature demonstrated that these proteins were related to TG-2.

Where were these TG-2 ligands located in the cells? Using centricollation technique to separate cell lysate through stepwise density extraction (Appendix A5), the sub-cellular localisation of these potential TG-2 binding partners could then be determined by referring to an approximate organelle localisation chart provided by Prospect Biosystems (Figure 3.5). The chart showed sucrose density (%) corresponding to a known organelle based on particle diameter (μm). Most of the organelles fell within the sucrose density of 14 - 50%. Hence, gross centricollation was first carried out at sucrose density of 8.5%, 20%, 30% and 40% (Figure 3.6). From the gross centricollation result, most of the potential TG-2 ligands were found in the 8.5% and 20% sucrose fractions (SF); thus further fractionations were performed in finer 8.5%, 10%, 15% and 20% SF.

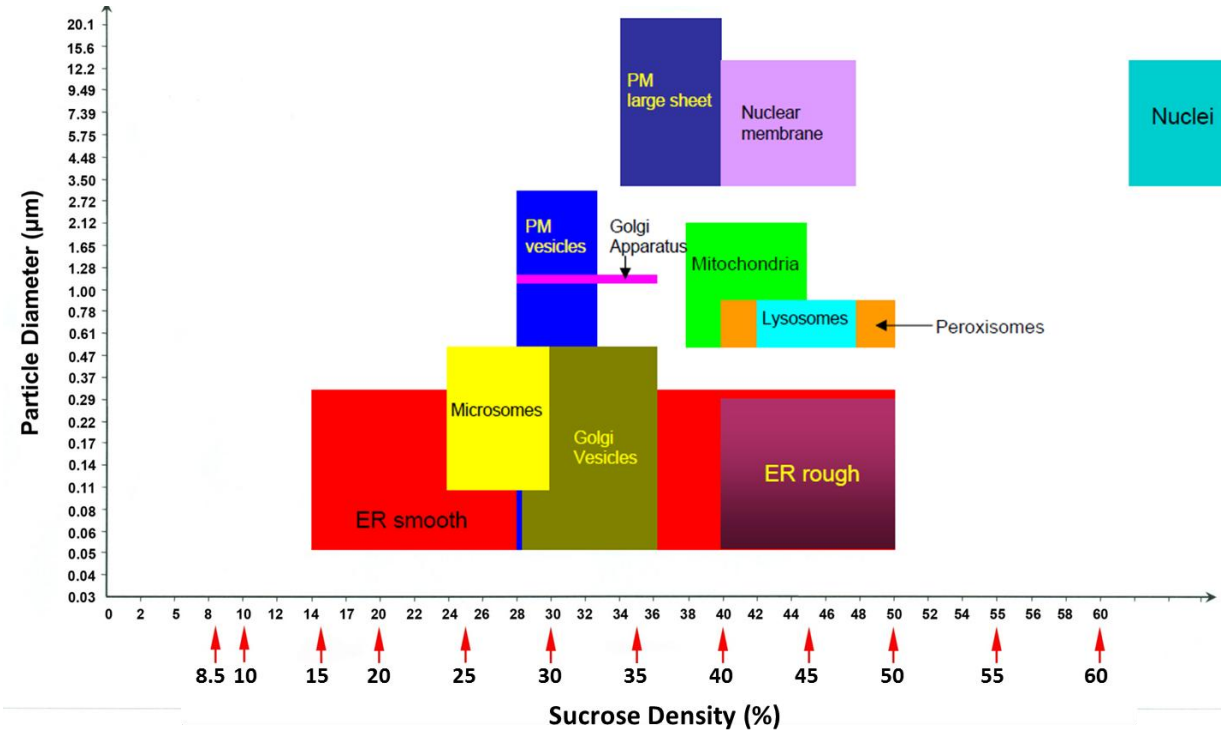

Figure 3.5. Figure showing the approximate distribution of organelles at different sucrose density (%) versus particle diameter (µm). Red arrows indicate pre-defined sucrose density media (%) at 8.5, 10, 15, 20, 25, 30, 35, 40, 45, 50, 55 and 60%.

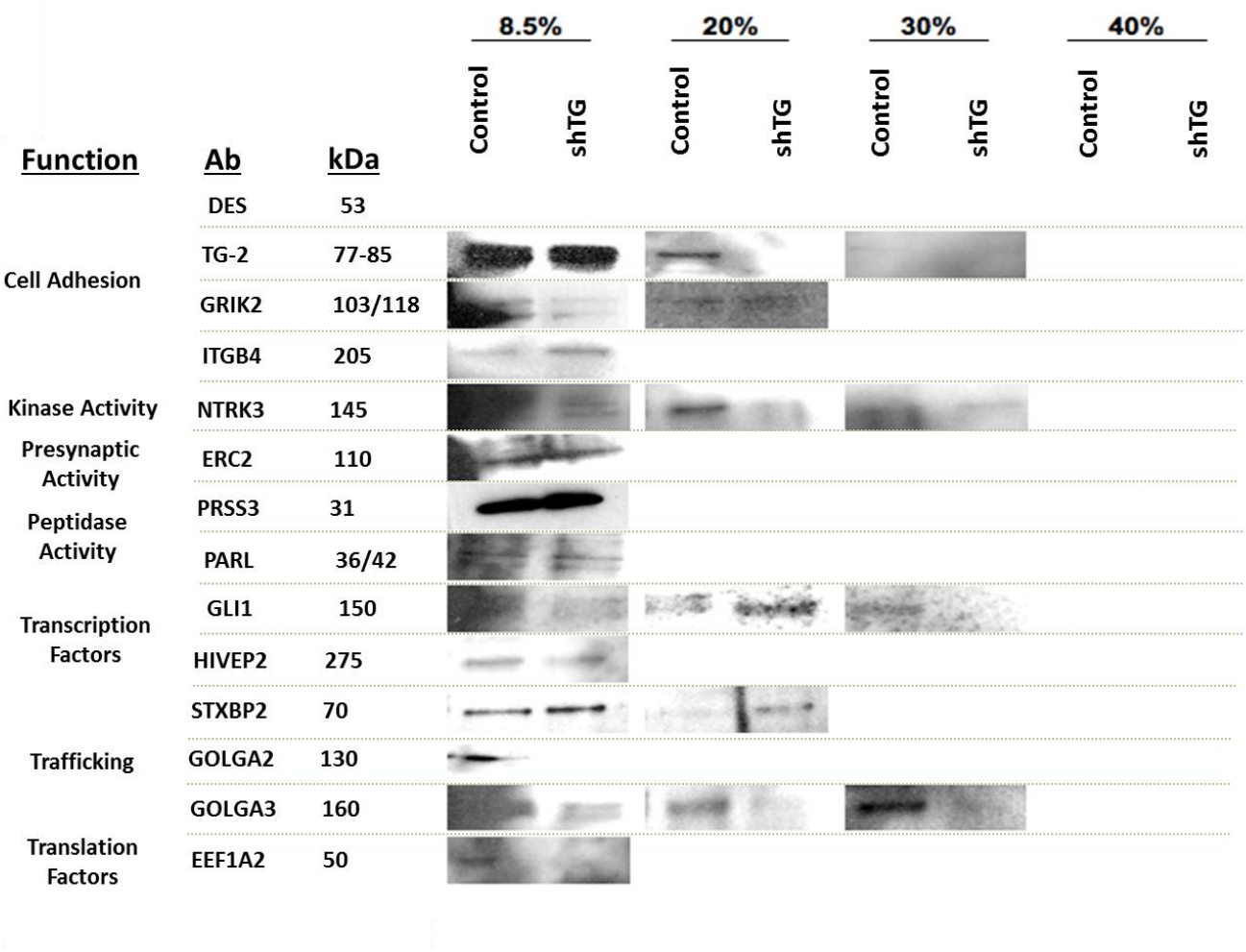

Figure 3.6. Western blotting images showing TG-2 ligands expression levels in centricollated control shRNA and shTG cell lysates. Gross sucrose fractions of 8.5%, 20%, 30%, and 40% were used. Most of the proteins of interest were found in the 8.5% and 20% sucrose fractions.

3.7 Grouping of TG-2 Binding Partners

As mentioned in Section 3.6, since most of the TG-2 ligands fell between 8.5% to 20% SFs, hence immunoblotting was performed against the 15 TG-2 interacting proteins in this range of SFs. Using commercially available antibodies, western blotting consistently detected 7 out of the total 15 TG-2 binding proteins. The TG-2 interacting proteins were categorised into three groups according to how TG-2 (control scrambled shRNA vs shTG cells) affected the pattern of localisation in various SFs (Figure 3.7). The relative intensity for each individual western blot band was also quantitatively measured (Figure 3.7B).

Group 1 consisted of desmin (DES), presenilin associated, rhomboid-like protein (PARL), neurotrophic tyrosine kinase, receptor, type 3 (NTRK3), and serine protease (PRSS3). Proteins falling into this group had lower expression of proteins in shTG compared to control shRNA cells in all (DES and PARL) or in specific fractions (NTRK3 and PRSS3). The ratio of relative intensities between control and shTG cells was around 3:1.

Group 2 consisted of proteins which were lower in shTG cells in one SF, but showed a reversal trend in other SFs. This group included Golgi-associated protein (GOLGA2) and integrin beta-4 (ITGB4). For example in GOLGA2, shTG had higher protein concentration than control cells in 8.5% SF, but it had lower concentration of protein than control in 10%, 15% and 20% SFs. The ratio of relative intensities between control and

shTG cells corresponding to each SF was approximately 1:3, 3:2, 3:2, 2:1 in GOLGA2; and 1:2, 3:2, 2:2, 2:1 in ITGB4

Protein in Group 3, such as Syntaxin binding protein (STXBP2), expressed similar concentration in both control and shTG cells in all the 4 SFs. STXBP2 had relative intensity ratios of 1:1,1:2,1:2, 1:1 in control and shTG cells for each SF. The band intensities in the 10% and 15% SFs were slightly higher in shTG cells compared to control. However, when compared to repeated experiments, STXBP2 had consistently similar expressions in control and shTG cells throughout the SFs.

A

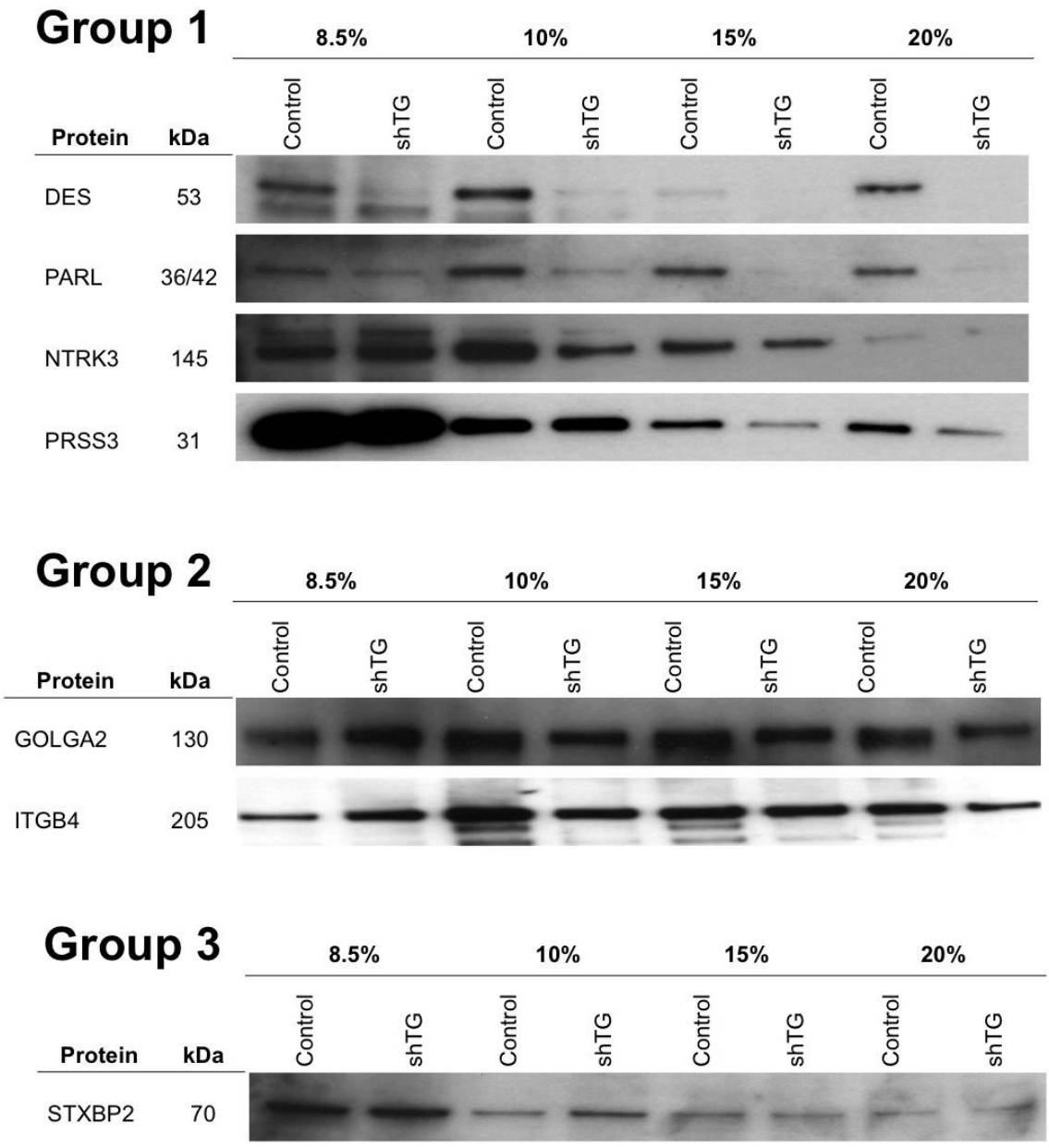
Group 1
8.5%
10%
15%
20%
Control
shTG
Protein
kDa
DES
53
PARL
36/42
NTRK3
145
PRSS3
31
Group 2
GOLGA2
130
ITGB4
205
Group 3
STXBP2
70

B

Group 1

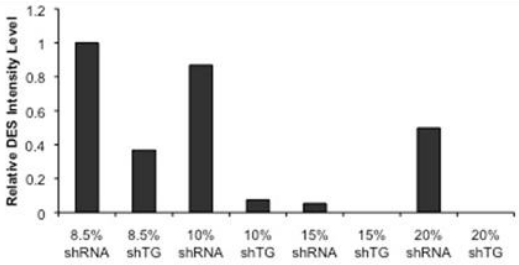

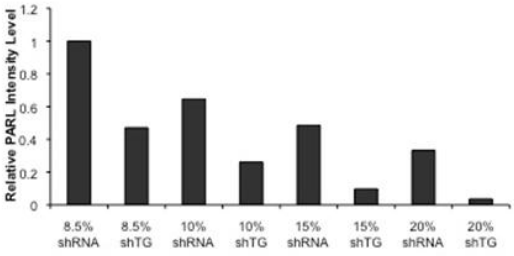

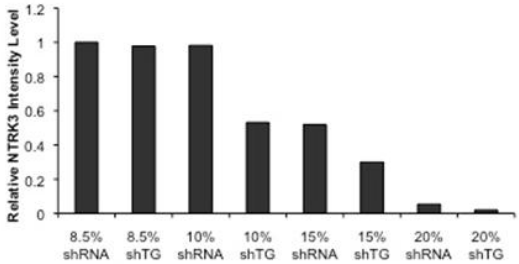

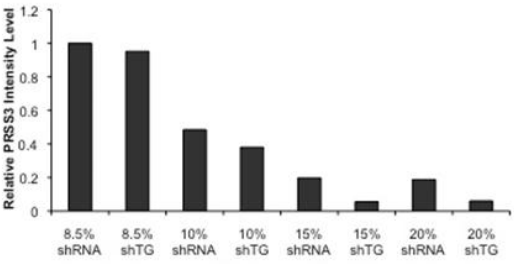

Group 2

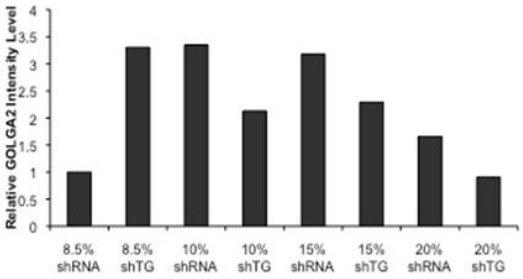

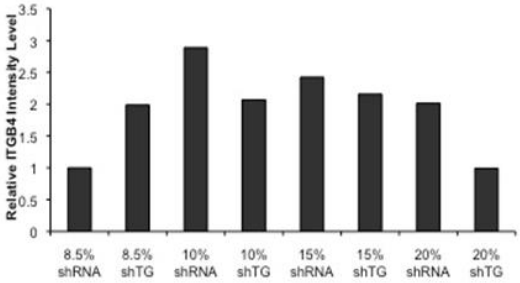

Group 3

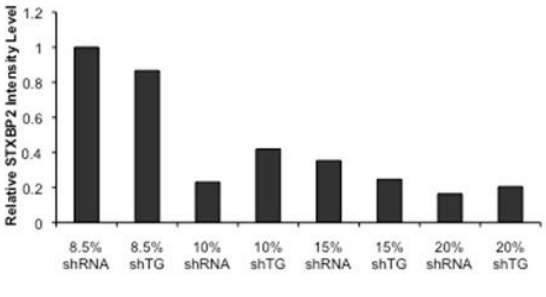

Figure 3.7. Representative western blot images showing TG-2 ligands expression levels in centricollated cell lysates. (A) Sucrose fractions of 8.5%, 10%, 15%, and 20% were used. Group 1 ligands: These were characterised by lower expression of proteins in shTG compared to control (scrambled shRNA) in all (DES and PARL) or in specific fractions (NTRK3 and PRSS3). Group 2 ligands: These were characterised by their reduced expression in one of the SFs, but showed an increased expression in other SFs. Group 3 ligand: syntaxin binding protein (STXBP2), which was characterised by the similar expression patterns between shTG and control in all the fractions tested. Three independent experiments were performed. (B) Densitometry showing relative intensity levels of various TG-2 ligands according to different density sucrose fractions from western blot results. Group 1: This group consistently showed a lower protein expression in shTG cells compared to control shRNA cells in all the sucrose fractions. The members of this category include DES, PARL, NTRK3 and PRSS3. Group 2: Comparing the expression level in shTG and shRNA cells, this group consisted of proteins that showed higher expression in shTG in one sucrose fraction, but showed lower expression level in shTG in another fraction. GOLGA2 and ITGB4 fell into this category. Group 3: shTG and shRNA cells were found to have relatively similar expression patterns in all sucrose fractions. This group consisted of the protein STXBP2.

3.8 Characterisation of Organelles in Different Sucrose Fractions

The characterisation for known organelles in different SFs from 8.5%, 10%, 15%, to 20% is shown in Figure 3.8. Organelles such as recycling endosomes, endoplasmic reticulum, and mitochondria were only found in particular SFs. Recycling endosomes were predominantly found in the 8.5-15% SFs. Endoplasmic reticulum were only present in the 8.5% SF. Mitochondria were only found in the 10% SF.

All the other organelles, for example early endosomes, late endosomes, secretory vesicles and lysosomes, showed different immunoreactivities intensities in 8.5-20% SFs. Early endosomes were predominantly expressed in the range of 8.5%-15% SFs. The expressions of late endosomes (RAB7), recycling endosomes (RAB11A) and the secretory vesicles (RAB27A) were lower in shTG cells compared to control. On the other hand, the reduction of TG-2 did not affect the immunoreactivity against lysosomes (LAMP1), early endosomes (EEA1), mitochondria (RAB3D) and endoplasmic reticulum (PDI).

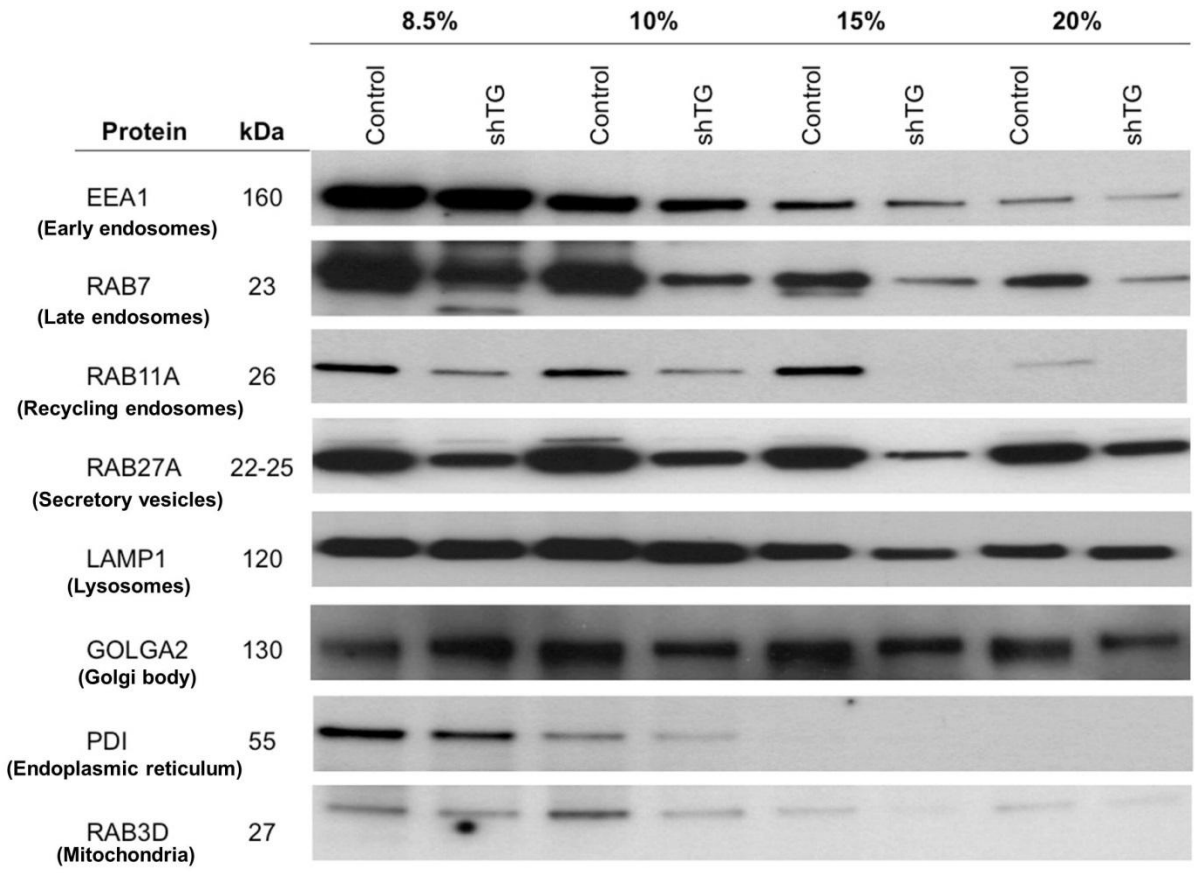

Figure 3.8. Western blots showing expression levels of organelle markers according to various densities of sucrose fractions in centricollated control and shTG cells. Late endosome (RAB7), recycling endosome (RAB11A) and the secretory vesicle (RAB27A) showed decreased expressions in shTG compared to control cells. The expression level of early endosome (EEA1), lysosomal (LAMP1), mitochondria (RAB3D) and endoplasmic reticulum (PDI) expressions were not affected by the status of TG-2. Early endosomes, late endosomes, secretory vesicles and lysosomes were present in all sucrose fractions. Recycling endosome, endoplasmic reticulum and mitochondria were not present in all fractions, for example recycling endosomes were mostly found in the 8.5%-15% range, while endoplasmic reticulum and mitochondria were mostly found in the 8.5% and 15% sucrose fractions respectively.

3.9 Discussion

Depending on sub-cellular localisation, TG-2 proteins in different locations had different functions; for example cell surface TG-2 had different functions from intracellular TG-2 [60, 61]. These were previously studied using non-ocular cell types such as neuroblastoma cells [135], human and mouse fibroblasts [141], Swiss 3T3 murine fibroblasts and primary vascular endothelial cells [61]. In this study, proteins binding to TG-2 had different protein concentrations and were present in different cell fractions. TG-2 was predominantly present in the lower density sucrose fractions (SF) as immunoreactivity against TG-2 was found in 8.5%, 10%, 15% and 20% fractions. This suggested that TG-2 may have a role in protein trafficking in these SFs.

TG-2 binding proteins were categorised into 3 groups according to the way TG-2 status affected the protein distribution. Group 1 had lower expression of binding proteins in shTG compared to control in all or specific SFs. This group consisted of Desmin (DES), presenilin associated, rhomboid-like protein (PARL), neurotrophic tyrosine kinase, receptor, type 3 (NTRK3) and serine protease (PRSS3). Group 2 included two members: integrin β4 protein (ITGB4) and Golgi associated protein, golgin-A2 (GOLGA2). Binding proteins that fell in this group had lower expression in shTG cells in one SF, but showed a reversal trend in other SFs. Group 3 was made up of Syntaxin binding protein (STXBP2), which expressed similar concentration in both control and shTG cells in all the four SF. Recycling endosomes, endoplasmic reticulum, and mitochondria were found in specific SFs. Meanwhile, early endosomes, late endosomes, secretory vesicles and lysosomes were present in all the SFs tested.

The current study differs from previous literatures, all of which examined sub-cellular trafficking and cell adhesion, in the use of high-speed centricollation to fractionate cell lysates. There are few or no reports that employ this relatively new centricollation technology to study sub-cellular trafficking. Instead, most studies had chosen to use ultracentifugation as a tool for protein isolation to evaluate sub-cellular trafficking in various cell types [142, 143]. These studies predominantly evaluated the sub-cellular localisation of specific proteins but did not study in the context of cell motility processes or wound healing.

This work shares some similarities with a study by Zemskov *et al* whereby they investigated TG-2-regulated trafficking of low-density lipoprotein receptor-related protein 1 (LRP1) from cell surface to inside of the cells and other sub-cellular compartments using methods similar to this current study [141]. Similar to this work, Zemskov's study used fractionation to analyse the membrane distribution of various proteins. Unlike the current study that first carried out gross fractionations over a wider range of SFs (8.5% - 40%), followed by greater resolution at finer range from 8.5%, 10%, 15% to 20% SFs, Zemskov's study only included SFs at 5%, 35% and 45%. In addition, instead of centricollation, fractionation by ultracentrifugation was performed in Zemskov's study. Both studies had evaluated a wide range of organelles, except that there was no systemic characterisation of the SFs in Zemskov *et al'*s report. Apart from the distribution of LRP1, Zemskov *et al* did not examine how TG-2 affected the trafficking of other proteins; whereas in the current study, TG-2 binding proteins were identified and their relative distribution between cellular compartments were reported.

The localisation of late endosomes and lysosomes using RAB7 and LAMP1 respectively was consistent with published literature [144]. In the current study, RAB7 was detected in 8.5% and 10% SFs; while de Araujo *et al* detected RAB7 in 6-11% SFs. LAMP1 was detected in 8.5%, 10%, and 20% SFs in this study; while it was detected in 6-16% SFs in de Araujo *et al*'s data.

3.9.1 Possible Roles of TG-2 Binding Proteins

A group of TG-2 interacting proteins which may have important roles in wound healing response was discovered in the current study. The possible roles of these seven TG-2 interacting proteins are discussed below.

The binding of integrin β4 (ITGB4) with plectin was shown to be important for the formation and stability of hemidesmosomes (HDs) [145-147]. With the formation of β4-plectin complex, HDs could mediate the adhesion of epithelial cell to the underlying basement membrane [145]. The removal of integrin β4 genes in mice resulted in the lack of hemidesmosomes, causing the fragile attachment of the tissue to the basal lamina [146]. The loss of integrin β4 was not compensated by the other integrins in the tissues. Hence, patients expressing a null mutated integrin β4 suffered from epidermal blistering due to poor epidermis adhesion to the basement membrane [148]. Apart from its structural adhesive role, integrin β4 also acted as a signalling component involved in cell migration [149-151]. Joly *et al* reported that integrin β4 interacted with Laminin-5 and

influenced epithelial cell adhesion, signalling and migration properties [151]. Another study showed that the phosphorylation of integrin β4 at specific site was important for HD disassembly at the trailing edge of cells during cell migration [150]. Pullar *et al* demonstrated that integrin β4 could coordinate with epidermal growth factor to initiate and maintain cathodal migration, with Rac1 as a common downstream target [149]. From these findings, it is evident that integrin β4 may have a crucial role in cell adhesion and migration possibly in wound healing as well.

Desmin (DES) is a type III intermediate filament that may have an important role in strengthening and maintaining the integrity of the myofibroblasts and the corneal stroma [152]. Injury in the cornea was reported to increase the desmin expression in the stromal cells, which then enhanced the stromal strength and helped in the contraction of the wound in incisional injuries [152]. Capetanaki *et al* reported that skeletal muscle cells in desmin null mice had poor cell adhesion and showed increased intercellular space [153]. Another study showed that desmin could bind to alpha-crystallin, a heat-shock protein, in the leading edge of the migrating lens epithelial cells [154]. Hence, desmin may play an important role in cell adhesion and migration, which is essential in wound healing and to maintain normal cell metabolism.

Golgin subfamily A member 2 (GOLGA2) is a cis-Golgi matrix protein that plays an important role in the stacking of Golgi cisternae, maintenance of Golgi structure and glycosylation. GOLGA2 was reported to be involved in subcellular vesicle trafficking of proteins to various cellular compartments [155, 156]. Cordell *et al* implicated that

GOLGA2 and its binding protein were involved in the delivery of non-classically secreted proteins to the plasma membrane [157]. Another study by Diao *et al* reported that knocking down GOLGA2 significantly inhibited the transport from endoplasmic reticulum to golgi [158]. They suggested that GOLGA2 was involved in membrane tethering at the endoplasmic reticulum to the Golgi intermediate compartment and cis-Golgi [158]. Meanwhile, Kodani *et al* found that GOLGA2 regulated centrosome organization and function through the Rho GTPase Cdc42 and Tuba [159]. During cell migration, Cdc42 would control polarisation at the leading edge of the cell and the re-orientation of the Golgi apparatus. These evidences suggested that GOLGA2 was involved in protein trafficking and may have an important role in cell migration.

Protein serine 3 or mesotrypsin (PRSS3) is an enigmatic trypsin isoform resistant to natural trypsin inhibitors and was reported to be involved in the metastasis of various cancer cells [160-162]. A study in early-stage non-small lung cancer cells found that overexpression of PRSS3 significantly increased transendothelial migration and a similar phenomenon in pancreatic cancer cells showed increased proliferation, invasion and metastasis, suggesting a potential role for mesotrypsin in metastasis [160, 163]. Another paper by Hockla *et al* reported that up-regulation of PRSS3 in breast cancer cells increased malignant tumour growth [161]. They also suggested that mesotrypsin could act through proteolysis of extracellular or cell surface targets to promote malignant growth [161]. Since proteolysis of extracellular matrix is known to be essential for cell movement and migration, hence mesotrypsin may play an important role in cell migration.

Neutrotrophic tyrosine kinase, receptor, type 3 protein (NTRK3) is a cell surface receptor responsible for the proliferation and differentiation of neurally derived cells. Studies by Yamauchi *et al* reported that NTRK3 could enhance the migration of premyelinating Schwann cells via activation of Rho GTPases Rac1 and Cdc42 as well as the downstream c-Jun N Terminal kinase cascade (JNK) [164, 165]. The ability of NTRK3 to regulate cell motility through Rho GTPase pathways suggests that its interaction with TG-2 may enhance the cell migratory response.

Presenilin-associated rhomboid-like protein (PARL) is a mitochondrial resident rhomboid serine protease which encodes mitochondrial integral membrane proteins. PARL knock-out mice would have impaired mitochondrial cristae junctional sealing and woulddie postnatally due to massive apoptosis [166]. Currently no literature has directly related the function of PARL to cell adhesion and migration. Mitochondrial fission and fusion events were linked to T lymphocytes polarisation and movements as well as to cancer cell migration and invasion [167]. Since PARL is involved in mitochondria expression, PARL may indirectly influence cell migration and adhesion through mitochondria and other mitochondrial interacting proteins.

Syntaxin binding protein 2 (STXBP2, also known as MUNC18-2) is important for regulating intracellular granule trafficking. STXBP2 was also reported to control the assembly of SNARE complex [168, 169]. Skalski *et al* have reported that inhibition of SNARE mediated trafficking pathway affected cell spreading and cell adhesion [170,

171]. Hence, the interaction between STXBP2 and TG-2 may influence cell spreading and adhesion.

3.9.2 Proposed Hypothesis

The following hypotheses on the role of TG-2 and the trafficking of its interacting proteins are proposed based on existing literatures and known protein functions: Group 1 proteins consisted of DES, PARL, NTRK3, and PRSS3; these had higher protein expression in control compared to shTG. In this case, TG-2 is proposed to either act as an adaptor protein, or as an upstream regulator for the transcription of interacting protein. TG-2 acting as an adaptor protein may bind and sequester its interacting protein in particular cellular compartments. Hence, TG-2 deficiency may cause non-differential accumulation of interacting partners in other cell compartments. TG-2 was reported to act as an adaptor protein for β1 and β3 integrins in subcellular compartments [29]. Alternatively, TG-2 may also act as an upstream regulator that modulated the transcription of the binding proteins. The increase in TG-2 expression would therefore increase the interacting protein expression in all the cell compartments.

Group 2 members GOLGA2 and ITGB4 showed a reversal pattern of protein expression from 8.5% to 10% SFs between control and shTG. In the 8.5% SF, an accumulation of TG-2 interacting proteins were observed in shTG, but not in the 10% and higher SFs. On the contrary, the control cells showed a higher protein expression in the 10% SF. TG-2 is proposed to act as a carrier protein which can translocate GOLGA2 and ITGB4 from one

compartment (8.5% SF) to another cellular compartment (10% and higher SFs). Hence, deficiency in TG-2 may hinder the removal of its interacting proteins from 8.5% SF causing an accumulation in that compartment. It was reported that fibronectin could act as a carrier protein for extracellular TG-2 [64]. Thus, it would not be surprising if intracellular TG-2 exhibits a similar type of relationship with its ligands.

Subcellular TG-2 status most likely did not affect the trafficking of group 3 proteins. This was because similar immunoreactivities were observed against STXBP2 between control and shTG cells in all tested SFs, suggesting that STXBP2 was probably unaffected by TG-2 concentration. In Chapter 4 of this thesis, TG-2 was found to regulate wound closure rate. In combination with the current findings, TG-2 is hypothesised to affect wound healing via trafficking of crucial molecules essential for cell migration and adhesion.

3.10 Conclusion

The current study employed a novel density based protein separation technique known as centricollation to elucidate the biological function of specific molecules; it is particularly powerful when combined with traditional cell biology techniques. This was not done before and hence, this current study may provide an idea of how to fully utilise this technology in the future. In this study, centricollation was used to explore the sub-cellular localisation of TG-2 and its interacting partners. TG-2 was found to be involved in the trafficking of sub-cellular proteins which may regulate the biological and cellular functions relevant to wound healing processes. The current study provided an insight on TG-2's mechanism, its trafficking pathway and associated ligands. This may help in the future development of therapies for corneal epithelial wound healing.

Key Findings

a. Seven proteins that interacted with different TG-2 fragments were identified.

b. TG-2 binding proteins were categorized into 3 groups according to the way TG-2 status affected the protein distribution.

c. TG-2 status could affect some of the sub-cellular concentrations of its binding proteins such as DES, PARL, NTRK3, PRSS3, ITGB4 and GOLGA2; and organelles such as recycling endosomes, endoplasmic reticulum, and mitochondria.

CHAPTER 4. TRANSGLUTAMINASE-2 IN CORNEAL EPITHELIAL MIGRATION AND ADHESION

4.1 TG-2 in Cell Adhesion and Migration

It was recently reported in literature that cell adhesion and migration may be affected by the involvement of cell surface TG-2 in cell-matrix interactions [36, 65]. Gentile *et al* first showed that overexpression of TG-2 increased fibroblast cell adhesion to the substratum, together with increased resistance to trypsin detachment [44]. Gaudry *et al* confirmed the involvement of cell surface TG-2 in cell adhesion by reporting that cell adhesion points had higher concentrations of TG-2 [172]. Endothelial cells with reduced expression of TG-2 were shown to decrease cell adhesion, spreading and stabilisation of melanoma adhesion under laminar flow [173, 174]. In addition, TG-$2^{-/-}$ mouse embryonic fibroblasts were reported to migrate slower compared to the fibroblasts derived from wild-type mice [82]. A similar observation was reported in human retinal pigment epithelial (RPE) cells whereby the blocking of TG-2 reduced cell adhesion and migration [175].

The *in vivo* wound healing experiment previously done by our laboratory reported that mice with homozygous TG-2 deletion (TG-$2^{-/-}$) showed delayed corneal wound closure in contrast to their wild type (TG-$2^{+/+}$) counterparts (Figure 4.1A). From day 3 onwards, the remaining unclosed epithelial defects were significantly different ($p< 0.05$) (Figure 4.1B). Immunofluorescence staining showed that TG-2 was present in the corneal epithelial

layers and basement membrane of TG-$2^{+/+}$ mice, but absent in the TG-$2^{-/-}$ mice (Figure 4.1C).

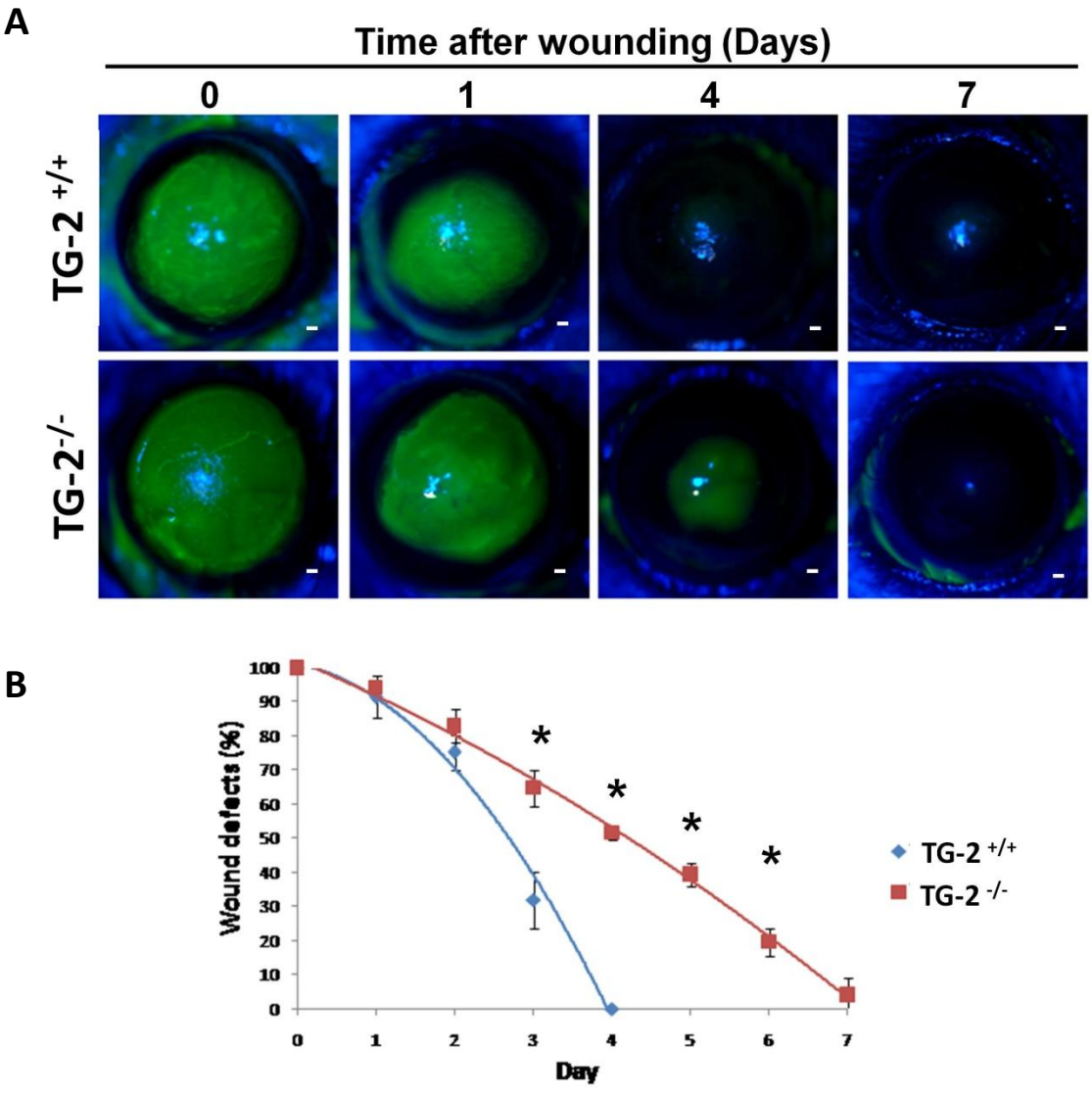

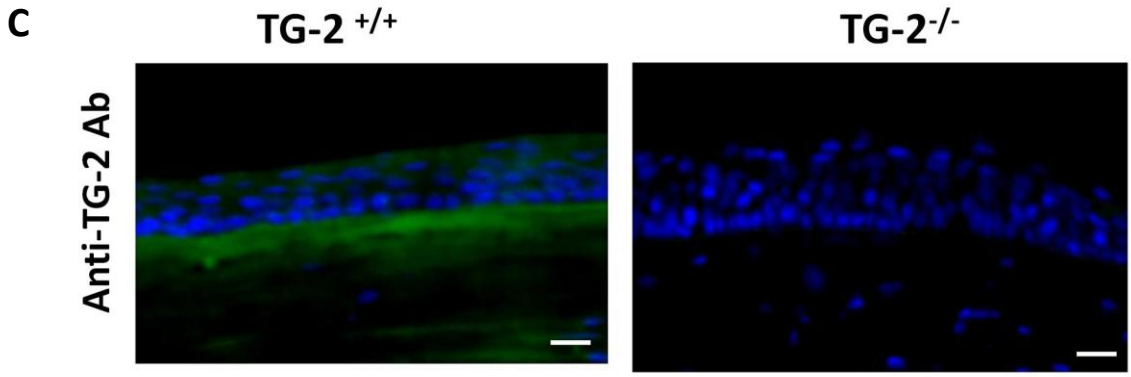

Figure 4.1. The corneal epithelial layers and the basement membrane of homozygous transglutaminase (TG)-2 deleted (TG-$2^{-/-}$) mice showed delayed corneal wound closure compared to wild type (TG-$2^{+/+}$) mice. (A) Representative microscopy images showing corneal epithelial wound stained with topical fluorescein dye (green) after the corneal epithelium was removed from the TG-$2^{+/+}$ and TG-$2^{-/-}$ mice. Scale bar = 100 μm. (B) Line graph showing the percentages of unclosed wound (vertical axis) over time (horizontal axis) in TG-$2^{+/+}$ and TG-$2^{-/-}$mice, 5 mice were used for each genotype and 3 independent experiments were done. *: $p < 0.05$. (C) Picture showing immunofluorescence staining of the central cornea without defect in TG-$2^{+/+}$ and TG-$2^{-/-}$ mouse. Primary antibody against TG-2, FITC conjugated secondary antibody (green) and DAPI nuclear counterstaining (blue) were used. Scale bar = 50 μm.

4.2 Hypothesis and Specific Aims

Since TG-2 is ubiquitously present in human corneal epithelium and TG-2 is known to be related to cell surface integrins and matrix proteins, we hypothesised that TG-2 affects wound healing processes through cell adhesion, migration and interaction with focal adhesion proteins.

Specific Aims

To study the functional significance of TG-2 on cell adhesion and migration in corneal epithelial wound closure.

a. To investigate the role of TG-2 in cell migration, adhesion and proliferation using *in vitro* techniques such as cell scratching assay, cell migration assay, immunofluorescence staining and trypsinisation assay.
b. To evaluate the possible interaction of TG-2 and focal adhesion proteins in cultured human corneal epithelial cells by performing western blot against focal adhesion proteins.
c. To determine if TG-2 affects paxillin incorporation in adhesion complexes by checking its *in vitro* kinase activity.
d. To check the effects of TG-2 on JNK through co-immunoprecipitation and western blotting.

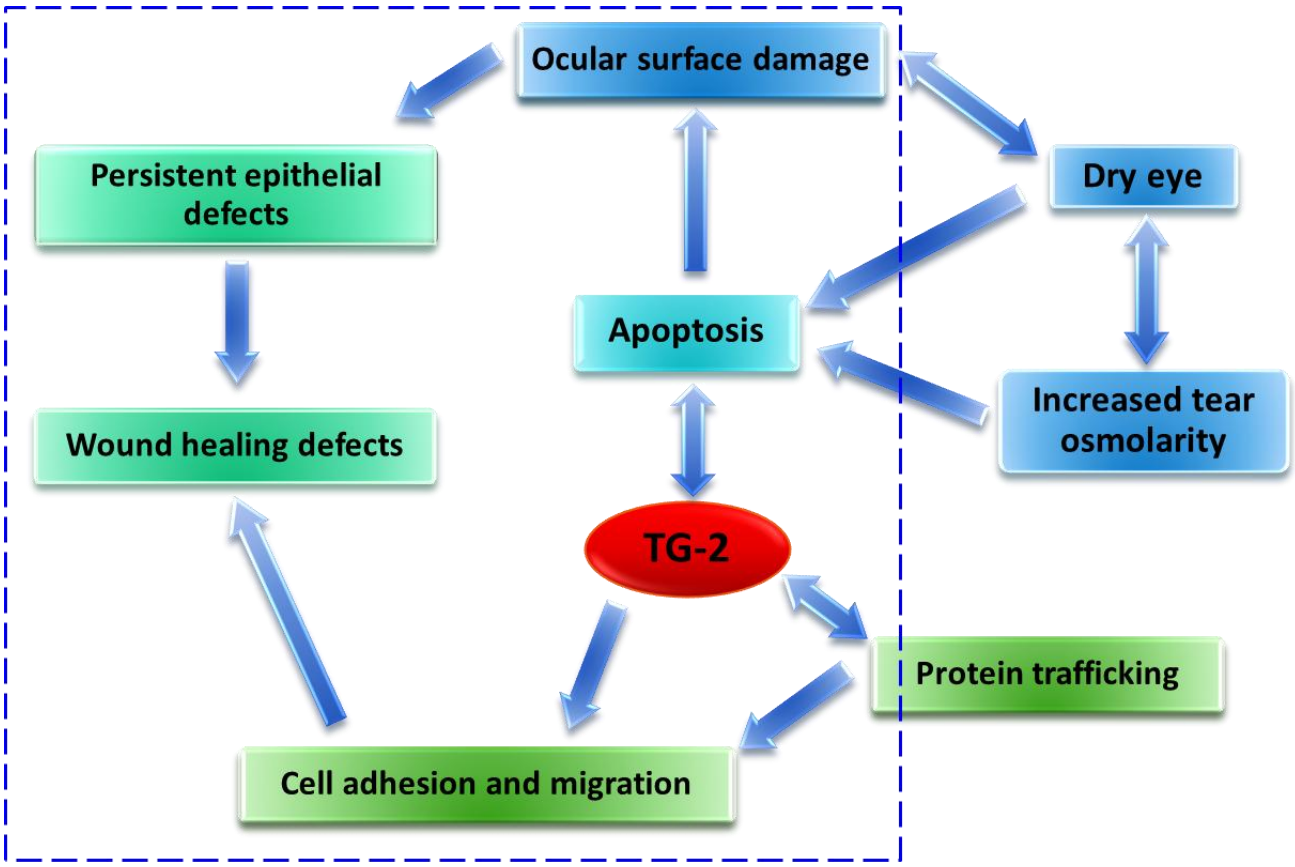

Figure 4.2. Schematic showing the focus of this chapter, as depicted by the blue square. The main objective of this chapter is to elucidate the role of TG-2 in wound healing.

4.3 Methodology

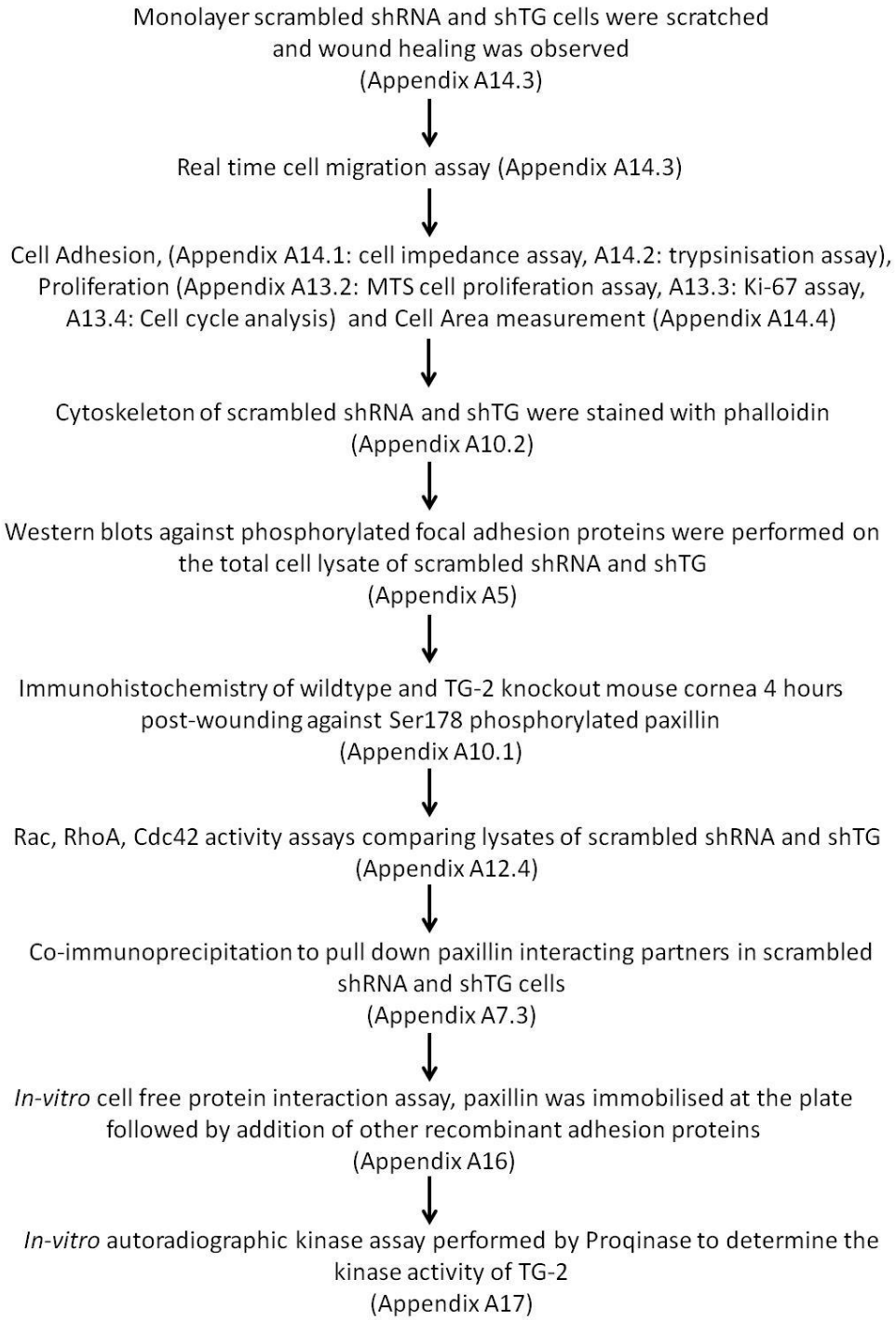

Methodology Flow Chart 4. Flow chart showing general methodology to study the role of TG-2 on cornea epithelial wound healing and relevant wound healing processes consist of cell adhesion, spreading and migration. The detailed protocol for each technique is described in the Appendix.

4.4 Delayed Wound Closure in TG-2 Deficient Cells

As mentioned in Figure 4.1, our *in vivo* mouse cornea wound healing experiment showed that TG-2 knockout mice had slower wound closure compared to their wild type counterparts. The same phenomenon was observed in *in vitro* scratch test assay using immortalised human corneal epithelial cells. The closure of a uniformly scratched wound took 12 hours in control shRNA cells, whereas the wound closure was delayed and not evident in shTG cells after 48 hours (Figure 4.3). Since TG-2 could interact with extracellular matrix fibronectin during cell adhesion and migration [65], the experiment was performed on both uncoated and fibronectin-coated surfaces (fibronectin coating methods at Appendix A3.3). The result was independent of the presence of the fibronectin coating on the culture vessel. This was because control cells always closed their scratched wounds more rapidly than the shTG cells regardless of the presence of fibronectin (Figure 4.3B). From 6 hours post scratching onwards, there were significant differences in the width of the residual wound between shTG and control cells ($p < 0.05$) (Figure 4.3B).

Statistical analysis (General Linear Model, Appendix A18) was performed from 2 to 14 hours after scratching. The analysis reported that the 'within subject' factor (time) was significant ($p < 0.001$) whereas the TG-2 status and fibronectin coating were significant for the 'between subject' factors ($p < 0.001$). Upon post-hoc analysis, the wound in control cells grown on fibronectin coated surfaces closed significantly faster than shTG cells, regardless of whether shTG cells were grown on fibronectin coated ($p = 0.001$) or uncoated surfaces ($p = 0.005$). On the other hand, on uncoated surfaces, the wound of

control cells closed faster than shTG cells, again regardless of whether shTG cells were grown on fibronectin coated ($p = 0.001$) or uncoated surfaces ($p = 0.004$). There was no significant difference in wound width between shTG cells grown on plates with or without the coating of fibronectin ($p = 0.885$). Hence, fibronectin coating did not affect the closure of the wound in shTG cells.

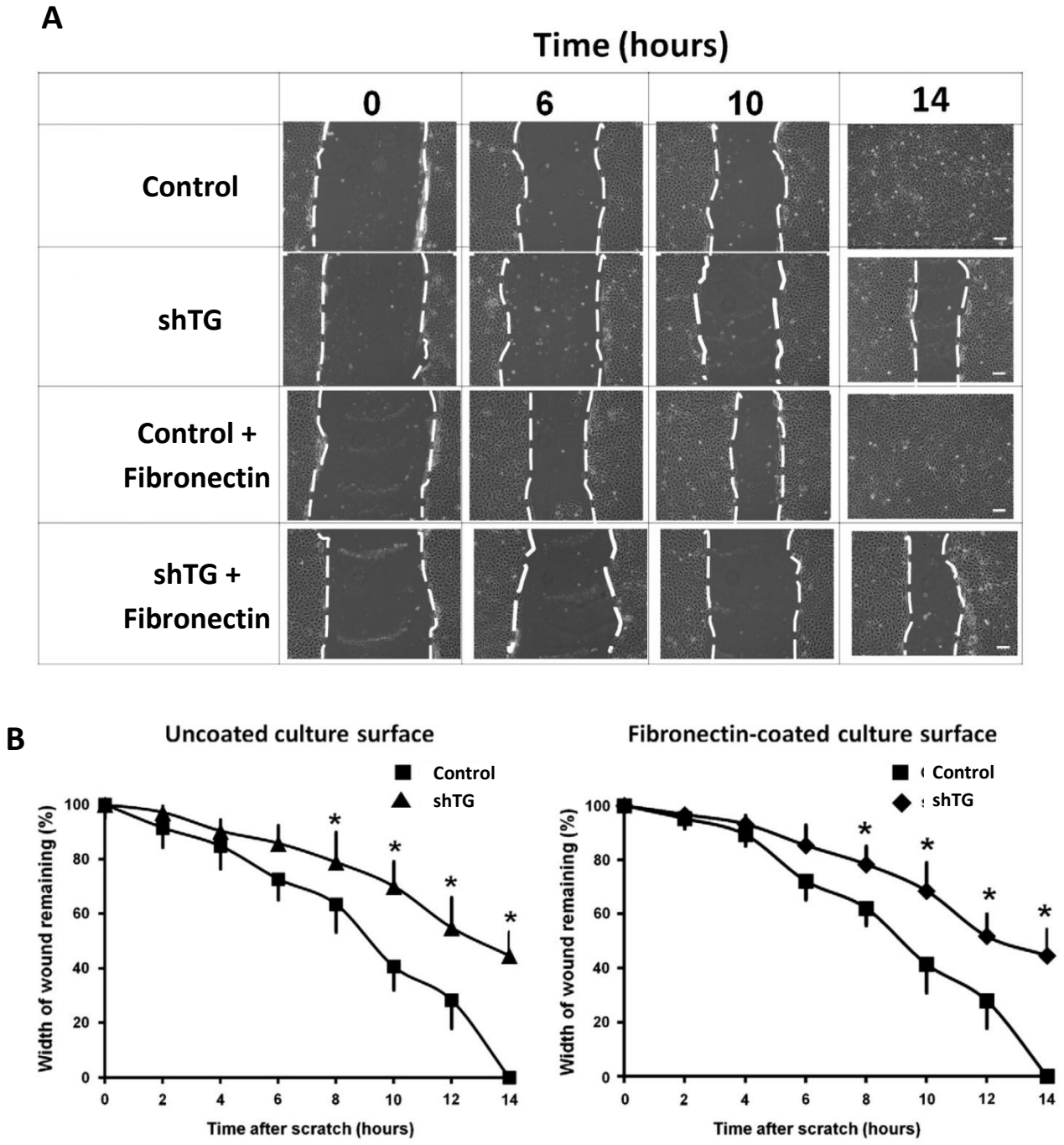

Figure 4.3. TG-2 knockdown in human corneal epithelial cells caused delayed wound closure. (A) Phase contrast microscopy images at different time points. A uniform width scratched strip was created on confluent layer of control or shTG cells. The cells were grown on either uncoated or fibronectin-coated surfaces. Scale bar = 50 μm. (B) Line graph showing the percentages of defect remaining (vertical axis) over time post-scratching (horizontal axis) in control and shTG cells, n = 6 independent experiments. *: $p < 0.05$

4.5 *In vitro* Study of TG-2 Deficiency in Cell Migration and Adhesion

4.5.1 TG-2 Deficiency Reduced Cell Migration Speed

A 2-D *in vitro* cell migration assay was performed to study whether the speed of cell migration at the wound edge affected the duration of wound closure. Fifty random cells were selected at the advancing edge and their centroids were recorded at 10 minute intervals for around 16 hours with time-lapse microscopy (Figure 4.4A). On uncoated culture surfaces, control shRNA cells migrated at significantly higher speed ($p < 0.0001$) (uncoated: 0.42 ± 0.05 μm/min) compared to shTG cells (uncoated: 0.31 ± 0.03 μm/min); with the migration speed difference of 0.11 μm/min (Figure 4.4B, top). Similarly, control shRNA cells also migrated faster on fibronectin-coated plates, with 0.12 μm/min difference of migration speed between control (0.66 ± 0.05 μm/min) and shTG cells (0.54 ± 0.05 μm/min) (Figure 4.4B, bottom).

Statistical analysis with dependent variable consisting of cell speed at different time period showed that the 'between subject' factors (fibronectin status, TG-2 status) were significant ($p = 0.001$). The significance in the time factor ($p < 0.001$) may indicate the increase in speed for the first 25 time points (first 4 hours) (Figure 4.4C). Post hoc testing showed that control cells migrated faster on fibronectin coated surfaces compared to the other three setups (all $p < 0.001$). On uncoated plates, control cells migrated significantly faster than shTG cells ($p < 0.001$); shTG cells grown on fibronectin coated surfaces migrated faster compared to shTG cells grown on uncoated plates ($p < 0.001$). The cell

migration speed between control cells cultured on uncoated plates and shTG cells grown on fibronectin-coated plates ($p = 1.0$) was no different.

To evaluate whether the reduction in shTG cells' migration speed was due to a delay in the initiation of cell movement, the data was analysed in segments of 6 hours (Figure 4.4C). ShTG cells did not show a delay in the initiation of cell movement in the first hour compared to the control shRNA cells. In the first 6 hours, all four conditions showed an increase in free-space movement, subsequently reaching a more stable level, followed by a decline in velocity. The migration velocity was significantly lower in shTG compared to the control cells ($P < 0.001$), whether on uncoated (Figure 4.4D) or fibronectin-coated polystyrene surfaces (Figure 4.4E). This trend continued for the next 6 hours, but in later phases (>12 hours).

Using in-house developed software, the effects of TG-2 on cell directionality was evaluated (Method see Appendix A18.3). The data was analysed in segments of 4 hours. For every segment, shTG cells had higher population of cells at higher oscillation mean range compared to the control cells. By measuring the lateral deviation of individual cells during migration, shTG cells showed higher amplitude of cell movement, suggesting some loss of precise directionality (Figure 4.5).

A

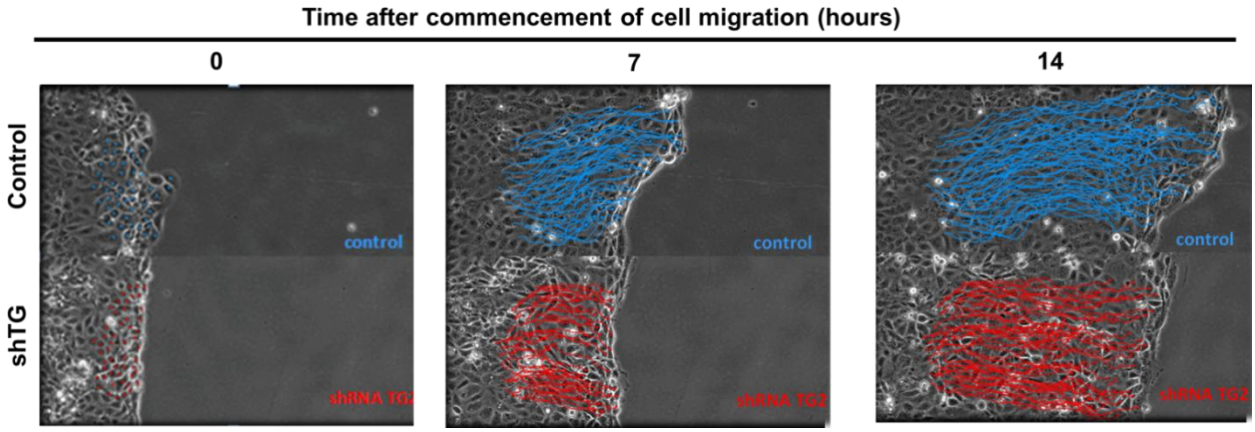

B **Polystyrene surface with no fibronectin coating**

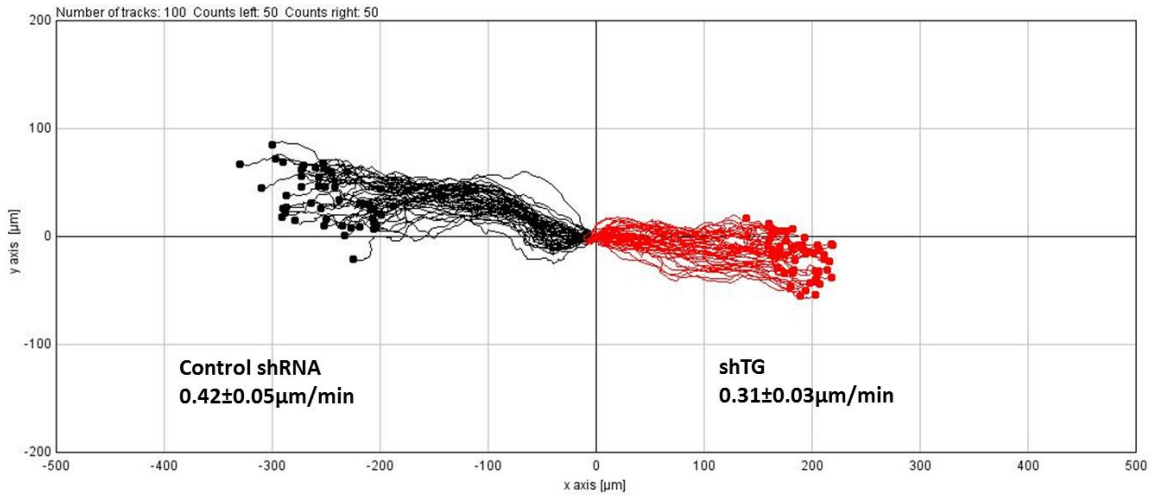

Polystyrene surface with fibronectin coating

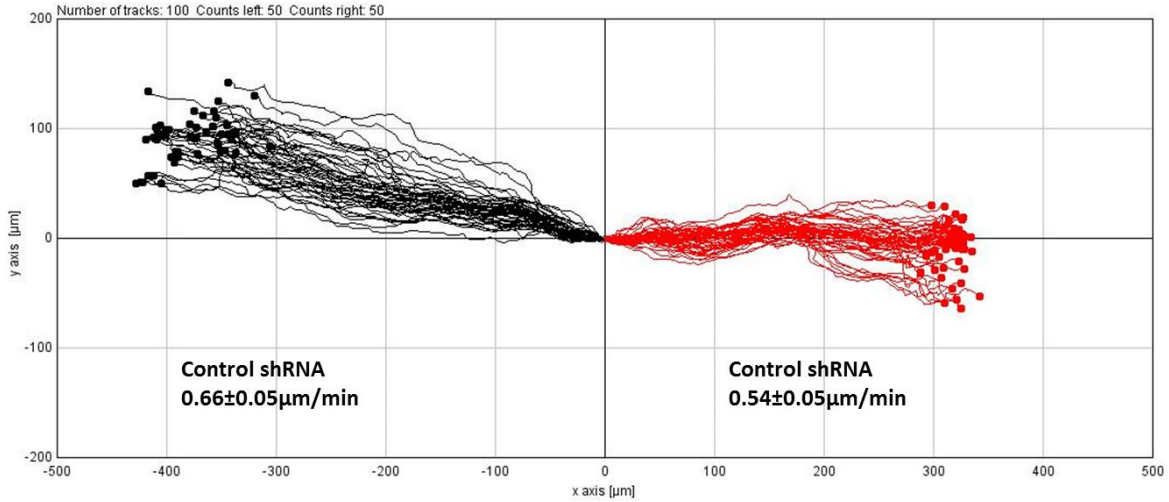

C

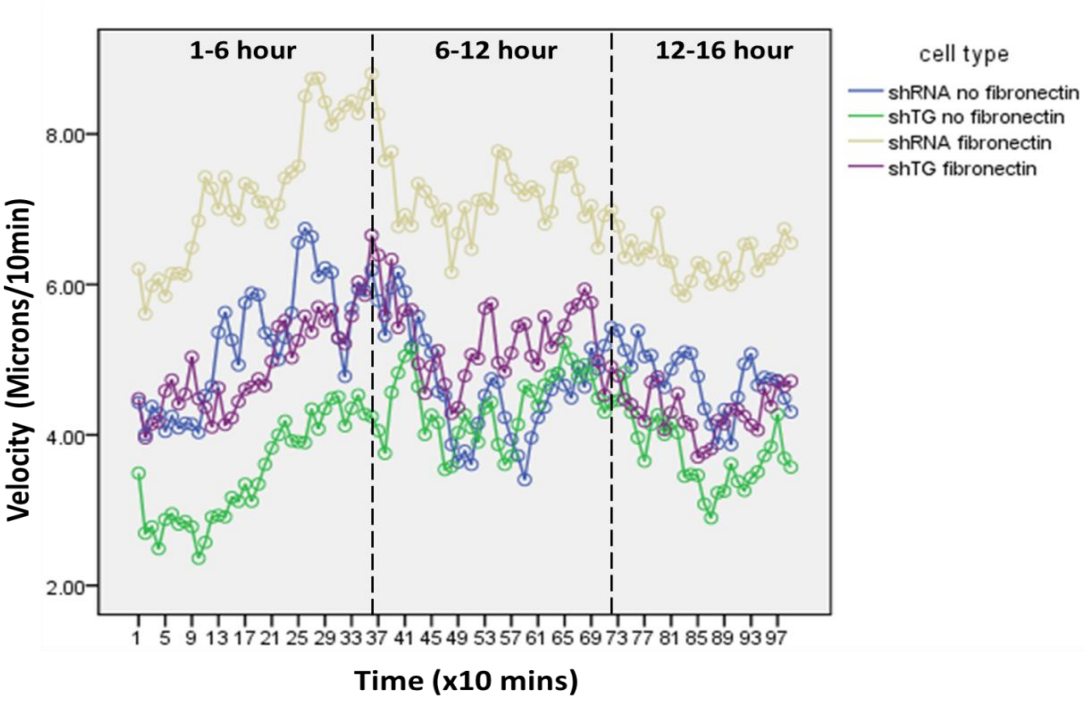
1-6 hour
6-12 hour
12-16 hour
cell type
shRNA no fibronectin
shTG no fibronectin
shRNA fibronectin
shTG fibronectin
Velocity (Microns/10min)
8.00
6.00
4.00
2.00
1 5 9 13 17 21 25 29 33 37 41 45 49 53 57 61 65 69 73 77 81 85 89 93 97
Time (x10 mins)

D

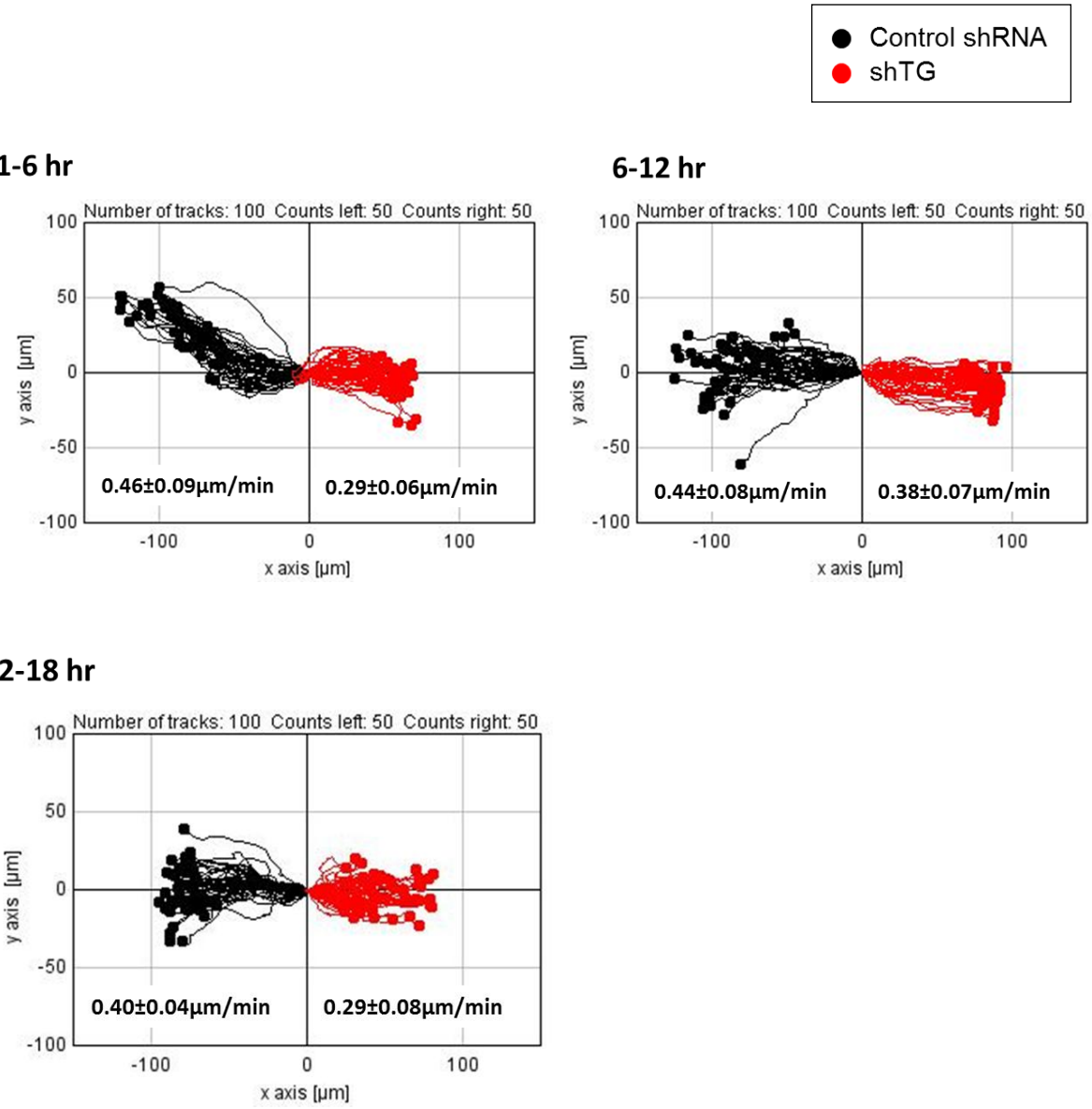

E

		1-6hr		6-12hr		12-18hr	
		shRNA	shTG	shRNA	shTG	shRNA	shTG
Velocity of cells (µm/min)	Uncoated	0.46±0.09	0.29±0.06	0.44±0.08	0.38±0.07	0.40±0.04	0.29±0.08
	Fib coated	0.70±0.04	0.55±0.08	0.69±0.07	0.58±0.04	0.58±0.06	0.44±0.06

Figure 4.4. Figures showed results of non-traumatic cell migration assay. Fifty adjacent cells were randomly selected at the advancing edge of the confluent cell sheet. Migration of cells was recorded every 10 min over 16 hours using live cell time-lapse microscopy. The centroid positions of the cells, consisting of either scrambled shRNA (control) or shTG cells, were tracked using ImageJ software. (A) Phase contrast microscopy images at 0, 7 and 14 hours after removal of culture cylinder. Blue and red lines represented the migratory tracks of the cells. Scale bar = 50 μm. (B) Line plots showing cell migration and mean velocity of 50 adjacent cells randomly selected at the advancing edge for each condition, whereby the initial cell positions were normalised to the plot origin. Top: Cell migration using cells cultured on polystyrene surface without fibronectin coating. Bottom: Cell migration with cells cultured on polystyrene surface coated with human fibronectin. (C) General linear model (GLM) analysis showing the mean velocity of 50 contiguous shRNA or shTG cells on uncoated plates, recorded every 10 minutes over a period of 16 hours. (n = 2 independent experiments). (D) Line plots showing segments of cell migration in period of 6 hours. Mean velocity of each time period was calculated. (E) Table showing the mean velocity of 50 randomly selected control shRNA or shTG cells at the advancing edge for each condition, on either uncoated or fibronectin-coated plates, recorded every 10 minutes and analysed in segments of every 6 hours. Mean velocity of each time period was calculated.

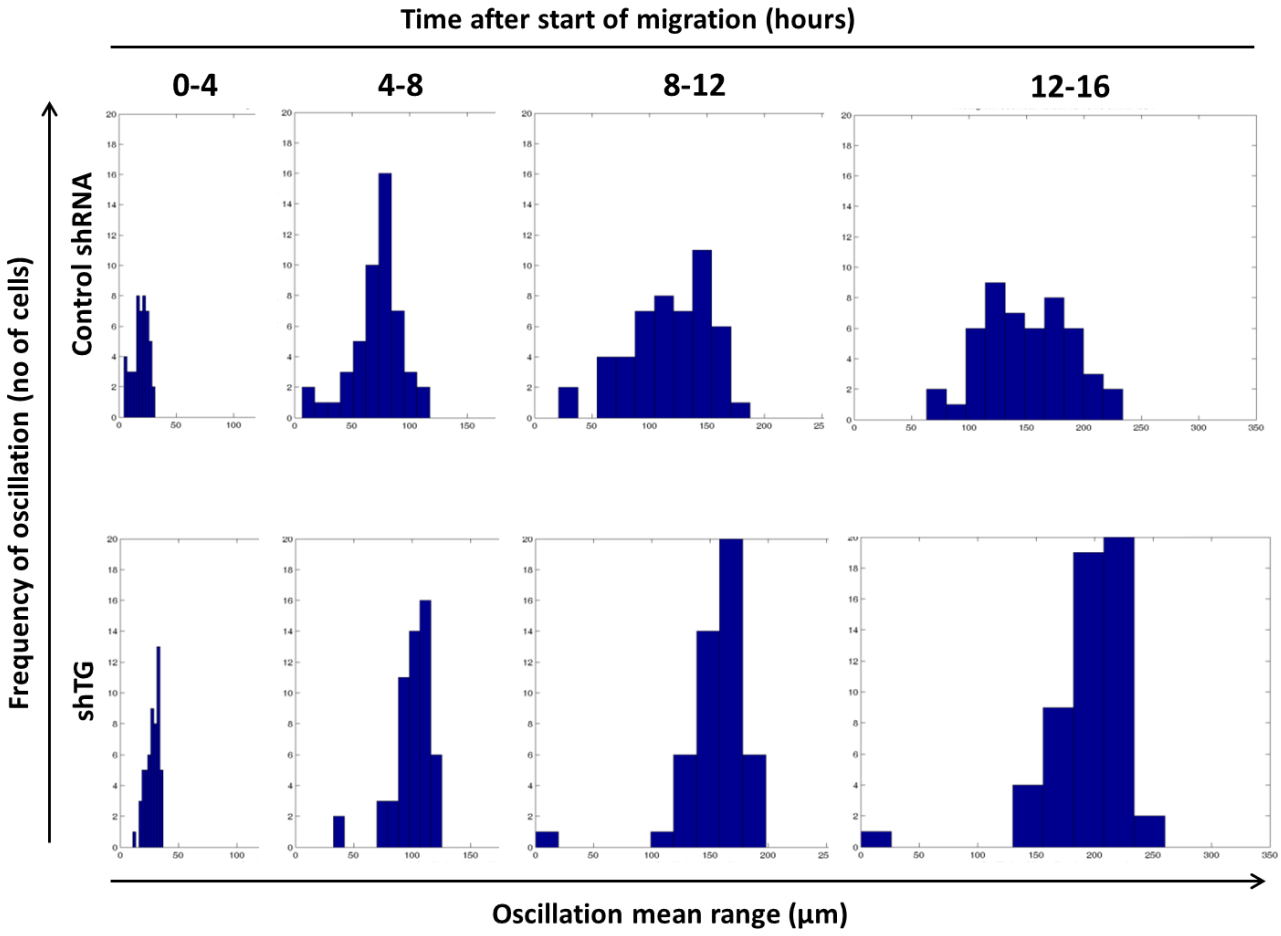

Figure 4.5. Histograms showing the distribution of numbers of cells (y-aixs) against the oscillation of cells in micrometre (x-axis) over time between control shRNA and shTG cells on fibronectin coated surfaces.

4.5.2 TG-2 Deficiency Reduced Cell Adhesion/Spreading

During the *in vitro* scratch test, shTG cells had the tendency to fold back on themselves at the advancing edge, which indicated signs of reduced adherence to the underlying culture surface. By measuring and analysing the change of impedance, cellular behaviors such as cell attachment, proliferation and cellular responses to pharmacological stimuli could be quantified. shTG cells showed significant reduction in cell impedance compared to its control counterpart ($p < 0.001$) from 1 to 6 hours after initial seeding on polystyrene surfaces (Figure 4.6A). Factors that potentially caused the decreased impedance in shTG cells were assessed individually. The MTS cell proliferation assay performed on non-confluent monolayer cells showed no difference in proliferation rate between shTG and control cells (Figure 4.6B). This was supported by steady state cell cycle analysis (Figure 4.6C) which also indicated no difference in proliferation rates between the two cell types. Consistent with the findings, there was a low proportion of Ki-67 positive cells at 6 hours after scratching and there was no significant difference ($p = 0.59$) between shTG [14/581 (95%CI: 0.0136– 0.0415)] and control shRNA [11/368 (95%CI: 0.0156–0.0550)] (Figure 4.6D).

The mean cell area between phalloidin-stained shTG (555 ± 161 μm^2) and control shRNA cells (682 ± 218 μm^2), measured 24 hours after seeding on fibronectin-coated surfaces, was significantly different ($p < 0.0001$) (Figure 4.6E). Interestingly, in the absence of fibronectin coating, there was no significant difference in the cell area between control and shTG cells (Figure 4.6E, Left). There was no significant difference between groups in their nuclei area ($p > 0.05$ ANOVA in Figure 4.6E, Right). Time-lapse microscopy

showed that shTG cells detached faster than control shRNA cells after diluted trypsin was added to the uncoated polystyrene plates (Figure 4.6F).

In summary, the delay of wound closure in shTG cells compared to control may be due to differences in cell adhesion, spreading and/or migration, but was not attributable to cell proliferation.

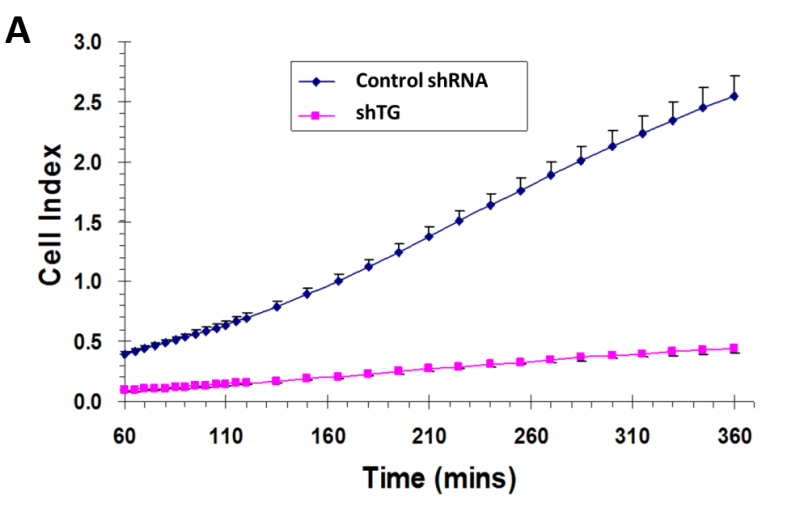

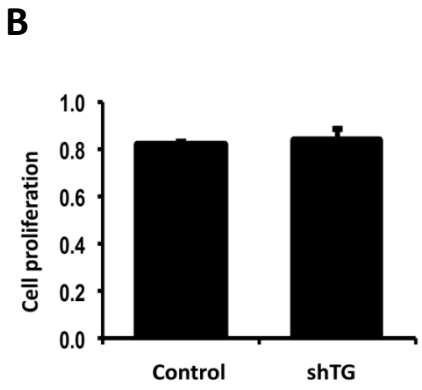

C

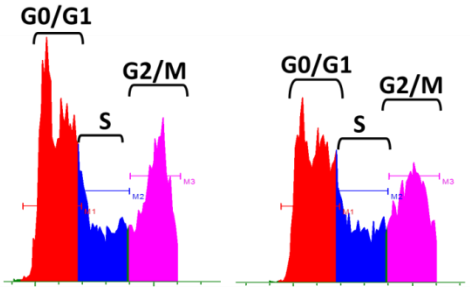

	% of cells in each cell cycle progression stage	
	Control shRNA	shTG
G0/G1	49.5	47.1
S	20.0	21.4
G2/M	30.5	31.5

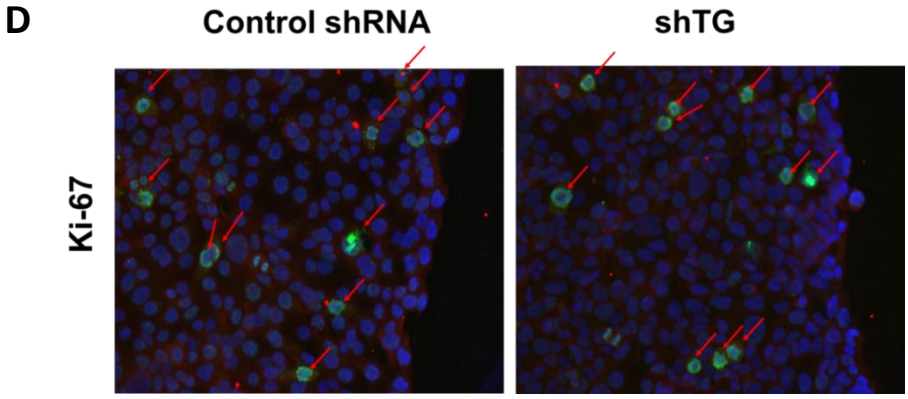

E

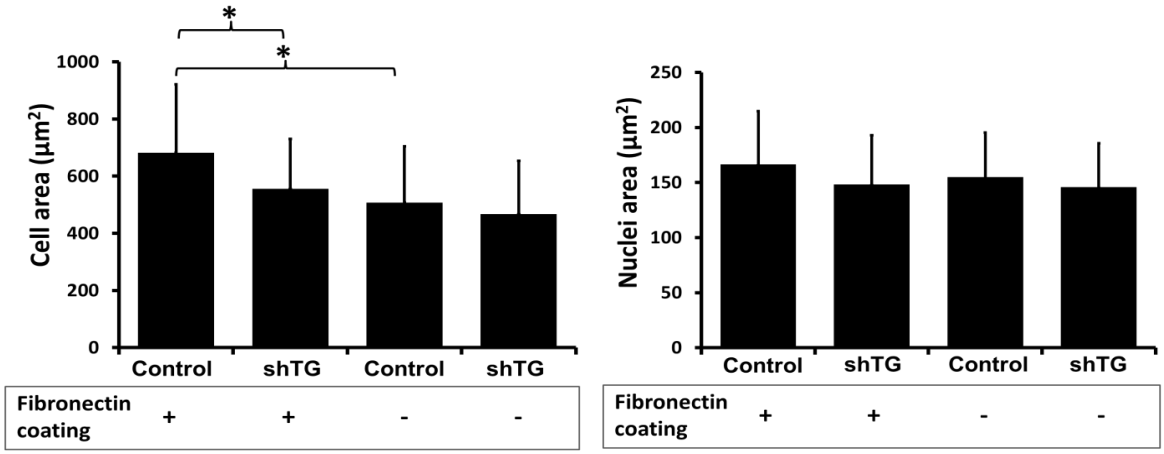
*
*
1000
800
600
400
200
0
Cell area (µm²)
Control
shTG
Control
shTG
Fibronectin coating
+
+
-
-
250
200
150
100
50
0
Nuclei area (µm²)
Control
shTG
Control
shTG
Fibronectin coating
+
+
-
-

F

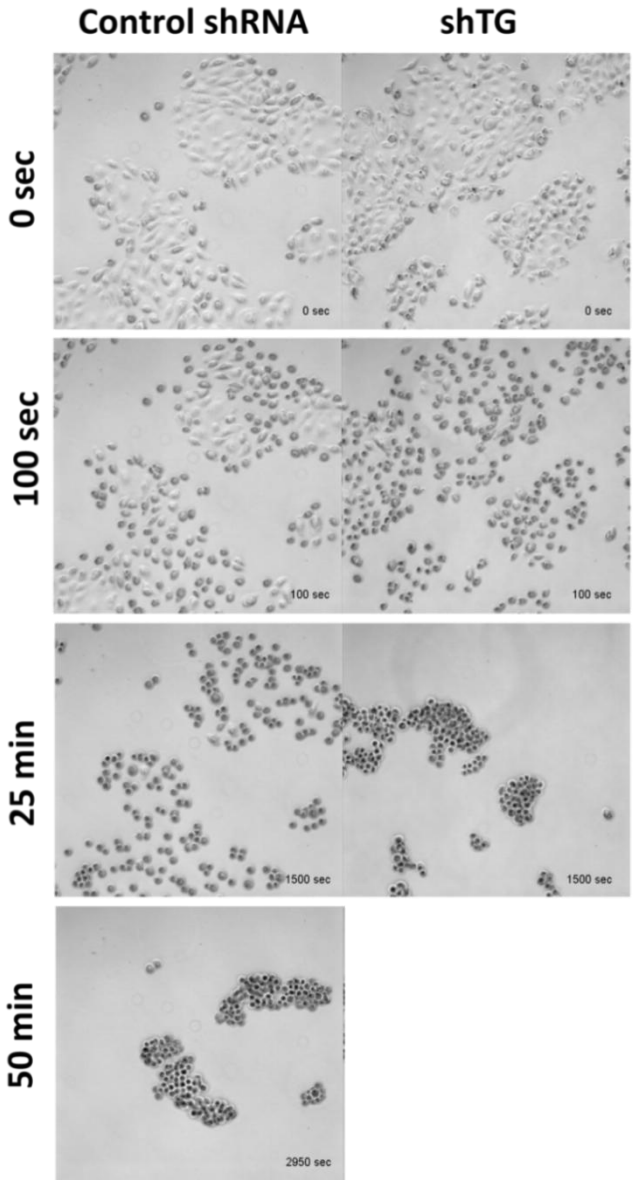
Control shRNA
shTG
0 sec
100 sec
25 min
50 min
0 sec
0 sec
100 sec
100 sec
1500 sec
1500 sec
2950 sec

Figure 4.6. The reduced cell impedance in TG-2 knockdown corneal epithelial cells was due to the decrease in cell adhesion and spreading, but not cell proliferation. (A) Five million each of control shRNA or shTG cells were seeded on polystyrene surfaces in triplicate. Cell impedance value (cell index) was recorded over time. (B) Bar graph showing MTS assay which measured the cell proliferation rate of control shRNA and shTG cells grown on polystyrene surfaces. Y-axis denotes the cell proliferation measured at A490. (C) Cell cycle analysis showed the percentage of cells in G0/G1, S, and G2/M phases in control shRNA and shTG cells. (D) Representative microscopy images of cells stained positively with Ki-67 (green). Control shRNA or shTG cells were seeded on polystyrene surfaces till confluent and a single uniform width scratched wound was administered. Six hours after scratching, cell proliferation (red arrows) was determined by Ki-67 stains. Cell nuclei were counterstained with DAPI (blue). Scale bar = 50 μm. (E) Bar graph showing cell (left) and nuclei (right) area of control shRNA and shTG cells grown on either fibronectin-coated (+) or uncoated (−) polystyrene plates for 24 hours. The areas were calculated by randomly choosing more than 50 adhering cells. N= 3 independent experiments.*: $p < 0.001$. (F) Time-lapse images of control shRNA and shTG cells after addition of diluted 0.005% Trysin-EDTA in PBS at 37°C, 5%CO_2. Imaging was stopped when all cells had detached, which was after 25 minutes for shTG cells, or after 50 minutes for control shRNA cells.

4.6 TG-2 Deficiency Disrupts Actin Cytoskeleton

To evaluate the effects of TG-2 on actin cytoskeleton, filamentous (F)-actin was stained with phalloidin 3 hours after scratching in control shRNA and shTG cells (Figure 4.7). The cortex at the advancing edge and cell-cell junctions of control shRNA cells showed stronger staining of phalloidin compared to shTG cells, indicating condensation of F-actin in the control cells. Also, majority of the control shRNA cells at the advancing edge formed lamellipodia in line with the direction of cell migration. On the other hand, shTG cells exhibited disrupted F-actin pattern. At the advancing edge of shTG cells, the presence of large gaps at the advancing edge showed signs of cells detachment. Also, lamellipodia at the advancing edge seemed to be extended in the direction of the wound and also perpendicularly to the wound (Figure 4.7, right: white arrows).

Rho family of small GTPases such as RhoA, Rac and Cdc42 are known to regulate actin organisation, cell adhesion and migration [176, 177]. The Rho family proteins alternated between an active GTP-bound state and an inactive GDP-bound state and their activation could be quantified by performing G-Lisa activation assays (See methods at Appendix A12.4). The status of TG-2 in the cells did not affect the level of RhoA; whereas shTG cells showed significant reduction in activation of Rac and Cdc42 compared to control cells ($P < 0.05$) (Figure 4.7B).

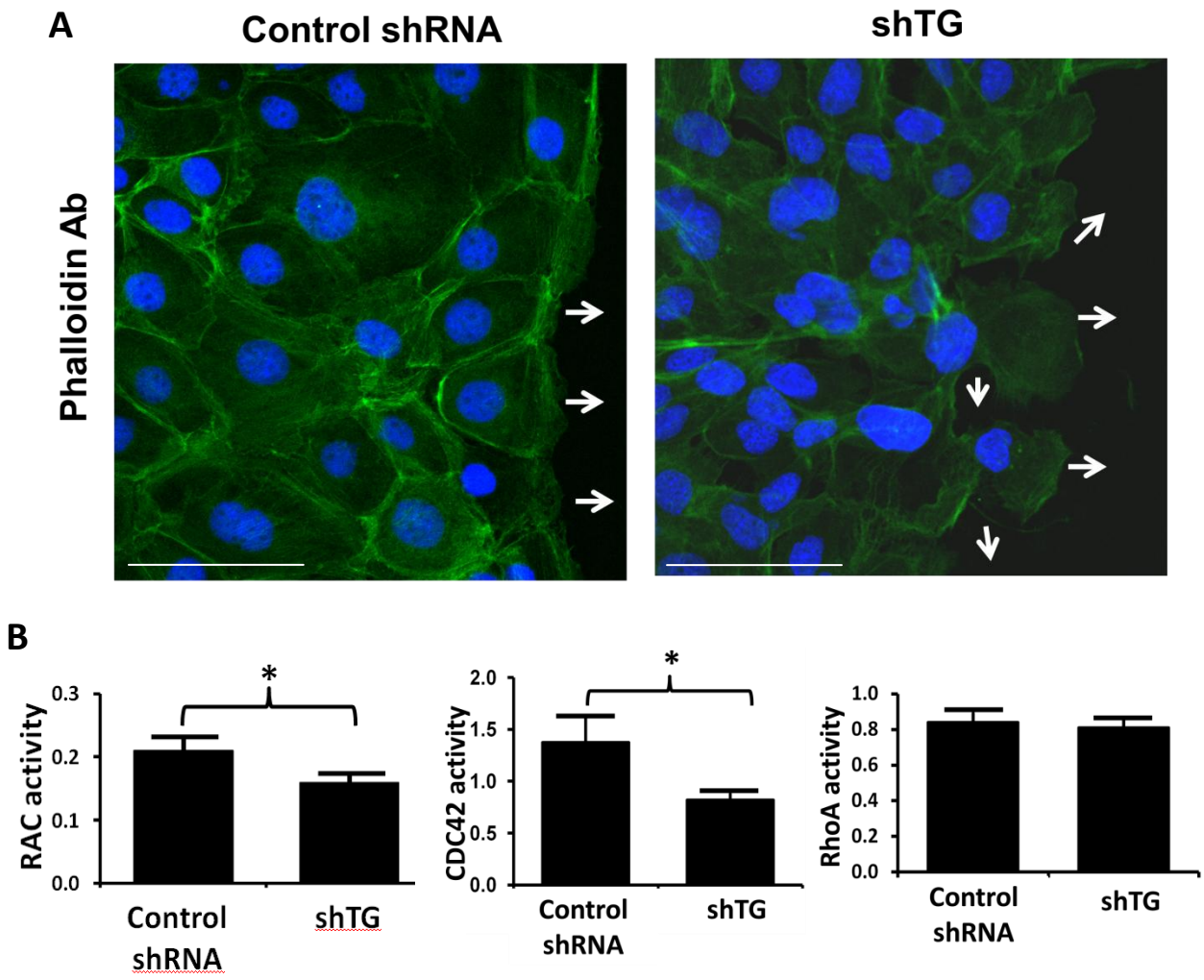

Figure 4.7. Figures showing FITC-conjugated phalloidin staining and Rac, Cdc42, RhoA activation assays in control shRNA and shTG cells. (A) Representative images of FITC-conjugated phalloidin staining (green) in control shRNA and shTG cells on uncoated polystyrene surfaces, 3 hours after *in vitro* scratching. Blue staining indicated nuclei stained with DAPI. White arrows show the directions of lamellipodia. Scale bar = 50 μm. (B) Activation assays for RAC (left), Cdc42 (middle) and RhoA (right). Subconfluent control shRNA and shTG cells were lysed and activation assays were performed. Absorbance was read at 490nm. Three independent experiments were performed. Height of bars = mean of fluorescence, error bars = standard deviation, *: $p < 0.05$.

4.7 Interaction and Effects of TG-2 with Focal Adhesion Proteins

4.7.1 TG-2 Deficiency Reduced Phosphorylation of Ser178 Paxillin

Kimura *et al* reported that the phosphorylation of paxillin at Ser178 was important for cell migration in cultured human corneal epithelial cells [101], which were the same type of cells used in this project. They reported that when Ser178 paxillin was replaced with alanine, an amino acid which cannot be phosphorylated, wound closure rate was significantly decreased in human corneal epithelial cells expressing these mutant proteins [101]. Since Kimura *et al* had used the same cell types as this project, would TG-2 have any effect on the phosphorylation of paxillin at Ser178?

To investigate TG-2's role in phosphorylating integrins and focal adhesion complexes in control shRNA or shTG cells, control shRNA and shTG cells were seeded in serum-free medium and incubated overnight to reach a confluency of 60-70% on uncoated polystyrene surfaces (Figure 4.8A-E). To detect the phosphorylation of focal adhesion proteins, western blotting was performed on the lysate of control shRNA and shTG cells using specific antibodies targeting phosphorylated focal adhesion proteins. Total protein of each focal adhesion protein was also probed to show that the change in phosphorylated protein level was not due to the change in the total protein.

Phosphorylation of paxillin at Ser178 was reduced in shTG cells compared to control cells (Figure 4.8A). This observation was consistent with the *in vivo* result in Figure 4.2, which also showed reduced phosphorylated paxillin at Ser178 at the advancing edge of

TG-$2^{-/-}$ mice cornea epithelium 4 hours after abrasion in contrast to wild type TG-2 mice. The amount of TG-2 in the cells did not affect the phosphorylation of β-1 integrin at Ser785 (Figure 4.8B). Some literatures reported that corneal epithelium did not have β-3 integrin [178, 179]. However, β-3 integrin was successfully detected in the cultured corneal epithelial cells as shown in Figure 4.9C. There was a reduction in the phosphorylation of Tyr747 at β-3 integrin shTG cells in contrast to the control cells (Figure 4.8C). There was also reduced phosphorylation at Tyr822 of vinculin (Figure 4.8D) and focal adhesion kinase (FAK) at Tyr925 in shTG cells compared to control cells, but there was no difference at Tyr576 of FAK (Figure 4.8E).

Since shTG cells exhibited less cell spreading on fibronectin coated surfaces (Figure 4.6E), the phosphorylation levels of some of these focal adhesion proteins (Ser178 paxillin, Tyr747 β-3 integrin, Tyr822 Vinculin) were repeated in serum-free medium on uncoated surfaces. Similar results were observed when the same experiments were repeated on fibronectin-coated surfaces (Figure 4.9).

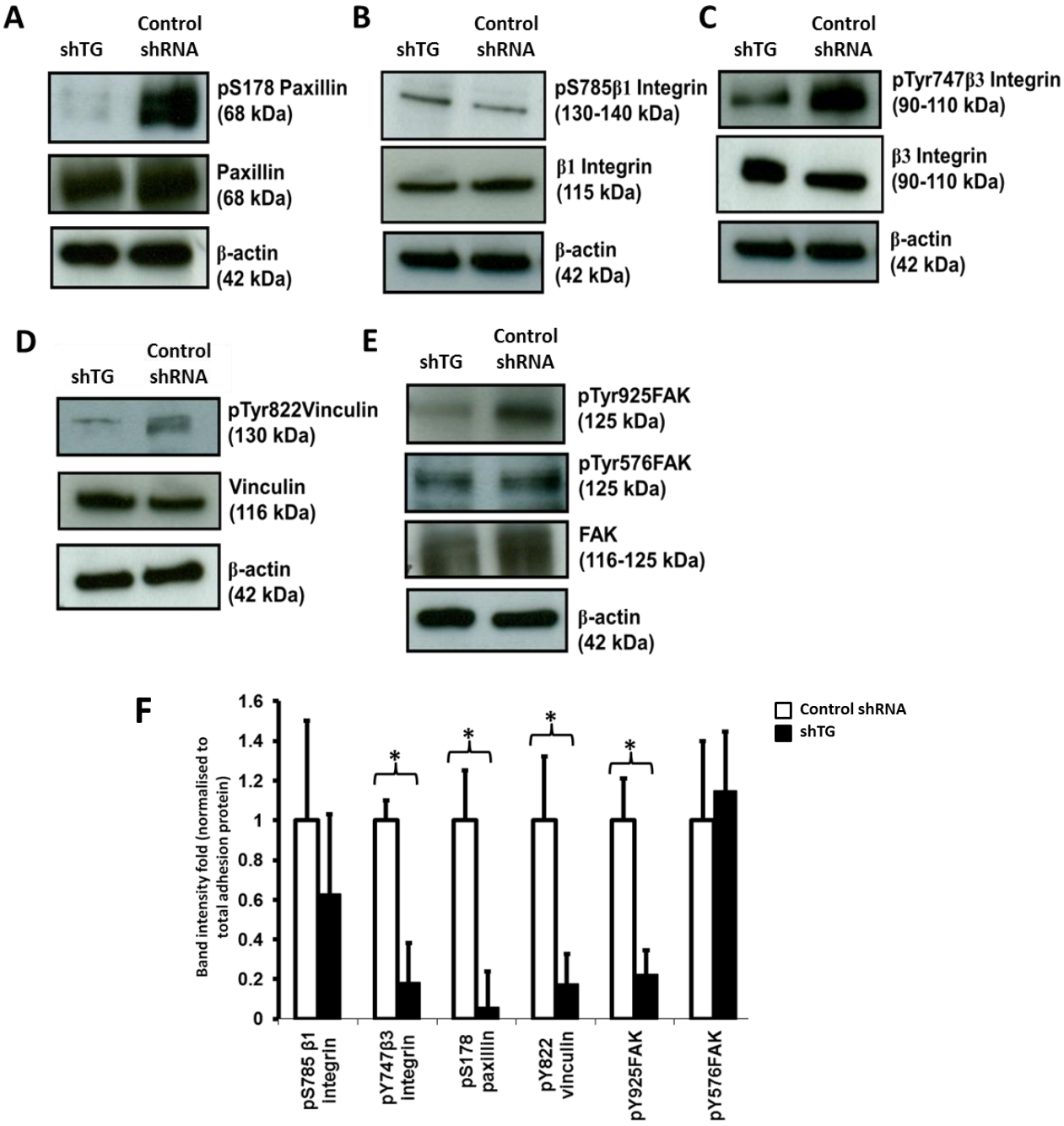

Figure 4.8. Figures showing western blot images of shTG and control shRNA cell lysate on primary antibodies against various adhesion proteins. (A) total paxillin and pS178 paxillin, (B) total β1 integrins and pS785 β1 integrins, (C) total β3 integrins and pY747 (D) total vinculin and pY822 vinculin (E) total focal adhesion kinase (FAK), pY925 FAK and pY576 FAK. β actin was used as loading control. (F) Densitometry analysis showing fold change in band intensity of targeted protein normalised to total adhesion protein. *: $p<0.05$

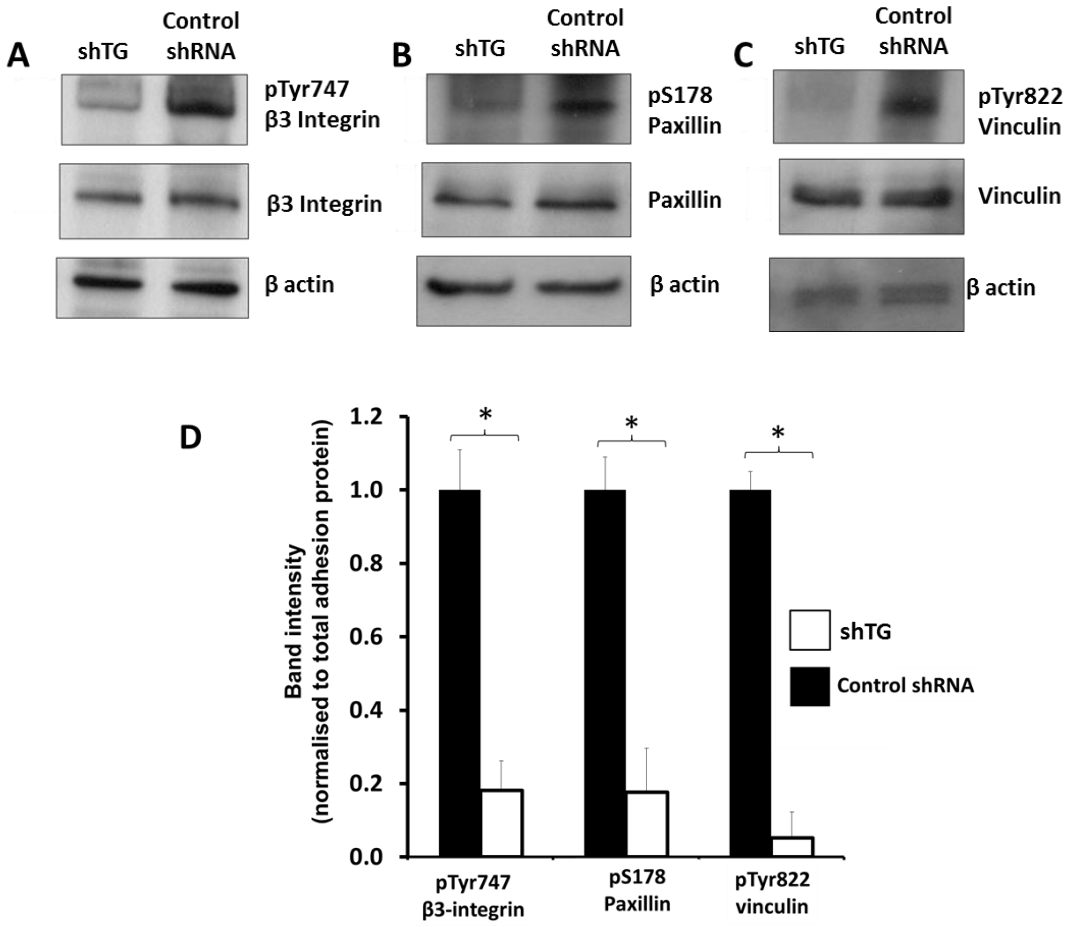

Figure 4.9. Human corneal epithelial cells with TG-2 deficiency reduced the phosphorylation of several focal adhesion proteins. (A-C) Control shRNA or shTG cells were seeded on fibronectin-coated plates followed by 5 hours of serum starvation. Western blots were then performed using 50μg of total cell lysates using primary antibodies specific for phosphorylated and total (A) β3 integrin, (B) paxillin and (C) vinculin; β actin was used as loading control. (D) Bar chart showing densitometry of western blots. For each of the protein of interest, the phosphorylated protein intensities were normalised to the total protein intensities. The resulting value were expressed as fold change comparing to the intensity of control cells (n= 3 independent experiments). * $p < 0.05$ using the Mann Whitney *U* test.

4.7.2 TG-2 Interacts with Paxillin in In vitro

In previous sections, it has been shown that TG-2 is crucial for corneal epithelial cell adhesion and migration. In addition, the phosphorylations of focal adhesion proteins such as integrin β-3, vinculin, paxillin and FAK at specific tyrosine/serine residues were associated with TG-2 status. However, there is no known relationship between TG-2 and the focal adhesion proteins, beyond the fact that TG-2 could interact with integrin β1 and β3 at cell surface to bind fibronectin [29, 180]. Hence, co-immunoprecipitation using anti-paxillin antibody was used to examine whether recombinant TG-2 could interact with vinculin, paxillin and FAK.

Co-immunoprecipitation data showed that anti-paxillin antibody successfully pulled down TG-2 in both shTG and control shRNA cell lysates (Figure 4.10). Control shRNA cells had more TG-2 proteins compared to shTG (Figure 4.10, leftmost 2 columns, row 1) while similar amounts of paxillin were pulled down in the assay (Figure 4.10, leftmost 2 columns, row 2). Vinculin and FAK were also co-immunoprecipitated by anti-paxillin antibody (Figure 4.10, leftmost 2 columns, rows 3, 4,), suggesting that these were *bona fide* mature focal adhesion complexes whose components separated under denaturing conditions. The amount of TG-2 did not affect the binding of FAK or vinculin to the paxillin-containing complex (Figure 4.10, leftmost 2 columns, rows 3, 4). Even when pre-clearing had been performed, TG-2 in the lysate may still be able to interact non-specifically with the streptavidin agarose resin during incubation; this was why negative

control experiments without paxillin antibodies to pull down were performed. (Figure 4.10, rightmost 2 columns).

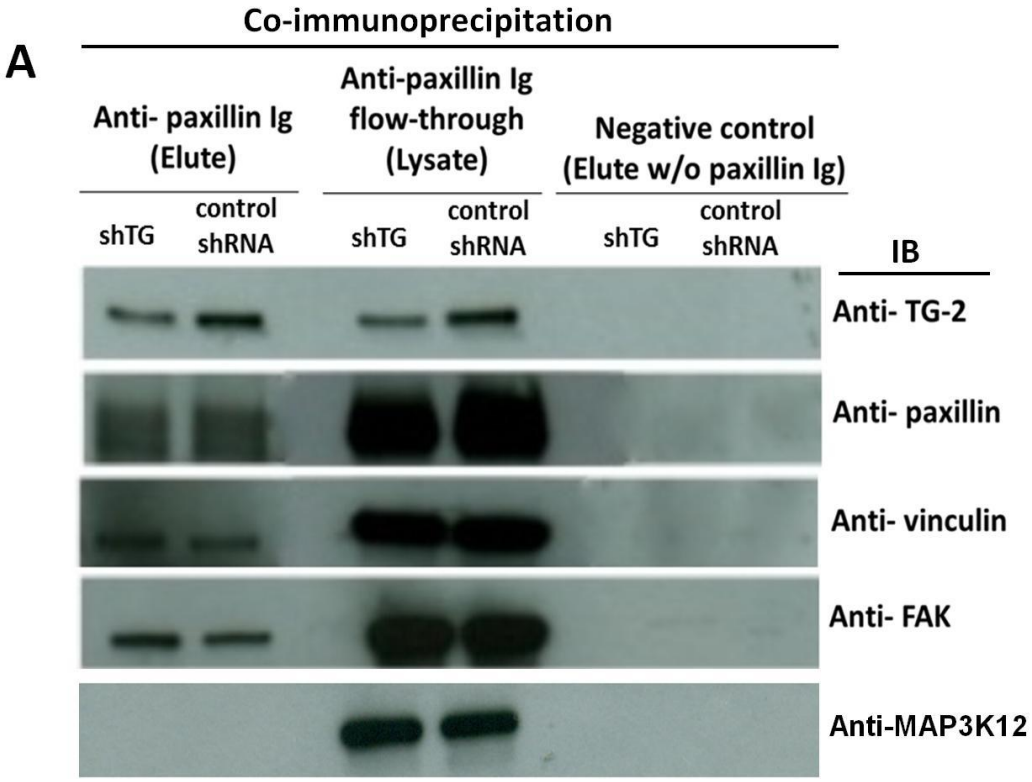
A
Co-immunoprecipitation
Anti- paxillin Ig (Elute)
Anti-paxillin Ig flow-through (Lysate)
Negative control (Elute w/o paxillin Ig)
shTG
control shRNA
shTG
control shRNA
shTG
control shRNA
IB
Anti- TG-2
Anti- paxillin
Anti- vinculin
Anti- FAK
Anti-MAP3K12

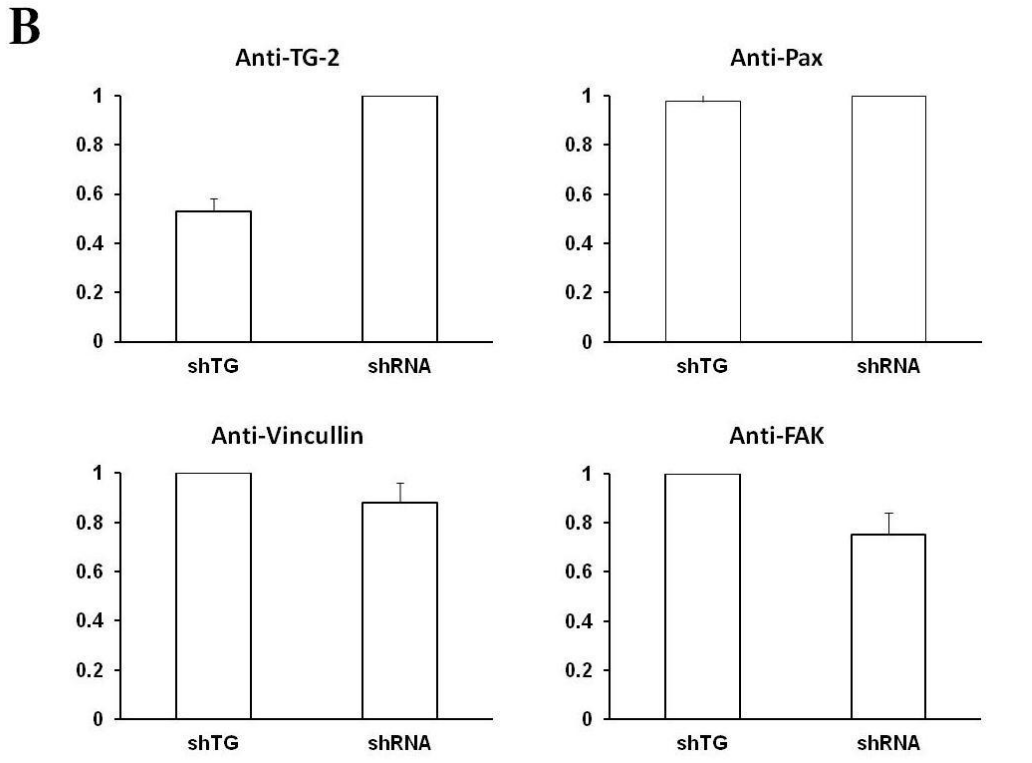
B
Anti-TG-2
Anti-Pax
Anti-Vincullin
Anti-FAK
1
0.8
0.6
0.4
0.2
0
shTG
shRNA

Figure 4.10. Co-immunoprecipitation of shTG and control cell lysate against anti-paxillin. (A) Total cell lyate from cell line shTG and control shRNA was immunoprecipitated with or whithout anti-paxillin. Elute and flow-through were used for western blotting with antibodies against TG-2 and focal adhesion proteins: paxillin, vinculin and FAK. Elute from plain streptavidin agarose beads without adhering antibody was used as negative control. (B) Bar chart showing the densitometric quantification of the proportion of proteins pulled down with paxilllin, using paxillin antibody, from shTG and shRNA cell lysate. Height of bars represents mean of ratios of 3 experiments, error bars indicate standard deviation.

The binding of TG-2 to paxillin was confirmed by an *in vitro* label-free assay which studied the interactions between TG-2 and focal adhesion proteins such as paxillin, vinculin and integrin (Methods at Appendix A16). This assay used an optic grating sensor technique, Enspire Multimode Plate Reader (Perkin Elmer, MA, USA), to evaluate *in vitro* protein interactions. The readout of this assay would measure changes in the index of refraction upon a binding event, indicated by a shift of wavelength of the incident light. The wells in the microplate were pre-coated and incubated overnight with recombinant paxillin protein. When different concentrations of TG-2 and αVβ3 integrin recombinant proteins were added to the immobilised paxillin protein, spectral shifts were detected after equilibrium (Figure 4.11A, B), suggesting both TG-2 and αVβ3 integrin could individually bind to the paxillin proteins. On the contrary, the addition of increasing concentration of recombinant vinculin to the immobilised paxillin showed minimal change in the spectral shift, hence the binding of vinculin to paxillin was not conclusive (Figure 4.11C).

In the context where TG-2 had already interacted with paxillin, the addition of αVβ3 integrin (Figure 4.11D left) or vinculin (Figure 4.11D right) caused additional interactions, which may be due to the binding of these two molecules to the pre-existing TG-2/paxillin complex, or that the two additional molecules enhanced the TG-2/paxillin interaction. When TG-2 was added to the integrin/paxillin complex (Figure 4.11E), there was a further increase in the spectral shift; implying that either the newly added TG-2 had bound to the integrin/paxillin complex, or that it had enhanced the binding of previously added integrin to the immobilised paxillin. Spectral shift occurred after the addition of

TG-2 to the solution containing vinculin (Figure 4.11F). This increase in spectral shift suggested that the newly added TG-2 had bound to the immobilised paxillin, implying that the interactions between TG-2 and paxillin were stronger than the vinculin paxillin interactions. These experiments were done in pH 7.0. Experiments repeated at pH 4.3 showed similar results (data not shown).

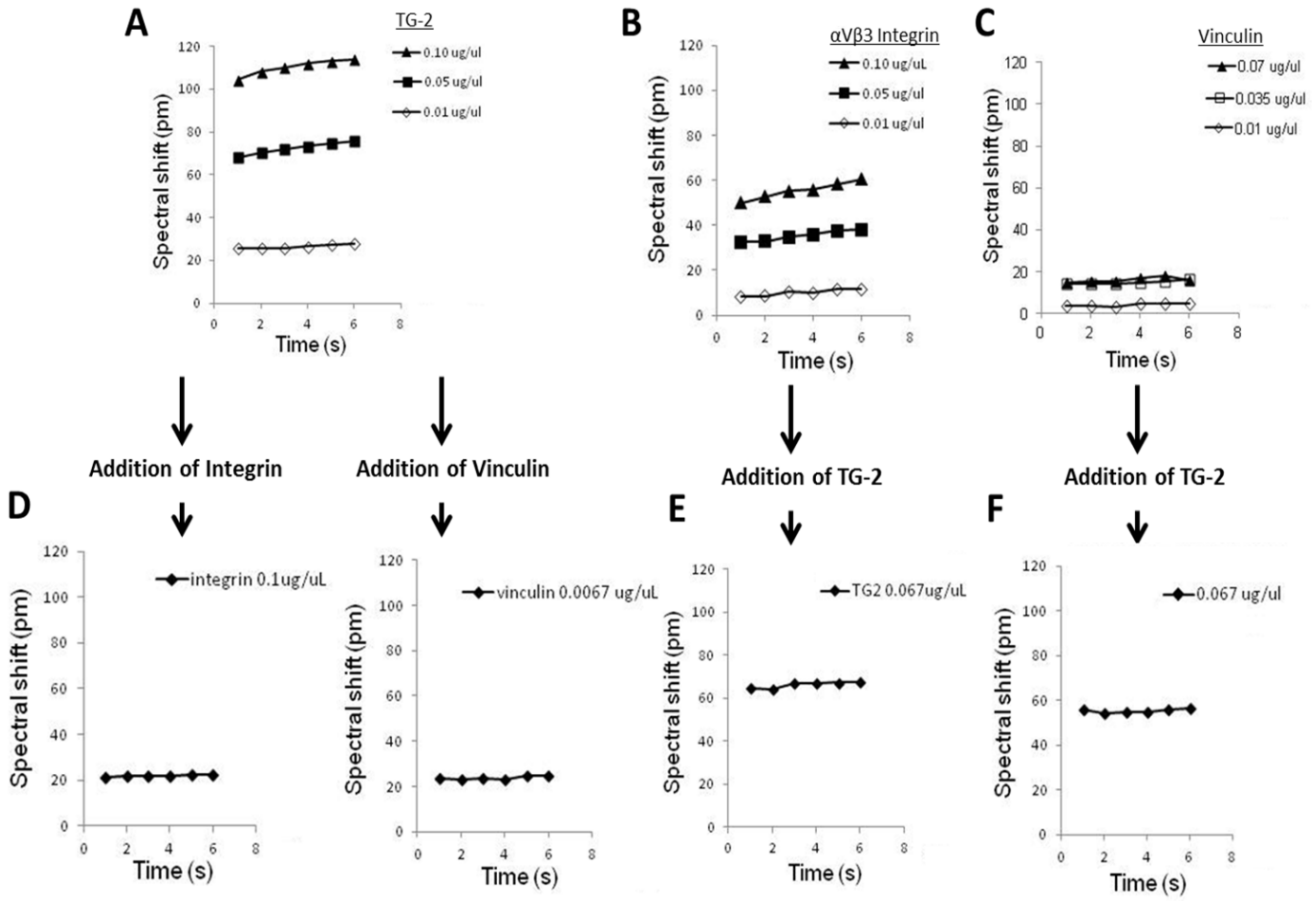

Figure 4.11. Graphs showing Enspire Label-free biochemical assay which showed a spectral shift after the addition of recombinant proteins to immobilised paxillin. Paxillin recombinant protein was first immobilised at a final concentration of 0.05µg/µL. After the immobilised paxillin was in equilibrium, the spectral shift was reset arbitrarily to zero picometres before adding a second recombinant protein, either TG-2, αVβ3 Integrin or Vinculin, at the indicated concentrations. The spectral shift was then measured and recorded (Top row: A, B, C). These spectral shifts were again reset to zero before the addition of the next recombinant protein. The new shifts were then recorded (Bottom row: D, E, F).

4.7.3 TG-2 Cannot Phosphorylate Paxillin Directly

Since TG-2 deficiency reduced the phosphorylation of paxillin at Ser178, I would want to find out next how TG-2 would affect the phosphorylation of paxillin. Can TG-2 act as a kinase to phosphorylate paxillin?

An *in vitro* autoradiographic kinase assay was performed to examine whether TG-2 itself could phosphorylate paxillin (Methods at Appendix A17.1). Strong bands were detected for the two positive controls at the expected molecular weight of paxillin in lane 9 (JNK is known to phosphorylate paxillin [101]), and Histone H1 in lane 10 (CDK2-CyclinE1 is known to phosphorylate Histone H1 [181]) (Figure 4.12A, Lane 9 and 10), indicating the reliability of the *in vitro* kinase assay with respect to the assay procedure.

No bands could be detected for paxillin and TG-2 in Figure 4.12A from lanes 1 to 8, showing that TG-2 neither phosphorylated paxillin (Figure 4.12A, Lanes 3-8) nor auto-phosphorylated itself (Figure 4.12A, Lane 1) in this experiment. Also, no protein auto-phosphorylation activity could be found for the paxillin preparation alone (Figure 4.12A, Lane 2).

Since TG-2 itself could not phosphorylate paxillin, could TG-2 recruit or activate another kinase to phosphorylate paxillin? A panel of 190 known Serine/Threonine kinases was screened to identify the protein kinase that could phosphorylate paxillin. This phosphorylation profiling showed a differential ability of paxillin to act as a substrate for

the tested kinases. JNK1 was found to have the highest relative activities (Figure 4.12B). The full tested panel of the 190 Serine/Threonine kinases is shown in Appendix D, Figure A11. To confirm that JNK1 could act as a kinase to phosphorylate paxillin, a radioactive protein kinase filter-binding assay was performed (Methods at Appendix A17.2). Briefly, radioactive ATP was added together with a fixed concentration of JNK and increasing concentration of paxillin protein. The kinase activity dependent transfer of the radioactive phosphate was determined with a microplate scintillation counter. Figure 4.13 showed that paxillin could act as a substrate for the tested kinase JNK1.

A

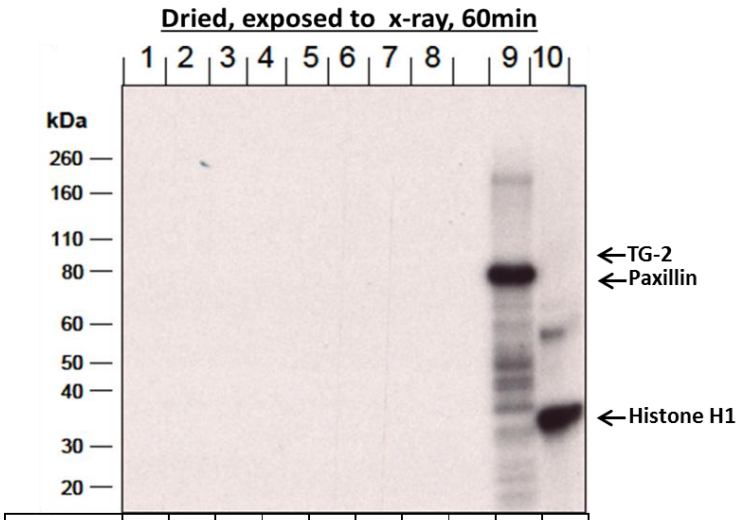

Lane	1	2	3	4	5	6	7	8	9	10
TG-2	100	0	50	50	50	100	100	100	0	0
Paxillin	0	500	500	500	500	500	500	500	500	0
Histone	0	0	0	0	0	0	0	0	0	500
JNK1	0	0	0	0	0	0	0	0	50	0
CDK2-CycE	0	0	0	0	0	0	0	0	0	50

B

Kinase (ProQinase Lot #)	Activity raw values	Kinase autophos., normalized mean n=3	Substrate-BG, mean of 2 singlicates	Activity values, corrected (A-C)	Activity Ratio (A-C)/B
JNK1 (Lot005)	3986	43	394	3592	84.34
PKA (Lot002)	7600	87	394	7206	82.43
MARK2 (Lot002)	24606	330	394	24212	73.30
DYRK1B (Lot001)	6317	81	394	5923	73.12
NEK7 (Lot002)	22181	304	394	21787	71.64
PRKX (Lot001)	5872	77	394	5478	71.14
GRK2 (Lot001)	16225	232	394	15831	68.17

Figure 4.12. Figures showing autoradiogram of in vitro kinase activities as well as a library of Serine/Threonine kinases to identify the protein kinase that phosphorylates paxillin. (A) Autoradiogram shows *in vitro* kinase activities of proteins. Samples were loaded on a 4-12% SDS-PAA gel and analysed by electrophoresis. The gel was dried and exposed to x-ray film for 60 min. Paxillin and different concentrations of TG-2 were loaded into lane 1-8. Lane 9 and 10 were positive controls with known kinase activities; which were phosphorylation of paxillin by JNK1, and phosphorylation of Histone H1 by CDK2-CyclinE1 respectively. (B) A library of 190 Serine/Threonine kinases was screened to identify the protein kinase that can phosphorylate paxillin. JNK1 was found to have the highest relative activities. The activity ratio value described the ratio between the activity of the particular kinase with and without sample protein.

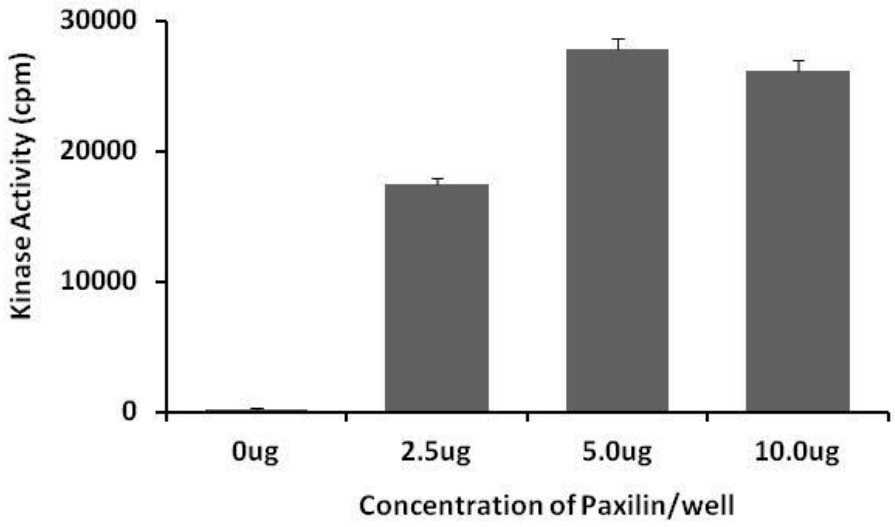

Figure 4.13. Barchart showing activity value (in counts per minute, cpm) of JNK1 with paxillin substrate. Reaction cocktails containing radioactive ATP and 5ng per well of JNK1 protein were added with different concentrations of paxillin protein (0ug, 2.5ug, 5.0ug and 10.0ug). Kinase activity dependent transfer of 33Pi was determined with a microplate scintillation counter. Error bars= standard deviation. Three independent experiments were done.

4.7.4 Interaction of TG-2 and JNK

Since the phosphorylation of Ser178 of paxillin in corneal epithelial cells was JNK-mediated, I would be interested to determine if TG-2 could affect recruitment of JNK to the focal adhesion complex. First, immunoblots were done against recombinant TG-2, paxillin and JNK at various concentrations to ensure that these proteins could be detected. 1µg of TG-2 and paxillin recombinant protein respectively could be pulled down by anti-paxillin during co-immunoprecipitation, while 5µg of JNK was needed for anti-paxillin to successfully pull it down (Figure 4.14A).

Co-immunoprecipitation with anti-paxillin antibody confirmed that recombinant TG-2 protein can bind to paxillin complexes, which also bound JNK (Figure 4.14B). However, when TG-2 concentration was increased (1µg, 2.5µg, 5µg) in the presence of fixed concentrations (1µg) of paxillin and JNK, there was no corresponding increased in the intensity of JNK in the immunoblots, suggesting that the amount of JNK in the complex did not increase in a TG-2 dependent manner (Figure 4.14B, C). When recombinant proteins were mixed with the resin without the paxillin Ig, further washing of the resin would have removed any adhered proteins, showing that none of the adhesion proteins could bind directly to the streptavidin resin (Figure 4.14B, negative control in leftmost column). Further negative controls for the immunoblots performed without primary anitbodies for the JNK, TG-2 and paxillin were performed (data not shown).

If JNK was the mediator that phosphorylated paxillin, what was the relationship between TG-2 and JNK? I have shown in Figure 4.14B that increasing TG-2 did not increase the JNK in the complex, which implied that TG-2 was not involved in recruiting JNK to the complex. Since Robitaille *et al* reported that TG-2 could crosslink and activate MAP3K12 (also known as DLK) and subsequently activate downstream JNK in human neuroblastoma cells [182], could TG-2 also recruit JNK via this mechanism in human corneal epithelial cells? Referring to co-immunoprecipitation in Figure 4.10, anti-paxillin successfully pulled down TG-2 and other focal adhesion proteins but failed to pull down MAP3K12. This showed that MAP3K12 was not part of the adhesion complex. If TG-2's crosslinking function was involved in this context, it may be via unknown mechanisms such as an unidentified upstream kinase that was recruited to the complex. Alternatively, JNK could have been activated and phosphorylated by unknown TG-2 dependent mechanisms and then recruited to the adhesion complex.

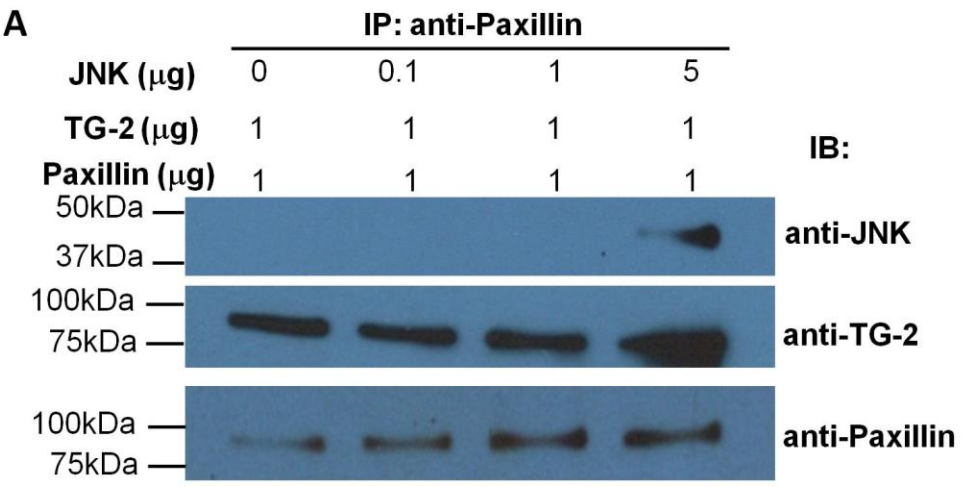
A
IP: anti-Paxillin
JNK (μg) 0 0.1 1 5
TG-2 (μg) 1 1 1 1
Paxillin (μg) 1 1 1 1
IB:
50kDa
37kDa
anti-JNK
100kDa
75kDa
anti-TG-2
100kDa
75kDa
anti-Paxillin

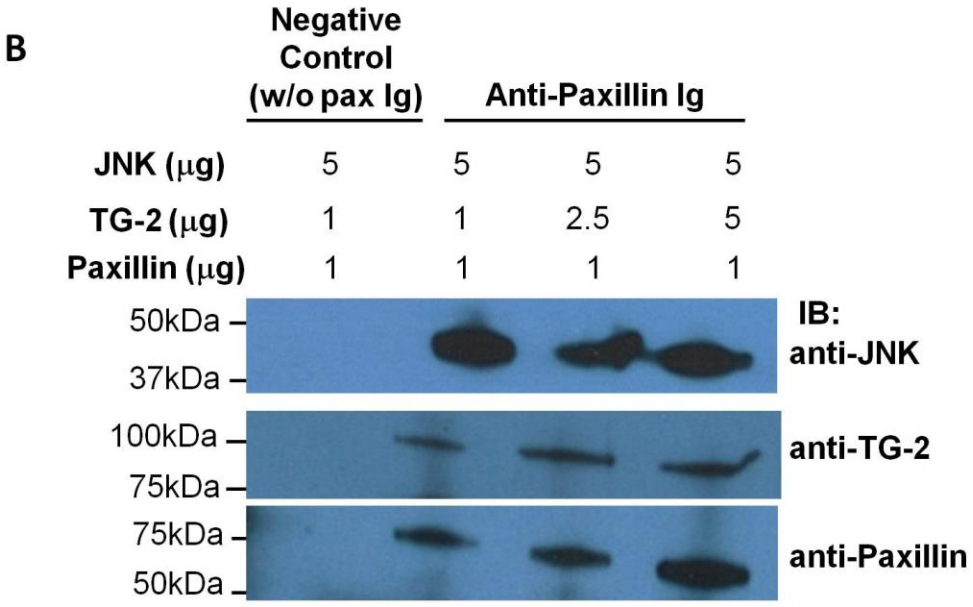
B
Negative Control (w/o pax Ig)
Anti-Paxillin Ig
JNK (μg) 5 5 5 5
TG-2 (μg) 1 1 2.5 5
Paxillin (μg) 1 1 1 1
50kDa
37kDa
IB: anti-JNK
100kDa
75kDa
anti-TG-2
75kDa
50kDa
anti-Paxillin

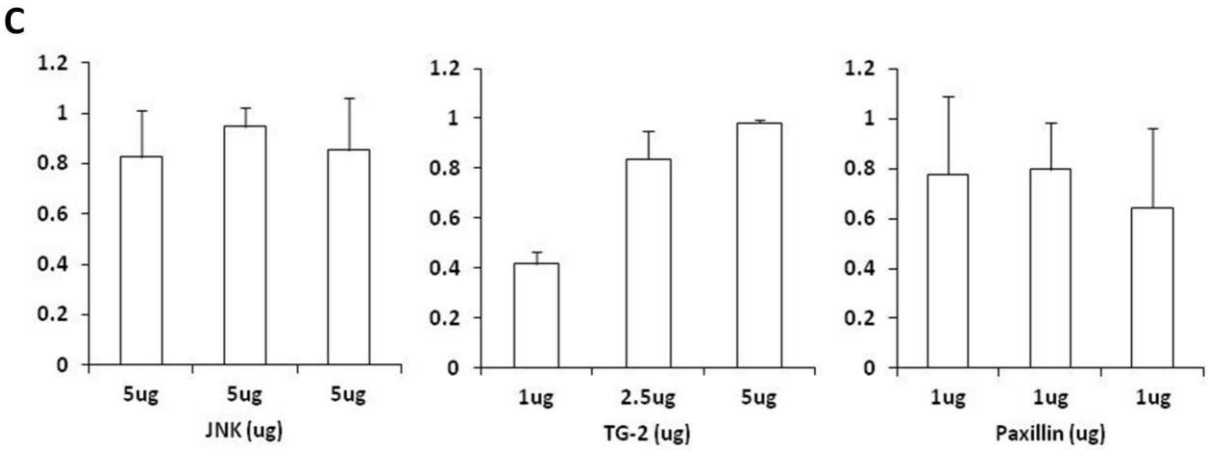
C
1.2
1
0.8
0.6
0.4
0.2
0
5ug 5ug 5ug
JNK (ug)
1ug 2.5ug 5ug
TG-2 (ug)
1ug 1ug 1ug
Paxillin (ug)

Figure 4.14. Cell free *in vitro* immunoprecipitation and western blotting. Immunoprecipitation was performed using mixture of human recombinant proteins TG-2, JNK and paxillin. The recombinant proteins mixture was incubated at 4^{o}C overnight followed by immunoprecipitation with anti-paxillin. Western blotting was then carried out on the pulled down proteins with anti-TG-2, anti-JNK and anti-paxillin. (A) Increasing concentration of recombinant JNK protein (0, 0.1, 1 and 5 µg) was added with fixed amount (1 µg) of TG-2 and paxillin proteins respectively in co-immunoprecipitation. (B) Fixed concentration of JNK and paxillin at 5µg and 1µg respectively per 200 µl reaction volume was added, while increasing concentration of TG-2 at 1µg, 2.5µg and 5µg per reaction was added. Negative control consisted of recombinant proteins mixed with streptavidin agarose resin without paxillin Ig (negative control in leftmost column). (C) Bar graphs showing densitometry for the anti-paxillin pulled down TG-2 and JNK proteins.

4.8 Discussion

Together with previous findings, this study demonstrated a novel mechanism of TG-2, i.e. TG-2 could bind and was required for the phosphorylation of adhesion molecules. More than one experimental approach was employed in this study such as cell scratching assay, cell migration assay, trypsinisation assay, western blotting and kinase assay; which were used to supplement the *in vivo* mouse corneal scratch wound data.

An *in vitro* scratch wound of cultured human corneal epithelial cells with reduced TG-2 (Figure 4.3), supported by an *in vivo* corneal abrasion experiment in TG-2 knockout and wild type mice (Figure 4.1), helped to provide evidence that TG-2 played an important role in corneal epithelial wound healing for the first time. The status of TG-2 did not affect cell cycle progression and cell proliferation (Figure 4.6A-D); while the presence of TG-2 increased cell adhesion, spreading (Figure 4.6E, F) and cell migration speed (Figure 4.4B).

Cell adhesion and spreading are essential to cell movement. The involvement of TG-2 in cell adhesion and/or migration have been reported in various cell types such as retinal pigment epithelial cells [175], osteoblast cells [68], breast cancer [183], enthothelial cells [173], monocytes [65] and metastatic melanoma cells [174]. Interestingly, shTG cells had significantly smaller cell areas compared to control shRNA cells when cultured on fibronectin-coated surfaces, but had comparable cell area to control cells when grown on uncoated surfaces (Figure 4.6E). A similar observation was also reported by Jones *et al* whereby antisense TG-2 transfected human endothelial cells showed reduced cell

spreading [173]. This difference in cell area between control shRNA and shTG cells was possibly due to the interaction between fibronectin, TG-2 and integrin, likely because it was well known that TG-2 could act as an integrin-associated coreceptor for fibronectin [29]. Control shRNA cells had higher amount of TG-2 compared to shTG cells, hence they could interact better with the underlying fibronectin coating, contributing to the bigger cell area.

Cytoskeleton is a structure that is responsible to maintain cell shape, to organise the organelles within cells, and to provide mechanical support for cells to carry out crucial biological activities such as motility and division [184]. When TG-2 was reduced in cultured human corneal epithelial cells (shTG cells), the cytoskeleton organisation was deranged (Figure 4.7A) and the cells showed slower migration velocity compared to the control cells (Figure 4.4B). This highlighted the importance of TG-2 in cell adhesion and migration.

Literatures had reported that extracellular TG-2 induced integrin clustering, potentiating outside-in signalling leading to the stimulation of downstream Rho proteins [75]. Small GTP-binding proteins of the Rho family such as RhoA, Rac and Cdc42, were known for regulating actin dynamics essential for cell migration [177]. RhoA promoted actin filament assembly, mediated cell contractility and controlled the retraction of tail in migrating cells; while Rac and Cdc42 initiated the formation of lamellipodium and filopodia [185]. In addition, Rac and Cdc42 also mediated the formation of focal adhesion complexes, which were different from the focal adhesions induced by RhoA

[176, 177]. In cells with reduced TG-2, there was a reduction in Rac and Cdc42 activity relative to control cells (Figure 4.7B). Although the activity of RhoA was not significantly different in the experiment, literature had reported that extracellular TG-2 elevated RhoA levels via clustering of β-1 integrin as well as down-regulation of the Src-p190RhoGAP pathway [75]. However, the study of adhesion molecules clustering is not in the scope of this report.

This was the first study to examine the interactions between TG-2 and focal adhesion proteins. Previous publications had only studied the interaction of extracellular TG-2 with integrin in the regulation of cell adhesion and migration [29, 186]. Previously, it was widely accepted that corneal epithelium had β-1 integrin, but not β-3 integrin. Here, by using specific antibodies targeting β-3 integrin and phosphorylated Tyr747 β-3 integrin, we showed that β-3 integrin was present and activated in a TG-2 dependent manner in human cornea epithelial cells (Figure 4.8C). The presence of β-3 integrin in human cornea epithelium was further supported by the expression of β-3 integrin transcript and protein in primary corneal epithelial cells derived from cadaveric limbal explant tissue (Appendix D, Figure A10). This was confirmed by another unrelated Gene Chip project from our laboratory which showed that β-3 integrin transcripts were present in both the corneal epithelial cell line and primary cultured corneal epithelial cells (Appendix D, Figure A10).

It has been reported that phosphorylation of β-3 integrin at Tyr747 was crucial for both inside-out and outside-in signaling [187] and recruitment of signalling proteins [188]

during cell adhesion [189]. TG-2 status also affected the phosphorylation of vinculin at Tyr822 and FAK at Tyr925 (Figure 4.8D, E). The phosphorylation of vinculin at Tyr822 has not yet been related to functions in control of cell shape and migration [190]. However, it was reported that since Tyr822 is located close to the flexible hinge region of vinculin, phosphorylation at this site maybe important to maintain its open conformation, which may affect the subsequent binding of talin [191]. In strain stimulated intestinal epithelial cell migration, the phosphorylation of FAK at Tyr925 was required for Rac1 mediated downstream activation of PI3K/AKT pathway [192]. Also, it has been reported that in mouse embryonic fibroblasts, FAK phosphorylation at Tyr925 was required for cell migration and formation of cell edge protrusion [193].

Immunoblotting using phosphoserine-specific antibody showed that shTG cells had reduced phosphorylation of paxillin at serine 178 relative to control cells (Figure 4.8A). This was a robust finding because it showed that TG-2 did not need specific extracellular ligands to phosphorylate paxillin. Previously, literatures had reported that TG-2 dependent adhesion signaling required specific interaction with syndecan-4 and fibronectin [194]. The relationship between TG-2 and paxillin phosphorylation was also supported by our i*n vivo* preliminary data (Figure 1.2), strongly suggesting that TG-2 could mediate corneal epithelial wound closure through phosphorylation of paxillin at Ser178.

The phosphorylation of paxillin at Ser178 leads to the downstream recruitment and activation of signalling molecules, thus mediating focal adhesion dynamics. Huang *et al*

reported that the phosphorylation of paxillin on Ser178 by c-Jun N-terminal kinase (JNK) was required for the association of FAK to paxillin [195]. This binding of FAK then promoted the phosphorylation of paxillin at Tyr 31 and Tyr 118, which then led to the subsequent recruitment of vinculin [196, 197]. This suggested that the phosphorylation of paxillin at Ser178 may be upstream of the phosphorylation of FAK and vinculin.

The success of pulling down TG-2 protein using paxillin-bound agarose beads in shTG and control shRNA cell lysates suggested that TG-2 could interact directly with recombinant paxillin. This was supported by the Enspire cell free assay whereby the addition of increasing concentration of recombinant TG-2 to immobilise paxillin caused a spectral shift in Figure 4.11. Another piece of evidence was that paxillin was detected in shTG and control shRNA cell lysate by a specific anti-paxillin antibody (Figure 4.8A).

Previous studies by Mishra *et al* had reported that TG-2 could act as a kinase and phosphorylate IGFBP-3, p53 and histones [198-200]. However, after performing kinase assay using increasing concentration of TG-2 against fixed concentration of paxillin, there were no bands observed on the blot upon X-ray exposure, indicating that TG-2 itself could not act as a kinase to phosphorylate paxillin. After screening a library of known serine/threonine kinases, JNK1 was a more probable candidate to phosphorylate paxillin as a kinase. The kinase activity of JNK1 with its substrate paxillin was then confirmed using a radioactive protein kinase assay, which is the gold standard for the quantification of protein kinase activity involving the incorporation of γ-^{33}P-labeled ATP into a substrate [107]. Consistent with this finding, Kimura *et al* reported that

phosphorylated JNK co-localised with paxillin at the wound margin through immunostaining [101]. They also found that when JNK inhibitor was added to the cultured human corneal epithelial cells, there was a reduction in phosphorylation of paxillin at Ser178, but not the paxillin expression level. This was supported by Huang *et al* who reported that overexpression of JNK1 enhanced the phosphorylation of paxillin in HEK-293 cells [201].

If JNK was the kinase that phosphorylated paxillin, what was the relationship between TG-2 and JNK? The effects of TG-2 on JNK had been reported, for example, the silencing of TG-2 reduced the expression of pJNK [202, 203]. Also, several studies showed that JNK could modulate the phosphorylation of paxillin at Ser178 and the formation of focal adhesions in corneal epithelial cells [101, 195, 204]. Earlier in this chapter, I showed that increasing TG-2 did not increase JNK in the complex, implying that TG-2 was not involved directly in recruiting JNK to the complex. Since TG-2 could not directly recruit JNK, could TG-2 recruit JNK indirectly through other kinases? Robitaille *et al* reported that TG-2 could crosslink and activate dual leucine zipper kinase (DLK, otherwise known as MAP3K12), and subsequently activate downstream JNK in fibroblasts and human neuroblastoma cells [202, 205]. Could TG-2 also activate downstream JNK through MAP3K12 in human corneal epithelial cells? Unfortunately, this specific mechanism was probably not active in our cell context since MAP3K12 could not be pulled down by paxillin antibody in our co-immunoprecipatation study. This showed that MAP3K12 was not part of the adhesion complex in human corneal epithelial cells. TG-2 may be involved in JNK activated paxillin pathway via unknown mechanisms

such as through an unidentified upstream kinase that is recruited to the focal adhesion complex. Alternatively, JNK could be activated by unknown TG-2 dependent mechanisms, followed by recruitment to the adhesion complex.

Since TG-2 can bind directly to paxillin, it is important to know the specific domain of both TG-2 and paxillin that was involved in this interaction. The interaction between TG-2 and paxillin may differ in various cell substrates and tissue origins. We suggest that TG-2 may interact with the LD domains in the amino terminal region of paxillin to affect the recruitment of other proteins, since LD domains are known to have various protein binding sites [206].

4.9 Conclusion

In summary, this project proposed that TG-2 can improve wound closure in corneal epithelial cells through phosphorylation of fundamental focal adhesion proteins. Since serine phosphorylation of paxillin has been associated with cell adhesion and migration in fibroblasts and epithelial cells [96, 101], and TG-2 has been shown to mediate adhesion in different cell type [44, 65]; hence TG-2 dependent serine phosphorylation of paxillin may act as a signal transduction mechanism for cell adhesion and migration in stratified epithelium. Also, I have showed that TG-2 can interact with paxillin in human corneal epithelial cells. The interaction between paxillin and TG-2 may be important as a potential therapeutic target since wound healing is deranged in most ocular surface diseases. In disease conditions, cell adhesion and wound closures may be improved by increasing this paxillin-TG-2 interaction. Further studies also need to focus on the interaction of TG-2 with different focal adhesion proteins and identify the sequence of signaling. This can help to decipher TG-2's role in ocular surface diseases such as recurrent corneal erosions, pterygium and corneal epitheliopathy in dry eye.

Key Findings

a. TG-2 deficiency delayed wound closure, both *in vitro* and *in vivo*. The lack of TG-2 reduced cell migration velocity and cell adhesion/spreading, exhibited deranged actin cytoskeleton and reduced in Rac and Cdc42 protein activities.

b. TG-2 deficiency reduced phosphorylation of Tyr747 integrin β3, Tyr822 vinculin, Tyr925 FA, and most notably Ser178 paxillin.

c. TG-2 bound to paxillin but TG-2 could not phosphorylate paxillin. JNK1 is the proposed kinase that could phosphorylate paxillin.

d. TG-2 concentration did not affect JNK. TG-2 could not indirectly activate JNK through DLK (also known as MAP3K12) in HCE-T cells.

CHAPTER 5. CONCLUSION AND FUTURE DIRECTIONS

Key Findings

1. The role of TG-2 in hyperosmolarity-mediated mitochondrial cell death has been evaluated as follows (Chapter 2):
    a. Hyperosmolar treatment mediated cell death and reduced cell viability in cultured human corneal epithelial cells.
    b. Hyperosmolar stimulation caused the release of cytochrome-c and mitochondrial depolarisation.
    c. TG-2 was present in mitochondrial extract. Hyperosmolar stimulation did not further increase the mitochondrial depolarisation in TG-2 overexpressing cells compared to cells with endogenous TG-2; while in TG-2 deficient cells, hyperosmolar conditions induced less amount of mitochondrial depolarisation, indicating a partial dependence on TG-2 function.
    d. TG-2 overexpression increased transamidase activity, reduced cornea epithelial cell proliferation and increased caspase-3/7 and 9 activity.
2. The interacting partners of TG-2 which are cell adhesion or cell migration related were discovered and characterised as follows (Chapter 3):
    a. Seven proteins that interacted with different TG-2 fragments were identified.
    b. TG-2 binding proteins were categorized into 3 groups according to the way TG-2 status affected the protein distribution.

c. TG-2 status could affect some of the sub-cellular concentrations of its binding proteins such as DES, PARL, NTRK3, PRSS3, ITGB4 and GOLGA2; and organelles such as recycling endosomes, endoplasmic reticulum, and mitochondria.

3. The functional significance of TG-2 on cell adhesion and migration in corneal epithelial wound closure was evaluated as follows (Chapter 4):
    a. TG-2 deficiency delayed wound closure, both *in vitro* and *in vivo*. The lack of TG-2 reduced cell migration velocity and cell adhesion/spreading, exhibited deranged actin cytoskeleton and reduced in Rac and Cdc42 protein activities.
    b. TG-2 deficiency reduced phosphorylation of Tyr747 integrin β3, Tyr822 vinculin, Tyr925 FA, and most notably Ser178 paxillin.
    c. TG-2 bound to paxillin but TG-2 could not phosphorylate paxillin. JNK1 is the proposed kinase that could phosphorylate paxillin.
    d. TG-2 concentration did not affect JNK. TG-2 could not indirectly activate JNK through DLK (also known as MAP3K12) in HCE-T cells.

5.1 Summary and Discussion

TG-2 is a ubiquitous, multi-functional protein that is expressed in corneal epithelial cells. In Chapter 1 of this thesis, it was demonstrated for the first time that hyperosmolar stimulation mediated mitochondrial depolarisation in human corneal epithelial cells is partially dependent on TG-2 function. Contrary to reports that TG-2 was not present in mitochondria [121, 207], TG-2 was successfully detected in the mitochondrial extract of cultured human corneal epithelial cells. Overexpression of TG-2 increased cellular transamidase activity and reduced cell proliferation. Importantly, when compared to pSG5 (vector alone) transfection, overexpression of TG-2 increased the proportion of mitochondrial depolarised cells. Our findings were supported by Piancentini *et al*'s work, which showed that TG-2 overexpression sensitised cells to apoptosis through the increase of mitochondrial membrane potential [122]. Hyperosmolar conditions caused a significant reduction in mitochondrial potential and decreased cell proliferation in HCE-T. The fold change of mitochondrial depolarisation in TG-2 overexpressing cells was less than those in cells with endogenous TG-2, suggesting that the presence of endogenous TG-2 had already saturated the requirement for TG-2.

Since defective wound healing reduces cornea transparency and affects visual function, in Chapter 2, this study was then extended to identify the interacting protein partners of TG-2 and their protein transportation, which may affect cell adhesion and migration. TG-2 was found to be involved in the trafficking of sub-cellular proteins relevant to wound healing processes. TG-2 deficiency reduced the expression of desmin, mitochondrial intramembrane cleaving protease (PARL), protein tyrosine kinase (NTRK3), and serine

protease (PRSS3) in all (8.5%, 10%, 15%, and 20%) the sucrose fractions (SF) tested. Integrin beta-4 protein and the Golgi associated protein (GOLGA2) showed a reverse expression pattern between subcellular compartments; whereby compared to control, both the proteins had higher expression levels in the 8% SF, but decreased in the subsequent 10%, 15% and 20% SFs. On the other hand, syntaxin binding protein (STXBP2) had similar amounts of protein between shTG and control in all SFs tested. Furthermore, the decrease in TG-2 level reduced the expression of organelles markers for late endosomes, secretory vesicles and recycling endosomes, suggesting that TG-2 levels may mediate cell adhesion and migration through protein transport and alteration of organelle functions. What differed this study from a previous report [141], which both examined sub-cellular trafficking and cell adhesion, was the use of centricollation, a novel protein fractionation technology to separate cell lysates through stepwise density extraction.

Since wound healing is deranged in many of the common ocular surface diseases, in Chapter 3, this work was further extended to elucidate the functions of TG-2 in wound healing which involved epithelial cell adhesion and migration. Cells with reduced TG-2 showed lower cell impedance compared to control, due to differences either in cell proliferation, spreading or adhesion. There was no significant difference in cell cycle progression, and the proportion of proliferating (Ki-67 positive) cells between shTG and control cells. However, control cells required a longer time to detach after trypsinisation compared to shTG cells. When cultured on fibronectin coated surfaces, shTG cells showed smaller cell spreading areas, deranged cytoskeleton organization, slower migration velocity and reduced Rho protein activity compared to the control cells,

indicating the importance of TG-2 in cell adhesion and migration. Upon further investigation, cells with reduced TG-2 showed decreased phosphorylation of adhesion proteins at specific residues. Among them, the most notable residue was Serine 178 paxillin, since it was previously reported, using the same cultured human corneal epithelial cells as in our experiment, to play an important role in adhesion and migration. However, TG-2 itself could not directly phosphorylate paxillin. After screening a library of kinases, JNK1 was found to be the highest possible kinase candidate to phosphorylate paxillin. The kinase activity of JNK1 with paxillin substrate was confirmed via radioactive kinase assay. TG-2 can bind to paxillin and JNK, hence we proposed that TG-2 is present in the FA complex. However, TG-2 neither can directly recruit JNK nor indirectly through DLK (also known as MAP3K12) in HCE-T cells. Taken together with the previous findings, JNK mediated the serine phosphorylation of paxillin through unknown kinase in a TG-2 dependent fashion. This activated JNK or paxillin may then phosphorylate other adhesion proteins, leading to the maturation of the FA complex, thus regulating corneal epithelial cell adhesion and migration.

Literatures had reported that C-jun N-terminal kinase (JNK), extracellular signal-regulated kinase (ERK), and mitogen-activated protein kinase (MAPK) signalling pathways were involved in hyperosmolar-induced corneal epithelial apoptosis [99, 104, 122]. However, these publications did not evaluate the role of TG-2 in the JNK, ERK, or MAPK signalling pathways. In addition, Kimura *et al* reported the JNK-dependent serine phosphorylation of paxillin in corneal epithelial cells, but did not study the role of TG-2 in this pathway [101]. The current work is the first study to connect the missing links

between TG-2, apoptosis and wound closure related cell motility processes which involved cell adhesion and migration. We reported that JNK1 may act as a kinase in TG-2-mediated corneal epithelial cell migration and adhesion by modulating the paxillin phosphorylation and the subsequent formation of focal adhesions.

5.2 Strengths

More than one experimental approach was employed in these studies to elucidate the role of TG-2 in common biological processes.

In Chapter 2, cell impedance assay allowed real time monitoring of cell viability, number, morphology, and adhesion degree in cell-based assays without the use of labels which may potentially affect cell functions. Quantitative assays such as TG-2 transamidase activity assay and cell-based caspase-3/7 and 9 assays were performed and they are different from other semi-quantitative techniques such as Western blot. For example, an optimised TG-2 transamidase activity assay could be used to accurately determine the transglutaminase activity in protein samples, since TG-2 concentration was proportional to detectable TG-2 crosslinking activity within a linear range. HCE-T overexpressing TG-2 showed at least 50% more of the transamidase activity than the cells transfected with pSG5 vector. Since it was reported that hyperosmolarity could increase transamidase activity in primary corneal epithelial cells [111], hence the current method of TG-2 overexpression in corneal epithelial cells may be a suitable means to study the effect of hyperosmolar stimulation on TG-2. Instead of using TG-2 inhibitor, various approaches were employed in this study to alter the TG-2 function; for example, overexpression of TG-2 and RNA interference targeting TG-2 sequence, thus permitting the evaluation of specific TG-2-related cell function.

In Chapter 3, a novel density based protein separation technique known as centricollation was employed to elucidate the biological function of TG-2 binding proteins. Centricollation is a stepwise protein separation technology where low volumes can be processed quickly under non-denaturing condition with high recovery yield. This technology is particularly powerful when used together with conventional cell biology methods. TG-2 protein interacting partners were listed based on an unbiased proteomics method (LC-LC/MS) followed by a detailed database search. Ligands bound to TG-2 domains were then pulled down by immunoprecipitation and their identities were determined by western blotting using specific antibodies. The fact that the same molecules were discovered from repeated co-IP experiments increased the confidence of the interaction.

In Chapter 4, the effect of TG-2 on cell migration was studied both *in vitro* via cultured human cornea epithelial cells in cell culture scratch test and non-traumatic cell migration assay, and *in vivo* via TG-$2^{+/+}$ and TG-$2^{-/-}$ mice cornea scratch test. Cell migration speed was quantified in real time and cell directionality was analysed using ImageJ software as well as cell oscillation software developed by our collaborator. The effect of TG-2 on cell proliferation was studied using 3 different experimental approaches consisting of Ki-67 staining, tetrazolium MTS assay and cell cycle progression assay. This was because both Ki-67 staining and tetrazolium MTS assay were not so specific but they could be performed on attached cells; on the other hand, cell cycle progression assay was specific but can only be done on trypsinised cells, which may have some cells lost during the trypsinisation stage.

5.3 Limitations

There were several limitations in this work. Instead of primary human corneal epithelial cells, SV-40 immortalised corneal epithelial cells, which may not be representative of the native human corneal epithelial cells, were used. The use of immortalised cell lines was necessary due to several reasons: for example, primary corneal epithelial cell culture medium was relatively costly; different batches of primary cells had different phenotypes after passaging; the scarcity of human cornea tissues; the translational therapeutic implications of using human cells; as well as the high demand of cells for different types of experiments, such as mitochondrial extraction and overexpression by plasmid transfection.

Since there were only cultured cells used in these experiments, it may be important to conduct experiments on mice with genetically modified TG-2 function in order to verify the *in vivo* relevance of the *in vitro* cell culture data. Another limitation was that only a single sequence of shRNA targeting TG-2 was employed, hence there was a chance of off target effects.

The main limitation of centricollation technique was that particle size could not be used as a criterion to separate entities. Ideally, more purified fractions could be obtained, if centricollation was used together with a size exclusion method, or a technique based on particle diameter such as asymmetric field flow fractionation. Besides, the molecules discovered by mass spectrometry may not be definite ligands in living cells. This is because after cell lysis, TG-2 may non-specifically interact with other molecules. Also,

after cell lysis, molecules that were already sequestered and separated spatially may be brought into close proximity and interacte with TG-2.

When the role of TG-2 in wound healing was evaluated, we tried to rescue TG-2 in the cell migration assay by either adding recombinant human TG-2 protein into the culture media, or by coating the culture surfaces with recombinant human TG-2 protein. However, the rescue effect was inconsistent. This outcome could be due to the inadequate amount of TG-2 added, the added TG-2 had low activity, or the failure of the added TG-2 to localise at the right location. We did not over-express TG-2 in corneal epithelial cells to rescue cell migration because this technique caused cell apoptosis, hence it would require a large amount of cells to produce a confluent cell sheet for scratch test assays.

The interaction between TG-2 and paxillin was not studied using living cells. In co-immunoprecipitation, it was possible that the binding of TG-2 to paxillin may occur after cell lysis and this interaction may not occur within intact living cells. This limitation could be partially overcome by performing live cell imaging with fluorescence labeling of paxillin and TG-2 to check for colocalisation. However, imaging approaches may not work because TG-2 is ubiquitous in all parts of the cell and may colocalise with any other molecule that was expressed.

Results of the kinase screening assays may not be totally relevant in our biological context because these were purely *in vitro* assays consisting of only cell free pure recombinant proteins. In cellular systems, more work could be performed in the future by

deleting or expressing inactive mutants of JNK1 to confirm the *in vivo* effects. However the main focus of this project is not the kinase activity of JNK1 but rather the relationship between TG-2 and JNK1.

5.4 Clinical Significance and Future Studies

The findings in this study suggest that TG-2 plays an important role in ocular surface diseases, especially in cornea wound healing related diseases such as persistent corneal epithelial defects or recurrent corneal erosion in dry eye patients. Hence, TG-2 deserves to be evaluated as a potential therapeutic target. TG-2 related strategies may be used together with conventional therapy, or as an adjuvant therapy.

Since TG-2 is involved in hyperosmolarity-mediated mitochondrial cell death in corneal epithelial cells, mitochondria protecting agents may be important in the treatment of dry eye, such as cyclosporine A (CsA). Literatures reported that CsA could inhibit mitochondrial permeability transition, which is the sudden increase of membrane permeability due to high concentrations of calcium ions causing swelling and uncoupling of the mitochondria, thereby reducing damage and preventing apoptosis [208, 209]. In addition, CsA is already a FDA approved ophthalmic drug commonly used for treatment of chronic dry eye condition to increase tear production [210]. Although topical CsA has shown beneficial effects in treating dry eye disease, many dry eye patients failed to show consistent therapeutic response to CsA [15]. Hence more work remains to be done to determine the effective and safe concentration of CsA for mitochondrial protection in ocular surface. Excitingly, SkQ1, a novel mitochondria-targeted antioxidant molecule aimed to reduce oxidative stress inside mitochondria, was recently reported to have attained positive results in US phase II clinical trial for treatment of dry eye disease, indicating the importance of mitochondrial protection in dry eye treatment.

In addition, TG-2 inhibitors may also be used to protect cells from hyperosmolar stress. Various cell penetrating and non-cell penetrating TG-2 inhibitors such as dansylcadaverine, 3-halo-4,5-dihydroisoxazoles, LDN-27219 and cystamine have been developed [211, 212]. Out of these TG-2 inhibitors, cysteamine, a FDA-approved reduced form of cystamine, has currently entered phase II clinical trial to determine its effectiveness in treating Huntington's disease, in which TG-2 is suspected of participating in its pathogenesis [213]. The development of new and better TG-2 inhibitors remains an active area of research.

This study has demonstrated the effects of TG-2 deficiency on protein transportation, cell adhesion, cell migration and wound closure. Since this work showed that TG-2 could interact with proteins that are involved in cell adhesion and migration, hence there is potential application of TG-2 in treating chronic corneal epithelial wounds that fail to heal within a predicted amount of time as most normal wounds would. TG-2 deficiency may be addressed by increasing TG-2 activity through an appropriate stimulus, such as increasing cytosolic calcium or by overexpressing TG-2 using a cDNA plasmid delivered via an eye drop formulation. Since some growth factors may affect specific cell types and wound healing pathways, it is suggested that combinations of growth factors may be better for complex wounds. For example, topical applications of platelet-derived growth factor (PDGF) and insulin were reported to increase the wound healing rate [214, 215]. Hence, topical TG-2 may be used in conjunction with growth factors such as epidermal growth factor (EGF) and transforming growth factor (TGF)-β1 to improve the corneal wound healing process [216, 217].

Since wound healing is affected in most of the ocular surface diseases, the interaction between paxillin and TG-2 may be important as a potential therapeutic target. In disease conditions, wounds that fail to heal may be improved by increasing this paxillin-TG-2 interaction, leading to the increase in cell adhesion and migration. On the other hand, disrupting this TG-2-paxillin interaction using TG-2 inhibitors may help to improve ocular surface diseases with aggressive cell migration that cause scarring. Since TG-2-paxillin interactions occur inside the cells, it is important to find a TG-2 inhibitor that can effectively penetrate inside cells without causing toxicity.

Cell migration, adhesion and proliferation are important aspects of malignant cancer cells metastasis. During this process of metastasis, cancer cells are dislodged from their primary tumour location, migrated, adhered and proliferated in a secondary environment. This metastasis process employs a similar pathway as wound healing, which also involves cell migration, adhesion and proliferation. As demonstrated by other cancer research, elevated expression of TG-2 has been associated with increased cancer metastasis and cell survival [218, 219]. Hence, strategies that inhibit TG-2 or its interacting proteins may be another direction in cancer research. For example, the identification of TG-2 interacting proteins related to cell migration and adhesion, as well as the discovery that TG-2 levels can affect phosphorylation of adhesion proteins, may have potential in targeting metastatic cancer, or as a new tool to study cell adhesion and migration in cancer research.

The question of whether TG-2 function is indeed beneficial in clinical setup is still under debate. *In vitro* cell culture experiments showed that TG-2-mediated mitochondrial apoptosis appeared to be highly dependent on the nature of the stimulus [117]. Moreover, although there were reports that the ocular surface of dry eye patients have higher expression of TG-2 [220], TG-2 may or may not be directly linked to dry eye disease. Furthermore, in clinical context, dry eye is a multifactorial disease involving immune cells, which is much more complex than *in vitro* cell culture conditions. Also, the role of TG-2 in different stages of the disease may change.

5.5 Conclusion

In conclusion, this thesis showed that TG-2 is involved in mitochondrial-induced apoptosis, cell motility processes and corneal epithelial wound closure. More work needs to be done to better understand the roles and mechanisms of TG-2 in various biological processes. The understanding of these pathways would help to devise combinatorial strategies for inhibition of apoptosis and improvement in ocular wound healing.

Application of TG-2 inhibitors to mouse models of some human diseases, such as Huntington's disease, has shown promising therapeutic potential [211]. However, the safety, efficacy and cellular localisation of TG-2 inhibitors should be evaluated in the context of human ocular cells before being developed into a topical ophthalmic drug.

BIBLIOGRAPHY

1. Knupp, C., et al., *The architecture of the cornea and structural basis of its transparency.* Adv Protein Chem Struct Biol, 2009. **78**: p. 25-49.
2. Lemp, M.A. and H.J. Blackman, *Ocular surface defense mechanisms.* Ann Ophthalmol, 1981. **13**(1): p. 61-3.
3. DelMonte, D.W. and T. Kim, *Anatomy and physiology of the cornea.* J Cataract Refract Surg, 2011. **37**(3): p. 588-98.
4. Klyce SD, B.R., *Structure and function of the cornea.* The cornea, 1987: p. 1–47.
5. Kinoshita, S., et al., *Characteristics of the human ocular surface epithelium.* Prog Retin Eye Res, 2001. **20**(5): p. 639-73.
6. MAURICE, D.M., *Chapter 1 - The Cornea and Sclera.* The Eye (Third Edition), 1984: p. 1-158.
7. Alarcon, I., et al., *Factors impacting corneal epithelial barrier function against Pseudomonas aeruginosa traversal.* Invest Ophthalmol Vis Sci, 2011. **52**(3): p. 1368-77.
8. Darlene A. Dartt, R.D., Patricia D'Amore, Jerry Niederkorn, *Immunology, Inflammation and Diseases of the Eye.* 2011: p. 134-139.
9. Wanda M. Haschek, C.G.R., Matthew A. Wallig, *Toxicology of the eye.* Haschek and Rousseaux's Handbook of Toxicologic Pathology, 2013: p. 2116-2122.
10. Stephen C. Pflugfelder, M.E.S., *Dry Eye: Inflammation of the Lacrimal Functional Unit.* 2005. **1**: p. 11-24.
11. Ohashi, Y., M. Dogru, and K. Tsubota, *Laboratory findings in tear fluid analysis.* Clin Chim Acta, 2006. **369**(1): p. 17-28.

12. Davidson, H.J. and V.J. Kuonen, *The tear film and ocular mucins.* Vet Ophthalmol, 2004. **7**(2): p. 71-7.

13. *The definition and classification of dry eye disease: report of the Definition and Classification Subcommittee of the International Dry Eye WorkShop (2007).* Ocul Surf, 2007. **5**(2): p. 75-92.

14. Tong, L., et al., *Association of tear proteins with Meibomian gland disease and dry eye symptoms.* Br J Ophthalmol, 2011. **95**(6): p. 848-52.

15. Stevenson, W., S.K. Chauhan, and R. Dana, *Dry eye disease: an immune-mediated ocular surface disorder.* Arch Ophthalmol, 2012. **130**(1): p. 90-100.

16. Lopez Bernal, D. and J.L. Ubels, *Artificial tear composition and promotion of recovery of the damaged corneal epithelium.* Cornea, 1993. **12**(2): p. 115-20.

17. Watson, S.L., M.H. Lee, and N.H. Barker, *Interventions for recurrent corneal erosions.* Cochrane Database Syst Rev, 2012. **9**: p. CD001861.

18. Dua, H.S., J.A. Gomes, and A. Singh, *Corneal epithelial wound healing.* Br J Ophthalmol, 1994. **78**(5): p. 401-8.

19. Tong, L., et al., *Molecular mechanism of transglutaminase-2 in corneal epithelial migration and adhesion.* Biochim Biophys Acta, 2013. **1833**(6): p. 1304-1315.

20. Mehta, K., *Mammalian transglutaminases: a family portrait.* Prog Exp Tumor Res, 2005. **38**: p. 1-18.

21. Nurminskaya, M.V. and A.M. Belkin, *Cellular functions of tissue transglutaminase.* Int Rev Cell Mol Biol, 2012. **294**: p. 1-97.

22. Thomazy, V. and L. Fesus, *Differential expression of tissue transglutaminase in human cells. An immunohistochemical study.* Cell Tissue Res, 1989. **255**(1): p. 215-24.

23. Chen, J.S. and K. Mehta, *Tissue transglutaminase: an enzyme with a split personality.* Int J Biochem Cell Biol, 1999. **31**(8): p. 817-36.

24. Metha, K., J. Turpin, and G. Lopez-Berestein, *Induction of tissue transglutaminase in human peripheral blood monocytes by intracellular delivery of retinoids.* Journal of leukocyte biology, 1987. **41**(4): p. 341-8.

25. Iismaa, S.E., et al., *Transglutaminases and disease: lessons from genetically engineered mouse models and inherited disorders.* Physiol Rev, 2009. **89**(3): p. 991-1023.

26. Folk, J.E., et al., *Polyamines as physiological substrates for transglutaminases.* J Biol Chem, 1980. **255**(8): p. 3695-700.

27. Pinkas, D.M., et al., *Transglutaminase 2 undergoes a large conformational change upon activation.* PLoS Biol, 2007. **5**(12): p. e327.

28. Fraij, B.M. and R.A. Gonzales, *Organization and structure of the human tissue transglutaminase gene.* Biochim Biophys Acta, 1997. **1354**(1): p. 65-71.

29. Akimov, S.S., et al., *Tissue transglutaminase is an integrin-binding adhesion coreceptor for fibronectin.* J Cell Biol, 2000. **148**(4): p. 825-38.

30. Zhang, W., et al., *Expression and distribution of tissue transglutaminase in normal and injured rat cornea.* Curr Eye Res, 2004. **28**(1): p. 37-45.

31. Fesus, L., V. Thomazy, and A. Falus, *Induction and activation of tissue transglutaminase during programmed cell death.* FEBS Lett, 1987. **224**(1): p. 104-8.

32. Condello, S., et al., *Transglutaminase 2 and NF-kappaB interplay during NGF-induced differentiation of neuroblastoma cells.* Brain Res, 2008. **1207**: p. 1-8.

33. Jang, G.Y., et al., *Transglutaminase 2 suppresses apoptosis by modulating caspase 3 and NF-kappaB activity in hypoxic tumor cells.* Oncogene, 2010. **29**(3): p. 356-67.

34. Singer, C.F., et al., *Tissue array-based expression of transglutaminase-2 in human breast and ovarian cancer.* Clin Exp Metastasis, 2006. **23**(1): p. 33-9.

35. Belkin, A.M., *Extracellular TG2: emerging functions and regulation.* FEBS J, 2011.

36. Zemskov, E.A., et al., *The role of tissue transglutaminase in cell-matrix interactions.* Front Biosci, 2006. **11**: p. 1057-76.

37. Zemskov, E.A., et al., *Unconventional secretion of tissue transglutaminase involves phospholipid-dependent delivery into recycling endosomes.* PLoS One, 2011. **6**(4): p. e19414.

38. Chou, C.Y., et al., *A crucial sequence for transglutaminase type 2 extracellular trafficking in renal tubular epithelial cells lies in its N-terminal beta-sandwich domain.* J Biol Chem, 2011. **286**(31): p. 27825-35.

39. Iismaa, S.E., et al., *GTP binding and signaling by Gh/transglutaminase II involves distinct residues in a unique GTP-binding pocket.* J Biol Chem, 2000. **275**(24): p. 18259-65.

40. Lorand, L. and R.M. Graham, *Transglutaminases: crosslinking enzymes with pleiotropic functions.* Nat Rev Mol Cell Biol, 2003. **4**(2): p. 140-56.

41. Casadio, R., et al., *The structural basis for the regulation of tissue transglutaminase by calcium ions.* Eur J Biochem, 1999. **262**(3): p. 672-9.

42. Gentile, V., et al., *Isolation and characterization of cDNA clones to mouse macrophage and human endothelial cell tissue transglutaminases.* J Biol Chem, 1991. **266**(1): p. 478-83.

43. Ikura, K., et al., *Amino acid sequence of guinea pig liver transglutaminase from its cDNA sequence.* Biochemistry, 1988. **27**(8): p. 2898-905.

44. Gentile, V., et al., *Expression of tissue transglutaminase in Balb-C 3T3 fibroblasts: effects on cellular morphology and adhesion.* J Cell Biol, 1992. **119**(2): p. 463-74.

45. De Laurenzi, V. and G. Melino, *Gene disruption of tissue transglutaminase.* Mol Cell Biol, 2001. **21**(1): p. 148-55.

46. Nanda, N., et al., *Targeted inactivation of Gh/tissue transglutaminase II.* J Biol Chem, 2001. **276**(23): p. 20673-8.

47. Fesus, L. and M. Piacentini, *Transglutaminase 2: an enigmatic enzyme with diverse functions.* Trends Biochem Sci, 2002. **27**(10): p. 534-9.

48. Szondy, Z., et al., *Transglutaminase 2-/- mice reveal a phagocytosis-associated crosstalk between macrophages and apoptotic cells.* Proc Natl Acad Sci U S A, 2003. **100**(13): p. 7812-7.

49. Bernassola, F., et al., *Role of transglutaminase 2 in glucose tolerance: knockout mice studies and a putative mutation in a MODY patient.* FASEB J, 2002. **16**(11): p. 1371-8.

50. Raghunath, M., et al., *Transglutaminase activity in the eye: cross-linking in epithelia and connective tissue structures.* Invest Ophthalmol Vis Sci, 1999. **40**(12): p. 2780-7.

51. Barathi, V.A., et al., *Transglutaminases (TGs) in ocular and periocular tissues: effect of muscarinic agents on TGs in scleral fibroblasts.* PLoS One, 2011. **6**(4): p. e18326.

52. Png, E., et al., *Hyperosmolarity mediated mitochondrial dysfunction requires transglutaminase-2 in human corneal epithelial cells.* J Cell Physiol, 2010.

53. Sohn, J., et al., *Novel transglutaminase inhibitors reverse the inflammation of allergic conjunctivitis.* J Clin Invest, 2003. **111**(1): p. 121-8.

54. Priglinger, S.G., et al., *Potential role of tissue transglutaminase in glaucoma filtering surgery.* Invest Ophthalmol Vis Sci, 2006. **47**(9): p. 3835-45.

55. Kim, Y.J., et al., *Glutathione transferase (class pi) and tissue transglutaminase (Tgase C) expression in pterygia.* Korean J Ophthalmol, 1998. **12**(1): p. 6-13.

56. Dalzell, M.D., *Dry eye: prevalence, utilization, and economic implications.* Manag Care, 2003. **12**(12 Suppl): p. 9-13.

57. Tovar-Vidales, T., et al., *Tissue transglutaminase expression and activity in normal and glaucomatous human trabecular meshwork cells and tissues.* Invest Ophthalmol Vis Sci, 2008. **49**(2): p. 622-8.

58. Riau, A.K., et al., *Aberrant DNA methylation of matrix remodeling and cell adhesion related genes in pterygium.* PLoS One, 2011. **6**(2): p. e14687.

59. Fujikawa, L.S., et al., *Fibronectin in healing rabbit corneal wounds.* Laboratory investigation; a journal of technical methods and pathology, 1981. **45**(2): p. 120-9.

60. Verderio, E.A., T. Johnson, and M. Griffin, *Tissue transglutaminase in normal and abnormal wound healing: review article.* Amino Acids, 2004. **26**(4): p. 387-404.

61. Gaudry, C.A., et al., *Cell surface localization of tissue transglutaminase is dependent on a fibronectin-binding site in its N-terminal beta-sandwich domain.* J Biol Chem, 1999. **274**(43): p. 30707-14.

62. Xian, X., S. Gopal, and J.R. Couchman, *Syndecans as receptors and organizers of the extracellular matrix.* Cell Tissue Res. **339**(1): p. 31-46.

63. Turner, P.M. and L. Lorand, *Complexation of fibronectin with tissue transglutaminase.* Biochemistry, 1989. **28**(2): p. 628-35.

64. Lorand, L., J.E. Dailey, and P.M. Turner, *Fibronectin as a carrier for the transglutaminase from human erythrocytes.* Proc Natl Acad Sci U S A, 1988. **85**(4): p. 1057-9.

65. Akimov, S.S. and A.M. Belkin, *Cell surface tissue transglutaminase is involved in adhesion and migration of monocytic cells on fibronectin.* Blood, 2001. **98**(5): p. 1567-76.

66. Akimov, S.S. and A.M. Belkin, *Cell-surface transglutaminase promotes fibronectin assembly via interaction with the gelatin-binding domain of*

fibronectin: a role in TGFbeta-dependent matrix deposition. J Cell Sci, 2001. **114**(Pt 16): p. 2989-3000.

67. Suzuki, K., et al., *Cell-matrix and cell-cell interactions during corneal epithelial wound healing.* Prog Retin Eye Res, 2003. **22**(2): p. 113-33.

68. Forsprecher, J., et al., *Enhanced osteoblast adhesion on transglutaminase 2-crosslinked fibronectin.* Amino Acids, 2009. **36**(4): p. 747-53.

69. Martinez, J., et al., *Transglutaminase-mediated processing of fibronectin by endothelial cell monolayers.* Biochemistry, 1994. **33**(9): p. 2538-45.

70. Isobe, T., et al., *Activity-independent cell adhesion to tissue-type transglutaminase is mediated by alpha4beta1 integrin.* Eur J Cell Biol, 1999. **78**(12): p. 876-83.

71. Toth, B., et al., *Over-expression of integrin beta3 can partially overcome the defect of integrin beta3 signaling in transglutaminase 2 null macrophages.* Immunol Lett, 2009. **126**(1-2): p. 22-8.

72. Herman, J.F., L.S. Mangala, and K. Mehta, *Implications of increased tissue transglutaminase (TG2) expression in drug-resistant breast cancer (MCF-7) cells.* Oncogene, 2006. **25**(21): p. 3049-58.

73. Hocking, D.C., J. Sottile, and P.J. McKeown-Longo, *Activation of distinct alpha5beta1-mediated signaling pathways by fibronectin's cell adhesion and matrix assembly domains.* J Cell Biol, 1998. **141**(1): p. 241-53.

74. Verma, A., et al., *Tissue transglutaminase regulates focal adhesion kinase/AKT activation by modulating PTEN expression in pancreatic cancer cells.* Clin Cancer Res, 2008. **14**(7): p. 1997-2005.

75. Janiak, A., E.A. Zemskov, and A.M. Belkin, *Cell surface transglutaminase promotes RhoA activation via integrin clustering and suppression of the Src-p190RhoGAP signaling pathway.* Mol Biol Cell, 2006. **17**(4): p. 1606-19.

76. Elisabetta Verderio*, A.S., *Significance of the Syndecan-4-Transglutaminase-2 Interaction.* TheScientificWorldJOURNAL, 2010.

77. Telci, D., et al., *Fibronectin-tissue transglutaminase matrix rescues RGD-impaired cell adhesion through syndecan-4 and beta1 integrin co-signaling.* J Biol Chem, 2008. **283**(30): p. 20937-47.

78. Guo, S. and L.A. Dipietro, *Factors affecting wound healing.* J Dent Res, 2010. **89**(3): p. 219-29.

79. Dolynchuk, K.N., R. Bendor-Samuel, and J.M. Bowness, *Effect of putrescine on tissue transglutaminase activity in wounds: decreased breaking strength and increased matrix fucoprotein solubility.* Plast Reconstr Surg, 1994. **93**(3): p. 567-73.

80. Clark, L.D., R.K. Clark, and E. Heber-Katz, *A new murine model for mammalian wound repair and regeneration.* Clin Immunol Immunopathol, 1998. **88**(1): p. 35-45.

81. Bowness JM, T.A., Wong T., *Increased transglutaminase activity during skin wound healing in rats.* Biochim Biophys Acta. , 1988.

82. Yiu, T.W., *The role of transglutaminase 2 in cell motility processes and its effect on cutaneous wound healing.* University of New South Wales, 2011.

83. Upchurch, H.F., et al., *Localization of cellular transglutaminase on the extracellular matrix after wounding: characteristics of the matrix bound enzyme.* J Cell Physiol, 1991. **149**(3): p. 375-82.

84. Haroon, Z.A., et al., *Tissue transglutaminase is expressed, active, and directly involved in rat dermal wound healing and angiogenesis.* FASEB J, 1999. **13**(13): p. 1787-95.

85. Raghunath, M., et al., *Cross-linking of the dermo-epidermal junction of skin regenerating from keratinocyte autografts. Anchoring fibrils are a target for tissue transglutaminase.* J Clin Invest, 1996. **98**(5): p. 1174-84.

86. Wang, L., et al., *Lateral Growth Limitation of Corneal Fibrils and Their Lamellar Stacking Depend on Covalent Collagen Cross-linking by Transglutaminase-2 and Lysyl Oxidases, Respectively.* J Biol Chem, 2014. **289**(2): p. 921-9.

87. Priglinger, S.G., et al., *Absence of scar formation in human donor cornea with prior laser in situ keratomileusis.* J Cataract Refract Surg, 2005. **31**(7): p. 1403-8.

88. Lo, S.H., *Focal adhesions: what's new inside.* Dev Biol, 2006. **294**(2): p. 280-91.

89. Turner, C.E., *Paxillin and focal adhesion signalling.* Nat Cell Biol, 2000. **2**(12): p. E231-6.

90. Wozniak, M.A., et al., *Focal adhesion regulation of cell behavior*. Biochim Biophys Acta, 2004. **1692**(2-3): p. 103-19.

91. Burridge, K. and M. Chrzanowska-Wodnicka, *Focal adhesions, contractility, and signaling.* Annu Rev Cell Dev Biol, 1996. **12**: p. 463-518.

92. Berrier, A.L. and K.M. Yamada, *Cell-matrix adhesion.* J Cell Physiol, 2007. **213**(3): p. 565-73.

93. Deakin, N.O. and C.E. Turner, *Paxillin comes of age.* J Cell Sci, 2008. **121**(Pt 15): p. 2435-44.

94. Brown, M.C., J.A. Perrotta, and C.E. Turner, *Serine and threonine phosphorylation of the paxillin LIM domains regulates paxillin focal adhesion localization and cell adhesion to fibronectin.* Mol Biol Cell, 1998. **9**(7): p. 1803-16.

95. Burridge, K., C.E. Turner, and L.H. Romer, *Tyrosine phosphorylation of paxillin and pp125FAK accompanies cell adhesion to extracellular matrix: a role in cytoskeletal assembly.* J Cell Biol, 1992. **119**(4): p. 893-903.

96. Bellis, S.L., et al., *Adhesion of fibroblasts to fibronectin stimulates both serine and tyrosine phosphorylation of paxillin.* Biochem J, 1997. **325 (Pt 2)**: p. 375-81.

97. Tong, L., et al., *A questionnaire-based assessment of symptoms associated with tear film dysfunction and lid margin disease in an Asian population.* Ophthalmic epidemiology, 2009. **16**(1): p. 31-7.

98. Schaller, M.D., *Paxillin: a focal adhesion-associated adaptor protein.* Oncogene, 2001. **20**(44): p. 6459-72.

99. Tong, L., et al., *Phospholipase D in the human ocular surface and in pterygium.* Cornea, 2008. **27**(6): p. 693-8.

100. Bukharova, T., et al., *Paxillin is required for cell-substrate adhesion, cell sorting and slug migration during Dictyostelium development.* J Cell Sci, 2005. **118**(Pt 18): p. 4295-310.

101. Kimura, K., et al., *Role of JNK-dependent serine phosphorylation of paxillin in migration of corneal epithelial cells during wound closure.* Invest Ophthalmol Vis Sci, 2008. **49**(1): p. 125-32.

102. Toth, B., et al., *Transglutaminase 2 is needed for the formation of an efficient phagocyte portal in macrophages engulfing apoptotic cells.* J Immunol, 2009. **182**(4): p. 2084-92.

103. Stephens, P., et al., *Crosslinking and G-protein functions of transglutaminase 2 contribute differentially to fibroblast wound healing responses.* Journal of cell science, 2004. **117**(Pt 15): p. 3389-403.

104. Luo, L., D.Q. Li, and S.C. Pflugfelder, *Hyperosmolarity-induced apoptosis in human corneal epithelial cells is mediated by cytochrome c and MAPK pathways.* Cornea, 2007. **26**(4): p. 452-60.

105. BM, M., et al., *Impaired wound healing and altered fibroblast cytoskeletal dynamics in Gh knockout mice.* 2002. **14**.

106. Balklava, Z., et al., *Analysis of tissue transglutaminase function in the migration of Swiss 3T3 fibroblasts: the active-state conformation of the enzyme does not affect cell motility but is important for its secretion.* J Biol Chem, 2002. **277**(19): p. 16567-75.

107. Hastie, C.J., H.J. McLauchlan, and P. Cohen, *Assay of protein kinases using radiolabeled ATP: a protocol.* Nature protocols, 2006. **1**(2): p. 968-71.

108. Liu, H., et al., *A link between tear instability and hyperosmolarity in dry eye.* Invest Ophthalmol Vis Sci, 2009. **50**(8): p. 3671-9.

109. Gilbard, J.P., R.L. Farris, and J. Santamaria, 2nd, *Osmolarity of tear microvolumes in keratoconjunctivitis sicca.* Arch Ophthalmol, 1978. **96**(4): p. 677-81.

110. Stewart, P., et al., *Effect of experimental dry eye on tear sodium concentration in the mouse.* Eye Contact Lens, 2005. **31**(4): p. 175-8.

111. Chen, Z., et al., *Hyperosmolarity-induced cornification of human corneal epithelial cells is regulated by JNK MAPK.* Invest Ophthalmol Vis Sci, 2008. **49**(2): p. 539-49.

112. Shin, D.M., et al., *Cell type-specific activation of intracellular transglutaminase 2 by oxidative stress or ultraviolet irradiation: implications of transglutaminase 2 in age-related cataractogenesis.* J Biol Chem, 2004. **279**(15): p. 15032-9.

113. Battelli, M.G., et al., *Oxidative stress to human lymphocytes by xanthine oxidoreductase activity.* Free Radic Res, 2001. **35**(6): p. 665-79.

114. Tong, L., et al., *Transglutaminase participates in UVB-induced cell death pathways in human corneal epithelial cells.* Invest Ophthalmol Vis Sci, 2006. **47**(10): p. 4295-301.

115. Niswander, J.M. and L.A. Dokas, *Hyperosmotic stress-induced caspase-3 activation is mediated by p38 MAPK in the hippocampus.* Brain Res, 2007. **1186**: p. 1-11.

116. Yang, P.M., et al., *Cadmium induces Ca2+-dependent necrotic cell death through calpain-triggered mitochondrial depolarization and reactive oxygen species-mediated inhibition of nuclear factor-kappaB activity.* Chem Res Toxicol, 2007. **20**(3): p. 406-15.

117. Tucholski, J. and G.V. Johnson, *Tissue transglutaminase differentially modulates apoptosis in a stimuli-dependent manner.* J Neurochem, 2002. **81**(4): p. 780-91.

118. Galluzzi, L., et al., *Mitochondrial control of cellular life, stress, and death.* Circ Res, 2012. **111**(9): p. 1198-207.

119. Tait, S.W. and D.R. Green, *Mitochondria and cell signalling.* J Cell Sci, 2012. **125**(Pt 4): p. 807-15.

120. Niizuma, K., H. Endo, and P.H. Chan, *Oxidative stress and mitochondrial dysfunction as determinants of ischemic neuronal death and survival.* J Neurochem, 2009. **109 Suppl 1**: p. 133-8.

121. Krasnikov, B.F., et al., *Transglutaminase activity is present in highly purified nonsynaptosomal mouse brain and liver mitochondria.* Biochemistry, 2005. **44**(21): p. 7830-43.

122. Piacentini, M., et al., *Transglutaminase overexpression sensitizes neuronal cell lines to apoptosis by increasing mitochondrial membrane potential and cellular oxidative stress.* J Neurochem, 2002. **81**(5): p. 1061-72.

123. Lesort, M., et al., *Impaired mitochondrial function results in increased tissue transglutaminase activity in situ.* J Neurochem, 2000. **75**(5): p. 1951-61.

124. Rodolfo, C., et al., *Tissue transglutaminase is a multifunctional BH3-only protein.* J Biol Chem, 2004. **279**(52): p. 54783-92.

125. Mastroberardino, P.G., et al., *"Tissue" transglutaminase contributes to the formation of disulphide bridges in proteins of mitochondrial respiratory complexes.* Biochim Biophys Acta, 2006. **1757**(9-10): p. 1357-65.

126. Mathers, W.D., et al., *Model for ocular tear film function.* Cornea, 1996. **15**(2): p. 110-9.

127. Hashimoto, S., et al., *Hyperosmolarity-induced interleukin-8 expression in human bronchial epithelial cells through p38 mitogen-activated protein kinase.* Am J Respir Crit Care Med, 1999. **159**(2): p. 634-40.

128. Shapiro, L. and C.A. Dinarello, *Hyperosmotic stress as a stimulant for proinflammatory cytokine production.* Exp Cell Res, 1997. **231**(2): p. 354-62.

129. Park, D., S.S. Choi, and K.S. Ha, *Transglutaminase 2: a multi-functional protein in multiple subcellular compartments.* Amino acids, 2010. **39**(3): p. 619-31.

130. Szondy, Z., et al., *Tissue transglutaminase (TG2) protects cardiomyocytes against ischemia/reperfusion injury by regulating ATP synthesis.* Cell Death Differ, 2006. **13**(10): p. 1827-9.

131. Virag, L. and C. Szabo, *BCL-2 protects peroxynitrite-treated thymocytes from poly(ADP-ribose) synthase (PARS)-independent apoptotic but not from PARS-mediated necrotic cell death.* Free Radic Biol Med, 2000. **29**(8): p. 704-13.

132. Chen, J.S., et al., *Drug-resistant breast carcinoma (MCF-7) cells are paradoxically sensitive to apoptosis.* J Cell Physiol, 2004. **200**(2): p. 223-34.

133. Shin, D.M., et al., *TGFbeta mediates activation of transglutaminase 2 in response to oxidative stress that leads to protein aggregation.* FASEB J, 2008. **22**(7): p. 2498-507.

134. Tatsukawa, H., et al., *Role of transglutaminase 2 in liver injury via cross-linking and silencing of transcription factor Sp1.* Gastroenterology, 2009. **136**(5): p. 1783-95 e10.

135. Milakovic, T., et al., *Intracellular localization and activity state of tissue transglutaminase differentially impacts cell death.* The Journal of biological chemistry, 2004. **279**(10): p. 8715-22.

136. Lesort, M., et al., *Distinct nuclear localization and activity of tissue transglutaminase.* J Biol Chem, 1998. **273**(20): p. 11991-4.

137. Kucerova, R., et al., *Cell surface glycoconjugate abnormalities and corneal epithelial wound healing in the pax6+/- mouse model of aniridia-related keratopathy.* Invest Ophthalmol Vis Sci, 2006. **47**(12): p. 5276-82.

138. McClintock, J.L. and B.P. Ceresa, *Transforming growth factor-{alpha} enhances corneal epithelial cell migration by promoting EGFR recycling.* Invest Ophthalmol Vis Sci, 2010. **51**(7): p. 3455-61.

139. Shankardas, J., M. Senchyna, and S.D. Dimitrijevich, *Presence and distribution of 14-3-3 proteins in human ocular surface tissues.* Mol Vis, 2008. **14**: p. 2604-15.

140. Mhawech, P., *14-3-3 proteins--an update.* Cell Res, 2005. **15**(4): p. 228-36.

141. Zemskov, E.A., et al., *Cell-surface transglutaminase undergoes internalization and lysosomal degradation: an essential role for LRP1.* J Cell Sci, 2007. **120**(Pt 18): p. 3188-99.

142. Wu, L. and S.L. Gonias, *The low-density lipoprotein receptor-related protein-1 associates transiently with lipid rafts.* J Cell Biochem, 2005. **96**(5): p. 1021-33.

143. Milano, S.K., et al., *Nonvisual arrestin oligomerization and cellular localization are regulated by inositol hexakisphosphate binding.* J Biol Chem, 2006. **281**(14): p. 9812-23.

144. de Araujo, M.E., L.A. Huber, and T. Stasyk, *Isolation of endocitic organelles by density gradient centrifugation.* Methods Mol Biol, 2008. **424**: p. 317-31.

145. de Pereda, J.M., et al., *Advances and perspectives of the architecture of hemidesmosomes: lessons from structural biology.* Cell Adh Migr, 2009. **3**(4): p. 361-4.

146. Dowling, J., Q.C. Yu, and E. Fuchs, *Beta4 integrin is required for hemidesmosome formation, cell adhesion and cell survival.* J Cell Biol, 1996. **134**(2): p. 559-72.

147. Spinardi, L., et al., *A recombinant tail-less integrin beta 4 subunit disrupts hemidesmosomes, but does not suppress alpha 6 beta 4-mediated cell adhesion to laminins.* J Cell Biol, 1995. **129**(2): p. 473-87.

148. Niessen, C.M., et al., *Deficiency of the integrin beta 4 subunit in junctional epidermolysis bullosa with pyloric atresia: consequences for hemidesmosome formation and adhesion properties.* J Cell Sci, 1996. **109 (Pt 7)**: p. 1695-706.

149. Pullar, C.E., et al., *beta4 integrin and epidermal growth factor coordinately regulate electric field-mediated directional migration via Rac1*. Mol Biol Cell, 2006. **17**(11): p. 4925-35.

150. Germain, E.C., T.M. Santos, and I. Rabinovitz, *Phosphorylation of a novel site on the {beta}4 integrin at the trailing edge of migrating cells promotes hemidesmosome disassembly.* Mol Biol Cell, 2009. **20**(1): p. 56-67.

151. Joly, D., et al., *Beta4 integrin and laminin 5 are aberrantly expressed in polycystic kidney disease: role in increased cell adhesion and migration.* Am J Pathol, 2003. **163**(5): p. 1791-800.

152. Chaurasia, S.S., et al., *Dynamics of the expression of intermediate filaments vimentin and desmin during myofibroblast differentiation after corneal injury.* Exp Eye Res, 2009. **89**(2): p. 133-9.

153. Capetanaki, Y., D.J. Milner, and G. Weitzer, *Desmin in muscle formation and maintenance: knockouts and consequences.* Cell Struct Funct, 1997. **22**(1): p. 103-16.

154. Maddala, R. and V.P. Rao, *alpha-Crystallin localizes to the leading edges of migrating lens epithelial cells.* Exp Cell Res, 2005. **306**(1): p. 203-15.

155. Rivero, S., et al., *Microtubule nucleation at the cis-side of the Golgi apparatus requires AKAP450 and GM130.* EMBO J, 2009. **28**(8): p. 1016-28.

156. Seemann, J., E.J. Jokitalo, and G. Warren, *The role of the tethering proteins p115 and GM130 in transport through the Golgi apparatus in vivo.* Mol Biol Cell, 2000. **11**(2): p. 635-45.

157. Cordell, P.A., et al., *Association of coagulation factor XIII-A with Golgi proteins within monocyte-macrophages: implications for subcellular trafficking and secretion.* Blood, 2010. **115**(13): p. 2674-81.

158. Diao, A., et al., *Coordination of golgin tethering and SNARE assembly: GM130 binds syntaxin 5 in a p115-regulated manner.* J Biol Chem, 2008. **283**(11): p. 6957-67.

159. Kodani, A., et al., *GM130-dependent control of Cdc42 activity at the Golgi regulates centrosome organization.* Mol Biol Cell, 2009. **20**(4): p. 1192-200.

160. Diederichs, S., et al., *S100 family members and trypsinogens are predictors of distant metastasis and survival in early-stage non-small cell lung cancer.* Cancer Res, 2004. **64**(16): p. 5564-9.

161. Hockla, A., D.C. Radisky, and E.S. Radisky, *Mesotrypsin promotes malignant growth of breast cancer cells through shedding of CD109.* Breast Cancer Res Treat, 2009.

162. Rinderknecht, H., et al., *Mesotrypsin: a new inhibitor-resistant protease from a zymogen in human pancreatic tissue and fluid.* Gastroenterology, 1984. **86**(4): p. 681-92.

163. Jiang, G., et al., *PRSS3 promotes tumour growth and metastasis of human pancreatic cancer.* Gut, 2010. **59**(11): p. 1535-44.

164. Yamauchi, J., et al., *Ras activation of a Rac1 exchange factor, Tiam1, mediates neurotrophin-3-induced Schwann cell migration.* Proc Natl Acad Sci U S A, 2005. **102**(41): p. 14889-94.

165. Yamauchi, J., et al., *The neurotrophin-3 receptor TrkC directly phosphorylates and activates the nucleotide exchange factor Dbs to enhance Schwann cell migration.* Proc Natl Acad Sci U S A, 2005. **102**(14): p. 5198-203.

166. Sekine, S., et al., *Rhomboid protease PARL mediates the mitochondrial membrane potential loss-induced cleavage of PGAM5.* J Biol Chem, 2012. **287**(41): p. 34635-45.

167. da Silva, A.F., et al., *Mitochondria dynamism: of shape, transport and cell migration.* Cell Mol Life Sci, 2014. **71**(12): p. 2313-24.

168. Sudhof, T.C. and J.E. Rothman, *Membrane fusion: grappling with SNARE and SM proteins.* Science, 2009. **323**(5913): p. 474-7.

169. Hackmann, Y., et al., *Syntaxin binding mechanism and disease-causing mutations in Munc18-2.* Proc Natl Acad Sci U S A, 2013. **110**(47): p. E4482-91.

170. Gonon, E.M., et al., *SNARE-mediated membrane traffic modulates RhoA-regulated focal adhesion formation.* FEBS Lett, 2005. **579**(27): p. 6169-78.

171. Skalski, M. and M.G. Coppolino, *SNARE-mediated trafficking of alpha5beta1 integrin is required for spreading in CHO cells.* Biochemical and biophysical research communications, 2005. **335**(4): p. 1199-210.

172. Gaudry, C.A., et al., *Tissue transglutaminase is an important player at the surface of human endothelial cells: evidence for its externalization and its colocalization with the beta(1) integrin.* Exp Cell Res, 1999. **252**(1): p. 104-13.

173. Jones, R.A., et al., *Reduced expression of tissue transglutaminase in a human endothelial cell line leads to changes in cell spreading, cell adhesion and reduced polymerisation of fibronectin.* J Cell Sci, 1997. **110 (Pt 19)**: p. 2461-72.

174. Menter, D.G., et al., *Transglutaminase stabilizes melanoma adhesion under laminar flow.* Cell Biophys, 1991. **18**(2): p. 123-43.

175. Priglinger, S.G., et al., *TGF-beta2-induced cell surface tissue transglutaminase increases adhesion and migration of RPE cells on fibronectin through the gelatin-binding domain.* Invest Ophthalmol Vis Sci, 2004. **45**(3): p. 955-63.

176. Allen, W.E., et al., *Rho, Rac and Cdc42 regulate actin organization and cell adhesion in macrophages.* J Cell Sci, 1997. **110 (Pt 6)**: p. 707-20.

177. Nobes, C.D. and A. Hall, *Rho, rac, and cdc42 GTPases regulate the assembly of multimolecular focal complexes associated with actin stress fibers, lamellipodia, and filopodia.* Cell, 1995. **81**(1): p. 53-62.

178. Stepp, M.A., *Corneal integrins and their functions.* Exp Eye Res, 2006. **83**(1): p. 3-15.

179. Nurminskaya, M.V. and A.M. Belkin, *Cellular functions of tissue transglutaminase.* International review of cell and molecular biology, 2012. **294**: p. 1-97.

180. Kotsakis, P., et al., *The role of tissue transglutaminase (TG2) in regulating the tumour progression of the mouse colon carcinoma CT26.* Amino Acids, 2011. **41**(4): p. 909-21.

181. Contreras, A., et al., *The dynamic mobility of histone H1 is regulated by cyclin/CDK phosphorylation.* Mol Cell Biol, 2003. **23**(23): p. 8626-36.

182. Robitaille, K., et al., *Tissue transglutaminase triggers oligomerization and activation of dual leucine zipper-bearing kinase in calphostin C-treated cells to facilitate apoptosis.* Cell Death Differ, 2004. **11**(5): p. 542-9.

183. Mangala, L.S., et al., *Tissue transglutaminase-induced alterations in extracellular matrix inhibit tumor invasion.* Mol Cancer, 2005. **4**: p. 33.

184. Jensen, M.H., E.J. Morris, and D.A. Weitz, *Mechanics and dynamics of reconstituted cytoskeletal systems.* Biochim Biophys Acta, 2015.

185. Yu, F.X., I.K. Gipson, and Y. Guo, *Differential gene expression in healing rat corneal epithelium.* Investigative ophthalmology & visual science, 1995. **36**(10): p. 1997-2007.

186. Takahashi, H., et al., *Tissue transglutaminase, coagulation factor XIII, and the pro-polypeptide of von Willebrand factor are all ligands for the integrins alpha 9beta 1 and alpha 4beta 1.* J Biol Chem, 2000. **275**(31): p. 23589-95.

187. Park, M.K., et al., *Novel participation of transglutaminase-2 through c-Jun N-terminal kinase activation in sphingosylphosphorylcholine-induced keratin reorganization of PANC-1 cells.* Biochimica et biophysica acta, 2011. **1811**(12): p. 1021-9.

188. Sit, S.T. and E. Manser, *Rho GTPases and their role in organizing the actin cytoskeleton.* Journal of cell science, 2011. **124**(Pt 5): p. 679-83.

189. Colak, G. and G.V. Johnson, *Complete transglutaminase 2 ablation results in reduced stroke volumes and astrocytes that exhibit increased survival in response to ischemia.* Neurobiology of disease, 2012. **45**(3): p. 1042-50.

190. Goldmann, W.H. and D.E. Ingber, *Intact vinculin protein is required for control of cell shape, cell mechanics, and rac-dependent lamellipodia formation.* Biochem Biophys Res Commun, 2002. **290**(2): p. 749-55.

191. Subauste, M.C., et al., *Vinculin modulation of paxillin-FAK interactions regulates ERK to control survival and motility.* J Cell Biol, 2004. **165**(3): p. 371-81.

192. Gentile, V., *Physiopathological roles of human transglutaminase 2.* Advances in enzymology and related areas of molecular biology, 2011. **78**: p. 47-95.

193. Deramaudt, T.B., et al., *FAK phosphorylation at Tyr-925 regulates cross-talk between focal adhesion turnover and cell protrusion.* Mol Biol Cell, 2011. **22**(7): p. 964-75.

194. Wang, Z., et al., *RGD-independent cell adhesion via a tissue transglutaminase-fibronectin matrix promotes fibronectin fibril deposition and requires syndecan-4/2 and {alpha}5{beta}1 integrin co-signaling.* J Biol Chem, 2010. **285**(51): p. 40212-29.

195. Huang, Z., D.P. Yan, and B.X. Ge, *JNK regulates cell migration through promotion of tyrosine phosphorylation of paxillin.* Cell Signal, 2008. **20**(11): p. 2002-12.

196. Varela, J.C., et al., *Microarray analysis of gene expression patterns during healing of rat corneas after excimer laser photorefractive keratectomy.* Investigative ophthalmology & visual science, 2002. **43**(6): p. 1772-82.

197. Schaller, M.D. and J.T. Parsons, *pp125FAK-dependent tyrosine phosphorylation of paxillin creates a high-affinity binding site for Crk.* Mol Cell Biol, 1995. **15**(5): p. 2635-45.

198. Mishra, S. and L.J. Murphy, *Tissue transglutaminase has intrinsic kinase activity: identification of transglutaminase 2 as an insulin-like growth factor-binding protein-3 kinase.* J Biol Chem, 2004. **279**(23): p. 23863-8.

199. Mishra, S. and L.J. Murphy, *The p53 oncoprotein is a substrate for tissue transglutaminase kinase activity.* Biochem Biophys Res Commun, 2006. **339**(2): p. 726-30.

200. Mishra, S., et al., *Phosphorylation of histones by tissue transglutaminase.* J Biol Chem, 2006. **281**(9): p. 5532-8.

201. Huang, C., et al., *JNK phosphorylates paxillin and regulates cell migration.* Nature, 2003. **424**(6945): p. 219-23.

202. Park, M.K., et al., *Novel participation of transglutaminase-2 through c-Jun N-terminal kinase activation in sphingosylphosphorylcholine-induced keratin reorganization of PANC-1 cells.* Biochim Biophys Acta, 2011. **1811**(12): p. 1021-9.

203. Gayer, C.P., et al., *Delineating the signals by which repetitive deformation stimulates intestinal epithelial migration across fibronectin.* American journal of physiology. Gastrointestinal and liver physiology, 2009. **296**(4): p. G876-85.

204. Miyamoto, Y., et al., *Paxillin is the target of c-Jun N-terminal kinase in Schwann cells and regulates migration.* Cell Signal, 2012. **24**(11): p. 2061-9.

205. Robitaille, K., et al., *Calphostin C-induced apoptosis is mediated by a tissue transglutaminase-dependent mechanism involving the DLK/JNK signaling pathway.* Cell Death Differ, 2008. **15**(9): p. 1522-31.

206. Png, E. and L. Tong, *Transglutaminase-2 in cell adhesion: All roads lead to paxillin?* Cell Adh Migr, 2013. **7**(5): p. 412-417.

207. Gundemir, S., et al., *Transglutaminase 2: a molecular Swiss army knife.* Biochim Biophys Acta, 2012. **1823**(2): p. 406-19.

208. Friberg, H., et al., *Cyclosporin A, but not FK 506, protects mitochondria and neurons against hypoglycemic damage and implicates the mitochondrial permeability transition in cell death.* J Neurosci, 1998. **18**(14): p. 5151-9.

209. Halestrap, A.P., et al., *Cyclosporin A binding to mitochondrial cyclophilin inhibits the permeability transition pore and protects hearts from ischaemia/reperfusion injury.* Mol Cell Biochem, 1997. **174**(1-2): p. 167-72.

210. Kymionis, G.D., et al., *Treatment of chronic dry eye: focus on cyclosporine.* Clin Ophthalmol, 2008. **2**(4): p. 829-36.

211. Siegel, M. and C. Khosla, *Transglutaminase 2 inhibitors and their therapeutic role in disease states.* Pharmacol Ther, 2007. **115**(2): p. 232-45.

212. Badarau, E., R.J. Collighan, and M. Griffin, *Recent advances in the development of tissue transglutaminase (TG2) inhibitors.* Amino Acids, 2013. **44**(1): p. 119-27.

213. Borrell-Pages, M., et al., *Cystamine and cysteamine increase brain levels of BDNF in Huntington disease via HSJ1b and transglutaminase.* J Clin Invest, 2006. **116**(5): p. 1410-24.

214. Lynch, S.E., et al., *Role of platelet-derived growth factor in wound healing: synergistic effects with other growth factors.* Proc Natl Acad Sci U S A, 1987. **84**(21): p. 7696-700.

215. Servold, S.A., *Growth factor impact on wound healing.* Clin Podiatr Med Surg, 1991. **8**(4): p. 937-53.

216. Pastor, J.C. and M. Calonge, *Epidermal growth factor and corneal wound healing. A multicenter study.* Cornea, 1992. **11**(4): p. 311-4.

217. He, J. and H.E. Bazan, *Epidermal growth factor synergism with TGF-beta1 via PI-3 kinase activity in corneal keratocyte differentiation.* Invest Ophthalmol Vis Sci, 2008. **49**(7): p. 2936-45.

218. Chhabra, A., A. Verma, and K. Mehta, *Tissue transglutaminase promotes or suppresses tumors depending on cell context.* Anticancer Res, 2009. **29**(6): p. 1909-19.

219. Kumar, S. and K. Mehta, *Tissue transglutaminase, inflammation, and cancer: how intimate is the relationship?* Amino Acids, 2011.

220. Aragona, P., et al., *Matrix metalloproteinase 9 and transglutaminase 2 expression at the ocular surface in patients with different forms of dry eye disease.* Ophthalmology, 2015. **122**(1): p. 62-71.

221. Araki-Sasaki, K., et al., *An SV40-immortalized human corneal epithelial cell line and its characterization.* Invest Ophthalmol Vis Sci, 1995. **36**(3): p. 614-21.

APPENDICES

Appendix A. List of Laboratory Techniques

A1. Cell Culture

A1.1. Immortalised Human Corneal Epithelial Cells

Primary human cornea epithelial cells were immortalised using recombinant simian virus 40 (SV40)-adenovirus vector [221]. This cell line retains the properties of normal corneal epithelial cells and has well developed desmosomes at intracellular junctions. In this thesis, this cell line will be referred as HCE-T, as large T antigen was expressed in every immortalised cell. Studies used passages from 80 to 98. The cells were grown in Dulbeco's modified Eagle's medium (DMEM)-F12 supplemented with 5% fetal bovine serum (FBS).

A1.2. Scrambled shRNA and shTG Cells

In this thesis, shTG referred to HCE-T cells stably transduced with short hair pin RNA (shRNA) targeting TG-2; while scrambled shRNA cells referred to HCE-T cells stably transduced with non-specific scrambled shRNA.

The sense and anti-sense sequences (5' to 3') of SiRNA against TG-2 were GGCCCGUUUUCCACUAAGAtt and UCUUAGUGGAAAACGGGCCtt respectively. This SiRNA targeted part of exon 3 of the TG-2 gene.

1. To study the effect of TG-2 reduction, silencing short hairpin RNA targeting TG-2 was subcloned into the pSM2 backbone.

2. Lipofectamine Plus reagent (Invitrogen, Grand Island, NY) was used to transfect the cloned vectors with retroviral packaging cell line PA317.
3. Six hours later, the medium was changed to fresh DMEM supplemented with 10% FBS, streptomycin (100 g/ml), penicillin (100 U/ml), and 2mML-glutamine, and cultured at 37ºC in 5% CO_2.
4. Viral supernatants from transiently transfected PA317 cells were then filtered with 0.45µm filters and stored at -80ºC.
5. HCE-T cells were seeded and allowed to adhere.
6. Twenty-four hours later, medium was replaced with the filtered viral supernatants.
7. Polybrene was added at 8 g/ml and cultured for 3 days.
8. Stably transduced cells were subsequently expanded in DMEM-F12 supplemented with 5% FBS and 0.15 g/ml of puromycin.

A1.3. Trypsinizing, Counting and Passaging Cells

1. Trypsin 0.05% (Invitrogen, Grand Island, NY) was warmed to 37ºC before use.
2. Cells were washed once in sterile phosphate buffered saline (PBS).
3. The volume of trypsin used should cover the surface of the cultured cells.
4. After the addition of trypsin, cells were incubated at 37ºC, 5% CO_2 for 5 to 10 minutes.
5. Gentle rocking was done to ensure complete detachment of cells from the dish.
6. Complete media with 5% FBS was added to neutralize the trypsin.
7. The cells were then centrifuged at 800-1000rpm for 5 minutes.

8. The supernatant was removed. The cell pellet was reconstituted with fresh complete media.
9. To count the cells, 10µL of tryphan blue was added to 10µL cell suspension.
10. 10µL of the tryphan blue/cell mixture was added into hemacytometer channel.
11. Cells were counted at all the 4 quadrants.
12. Desired amount of cells were seeded into new culture vessels.

A1.4. Freezing and Thawing cells

1. A freezing mixture of 70% complete media, 20% FBS and 10% DMSO was prepared.
2. At least one million cells were added to the freezing mixture in a cryo tube.
3. The cryo tubes were then placed into a freezing container containing isopropanol, and placed overnight at -80ºC.
4. The cryo tubes were then transferred into liquid nitrogen for long term storage.
5. Cells to be thawed in cryo vials were removed from liquid nitrogen and placed on ice.
6. One milliliter of warm complete media was added into the cryo vial to thaw the cells.
7. After complete thawing, the cells were spun down using similar centrifuge settings as passaging.
8. After aspiration of the supernatant, fresh culture media were added to re-suspend the cells.

Cells were then seeded and incubated in 5% CO_2, 37ºC.

A2. Preparation of Plasmids and Transfection

A2.1. Preparation of Luria-Bertani (LB) Broth and Agar Plate

1. LB broth and agar was made by adding LB broth pellet or LB agar powder to distilled water, as recommended by manufacturer.
2. The liquid broth and agar was then autoclaved.
3. Antibiotics such as kanamycin or ampicillin were added into the LB broth just before any experiment to facilitate selection of bacteria.
4. The LB broth was stored at room temperature.
5. For the LB agar, antibiotics were added to the liquid agar after cooling to 55ºC. About 20ml of agar was poured into each 10cm plate.
6. The poured agar plates were then cooled down before stored at 4ºC.

A2.2. Propagation of Plasmid DNA Expressing TG-2 Fragments

1. Four TG-2 domains: C terminal 1 (T1), C terminal 2 (T2), catalytic core (C), and N terminal (N) fragments were cloned respectively into pIRES-hrGFP II plasmid vector expressing Flag-tagged peptides (Figure A1). These plasmid DNAs were cloned by GenScript, NJ, USA.
2. The four TG-2 domains sequences were shown in Figure A2. These sequences were confirmed by DNA sequencing services (1st Base, Singapore) using primer as follows: 5’ - ATG GGC GGT AGG CGT GTA - 3’

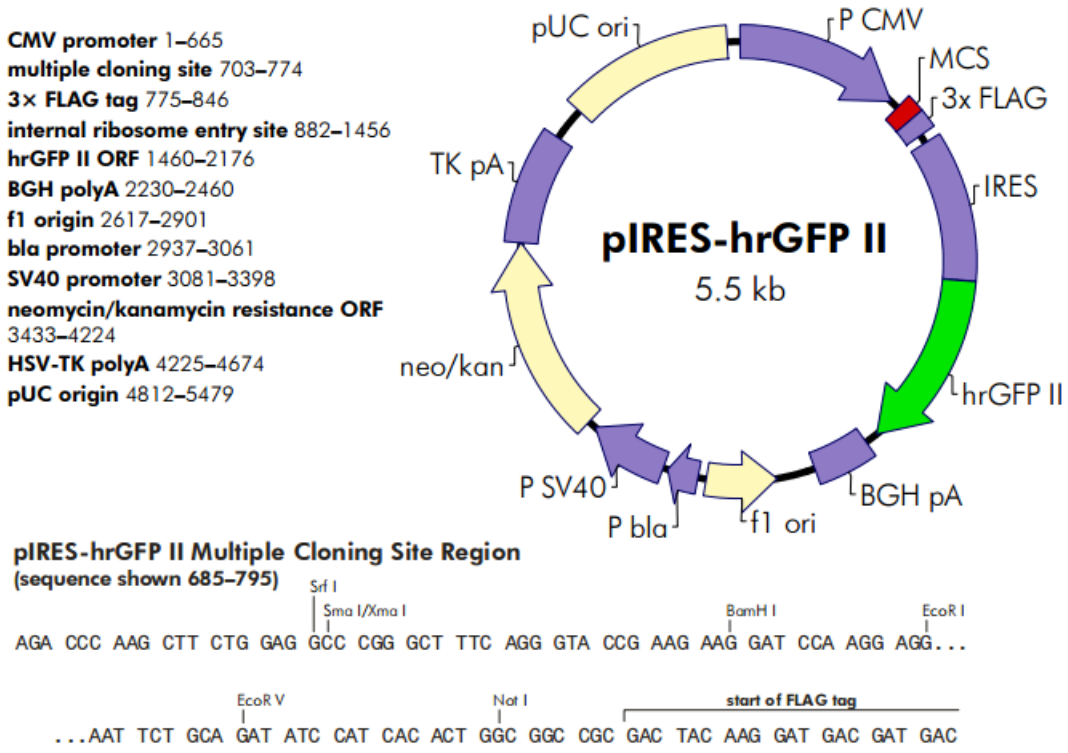

Figure A1. Circular map and features of pIRES-hrGFP II expression vector (Agilent Technologies, CA, USA). The piRES-hrGFPII vector is 5.5kb, contains a CMV promoter, neomycin/kanamycin-resistance gene, SV40 early promoter providing G418 resistance in mammalian cells and a bovine growth hormone polyadenylation sequence (BGHpA) for improved stability and translatability of mRNA. The gene of interest may be fused to three tandem FLAG epitopes.

TG-2 N Terminal (435 bp) ~16kD

GCCACCATGGCCGAGGAGCTGGTCTTAGAGAGGTGTGATCTGGAGCTGGAGACCAATGGCCG
AGACCACCACACGGCCGACCTGTGCCGGGAGAAGCTGGTGGTGCGACGGGGCCAGCCCTTCT
GGCTGACCCTGCACTTTGAGGGCCGCAACTACGAGGCCAGTGTAGACAGTCTCACCTTCAGTG
TCGTGACCGGCCCAGCCCCTAGCCAGGAGGCCGGGACCAAGGCCCGTTTTCCACTAAGAGAT
GCTGTGGAGGAGGGTGACTGGACAGCCACCGTGGTGGACCAGCAAGACTGCACCCTCTCGCT
GCAGCTCACCACCCCGGCCAACGCCCCCATCGGCCTGTATCGCCTCAGCCTGGAGGCCTCCAC
TGGCTACCAGGGATCCAGCTTTGTGCTGGGCCACTTCATTTTG CTCTTCAACGCCTGGTGC

TG-2 core (981 bp) ~37kD

GCC ACC ATG GCA GCG GAT GCT GTG TAC CTG GAC TCG GAA GAG GAG CGG CAG GAG
TAT GTC CTC ACC CAG CAG GGC TTT ATC TAC CAG GGC TCG GCC AAG TTC ATC AAG
AAC ATA CCT TGG AAT TTT GGG CAG TTT GAA GAT GGG ATC CTA GAC ATC TGC CTG ATC
CTT CTA GAT GTC AAC CCC AAG TTC CTG AAG AAC GCC GGC CGT GAC TGC TCC CGC
CGC AGC AGC CCC GTC TAC GTG GGC CGG GTG GTG AGT GGC ATG GTC AAC TGC AAC
GAT GAC CAG GGT GTG CTG CTG GGA CGC TGG GAC AAC AAC TAC GGG GAC GGC GTC
AGC CCC ATG TCC TGG ATC GGC AGC GTG GAC ATC CTG CGG CGC TGG AAG AAC CAC
GGC TGC CAG CGC GTC AAG TAT GGC CAG TGC TGG GTC TTC GCC GCC GTG GCC TGC
ACA GTG CTG AGG TGC CTG GGC ATC CCT ACC CGC GTC GTG ACC AAC TAC AAC TCG
GCC CAT GAC CAG AAC AGC AAC CTT CTC ATC GAG TAC TTC CGC AAT GAG TTT GGG
GAG ATC CAG GGT GAC AAG AGC GAG ATG ATC TGG AAC TTC CAC TGC TGG GTG GAG
TCG TGG ATG ACC AGG CCG GAC CTG CAG CCG GGG TAC GAG GGC TGG CAG GCC CTG
GAC CCA ACG CCC CAG GAG AAG AGC GAA GGG ACG TAC TGC TGT GGC CCA GTT CCA
GTT CGT GCC ATC AAG GAG GGC GAC CTG AGC ACC AAG TAC GAT GCG CCC TTT GTC
TTT GCG GAG GTC AAT GCC GAC GTG GTA GAC TGG ATC CAG CAG GAC GAT GGG TCT
GTG CAC AAA TCC ATC AAC CGT TCC CTG ATC GTT GGG CTG AAG ATC AGC ACT AAG
AGC GTG GGC CGA GAC GAG CGG GAG GAT ATC ACC CAC ACC TAC AAA TAC CCA GAG
GGG TCC TCA GAG GAG AGG GAG GCC TTC ACA AGG GCG AAC CAC CTG AAC AAA CTG
GCC GAG

TG-2 Terminal 1 (372 bp) ~15kD

GCCACCATGGAGAAGGAGGAGACAGGGATGGCCATGCGGATCCGTGTGGGCCAGAGCATGA
ACATGGGCAGTGACTTTGACGTCTTTGCCCACATCACCAACAACACCGCTGAGGAGTACGTCT
GCCGCCTCCTGCTCTGTGCCCGCACCGTCAGCTACAATGGGATCTTGGGGCCCGAGTGTGGCA
CCAAGTACCTGCTCAACCTCAACCTGGAGCCTTTCTCTGAGAAGAGCGTTCCTCTTTGCATCCT
CTATGAGAAATACCGTGACTGCCTTACGGAGTCCAACCTCATCAAGGTGCGGGCCCTCCTCGT
GGAGCCAGTTATCAACAGCTACCTGCTGGCTGAGAGGGACCTCTACCTGGAGAATCCA

TG-2 Terminal 2 (321 bp) ~12kD

GCCACCATGGTGGAGAATCCAGAAATCAAGATCCGGATCCTTGGGGAGCCCAAGCAGAAACG
CAAGCTGGTGGCTGAGGTGTCCCTGCAGAACCCGCTCCCTGTGGCCCTGGAAGGCTGCACCTT
CACTGTGGAGGGGGCCGGCCTGACTGAGGAGCAGAAGACGGTGGAGATCCCAGACCCCGTGG
AGGCAGGGGAGGAAGTTAAGGTGAGAATGGACCTGCTGCCGCTCCACATGGGCCTCCACAAG
CTGGTGGTGAACTTCGAGAGCGACAAGCTGAAGGCTGTGAAGGGCTTCCGGAATGTCATCATT
GGCCCCGCC

Figure A2. Nucleotide sequences of human TG-2 four fragments: N terminal, catalytic core, N-Terminal 1 and N-Terminal 2.

A2.3. Plasmid DNA Over-Expressing TG-2

1. Over-expression of TG-2 was achieved by a cDNA plasmid pSG5 coding for TG-2 (referred to as pSG5 TG-2 in thesis).
2. As controls, transfection with the pSG5 vector (Figure A3) was used.

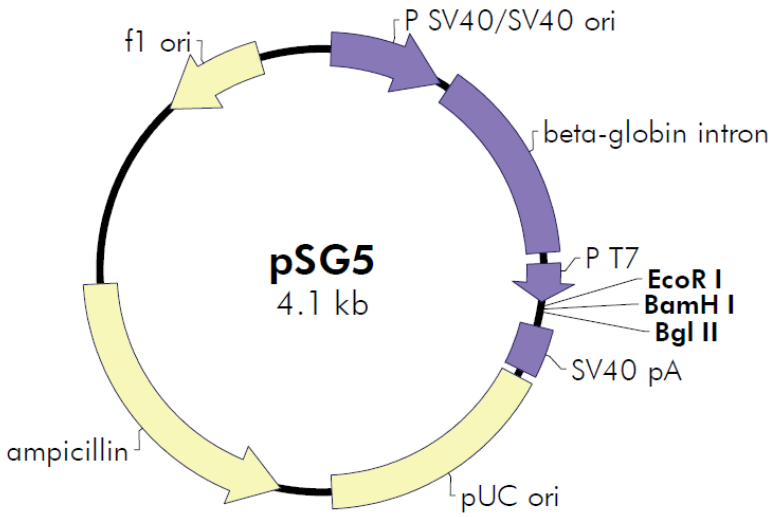

Feature	Nucleotide Position
SV40 promoter and SV40 origin of replication	28–366
β-globin intron	395–967
T7 promoter	1022–1040
EcoR I	1043
BamH I	1049
Bgl II	1055
SV40 polyA signal	1069–1202
pUC origin of replication	1342–2009
ampicillin resistance (*bla*) ORF	2160–3017
f1 origin of ss-DNA replication	3587–3893

Figure A3. Circular map and features of pSG5 vector (Agilent Technologies, CA, USA). The pSG5 vector is a eukaryotic expression vector which is 4.1kb in size. The gene of interest can be ligated into the vector via restriction sites EcoR I, BamH I, and Bgl II. The f1 origin can rescue ssDNA, the SV40 (simian virus 40) early promoter and origin allows overexpression of the recombinant gene, the T7 bacteriophage promoter mediates transcription of cloned inserts, and the β-globin intron II splices expressed transcripts.

A2.4. Plasmid Propagation, DNA Extraction, Purification and Quantification

1. The lyophilized plasmid DNA was dissolved in 20µL water and vortex diligently.
2. A tube of DH5α competent cells was thawed on ice.
3. The cells were gently mixed with pipette tip. 50µl of cells were aliquoted for each transformation reaction into a 1.5 ml microcentrifuge tube.
4. Five nanogram of plasmid DNA was added to the cells followed by gentle mixing.
5. The tubes were incubated on ice for 30 minutes.
6. The competent cells were heat shocked in a 42°C water bath for 20 seconds without shaking.
7. Tubes were then placed on ice for 2 minutes.
8. Pre-warmed 950µl of DMEM-F12 media was added to each tube.
9. The tubes were incubated at 37°C for 1 hour, shaking at 225 rpm.
10. 20-100µl of media containing the cells from each transformation was spreaded on pre-warmed selective agar plates.
11. The plates were incubated overnight at 37°C.
12. Individual transformed clones were picked using sterile inoculation loop. The colony was immersed into a 15mL tube containing 2mL LB broth with appropriate antibiotic.
13. The tube was then incubated 8 hours at 37ºC, shaking at 300rpm.
14. The bacteria LB broth was then transferred into a conical flask containing fresh 100mL LB with antibiotic.
15. The conical flask was then incubated overnight at 37ºC, shaking at 300rpm.

16. The next day, 500µL was removed from the bacteria LB broth and mixed with an equal volume of glycerol. This was stored at -80ºC to serve as a stock for future plasmid propagation.
17. DNA extraction was performed on the rest of the LB broth following instructions from the Qiagen Maxiprep kit. The cells were first harvested by centrifuging at 6000g for 15 mins at 4ºC.
18. The cell pellet was resuspended in 10mL Buffer P1 in a 50mL tube until no cell clumps remain.
19. Then 10mL of Buffer P2 was added. The solution was thoroughly mixed by vigorously inverting the tube 4-6 times until it turned into blue colour. This was followed by 5 minutes room temperature incubation.
20. 10mL of chilled Buffer P3 was added. The addition of P3 buffer produced a fluffy white material. The suspension was mixed thoroughly and vigorously by inverting the tube 4-6 times, until the suspension turned colourless. The suspension was incubated on ice for 20 minutes.
21. The suspension was mixed before centrifuging at 20,000g for 30 minutes at 4ºC. The supernatant was transferred into a fresh 50mL tube.
22. The supernatant was centrifuged again at 20,000g for 15 minutes at 4ºC. The supernatant was transferred into a fresh 50mL tube.
23. Meanwhile, a Qiagen-Tip 500 was equilibrated by flowing through 10mL of Buffer QBT.
24. The supernatant was pipetted to the Qiagen-Tip 500 and allowed it to enter the resin by gravity flow.

25. The Qiagen-Tip 500 was washed twice with 30mL of Buffer QC by gravity flow.
26. DNA was then eluted with 15mL of Buffer QF. The eluate was collected in a 50mL tube.
27. The DNA was precipitated by the addition of 10.5mL isopropanol to the eluted DNA. The solution was immediately mixed and centrifuged at 15,000g for 30minutes at 4ºC. The supernatant was carefully decanted as the pellet is loosely attached.
28. The DNA pellet was washed with 5mL of 70% ethanol and centrifuged at 15,000g for 10minutes. The resulting supernatant was carefully decanted without disturbing the pellet
29. The pellet was air-dried for 5-10 minutes. The DNA was then re-dissolve in 1mL TE buffer, pH8.
30. The DNA concentration was determined at 260nm.

A2.5. Plasmid Transfection

Optimization was first performed using HCET cells and PSG5 vector to determine suitable voltage and amount of plasmid DNA used (Figure A4).

1. Transient DNA plasmid transfection was done using electroporation. At least $1x10^6$ cells were needed per electroporation condition.
2. The cells were washed once with PBS, followed by trypsinisation and neutralization as described in A1.3.
3. The cells were then spun down at 1200rpm for 5 minutes.
4. The pellet was rinsed once with PBS.

5. Cell count was performed as described in A1.3. $1x10^6$ cells were aliquoted into 1.5mL Eppendorf tube.
6. The cells were spun at 1200rpm for 5 minutes.
7. The cell pellet was resuspended in 110μL of Solution R (Neon Transfection System 100μL Kit, Invitrogen).
8. One microgram of plasmid DNA was added and mixed gently with the re-suspended cells.
9. 4mL of Solution E was added into the microporation tube.
10. 100μL of cell suspension with added plasmid was taken up slowly avoiding bubbles using the Neon's electroporation pipette.
11. The MicroPorator-mini MP100 (DigitalBio, Seoul, Korea) was set up as follows: 1300V, 30ms, 1 pulse
12. After electroporation, the cells were seeded into vessel containing warmed complete media.

A4A

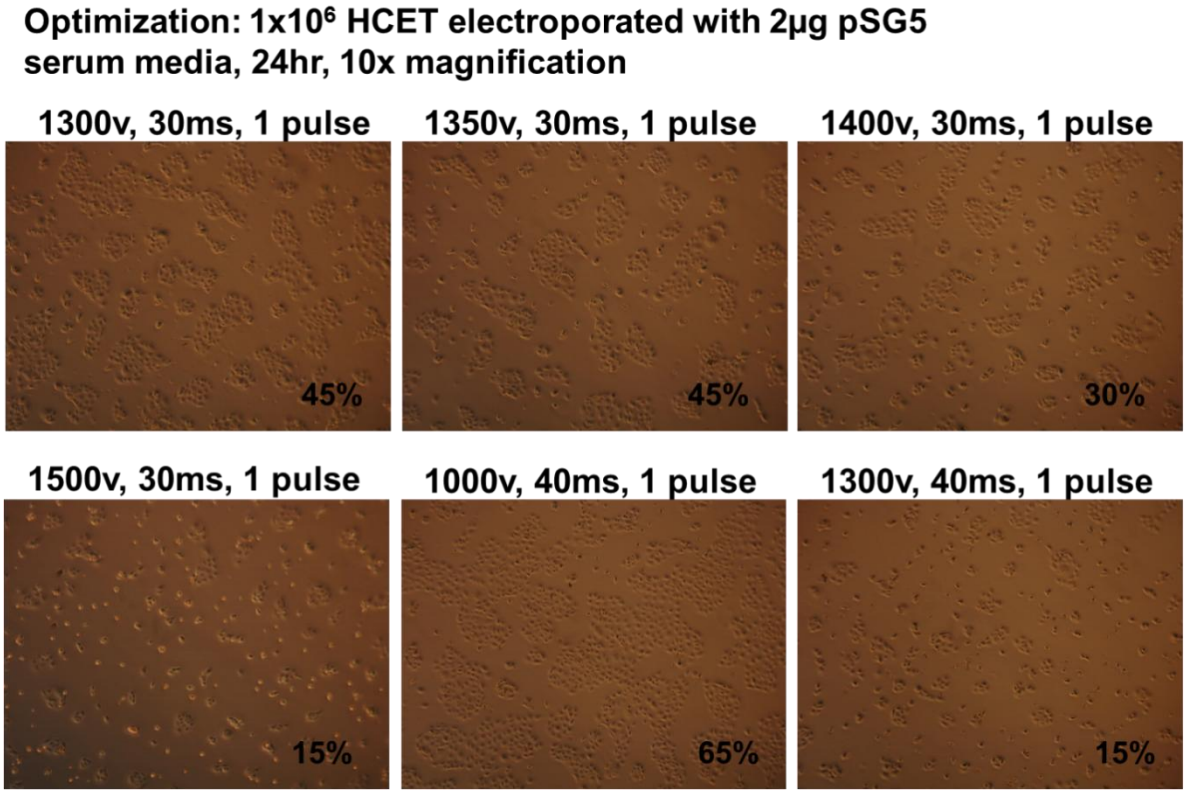
Optimization: 1x10⁶ HCET electroporated with 2µg pSG5
serum media, 24hr, 10x magnification
1300v, 30ms, 1 pulse
45%
1350v, 30ms, 1 pulse
45%
1400v, 30ms, 1 pulse
30%
1500v, 30ms, 1 pulse
15%
1000v, 40ms, 1 pulse
65%
1300v, 40ms, 1 pulse
15%

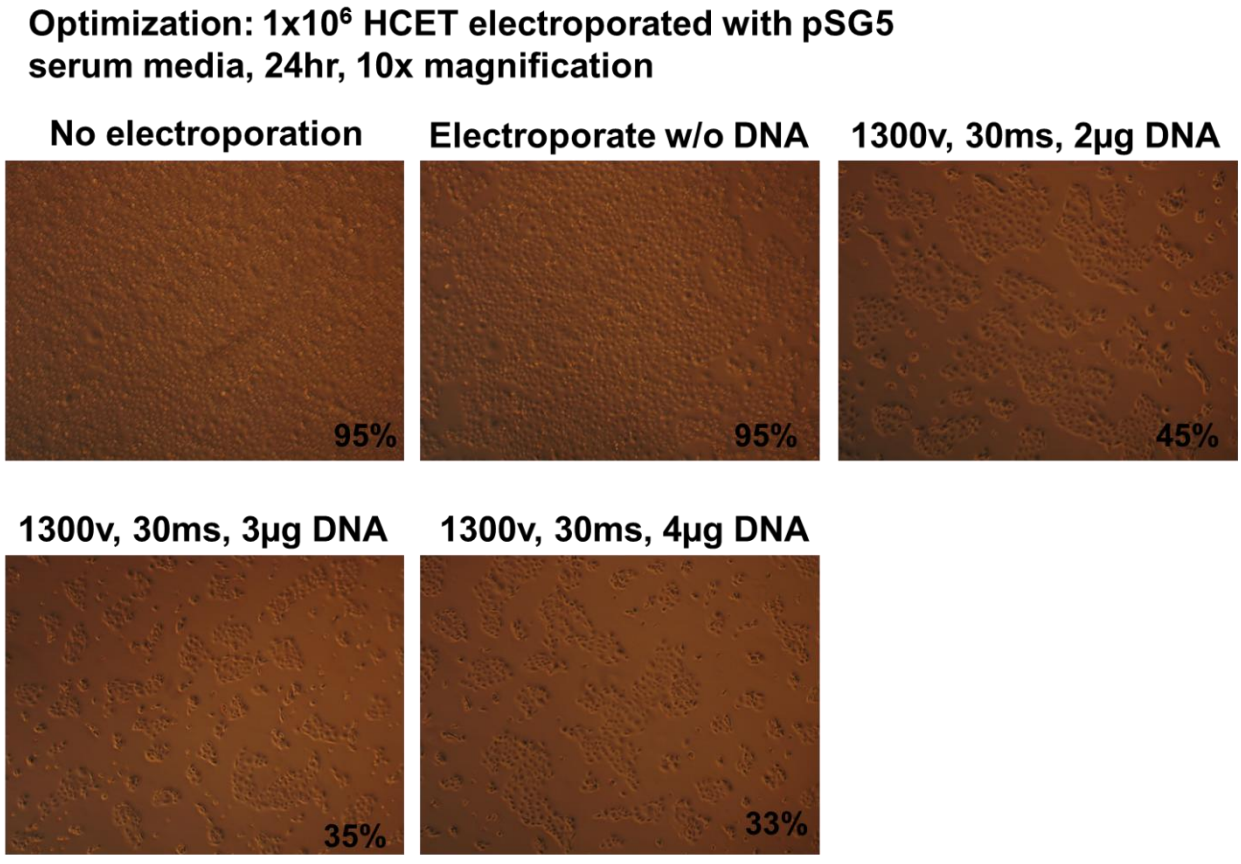
Optimization: 1x10⁶ HCET electroporated with pSG5
serum media, 24hr, 10x magnification
No electroporation
95%
Electroporate w/o DNA
95%
1300v, 30ms, 2µg DNA
45%
1300v, 30ms, 3µg DNA
35%
1300v, 30ms, 4µg DNA
33%

Optimization: 1x10^6 HCET electroporated with pSG5 serum media, 24hr, 10x magnification

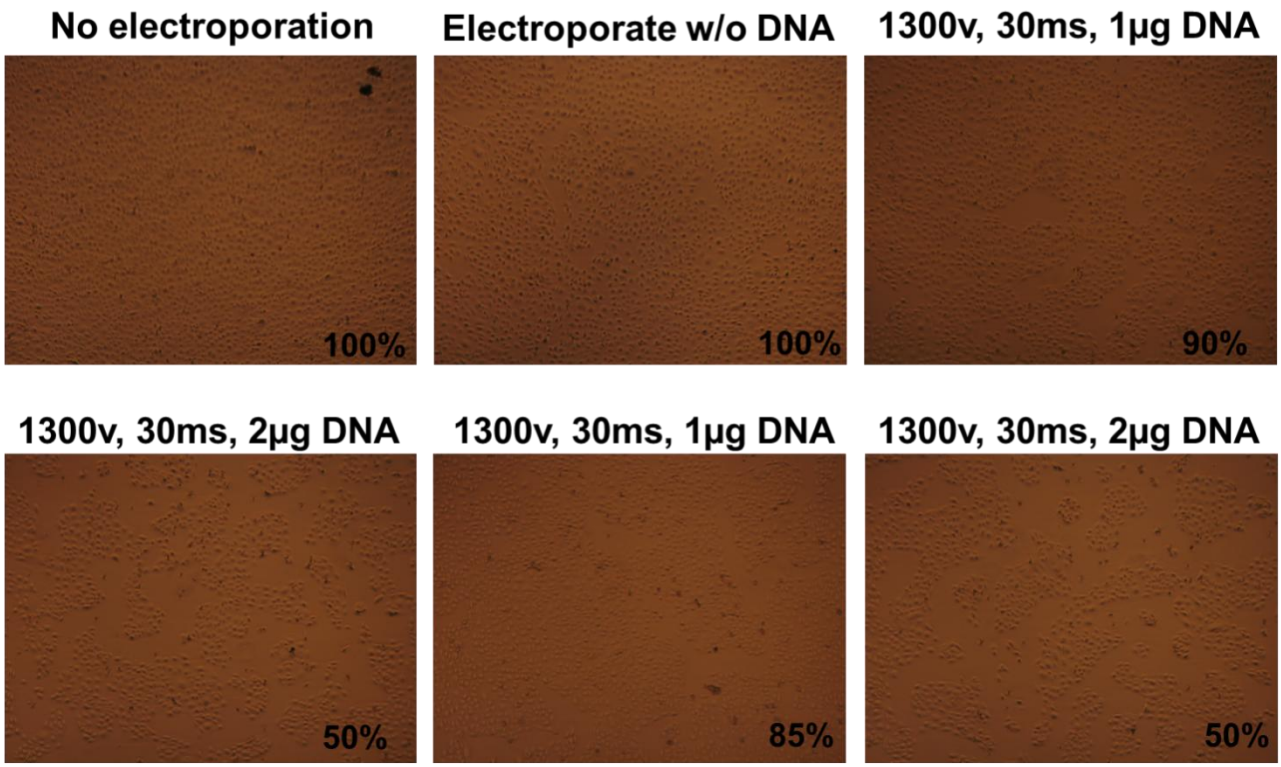

A4B

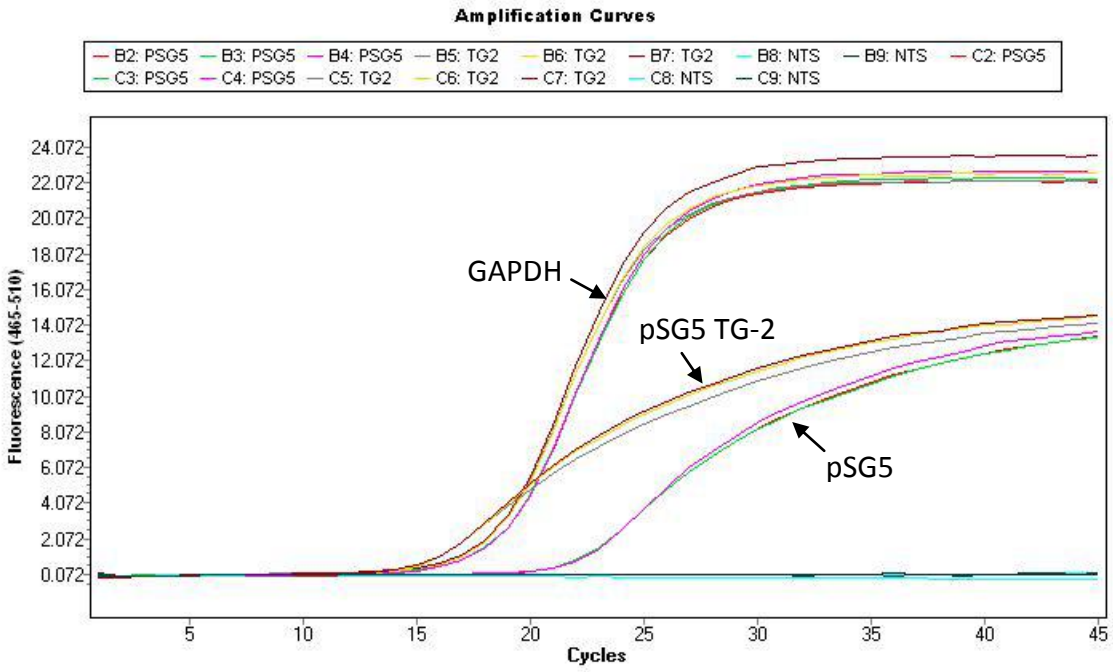

Figure A4. (A) Pictures showing optimization of electroporation conditions on immortalised human corneal epithelial (HCET) cells. Different parameters were tried: varied amount of plasmid DNA pSG5 were used (1-4µg), different electroporation timing (30 and 40ms) and different voltages (1000, 1300, 1350, 1400, 1500v) were used. The effectiveness of these electroporation parameters were determined by the amount of cell growth after 24 hours. After overnight incubation, 1300v, 30ms, 1 pulse with 1µg of plasmid DNA showed the highest cell survival of 85-90%. (B) To quantify the transfection efficiency, HCET cells were electroporated with 1µg of plasmid DNA pSG5 and pSG5 TG-2 respectively. The electroporation parameters of 1300v, 30ms, 1 pulse were used. Reverse transcription and real time quantitative PCR was then performed. GAPDH was used as a control.

A2.6. SiRNA Transfection

Short interfering (Si) RNA against TG-2 and fluorescein-conjugated SiRNA were used. The sense and anti-sense sequences (5' to 3') of the fluorescein-conjugated SiRNA were UUCUCCGAACGUGUCACGUdTdT and UUCUCCGAACGUGUCACGUdTdT respectively. Details of SiRNA transfection with the RNAiFect reagent have been previously described.(Chen et al 2005) Briefly, the ratio of siRNA to RNAifect used was 1:8. The silencing or non-silencing (control fluorescein-conjugated siRNA) siRNA (1 μg per well in the case of a single well in a 12 well plate) was applied at a final concentration of 67 nM with the fast-throw technique following the Qiagen protocol.

A3. Use of Chemical Inhibitors, Hyperosmolar Stimulation and Fibronectin Coating

A3.1. Caspase Inhibitor

Z-VAD-FMK (carbobenzoxy-valyl-alanyl-aspartyl-[O-methyl]-fluoromethylketone), a cell-permeable pan caspase inhibitor, was added to the culture media at a concentration of 20mM to inhibit caspases in cultured cells.

A3.2. Hyperosmolar stimulation

HCE-T cells were grown to 70-80% confluency before stimulation with hyperosmolar medium. The osmolarity suitable for experiment was determined through titration over a period of 24 hour (See Figure 2.1B). Sodium chloride was added to culture media to achieve osmolarity of 460mOsM (±5 mOsM), whereas control medium had osmolarity ranging from 290 to 305 mOsM. In every experiment, media osmolarity was determined and confirmed by VAPOR Pressure Osmometer 5520 (Wescor, UT).

A3.3. Fibronectin Coating on Polystyrene Surface

Fibronectin F0895 (Sigma stock 1mg/mL) was diluted to 1µg/mL in PBS. An eight well plate was coated with 200uL diluted fibronectin for 3hr, 37C. The amount of fibronectin added can be changed depending on the size of the dish/well. The amount of fibronectin should be enough to cover the surface of the dish/well. After incubation, the surface was wash once with PBS. Cells were then seeded on the coated surface.

A4. Cell Lysis

A4.1. Extraction of RNA and Quantification

1. RNeasy Mini kit from Qiagen was used to extract RNA from cells.
2. Cells were washed once with PBS.
3. 350 µL of RLT buffer was added per well of a 6 well plate (for less than $5x10^6$ cells). Cells were harvested using cell scraper.
4. The cells were homogenized using a 22-gauge needle for at least 5 times.
5. 350 µL (or the same volume as RLT buffer) of 70% ethanol was then added and mixed by pipetting.
6. The mixture was then transferred to an RNeasy spin column with 2mL collection tube and centrifuged for 15 s, at >8000g. The flow-through was discarded.
7. 700 µL of Buffer RW1 was added to the spin column and centrifuge for another 15s at >8000g. The flow through was discarded.
8. 500 µL of Buffer RPE was again added to the spin column and re-centrifuged for 2 minutes, at >8000g.
9. After discarding the flow through, the spin column was placed in a new 2mL collection tube and centrifuged dry at full speed for 1 minute.
10. After discarding the flow through, the column was placed in another new collection tube. 30 µL of RNase-free water was added and RNA was collected by centrifuging at >8000g, 1 minute.
11. 30µL RNase-free water from step 9 was added back into the spin column and centrifuged again at >8000g for 1 minute.

12. After extraction, RNA quantification was performed using Nanodrop at 260/280 (~1.8 is fine) and 260/230 (2.0-2.2 is fine).
13. The purified RNA was then stored at -80ºC.

A4.2. Total Proteins Extraction

1. Cell lysis buffer was prepared by adding 2.5µL of protease inhibitor, 10µL phosphatase inhibitor to 65µL of Radioimmunoprecipitation assay (RIPA) buffer.
2. Cells were washed once with cold PBS.
3. Cell lysis buffer was added to the cells (around 200µL needed for a 10cm plate). This is followed by incubation on ice for 5 minutes.
4. A sterile cell scrape was then used to harvest adherent cells. The cell suspension was then transferred to an eppendorf tube.
5. The cell suspension was homogenized on ice with sonicator for 20 seconds.
6. This is then followed by centrifugation at 10,000g for 15 minutes at 4ºC.
7. The cell lysate was aliquoted, snap freeze in liquid nitrogen and stored at -80ºC.

A4.3. Mitochondrial Protein Extraction

1. HCE-T cells were grown to 70-80% confluency, washed with PBS and trypsinised as described in A1.3.
2. The cells were pelleted down at 1,000 rpm for 5 minutes at 4ºC.
3. The cell pellet was re-suspended in cold PBS and pelleted down again.

4. After removal of supernatant, 1mL of mitochondrial extraction buffer (MSHE) buffer A was added and incubated on ice for 2 minutes.

   Composition of MSHE buffer A:

   0.21M mannitol, 0.07M sucrose, 10mM HEPES (pH 7.4), 1mM EDTA, 1mM EGTA, 0.15mM spermine, 0.75mM spermidine

   10µL of protease inhibitor was added freshly into 1mL of MSHE buffer A every time before use.
5. The suspension was spun at 1,600 rpm for 5 minutes at 4ºC.
6. After removal of supernatant, the pellet was re-suspended in 1mL of MSHE buffer A
7. Viable cells were checked with trypan blue and homogenized using a 27G needle, 60 times on ice, and verified by microscopy.
8. To pellet unbroken cells and nuclei, the suspension was spun at 800g for 3 minutes. The supernatant was retained and spun again at 11,000g for 15 minutes at 4ºC.
9. The resulting supernatant was the cytosolic fraction. The mitochondrial pellet was re-suspended in 200mL of MSHE buffer A, and was further purified by centrifugation at 1,000g for 5 minutes and at 11,000g for 15 minutes.
10. The protein concentrations of the extracted total protein mitochondrial protein were determined using BCA protein Assay kit as described in A4.4.

A4.4. Bicinchoninic Acid (BCA) Protein Assay

1. Protein samples were diluted 5 times with DEPC water. Triplicates of each sample were prepared.

2. Albumin standards provided by the BCA kit were diluted with nanopure water into concentrations from 1000µg/mL to 25µg/mL.
3. 10µL of standards and samples was pipetted into the microplate. Triplicates were done for each of them.
4. Working Reagent was prepared by mixing 50parts of Reagent A with one part of Reagent B.
5. 200µL of Working Reagent were added to every well containing either protein samples or standards.
6. The plate was incubated for 30 minutes at 37ºC.
7. The absorbance at 562nm was read using a spectrophotometer.

A5. Western Blotting

Protein concentration was determined using the BCA method as described in A4.3.

A5.1. Preparation of Buffers

1. The running buffer was a Tris/glycine/SDS running buffer from Biorad, CA, USA.
2. The transfer buffer was Tris/glycine transfer buffer from the same company with addition of 20% methanol, kept chilled before use.
3. TBST wash buffer is composed of 0.1% Tween 20 in Tris buffered saline.

A5.2. Gel Electrophoresis

1. The same mass of protein (40µg) was mixed with 4x loading dye containing 20% beta mercapethanol.
2. The samples were denatured at 99ºC for 10 minutes.
3. For identification of protein bands, 10µL of protein standard with known molecular masses was loaded in one lane.
4. The gel electrophoresis was carried out at 100 volts for around 1 hour and 30 minutes. The machine was stop when the dye front reached the bottom of the gel.

A5.3. Transfer and Blotting

1. PVDF membrane was activated with 100% methanol for 15 seconds, followed by soaking in water for 2 minutes. The membrane was then submerged in transfer buffer until ready to make the western sandwich.

2. After the gel has finished running, the front glass plate was removed and the gel was carefully detached. The gel was equilibrated for 10 minutes in transfer buffer.
3. The western sandwich was prepared in a tray containing the cold transfer solution. The sandwich was prepared in the following order: A fiber pad, a filter paper, the PVDF membrane, gel, a sheet of filter paper and a fiber pad. Bubbles were removed from the sandwich by rolling a pipette over the set-up.
4. The sandwich was then placed inside a cassette, whereby the PVDF membrane was closest to the transparent side of the cassette.
5. The sandwich was put in a transfer device. The black side of the cassette was placed next to the black side of the transfer cassette.
6. The transfer tank was filled the cold transfer buffer together with an ice and a stir bar.
7. The transfer was carried out at 20v overnight or 110v for 75 minutes.
8. After the run, the PVDF membrane was removed from the cassette. The PVDF membrane was washed 3x 5 minutes in TBST.
9. The membrane was blocked was blocked in 5% Bovine Serum Albumin (BSA) in TBST for one hour at room temperature.
10. This is followed by 3x 5 minutes washing in TBST at room temperature with shaking.
11. Primary antibody was added into 1% BSA in TBST and incubated at for 1 hour at room temperature with shaking. Alternatively, the primary antibody incubation can be left overnight at 4ºC with shaking.
12. This is followed by 3x 5 minutes washing in TBST at room temperature with shaking.
13. Secondary antibody in 1% BSA in TBST was incubated for 45 minutes at room temperature with shaking.

14. This is followed by 3x 5 minutes washing in TBST at room temperature with shaking.
15. Substrate was added to the membrane. The incubation time of the substrate depends on the strength of the substrate used.
16. The PVDF membrane was placed in a plastic bag and put into a cassette. A piece of film was put over the PVDF membrane for 1 minute.
17. Chemiluminescence captured by the film then detected using Kodak imaging system 2000R (CT, USA).
18. The image is then analysed by densitometry which evaluates the relative amount of protein staining.

A5.4. Densitometry

To prepare band image file:

1. Image J was used to open the image file.
2. The images were converted to 8 bit.
3. The band of interest was enlarged using "Magnifying Glass" tool.
4. The image was cropped by drawing a tight fitting rectangle around the band using the "Rectangle" tool.
5. The images were cropped by selecting "Image > Crop".
6. All the cropped images were then pasted on Powerpoint and saved as a TIFF file.

To measure band intensities:

7. The saved TIFF file was opened in ImageJ.

8. The image was converted to 8 bit again.
9. The image was enlarged using “Magnifying Glass” tool.
10. The rectangle tool was used to create a vertical rectangle in the first lane. To indicate that this is the first lane of the gel, “Analyse > Gels > Select First lane” was selected.
11. Using the mouse, click inside the rectangle and drag the box to the second lane. This lane was labeled as another lane by selecting “Analyse > Gels > Select next lanes”.
12. After dragging the last rectangle over the last lane, “Analyse > Gels > Plot lanes” was selected.
13. Image J will open a new window containing a mountain for each band. The mountain represents the density of the band.
14. The area inside the mountains was calculated by clicking the “magic wand” inside a mountain to calculate the area inside the mountain.
15. For loading control in western blot, the band intensity of each protein band was compared to the band intensity of its loading control.

A6. Centricollation

A6.1. Cell Lysis for Centricollation

1. Cell lysis buffer was prepared by adding 2.5µL of protease inhibitor, 10µL phosphatase inhibitor to 65µL of Radioimmunoprecipitation assay (RIPA) buffer.
2. Cells were washed once with cold PBS.
3. Cell lysis buffer was added to the cells (around 200µL needed for a 10cm plate). This is followed by incubation on ice for 5 minutes.
4. A sterile cell scrape was then used to harvest adherent cells. The cell suspension was then transferred to an eppendorf tube.
5. The cell suspension was centrifuged at centrifuged at 1200rpm for 5 minutes at 4ºC.
6. The cell pellet was re-suspended in homogenizing buffer (1mL of 8.5% GradiSpec with 2µL of 0.5M of Ethylenediaminetetraacetic acid (EDTA) and 10µL of protease inhibitor).
7. The cells were then homogenized for approximately 25 times with a 27G needle and syringe.
8. The homogenized suspension was centrifuged at 1000rpm for 5 minutes at 4ºC.
9. BCA was then carried out as described in section A4.3. Higher protein concentrations were diluted with homogenizing buffer to match the lower concentration.

A6.2. Centricollation

Enhanced density gradient extraction (Edge™) 200 System (Prospect Biosystems) is a bench-top, air-driven temperature-controlled ultracentrifuge system driven by centrifugal force for a stepwise extraction of particles.

1. As shown in Figure A5, 1 mL of samples with 8.5% GradiSpec solution was added into the SteriLiner.
2. The SteriLiner was then inserted into the rotor of the Edge 200 machine and spun for 5 minutes at 125,000g force.
3. After spinning, the supernatant was removed with a fine tip pipette without disturbing the pellet at the walls of the SteriLiner. The supernatant was kept in Eppendorf tube.
4. 100 uL of the next higher GradiSpec Sucrose Fraction (20%, 30%, 40%) was added into the same SteriLiner.
5. The centre hole of the SteriLiner was covered using parafilm. It was then vortexed for 1 minute until all the pelleted sample on the wall is re-suspended in the solution.
6. The parafilm was then removed and the same procedure from 2 to 4 was repeated until supernatants of the various sucrose fractions were obtained.
7. Gross fractionations were first performed using sucrose density solution at 8.5%, 20%, 30% and 40% (Figure A5).
8. To narrow down the range of sucrose density solution containing the interacting proteins and organelles, an approximate organelle localisation chart provided by Prospect Biosystems was referred (Figure 3.5).

9. After the range of sucrose density solution was narrowed down, centricollation was carried out using density solutions ranging from 8.5% to 20%.

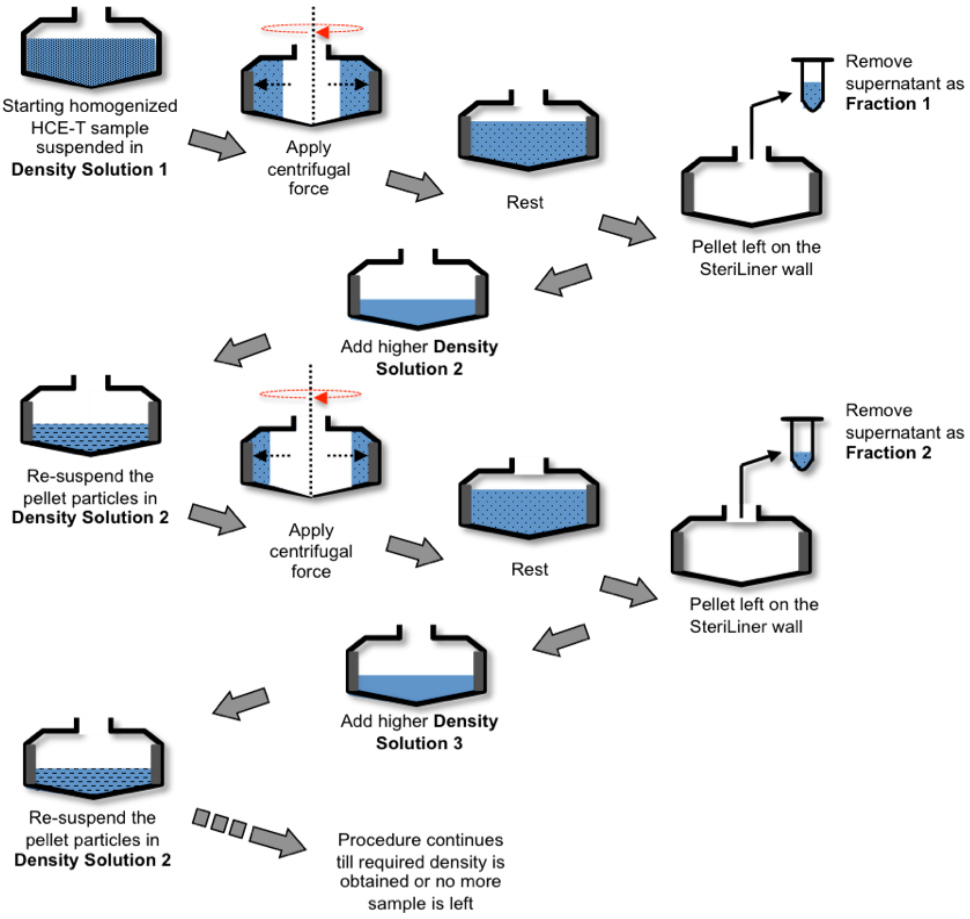

Figure A5. Diagram showing the process of centricollation. After homogenizing cell lysates with Density solution 1, samples were centrifuged and BCA was performed. Centricollation was carried out by adding 1 mL of sample to SteriLiner and rapidly spun at 125,000g for 5 minutes. After spinning, the sample was allowed to rest. The supernatant (Fraction 1) was carefully removed. The next higher Density Solution was added and the same procedure was repeated until supernatants of the various densities were obtained. This study mainly used Density Solution of 8.5%, 10%, 15% and 20%.

A7. Immunoprecipitation

A7.1. Co-Immunoprecipitation to Pull Down TG-2 Binding Partners

1. Cell lysate was collected as described in A4.2.
2. EZview Red ANTI-FLAG M2 affinity gel beads were mixed until uniformly suspended.
3. 40µL of the affinity gel beads was aliquoted into a 1.5mL eppendorf tube on ice.
4. 500µL of TBS buffer was added to the eppendorf tube with beads. The content was vortex and centrifuged for 30 seconds at 8200g.
5. Supernatant was carefully removed and the tube with beads was placed on ice.
6. 500µL of TBS buffer was again added to the beads. The content was vortex and centrifuged for 30 seconds at 8200g.
7. Cell lysate was spun at 8200g for 10 minutes at 4ºC.
8. 500 ug (200-1000µL) of cell lysate was added to the washed beads. The final volume was top-up to 1mL by adding lysis buffer.
9. The beads were gently shaken overnight at 4ºC.
10. This is followed by spinning down at 8200g for 30 seconds at 4ºC.
11. Supernatant was removed. Tube with beads was place on ice.
12. The beads were washed by adding 500µL TBS with brief vortexing.
13. Incubation was done at 4ºC for 5 minutes, followed by centrifugation for 30 seconds at 8200g.
14. Supernatant was carefully aspirated.
15. The beads were washed 2x with 500µL of TBS and brief vortexing.

16. After removing the final wash supernatant, the bound antigens can be eluted and analysed.
17. 3X FLAG peptide was dissolved in 0.5M tris HCl, pH 7.5, 1M NaCl to prepare stock solution at a concentration of 25µg/µL.
18. To prepare 5µg/µL of 3X FLAG peptide, the stock concentration was diluted 5-fold with water.
19. To prepare 3X FLAG Elution Solution at a concentration of 150ng/µL, 3µL of 5µg/µL 3X FLAG peptide was added to 100µL of TBS.
20. As a positive control, 1mL of TBS and 4µL of 50ng/µL FLAG-BAP fusion protein was added to a comparable tube of washed resin.
21. As a negative control, a comparable lysate volume from a lysate of cells not expressing FLAG fusion protein was used.
22. 100µL of 3X FLAG Elution Solution was added to each sample and control beads.
23. Samples and controls were incubated with gentle shaking for 30 minutes at 4ºC.
24. The beads were centrifuged at 8200g for 30 seconds.
25. Without disturbing the beads, the resulting supernatant was transferred to fresh tube.
26. For immediate use, the supernatant was store at 4ºC.

A7.2. Co-Immunoprecipitation to Pull Down Paxillin Interacting Partners

1. To pre-clear the lysate, 500ug lysate was incubated with 60ul of streptavidin agarose slurry for 1 hour by end-over-end mixing.
2. The lysate and agarose mixture was then centrifuged at 1000g at 4°C, 1 minute.
3. The supernatant was incubated with rabbit anti-paxillin conjugated to biotin (1:20), overnight at 4°C with end-over-end mixing.
4. The lysate and antibody mixture was incubated with 60ul of streptavidin agarose slurry for 2 hours at 4°C, with end-over-end mixing.
5. The lysate and agarose mixture was again centrifuged at 1000g at 4°C, 1 minute before the supernatant was removed and stored.
6. The remaining beads with bound protein complex were washed 4 times with binding buffer solution.
7. The washed agarose beads with the bound protein complex were boiled at 95°C, for 9 minutes in 50ul of 2X protein loading dye containing 20% reducing agent, to denature and release the bound protein from the agarose beads.

A7.3. Cell Free In Vitro Immunoprecipitation

1. Recombinant human proteins TG-2 (R&D system), JNK (Santa Cruz) and paxillin (Biolegend) were pre-cleared in 1.5mL tubes by mixing with streptavidin agarose resin for 1 hr at 4˚C.
2. The tubes were centrifuged at 1,000 g for 1 min at 4˚C. The supernatant was transferred to new tubes, and the streptavidin agarose beads were discarded.

3. JNK (5µg) and paxillin (1µg) were mixed with 1µg, 2.5 µg or 5 µg of TG-2 respectively in 1.5mL tubes.
4. Biotinylated anti-paxillin (10µg) was added to each tube, and PBS was added to make each tube to a final volume of 200µL.
5. The tubes were incubated overnight at 4˚C with end-over-end mixing.
6. The next day, the same amount of streptavidin agarose resin used for pre-clearing was added to each tube and the tubes were incubated at 4˚C for 2 hrs.
7. The supernatant was removed from each tube and resin beads were washed 5x with 500µL of cold PBS.
8. Fifty microliter of 2x protein loading dye was added to each tube and the tubes were heated at 95˚C for 10 min. The same volume from different samples was used for immuno blot with anti-TG-2, anti-JNK and anti-paxillin antibodies

A8. Liquid chromatography-tandem mass spectrometry (LC-MS/MS)

1. Protein digestion was performed using a trypsin digestion kit.
2. The lyophilized IP samples were first re-dissolved in 25 µL Extraction Buffer followed by 25µL of Digest Buffer.
3. Samples were reduced using 1.5µL of Tris (2-carboxyethyl)phosphine (TCEP), mixed and incubated for 20 minutes at 37ºC. Negative controls "immunoprecipitation" with pre-immune serum was also included
4. Samples were brought to room temperature and 1.5 µl of iodoacetamide was added, mixed and incubated for another 20 minutes at room temperature.
5. Trypsin digestion was then carried out by adding 1.5 µL of 1µg/µL Trypsin for 3 hours at 37ºC.
6. The digested samples were dried using speedvac.
7. 10 µL of loading buffer was added to re-dissolve samples and analysis was performed using LC-MS/MS.
8. Micro-capillary LC column (15 cm × 75 µm i.d.) was self-packed using PicoFrit (New Objectives, Woburn, MA) with integrated spray tip which was directly coupled with the nano-spray interface (Protana, Odense, Denmark) into ABI's QSTAR mass spectrometer. The packing material was Luna C18, 3µm, 100 Å (Phenomenex Torrance, CA).
9. Samples were loaded onto a trap column (C18, 0.3 x 5 mm, from Dionex, LC Packings) from Famos autosampler (Dionex, LC Packings) at 30 µL/min.

10. After a 5 min wash with acetonitrile/water (5/95, v/v with 0.1% formic acid), the system was switched (Switchos, Dionex, LC Packings) into line with the C18 capillary column.
11. Using an Ultimate solvent delivery system (Dionex, LC Packings), peptides were eluted by a linear gradient of acetonitrile (0.1% formic acid) from 5% to 55% over 35 min at flow rate of 300 nL/min.
12. Parameters for the nanospray and other instrumentation were set as follows: ionspray voltage (IS) = 1800 V, curtain gas (CUR) = 25, declustering potential (DP) = 60 V, focusing potential (FP) = 265 V, collision gas setting (CAD) = 5 for nitrogen gas, DP2=25. All data was acquired using information-dependent acquisition (IDA) mode with Analyst QS software (Applied Biosystems).
13. TOF-MS survey scan parameters were set as follows: 1 sec TOF MS survery scan in the mass range of 350~1200 Da followed by two product ion scans of 3 sec each in the mass range of 100~1800 Da. The "enhance all" function was used in the IDA experiments. Switching criteria were set to ions greater than m/z = 350 and smaller than m/z = 1200 with charge state of 2 to 4 and an abundance threshold of > 8 counts/s. Former target ions were excluded for 120s. IDA collision energy (CE) parameter script was used for automatically controlling the CE.
14. An example of the mass spectrogram is shown in Figure A6.

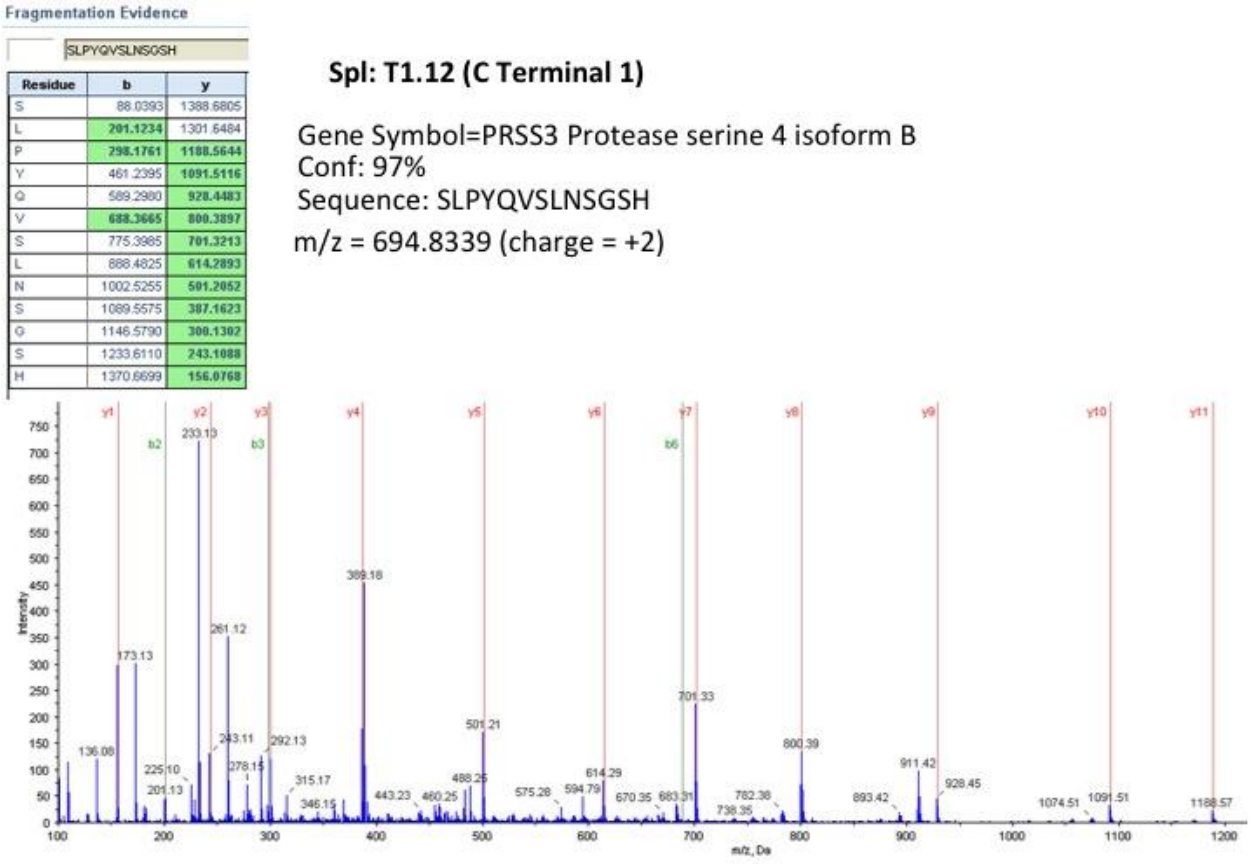

Figure A6. Mass spectrogram showing the ion fragment with peptide sequence that matches serine protease (PRSS) 3 in TG-2 C terminal.

A9. Mapping of Protein Ligands to TG Domains

1. Cells were lysed and immunoprecipitation was performed with anti-Flag antibodies as described in A7.
2. Elutes were sent for tryptic digest and nano LC/LC MS/MS as described in A8.
3. Using MASCOT protein database search, the potential binding partners of TG-2 was given a confidence level according to factors such as: not present in the negative control, not in a similar class as negative control proteins, a known protein, found with an antibody against TG-2, related to known TG-2 functions as documented in Gene Ontology, not repeated in different peptide fragments, and it is found in replicated experiments.
4. Each of these factors contributed 1 point. Only level 3 and 4 (3 or more point) ligands were considered for mapping to TG domains.
5. Proteins with functions clearly related to cell adhesion or trafficking were preferentially retained and the known relations of these proteins with TGM-2 plotted.
6. The functional relationships of these potential binding partners were constructed and validated using Pathway Studio Version 5.0.
7. Pathway Studio extracted related PubMed articles based on the mass-spectometry results. One article was limited to one intervening entity. To determine the relationships with TG-2, the abstracts of these published articles were manually chosen.
8. After generating a list of TG-2 related ligands, a search on the PubMed gene database was performed to classify entities according to their biological process.

9. Western blots were then carried out with the corresponding antibodies against the suggested ligands.

A10. Immunostaining

A10.1. Immunocytochemistry and Immunohistochemistry

1. Fixation was performed with 4% paraformaldehyde (PFA) in PBS for 15 minutes.
2. To make 50mL of 4% PFA:
    i. 2 gram of paraformaldehyde was added to 250 mL of conical flask or beaker.
    ii. 50 ml of water and a stirrer was added.
    iii. The mixture was heated at 100ºC until moisture was observed at the side of the glass beaker.
    iv. The beaker was placed on a magnetic mixer.
    v. Add in drops of 5M NaOH until solution becomes clear.
    vi. The beaker was removed from heat. Same number of drops as step v of 5M HCl was added.
    vii. 2.5mL of 20x PBS was added.
3. The slides were washed twice with PBS.
4. The cells/tissues were then permeabilised with 0.1% of Triton X-100 in PBS for 10 minutes.
5. This is followed by 3x 5minutes washing with PBS.
6. Blocking was performed with 1.5% BSA in PBS for 1hour in humidified chamber.
7. Excess blocking buffer was tapped off from the slides.
8. The slides were then incubated with primary antibody in 1.5% of BSA for 2 hours at room temperature in humidified chamber.
9. Washing was done 3x 5minutes with PBS.

10. Secondary antibody in 1% BSA in PBS was added to the slides at room temp for 1 hour in moist chamber.
11. Washing was done 3x 5minutes with PBS.
12. To stain the nucleus, the cells/tissues were incubated with Dapi in PBS (1:1000) for 10 minutes.
13. The slides were rinsed 3x with PBS
14. The slides were then mounted with 10µL of mowiol.
15. A coverslip was added on top of the glass slide. The side of the coverslip were sealed with transparent nail polish.
16. Slides were then observed under a microscope and fluorescent images were captured

A10.2. Immunofluorescence Staining with Phalloidin

1. Cells were grown for 24 hours to produce a confluent monolayer of cells on glass coverslip coated with fibronectin. The cells were submerged in DMEM-F12 supplemented with 5% FBS, at 37^{o}C, 5% CO_2 atmosphere.
2. After removing the medium, the monolayer was washed once with PBS.
3. Scratches were made with a 1 mL blue pipette tip.
4. After scratching, the monolayer was washed twice with PBS to remove cell debris.
5. Cells were incubated with fresh DMEM-F12 supplemented with 5% FBS, at 37^{o}C, 5% CO_2 atmosphere, for 3 hours.
17. The monolayer cells was washed with PBS and fixed with 4% paraformaldehyde (PFA) in PBS for 15 minutes
18. The slides were washed twice with PBS.

19. The cells/tissues were then permeabilised with 0.1% of Triton X-100 in PBS for 10 minutes.
20. This is followed by 3x 5minutes washing with PBS.
21. Blocking was performed with 1.5% BSA in PBS for 1hour in humidified chamber.
22. Excess blocking buffer was tapped off from the slides.
23. The slides were then incubated with phalloidin and DAPI in 1.5% of BSA for 30 min at room temperature in humidified chamber in the dark.
24. Washing was done 3x 5minutes with PBS
25. Excess liquid was removed from the coverslip by touching the corner on a paper towel. The coverslip was then inverted on a drop of mounting media on a glass slide
26. The coverslip and glass slide was left for 20 min to dry followed by sealing of the sides with transparent nail polish

A11. Polymerase Chain Reaction (PCR)

A11.1. Reverse Transcription

1. Reverse transcription was done to obtain cDNA from RNA (Figure A7). The RNA concentration was first measured using nanodrop.
2. The following were added into a nuclease-free microcentrifuge tube:

   1µg of RNA

   1µL of 10mM dNTP Mix

   1µL of 50µM random hexamer

   Sterile water to 8µL
3. The mixture was heated at 65°C for 5 minutes followed by incubation on ice for at least 1 minute.
4. The content of the tube was collected by brief centrifugation and the following were added:

   2µL of 10x First-Strand Buffer

   2µl 0.1M DTT

   4 µl of 25mM $MgCl_2$

   1 µl of RNaseOUT Recombinant RNase Inhibitor

   1µL of Superscript III RT
5. The solution was mixed by pipetting gently up and down.
6. The solution was incubated at 25°C for 10 minutes, then 50°C for 50 minutes.
7. The reaction was inactivated by heating at 85°C for 5 minutes followed by chilling on ice.

8. 1µL of RNase H was added to each tube and incubated at 37ºC for 20 minutes.

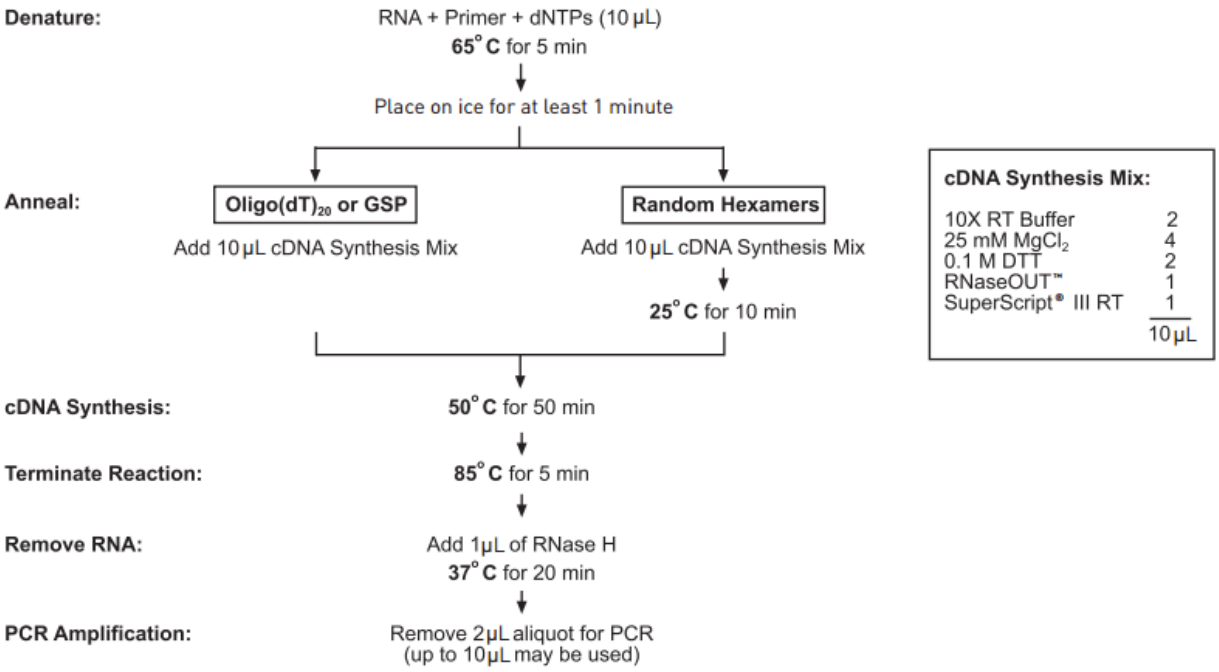

Figure A7. Diagram showing a summary of reverse transcription to obtain cDNA from RNA. The whole process involved denaturation of RNA strands at 65ºC, annealing of random primers along RNA transcript, cDNA synthesis followed by PCR amplification.

A11.2. Quantitative Real Time PCR (qPCR)

Real-time PCR was performed using specific Taqman probes. GAPDH gene was used as an endogenous control which quantifies relative gene expression in cDNA samples.

1. The sequences of the forward and reverse primers (50–30) to detect TG-2 were

   AGGGTGACAAGAGCGAGATG

   TGGTCATCCACGACTCCAC

2. The following were pipetted into the two 1.5mL eppendorf tubes labelled TG-2 and GAPDH.

Reagent	**Volume**
Water	17.1
2x master mix	45
Primer (Forward)	9
Primer (Reverse)	9
Taqman Probe	0.9
Total vol in PCR tube	81

3. 29.7µL of the mixed solution each was aliquot into 2 eppendorf tubes.
4. 3.3µL of cDNA was added into the tubes.
5. The solution was mixed by pipeting up and down followed by spinning down at 1000rpm for 5 minutes.
6. 10µL was pipetted into a well of the 384 PCR plate. Triplicates were done for each sample.
7. The rest of the solution from step 2 was use as a Negative Control. 10µL of negative control was pipetted into the PCR plate.
8. The plate was spun at 2000g for 3 minutes at 4ºC.
9. The PCR machine was set with the following parameters

Pre-incubation (1 cycle)		
95C	None	10.01 min

Amplification (45 cycles)		
95C	None	10 s
54C	None	10s
72C	Single	30s
Cooling (1 cycle)		
40C	None	1s

A12. Functional Assays

A12.1. Caspase Assay

Caspase-3 and -7 activities were measured using Caspase-Glo 3/7 assay while caspase-9 activity was measured using Caspase-Glo 9 assay. The Caspase-Glo Assay is a luminescent assay that is able to measure caspase-3/7 or 9 activities in living cells. Addition of the Caspase-Glo 3/7 or 9 Reagent caused cell lysis, followed by caspase cleavage of the substrate, and production of luminescent signal. Pro-luminescent caspase-3/7 or 9 substrate containing tetrapeptide sequence DEVD was provided. Once the substrate is cleaved, aminoluciferin is release and luminescent signal is generated.

1. 100µL of complete media containing $1.1x10^5$ cells/mL cells were grown in 96 wells white walled-plate. These are the sample wells.
2. 20µM of caspase inhibitor Z-Vad-FMK, as described in A3.1, was added into three of the wells which contained cells and incubated for 24 hours. These are the inhibitor wells.
3. The plate was equilibrated to room temperature.
4. 100µL of Caspase-Glo 3/7 or Caspase-Glo 9 reagents were to each well (blank, samples, inhibitor wells).
5. Plate was shake on a plate shaker for 30 seconds.
6. The plate was then incubated at room temperature for 2 hours.
7. Luminescent signal, which was proportional to the amount of caspase activity present, was measured using a microplate reader.

A12.2. Mitochondrial Depolarisation Assay

Mitochondrial membrane potential of various cells was studied by staining the cells with JC-1, a membrane permeable dye which exhibits membrane potential dependent accumulation in mitochondria. In live cells, JC-1 is a metachromatic probe which exists either as a green-fluorescent (~529 nm) monomer at depolarised membrane potentials, or as an orange-fluorescent (~590 nm) J-aggregate at hyperpolarized membrane potentials.

1. Non-adherent cells in the media were collected and adherent cells were trypsinised.
2. The cells were pelleted at 800rpm for 5 minutes.
3. The pelleted cells were resuspended in 1mL of media and incubated with 10µL of 200µM JC-1 dye for 30 minutes, at 37ºC and 5% CO_2.
4. As a positive control, 2µL of 2mM mitochondrial membrane disruptor CCCP was added.
5. Cells were washed once with PBS and spun down at 800rpm for 5 minutes at room temperature.
6. Cells were re-suspended by gently flicking the tubes.
7. 500µL of warm complete media was added.
8. Samples were analysed by flow cytometry performed at 488nm.
9. Healthy cells with intact mitochondria fluoresce red; while apoptotic cells fluoresce green.
10. An ellipse was use to delineate a population of cells with healthy mitochondria. The percentage of depolarised cells was computed by measuring the amount of cells falling outside the ellipse.

A12.3. Transglutaminase Colorimetric Microassay Kit

Cellular transglutaminase enzymes can catalyze the crosslinking of biotin cadaverine to CBZ-Gln-Gly peptides coated on 96-well plates. The greater the activity of the cellular transamidase enzymes, the more biotin will be cross-linked to these peptides.

1. 150µL per well of 1X diluent buffer was added and the plate was incubated for at least 30 minutes at 37°C.
2. Samples from cells or tissues were centrifuged before use.
3. The 1X diluent buffer was removed from the plate.
4. Per well, the following were dispensed:

   samples: 40 µL+10µL distilled water),

   positive control: 40µL TG (1/10 in NaCl 0.14M) + 10µL distilled water

   negative control: 40µL TG + 10µL of Negative control reagent

   one blank well for HRP substrate/chromogen solution only
5. 50 µL per well of reconstituted biotin-cadaverine/$CaCl_2$ was added.
6. Incubation at 37°C for 15 minutes.
7. The enzyme tracer solution was prepared at 1/2000.
8. The wells were washed 3x with PBS containing 0.1% Tween 20 or TBS containing 0.1% Tween 20.
9. 100 µL per well of 1/2000 diluted enzyme tracer solution was added.
10. The plate was incubated for 15 minutes at 37°C.
11. HRP substrate/chromogen solution was prepared.

12. The wells three times were washed 3x with PBS containing 0.1% Tween 20 or TBS containing 0.1% Tween 20.
13. 100µL per well of HRP substrate/chromogen solution was added.
14. Incubation at room temperature for 2 to 10 minutes.
15. 100µL per well of blocking reagent was dispensed.
16. The optical density of each well at 450nm was measured.

A12.4. G-LISA Kit

Traditionally, the Rho family proteins such as RhoA, Rac or Cdc42 assays had been performed using a conventional agarose beads affinity pull-down method. However, this method have several drawbacks such as time consuming, requiring large amount of total protein, limited in the number of samples that can be handled simultaneously and generating semi-quantitative results.

These G-LISA RhoA, Rac and Cdc42 kits from Cytoskeleton enabled Rho proteins to be measured in less than 3 hours, requires only 1-5% of the material needed for a conventional pull down assay, able to handle large number of samples and generated quantitative results.

The G-LISA kit contained a Rho protein-GTP binding protein linked to the wells of a 96-well plate. Active GTP-bound Rho present in cell lysates can bind to the wells. Specific antibody was then used to detect the bound active Rho proteins. The inactive GDP-bound Rho proteins were eliminated during washing steps.

A12.4.1. RhoA and Rac1/2/3 G-LISA Activation Assay

1. Cells with confluency of 50% were lysed and collected using cold lysis buffer as described in A4.2.
2. Total amount of proteins were quantified using BCA assay as described in A4.4.
3. The cell extracts were equalized with cold lysis buffer. Concentration of equalized protein must not > 2mg/mL or <0.4mg/mL.

   [(A-B)/B]*(vol of A)= ____ µL

   A= higher concentration lysates (mg/mL)

   B= most diluted lysates (mg/mL)
4. For Rho A assay, 60µL of lysis buffer and 120µL of ice cold binding buffer was added into microfuge tube.

   For Rac assay, 60µL of lysis buffer and 60µL of ice cold binding buffer was added into microfuge tube.
5. The tubes were vortexed for 3-5 seconds at high speed and then placed on ice. This is buffer blank sample.
6. For Rho A assay, 24µL of Rho Control Protein, 96µL of cold lysis buffer and 120µL of binding buffer was added into the microfuge tub.

   For Rac assay, 5µL of Rac Control Protein, 55µL of cell lysis buffer and 60µL of binding buffer was added into the microfuge tub.
7. The tubes were vortexed for 3-5 seconds at high speed and then placed on ice. This is positive control sample.
8. Strips of wells were taken out from the plate and placed on ice. 100µL of cold water was added to dissolve the powder in the wells.

9. Frozen cell lysates were thawed in room temperature water bath. Lysis buffer was added to respective tubes based on calculations from the equation in step 3.
10. 120µL of lysate for triplicate wells were aliquoted into fresh ice cold microfuge tubes.
11. Equal volume of cold binding buffer was added to each tube on ice.
12. Water was completely removed from the microplate wells by vigorously flicking the plate, followed by 5-7 hard and vigorous series of pats onto paper towels.
13. Plate was placed back on ice.
14. Each tube was immediately vortexed for 3-5 seconds with high speed.
15. 50µL of equalized cell lysate, buffer blank control or RhoA/Rac positive control was pipetted to triplicate wells respectively.
16. Plate was immediately placed on a cold orbital microplate shaker at 210rpm, 4ºC for exactly 30 minutes.
17. During the incubation, anti-RhoA primary antibody was prepared by diluting to 1/250 in Antibody Dilution Buffer.

    Anti-Rac primary antibody was prepared by diluting to 1/200 in Antibody Dilution Buffer.

    * Final volume of 500µL is enough for 1 strip (8 wells)
18. After 30 min, the solution was flicked out from the wells followed by washing 2x with 200µL room temperature wash buffer using. Wash buffer was vigorously removed after each wash.
19. The plate was placed on bench.

20. 200µL of room temperature Antigen Presenting Buffer was immediately pipetted into each well using a multi-channel pippettor. The wells were incubated at room temperature for exactly 2 minutes.
21. Antigen Presenting Buffer was vigorously flicked out and the inverted plate was patted 5-7 times.
22. The wells were then washed 3x with 200µL room temperature wash buffer and the wash buffer was vigorously removed.
23. 50µL of diluted anti-RhoA/anti-Rac primary antibody was added to each well and the plate was placed on the shaker at 250 rpm for 45 minutes in room temperature.
24. During the primary antibody incubation, for Rho A assay, secondary HRP labeled antibody was diluted to 1/62.5 in antibody dilution buffer; for Rac assay, secondary HRP labeled antibody was diluted to 1/100 in antibody dilution buffer.

    * The final vol of 500µL is enough for 1 strip of 8 wells.
25. Primary antibody was vigorously flicked out and the inverted plate was pat 5-7 times.
26. The wells were then washed 3x with 200µL room temp wash buffer and the wash buffer was vigorously removed every time.
27. 50µL of diluted secondary antibody was added to each well and shook at 200-400 rpm in room temperature for 45 minutes.
28. HRP detection reagent was prepared by mixing equal volume of reagent A with B into a fresh tube (50µL per well). Mixture must be protected from light.
29. Secondary antibody was vigorously flicked out and the plate was inverted and pat for 5-7 times.

30. The wells were washed 3x with 200µL room temperature wash buffer. The wash buffer was vigorously removed every time.
31. 50µL of HRP detection reagent was added into each well and incubated at 37ºC for 15 minutes in Rho A assay, but 20 minutes in Rac assay.
32. 50µL of HRP stop Buffer was added to each well.
33. Absorbance was measured at 490 nm using a microplate spectrophotometer.

A12.4.2. Cdc42 G-LISA Activation Assay

1. Cells with confluency of 20-30% were lysed and collected using cold lysis buffer as described in A4.2.
2. Total amount of proteins were quantified using BCA assay as described in A4.4.
3. The cell extracts were equalized with cold lysis buffer. Concentration of equalized protein must not > 2mg/mL or <0.4mg/mL.

[(A-B)/B]*(vol of A)= ____ µL

A= higher concentration lysates (mg/mL)

B= most diluted lysates (mg/mL)

4. 120µL of lysis buffer was aliquoted into a microcentrifuge tube. This is buffer blank sample.
5. 12µL of Cdc42 Control Protein and 108µL of cold lysis buffer was added into the microfuge tub. The tubes were vortexed for 3-5 seconds at high speed and then placed on ice. This is positive control sample for 2 wells.

6. Strips of wells were taken out from the plate and placed on ice. 100µL of cold water was added to dissolve the powder in the wells.
7. Frozen cell lysates were thawed on ice. Lysis buffer was added to respective tubes based on calculations from the equation in step 3.
8. Water was completely removed from the microplate wells by vigorously flicking the plate, followed by 5-7 hard and vigorous series of pats onto paper towels.
9. Plate was placed back on ice.
10. 50µL of equalized cell lysate, buffer blank control or Cdc42 positive control was pipetted to triplicate wells respectively.
11. Plate was immediately placed on a cold orbital microplate shaker at 210rpm, 4ºC for exactly 30 minutes.
12. During the incubation, anti-Cdc42 primary antibody was prepared by diluting to 1/20 in antibody dilution buffer.

    * Final volume of 500µL is enough for 1 strip (8 wells)
13. After 30 min, the solution was flicked out from the wells followed by washing 2x with 200µL room temperature wash buffer using. Wash buffer was vigorously removed after each wash.
14. 200µL of room temperature Antigen Presenting Buffer was immediately pipetted into each well using a multi-channel pippettor. The wells were incubated at room temperature for exactly 2 minutes.
15. Antigen Presenting Buffer was vigorously flicked out and the inverted plate was patted 5-7 times.

16. The wells were then washed 3x with 200µL room temperature wash buffer and the wash buffer was vigorously removed.
17. 50µL of diluted anti-Cdc42 primary antibody was added to each well and the plate was placed on the shaker at 250 rpm for 45 minutes in room temperature.
18. During the primary antibody incubation, secondary HRP labeled antibody was diluted to 1/62.5 in antibody dilution buffer.

    * The final vol of 500µL is enough for 1 strip of 8 wells.
19. Anti- Cdc42 primary antibody was vigorously flicked out and the inverted plate was pat 5-7 times.
20. The wells were then washed 3x with 200µL room temp wash buffer and the wash buffer was vigorously removed every time.
21. 50µL of diluted secondary antibody was added to each well and shook at 200-400 rpm in room temperature for 45 minutes.
22. HRP detection reagent was prepared by mixing equal volume of reagent A with B into a fresh tube (50µL per well). Mixture must be protected from light.
23. Secondary antibody was vigorously flicked out and the plate was inverted and pat for 5-7 times.
24. The wells were washed 3x with 200µL room temperature wash buffer. The wash buffer was vigorously removed every time.
25. 70µL of HRP detection reagent was added into each well and incubated at 37ºC for 10 minutes.
26. 140µL of stop Buffer was added to each well.
27. Absorbance was measured at 490 nm using a microplate spectrophotometer.

A13. Cell Viability/Proliferation Assay

A13.1. Crystal Violet

Crystal violet dye stains DNA. This assay is useful for obtaining quantitative information about the relative density of cells in multi-wells plate. Upon solubilisation of the dye, the amount of dye taken up by the cells can be quantitated in a plate reader.

1. Cells were counted and $1x10^6$ cells were transfected by electroporation as described in A2.5.
2. The cells were seeded in a six-well culture plate, incubated for 24h at 37ºC and 5% CO_2.
3. The cells were washed with PBS prior to staining with crystal violet solution.
4. One milliliter of crystal violet dye was added into each well and incubated in room temperature for 20 minutes.
5. The cells were carefully washed three times with PBS.
6. The crystal violet dye was then solubilised with 1ml of 1%SDS solution, followed by gentle shaking for 30minutes.
7. The absorbance was then measured using microplate reader at 595 nm.

A13.2. MTS Cell Proliferation Assay

The CellTiter 96® AQueous One Solution Reagent from Promega contains a tetrazolium compound [MTS: 3-(4,5-dimethylthiazol-2-yl)-5-(3-carboxymethoxyphenyl)-2-(4-sulfophenyl)-2H-tetrazolium] and an electron coupling reagent (PES: phenazine

ethosulfate). PES can combine with MTS to form an insoluble formazan product which has a purple color. The quantity of formazan product measured at 490nm absorbance is directly proportional to the number of living cells.

1. 50µL of complete media was added to 96-well plate and equilibrated in 37ºC, 5% CO_2 incubator for 30 minutes.
2. 5000 cells in 50µL were seeded in complete medium to the equilibrated 96-well plate.
3. The MTS colorimetric assay was performed by adding 20mL of the CellTiter 96 AQ_{ueous} One Solution Reagent directly to 96 wells plate containing 100µL of culture media.
4. The cells were incubated for 3 hours in humidified, 37ºC, 5% CO_2 atmosphere.
5. Absorbance was measured at 492nm with the microplate reader.

A13.3 Ki-67 Assay

Ki-67 is a nuclear antigen that is expressed in the late G1, S, M, and G2 phases of the cell cycle, but is absent from non-proliferation cells (G0 phase). The expression of the Ki-67 protein has been associated to cell proliferation. Hence, the fraction of cells that stain positive for the Ki-67 nuclear antigen is a highly accurate method of assessing the fraction of proliferating cells.

1. A monolayer of scrambled shRNA and shTG cells were scratched as described in Appendix A14.4.
2. After scratching the monolayer, the cells were washed twice with PBS.

3. Fresh DMEM-F12 media with 5% FBS was added to the wells containing the scratched monolayers.
4. The cells were incubated in humidified chamber for 6 hours at $37^{o}C$, 5% $CO_{2.}$
7. As described in Appendix A10.1, cells were fixed with 4% paraformaldehyde (PFA) in PBS for 15 minutes.
8. The slides were washed twice with PBS.
9. The cells/tissues were then permeabilised with 0.1% of Triton X-100 in PBS for 10 minutes.
10. This is followed by 3x 5minutes washing with PBS.
11. Blocking was performed with 1.5% BSA in PBS for 1hour in humidified chamber.
12. Excess blocking buffer was tapped off from the slides.
13. The slides were then incubated with anti-Ki-67 (1:40. Appendix B) in 1.5% of BSA for 2 hours at room temperature in humidified chamber.
14. Washing was done 3x 5minutes with PBS.
15. Secondary antibody in 1% BSA in PBS was added to the slides at room temp for 1 hour in moist chamber.
16. Washing was done 3x 5minutes with PBS.
17. To stain the nucleus, the cells/tissues were incubated with Dapi in PBS (1:1000) for 10 minutes.
18. The slides were rinsed 3x with PBS
19. The slides were then mounted with 10µL of mowiol.
20. A coverslip was added on top of the glass slide. The side of the coverslip were sealed with transparent nail polish.

21. Slides were then observed under a microscope and fluorescent images were captured
22. Positively-stained cells (green) within contiguous cells of a confluent area were counted 3 times in each cell type.

A13.4 Cell Cycle Analysis

1. 4×10^5 cells were cultured for 2 days.
2. Non-adherent and trypsinised cells were pelleted as described in A1.3.
3. Cells were re-suspended in 500µL PBS, transferred drop by drop to 4.5 mL of chilled 70% ethanol while gently vortexing and incubated in ethanol overnigh at 4ºC.
4. The cells were pelleted and resuspended in 5mL PBS at room temperature for 1 minute.
5. The cells were pelleted again by centrifugation and re-suspended in 200µL of GUAVA cell cycle reagent.
6. This is followed by 30 minutes room temperature incubation before analysis by mini-flow cytometry.

A14. Cell Adhesion and Migration Assay

A14.1. Cell Impedance

Xcelligence system (Roche Applied Science, Basel, Switzerland) measures cell proliferation by detecting the changes in impedance. The local ionic environment at the electrode/solution interface changes with the presence of cells on top of the electrodes. The impedance increased with increasing number of cells, displayed as cell index (CI) values. In addition, the quality of interaction between cells and electrodes can affect cell impedance. Hence, electrode impedance can be used to monitor cell viability, number, morphology, and adhesion degree in cell-based assays (Figure A8).

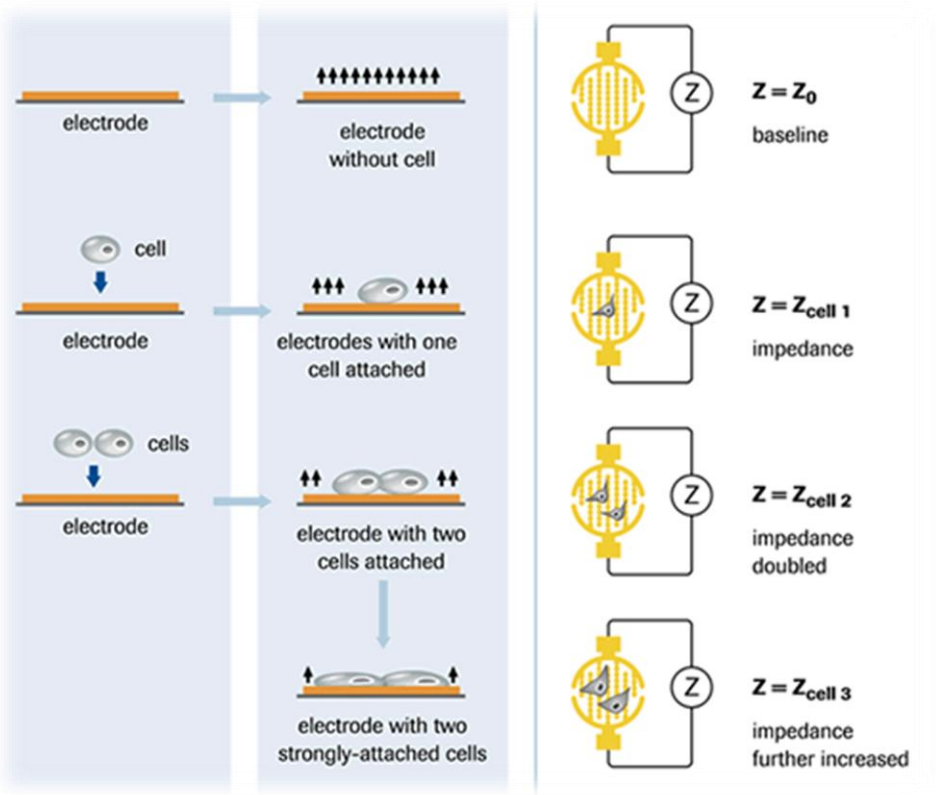

Figure A8. Diagram showing the electrode impedance in the Xcelligence system increases with increasing cell numbers and cell adhesion strength.

1. Five thousand cells were seeded in 200µL of cell culture media in each well of a 96-well plate, in quadruplicate.
2. The cells requiring hyperosmolar stimulation were seeded in fresh hyperosmolar media as described in A3.2.
3. Cell proliferation was monitored over 1 week.

A14.2. **Trypsinisation** *Assay*

1. Adherent cells at confluency of 50-60% were washed once with PBS.
2. The cells were incubated with PBS-diluted 0.005% Trypsin-EDTA at 37 °C, 5% CO_2 for 1 hour.
3. Photographs were taken periodically without mechanical perturbation.

A14.3. Real Time Cell Migration Assay

1. Scrambled shRNA or shTG cells were seeded in a 6mm (inside diameter) x 8mm (outer diameter) x 5mm (height) detachable culture glass cylinder filled with 100µL 5% DMEM-F12 supplemented medium.
2. After overnight incubation, the culture cylinder was removed.
3. The monolayer was washed with twice PBS to remove cell debris.
4. Fresh medium was added and cell migration was recorded every 10 minutes for 100 frames (around 16 hours).
5. The centroid positions of 50 randomly selected contiguous cells at the advancing edge, tracked every 10 min over 16 h by live cell time-lapse microscopy.

6. Cell centroids were computed after manually outlining cells using ImageJ software. Initial cell positions were normalised to plot origin.
7. The details of the ImageJ analysis is at Appendix A18.2

A14.4. Scratched Wound Assay

1. Scrambled shRNA or shTG cells were seeded in uncoated or fibronectin-coated 6-well tissue culture plates and grown for 24 hours to produce a confluent monolayer of cells. The cells were submerged in DMEM-F12 supplemented with 5% FBS, at 37^{o}C, 5% CO_2 atmosphere.
2. After removing the medium, the monolayer was washed once with PBS.
3. Straight scratches were made with a 1 mL blue pipette tip.
4. After scratching, the monolayer was washed twice with PBS to remove cell debris.
5. Re-epithelialization of the denuded area was determined using ImageJ software from images captured at fixed positions every 2 hour for 14 hours.
6. The details of the ImageJ analysis is at Appendix A18.2

A14.5. Cell Area Measurement

1. shTG or scrambled shRNA cells were cultured on uncoated or fibronectin-coated dishes with serum supplemented medium until 80% confluency.
2. The cells were washed twice with PBS.
3. Serum-free medium was added and incubated overnight.

4. The cells were seeded into uncoated or fibronectin precoated 8-well chamber slides and incubated overnight.
5. Using ImageJ software (National Institute of Health, USA), cell boundaries including cytoplasmic protrusions of non-overlapping cells were outlined manually on captured images (20× magnification, Axioplan 2 fluorescence microscope, Carl Zeiss, Oberkochen, Germany) and cell area was measured. Nuclear boundaries of the same cells were drawn to calculate nuclei areas.
6. The details of the ImageJ analysis is at Appendix A18.2

A15. Animal Work

A15.1. Mouse Model

Mice were handled according to guidelines in the Association for Research in Vision and Ophthalmology Statement for the Use of Animals in Ophthalmic and Vision Research and protocols approved by the Institutional Animal Care and Use Committee of SingHealth. Heterozygous TG-2-deleted mice ($Tgm2^{tm1.1Rmgr}$) originally on a mixed C57BL/6J-129S1/SvImJ strain background were established as previously described [46]. These heterozygous TG-2 deleted mice were backcrossed more than 12 generations to C57BL/6J to produce congenic heterozygote (TG-$2^{+/-}$) mice. The heterozygous TG-$2^{+/-}$ mice have >99.95% genomic homogeneity with C57BL/6J. Homozygous (TG-$2^{-/-}$) and wild type (TG-$2^{+/+}$) littermate founders were bred from the congenic C57BL/6J TG-$2^{+/-}$ mice.

A15.2. Assessing Corneal Wound Healing in Mouse

1. Mice were anesthetized by intra-peritoneal injection of ketamine hydrochloride (2mg/g body weight) and xylazine (0.4mg/g body weight).
2. Hind limb toe pinching was done to monitor the depth of anesthesia.
3. A trephine with diameter in 2mm was used to mark the central cornea.
4. The epithelium was peeled off using a forcep under a dissecting microscope.
5. Wound healing was accessed by instilling 10µL of fluorescein staining for 5 seconds in the mouse eye (sterile 1% Minimsfluorescein sodium solution, diluted 1:4 in sterile saline)

6. Excess fluorescein dye was rinsed off with sterile saline for 1 minute.
7. Digital camera photography was done in cobalt blue light with ultraviolet lightfilters.
8. Wound area was determined by the fluorescein staining and expressed as a percentage of total wounded corneal area.

A16. *In vitro* Label Free Protein Interaction Assay

1. Recombinant paxillin protein (Biolegend, 0.15ug/ul) was thawed on ice.
2. PBS pH4.3 and PBS pH7.5 were prepared.
3. 100uL of paxillin was mixed with 200uL of PBS pH7.5. 100uL of paxillin was mixed with 200uL of PBS pH4.3. The final concentration of paxillin in PBS is 0.05ug/uL.
4. 12uL of Pax-PBS 7.5 and Pax-PBS 4.3 was aliquoted into designated well.
5. Quick spin was performed on the micro plate.
6. The plate was sealed with PCR plate seal, followed by overnight incubation at 4°C.
7. The next day, vinculin (Abnova), TG-2 (R&D) and Integrin α5 β3 (R&D) recombinant protein were thawed.
8. The proteins were dilute with PBS pH7.5 to designated concentration

   TG-2 at 0.1, 0.05 and 0.01ug/uL

   Integrin αV β3 at 0.1, 0.05 and 0.01ug/uL

   Vinculin at 0.07, 0.035, 0.01ug/uL
9. Quick spin was performed on the micro plate.
10. The solution in the micro plate was removed by gently tapping the plate on tissue papers.
11. The micro plate was washed 3x with 30uL of PBS pH7.5. After every wash, the solution in the plate was removed by gently tapping the plate on tissue papers.
12. 15uL of PBS pH7.4 was added into each well. The micro plate was then spinned down.
13. This is then followed by incubation of the micro plate in the Enspire Multimode Plate Reader (Perkin Elmer, MA, USA) at 27°C for 2 hours.

14. 15uL of recombinant protein was added into each well.
15. Quick spin was performed on the micro plate.
16. The micro plate was read using the Enspire Multimode Plate Reader.
17. 15uL of the next proteins was added to each well.

    TG-2 at 0.0067ug/uL

    Integrin αV β3 at 0.1ug/uL

    Vinculin at 0.0067ug/uL
18. Quick spin was performed on the micro plate.
19. The micro plate was read using the Enspire Multimode Plate Reader.

A17. *In vitro* Kinase Assay

These experiments were outsourced to ProQinase GmbH, Freiburg, Germany.

A17.1. TG-2 Intrinsic Kinase Activity Assay

The ability of the putative protein kinase TGM2 to phosphorylate Paxillin was determined in an *in vitro* kinase activity assay experiment in comparison to the protein kinase JNK1 and the phosphorylation of Histone H1 by CDK2-CyclinE1 complexes.

1. The following buffers were prepared:

   Standard Assay Buffer (2.5x stock)
   125 mM HEPES-NaOH, pH 7.5
   7.5 mM MgCl2
   7.5 mM MnCl2
   7.5 µM Na-orthovanadate
   2.5 mM DTT

   Kinase Dilution Buffer (10x stock)
   500 mM HEPES-NaOH, pH 7.5
   2.5 mg/ml PEG20.000
   10 mM DTT

2. Reaction mixture was pipetted into a 1.5ml Eppendorf cups in the following order:

   10 µL of 2.5x Standard Assay Buffer
   7.5µL Substrate in 50mM HEPES pH7.5
   5µL Recombinant kinase in 1x Kinase Dilution Buffer
   2.5µL ATP + tracer (^{32}P-γ-ATP in H_2O approx 4.5*10^6 cpm/sample)
   Total volume is 25µL and the final assay concentration of ATP was 10µM.

3. The samples were mixed and incubated at 30°C for 60 mins.

4. The reaction was stopped by addition of 10µL 4x SDS sample-buffer and incubation at 95°C for 5 mins.

5. 20µL of the samples were loaded on a 4-12% Bis-Tris polyacrylamid gel and analysed by electrophoresis.
6. The gel was stained with colloidal coomassie solution for visualisation of protein loading and dried. For visualisation of transferred radioactive phosphate the gel was exposed to X-ray film (Kodak BioMax MR) for various periods of time.

A17.2. In vitro Autoradiographic Kinase Assay

1. A reaction cocktails was prepared as follows:

   60mM HEPES-NaOH, pH 7.5, 3 mM $MgCl_2$, 3mM $MnCl_2$, 3µM Na-orthovanadate, 1.2mM DTT, 50µg/ml PEG20000, 1µM ATP/[γ-^{33}P]-ATP (8. x 10^{05} cpm per well), protein kinase (1-400 ng/50µl) and sample protein (5 µg/50 µl).
2. The reaction cocktails were pipetted into a 96 well, V-shaped polypropylene plates in the following order:

   10 µl of kinase solution

   40 µl of buffer/ ATP/ test sample mixture
3. One well of each plate was used for a control containing no enzyme.
4. The assay plates were incubated at 30°C for 60 minutes.
5. The reaction cocktails were stopped with 20 µl of 10% (v/v) H_3PO_4.
6. The reaction cocktails were transferred into 96-well glass-fiber filter plates, pre-wetted with 150 mM H_3PO_4, followed by 10 min incubation at room temperature.
7. The filter plates were washed 3x with 250 µl of 150 mM H_3PO_4 and 1x with 20 µl of 100% ethanol.

8. The plate was dried for 30 min at 40°C
9. 50 µl of scintillator (Rotiszint Eco plus, Roth) were added to each well
10. The incorporation of ^{33}Pi ("counting of cpm") was determined with a microplate scintillation counter (Microbeta, Perkin Elmer).
11. The autophosphorylation activity of each kinase had previously been determined in two independent experiments
12. The mean autophosphorylation values (in cpm) had been calculated for each kinase at a given input of radioactivity. These autophosphorylation values were normalised to the counts used in the current experiment and subtracted from the corresponding raw data obtained with each kinase.
13. The background value of the protein sample (mean of two singlicate measurements) was subtracted from each raw value.

A18. Analysis

A18.1. Statistical Analysis

For continuous variables, all results shown are means ± SD. Statistical differences for cell areas were determined by ANOVA with post-hoc comparisons where the ANOVA is significant. The general linear model (GLM) procedure was used (SPSS, Inc.) for the evaluation of velocity of cell migration and gap width inin vitroscratch assays. The post hoc test option in the GLM procedure was used to evaluate for significant differences between the 4 conditions (cells with scrambled shRNA and shRNA targeting TG2, either with or withoutfibronectin), p values adjusted for multiple comparisons were evaluated for statisti-cal significance. For categorical variables, proportions (e.g.proportions of positively-labeled Ki-67 cells) were compared using the Chi square test, with $p \leq 0.05$ being considered significant.

A18.2. ImageJ Analysis

A. Loading

1. Image was loaded by clicking at: plugins > input-output > ICS/IDS
2. Video was loaded by clicking: file > open > file is in .ics format
3. Previous saved tracks were loaded by clicking: plugins > MTrackJ > load tracks > tracks are in mdf format
4. Frame numbers of a video can be reduced by clicking: plugins > stacks > stack reducer

B. Cell Area Measurement

5. Before starting measurement, a scale bar was drawn to match the ruler in the image, followed by clicking: analyse > set scale > value came out in um
6. Image properties were checked at: Image > properties > unit of length “um” > pixel width “0.6468750” > OK
7. After changing the properties, each pixel was made sure to have 0.6468750um (for 10x magnification) (20x magnification, 1 pixel= 0.323μm).
8. Image properties need to be changed every time a new image was opened because the measurement by default is in pixel
9. The tab “polygon selection” was selected, followed by outlining the border of the cells
10. Measurement of cell area was done by clicking: Analyse > measure

C. Tracking cells

11. The resolution of original picture is 1280 x 960 pixels
12. Before starting tracking cells, the image properties need to be changed by clicking: Image > properties > unit of length “um” > pixel width “0.6468750” > frame interval “10 min” >OK
13. After changing the image properties, each pixel is 0.6468750um. Each frame when tracking must be in 10 min interval, usually total frame is >= 145 frames.
14. The cells were magnified before tracking.
15. The centre of the cells was tracked instead of the dots in the cells.

16. New tracks were added by clicking: plugins > MTrackJ > add tracks
17. To tracking setting was set as follows: check “move to next time index after adding points”, “finish track after adding point at last time index”.
18. The display properties of the track at “configure displaying” can be changed. If there are multiple tracks which block the sight of next cells while tracking, the finished track can be hided: configure display > uncheck display finished track
19. The width of line can be changed: configure display > track width > 0
20. Different tracks can be assigned into the same cluster for future analysis. This will change the numbers and colour of the tracks. This is usually done after finishing all the tracks: cluster track > ctrl+ right click > right click > OK
21. To continue previous track: Continue tracks > add tracks

D. Save Files

22. File was saved by clicking: Save tracks
23. For the track files, it is a small file. The track file was changed to “.mdf” format.

E. Measuring Cell Tracks

24. Click “measure tracks” > display track, display points

F. Measure the Distance between First and Last Frame

25. Frame numbers was reduced by clicking: plugins > stacks > stack reducer (only first and last frame left). There are 2 ways to calculate length:
26. A) Using line drawing method: draw a straight line > connect first and last frame with straight line > press “ctrl + m” to measure > move straight line down the picture > get 10 measurements > get average
27. B) Plugin > analyse >grid > lines > 1000 pixels^2 > using multi tool, place dots on horizontal line > measure > On the same horizontal line, the corresponding points should have same Y, different Y > distance between 2 frames= Y1 – Y2

A18.3. Cell Oscillation Analysis

This cell oscillation analysis program was written by our collaborator Dr Earnest Mendoz from National University of Singapore. The cell track of a migrating cell was tracked using ImageJ as described in the Material and methods of Appendix A18.2C. The software will measure the cell oscillation by generating a directionality line that joins the origin of the cell track to its end point, the displacement of each cell from the directionality line was measured (Figure A9, green arrow). Mean of oscillation is the mean displacement of all the frames for each cell within certain time interval.

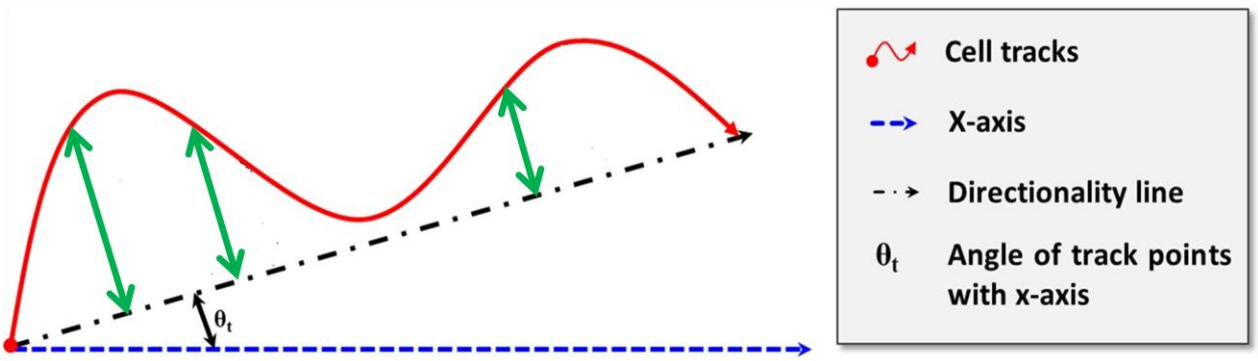

Figure A9. Diagram illustrates the theory behind the cell oscillation analysis software.

Appendix B. Antibodies List

Antigen	Antibody (catalog number)	Dilution	Species	Source
Transglutaminase-2	ab421	1: 50 (IF[a])	Rabbit	Abcam
Anti-(Ki) 67	18-0191Z	1:40 (IF[a])	Rabbit	Invitrogen
Phospho-β3 integrin (Tyr747)[b]	ab38460	1: 400 (western)	Rabbit	Abcam
		1: 50 (IF[a])		
Phospho-β1 integrin (S785)	ab5185	1: 200 (western)	Rabbit	Abcam
Phospho-vinculin integrin (Tyr 822)	V4889	1: 1000 (western)	Rabbit	Sigma
		1: 50 (IF[a])	Rabbit	
Phospho-Paxillin (S178)	A300-100A	1: 1000 (western)	Rabbit	Bethyl Laboratories
		1: 100 (IF[a])	Rabbit	
Phospho-FAK (Tyr576)	#07-157	1: 150 (western)	Rabbit	Millipore
Phospho-FAK (Tyr925)	#3284	1: 500 (western)	Rabbit	Cell Signaling
Integrin β3	ab34409	1: 400 (western)	Mouse	Abcam
Integrin β1	MAB1965	1: 200 (western)	Mouse	Millipore
Vinculin clone hVIN-1	V4505	1: 400 (western)	Mouse	Sigma
Paxillin	P1093	1: 500 (western)	Mouse	Sigma
FAK	610087	1: 200 (western)	Mouse	BD Biosciences
Talin	T3287	1: 500 (western)	Mouse	Sigma
β-Actin	ab8227	1: 1000 (western)	Rabbit	Abcam
β-Actin	A5441	1: 5000 (western)	Mouse	Sigma
Cytochrome C	556433	1: 1000 (western)	Mouse	BD Biosciences Pharmingen
Manganese superoxide dismutase (MnSOD)	611580	1: 500 (western)	Mouse	BD Biosciences Pharmingen
Anti-mitochondrial intramembrane cleaving protease (PARL)	sc-98994	1: 200 (western)	Rabbit	Santa-Cruz Biotechnology
Anti-Trk C (NTRK3)	sc-14025	1: 200 (western)	Rabbit	Santa-Cruz Biotechnology
Mesotrypsinogen (PRSS3)	sc-47127	1: 200 (western)	Goat	Santa-Cruz Biotechnology
Rho GTPase activating protein (ARHGAP)-17	sc-160145	1: 200 (western)	Goat	Santa-Cruz Biotechnology
Desmin (DES)	sc-34201	1: 200 (western)	Goat	Santa-Cruz Biotechnology
Unc 18-2 (STXBP2)	sc-23014	1: 200 (western)	Goat	Santa-Cruz Biotechnology
Glutamate receptor ionotropic kainate (GRIK)2	sc-26478	1: 200 (western)	Goat	Santa-Cruz Biotechnology
ELKS/RAB6 interacting/CAST family member (ERC)2	sc-70271	1: 200 (western)	Goat	Santa-Cruz Biotechnology
Golgi-associated protein (GOLGA)2	sc-16268	1: 200 (western)	Goat	Santa-Cruz Biotechnology
GLI family zinc finger (GLI)-1	sc-6153	1: 200 (western)	Goat	Santa-Cruz Biotechnology
Golgin 160 (GOLGA3)	sc-79966	1: 200 (western)	Goat	Santa-Cruz Biotechnology
Integrin beta (ITGB) 4	sc-6629	1: 200 (western)	Goat	Santa-Cruz Biotechnology
Human immunodeficiency virus type I enhancer binding protein (HIVEP)2	sc-10682	1: 200 (western)	Goat	Santa-Cruz Biotechnology
Anti-human eukaryotic translation elongation factor 1 alpha 2 (EEF1A2)	sc-68482	1: 200 (western)	Rabbit	Santa-Cruz Biotechnology
Centrosome-associated protein (CEP) 350	NB-100-59811	1: 200 (western)	Rabbit	Novus Biological
Anti-mouse IgG (whole molecule) FITC	F2012	1: 800 (western)	Goat	Sigma
Anti-rabbit Alexa Fluor 488	A11070	1: 800 (western)	Goat	Invitrogen
Anti-mouse HRP	A9044	1: 5000 (western)	Goat	Sigma
Anti-rabbit HRP	A0545	1: 5000 (western)	Goat	Sigma
Anti-goat IgG	F7367	1: 400 (western)	Mouse	Sigma
Anti-MAP3K12 mAb	LS-C158096	1: 800 (western)	Mouse	LSBio
Protein disulphide isomerase (PDI) (F-11)	sc-166474	1: 200 (western)	Mouse	Santa-Cruz Biotechnology
Lysosomal associated membrane protein (LAMP)-1 (H5G11)	sc-18821	1: 200 (western)	Mouse	Santa-Cruz Biotechnology
Early endosome antigen (EEA)1	E3906-200UL	1: 200 (western)	Rabbit	Santa-Cruz Biotechnology
RAB7	R4779-200UL	1: 200 (western)	Rabbit	Santa-Cruz Biotechnology
Manganese Superoxide Dismutase (MnSOD)	611580	1: 200 (western)	Mouse	BD Biosciences Pharmingen

[a] Immunofluorescence staining.

[b] Although called integrin beta 3-phospho-Y773 antibody in manufacturer's catalog, it refers to the same tyrosine residue because amino acid counting from N terminus of propeptide.

Appendix C. List of Reagents and Chemicals

Item	Product Number	Company	Country of Origin
SuperScript® III Reverse Transcriptase	18080051	Life Technologies	CA, USA
Random Hexamers	N8080127		
Dulbecco's modified Eagle medium: nutrient mixture F12 (DMEM-F	11320-033		
Fetal bovine serum (FBS)	16000-044		
Puromycin	A1113802		
Penicillin-Streptomycin	15140148		
Lipofectamine Plus Reagent	15338-100		
MitoProbe™ JC-1 Assay Kit for Flow Cytometry	M34152		
Neon 100 µL Transfection Kit	MPK10096		
GUAVA cell cycle reagent	4500-0220	Millipore	MA, USA
Culture glass cylinder		Bioptechs	PA, USA
Phosphate Buffered Saline (PBS)	SH30256.01	GE Healthcare	NJ, USA
Dimethyl sulfoxide (DMSO)	472301	Sigma	MO, USA
RIPA buffer	R0278-50ML		
Protease inhibitor cocktail	S8820		
Trypsin–EDTA	T4174-100ML		
Tryphan blue	T8154-20ML		
Pan-caspase inhibitor Z-VAD-FMK	V116-2MG		
Mitochondrial extraction buffer (MSHE) A	MITOISO1-1KT		
Polybrene	107689		
Purified pig liver TG-2	T5398-1UN		
Bovine Serum Albumin	A9418-500G		
Paraformaldehyde	P6148-500G		
pSG5 vector	216201	Stratagene	CA, USA
phrGFPII-N plasmids	240145		
Sodium chloride (NaCl)	1.16224.9011	Merck	Darmstadt, Germany
ProteoExtract-All-In-One Trypsin Digestion Kit	650212		
BCA protein assay kit	23225	Pierce Biotechnology	IL, USA
Supersignal West Pico chemiluminescent substrate	34077		
Supersignal West Dura chemiluminescent substrate	34075		
Supersignal West Femto chemiluminescent substrate	34094		
Nitrocellulose membrane	162-0115	Bio-Rad Laboratories	CA, USA
Non-fat milk powder	170-6404XTU		
Beta-mercaptoethanol	161-0710		
4–20% pre-cast SDS-polyacrylamide gel	456-1096		
Triton X-100	161-0407		
Tween 20	170-6531		
LB Agar powder	166-0472EDU		
LB broth pellet	166-0412		
CellTiter 961 AQueous Non-Radioactive Cell Proliferation Assay	G3582	Promega	WI, USA
Caspase-Glo 3/7 caspase activity kits	G8090		
Caspase-Glo 9 caspase activity kits	G8210		
TG colorimetric assay kit	opr0001	CovaLab	Lyon, France
Crystal violet staining solution	C581-25	Fisher Scientific	NJ, USA
10x Tris-buffered saline	BUF-3030-10X4L	1st Base	Singapore
0.1M EDTA	BUF-1051-500ml-pH7.4		
Water, DEPC treated	BUF-1170-1L		
GradiSpec Discovery Reagent Kits	PB 203D	Prospect Biosystem	NJ, USA
Fibronectin precoated 8-well chamber slides	EW-13004-28	BD Bioscience	MA, USA
Phosphatase inhibitors	4906845001	Roche	Basel, Switzerland
Rac1 G-LISA Activation Assay	BK126	Cytoskeleton	Denver, USA
RhoA G-LISA Activation Assay	BK121		
Cdc42 G-LISA Activation Assay	BK127		
Phalloidin, Alexa Fluor 568	A12380	Molecular Probes	Basel, Switzerland

Appendix D. Supplementary Information

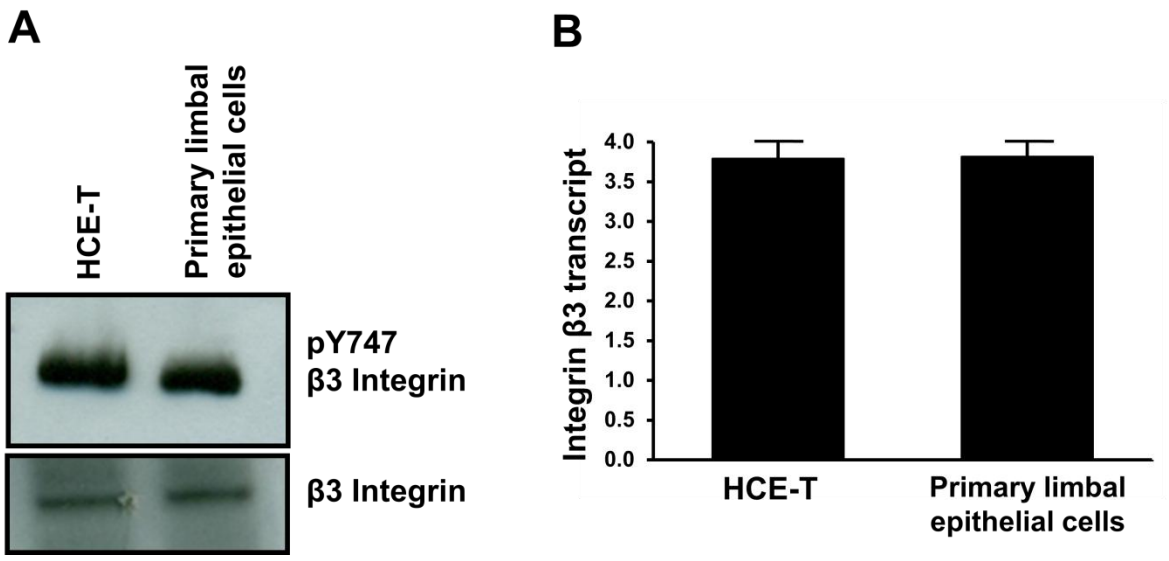

Figure A10. β3 integrin is expressed in cultured human corneal epithelial cell (HCE-T) and primary human limbal epithelial cells. (A) Representative western blots images of cultured HCE-T and primary human limbal epithelial cell lysate probed with primary antibodies against β3 integrin phosphorylated at Tyr747 (pTyr747 β3 integrin) and total β3 integrin. (B) Bar chart showing normalised values of β3 integrin transcript detected by gene chip. This intensity had been normalised to the median probe signal of all transcripts (> 23,000 genes) in Affymetrix microarray chip U133A for human genes (n =14 independent samples of cultured HCE-T cells and primary limbal epithelial cells grown from different donors).

A11

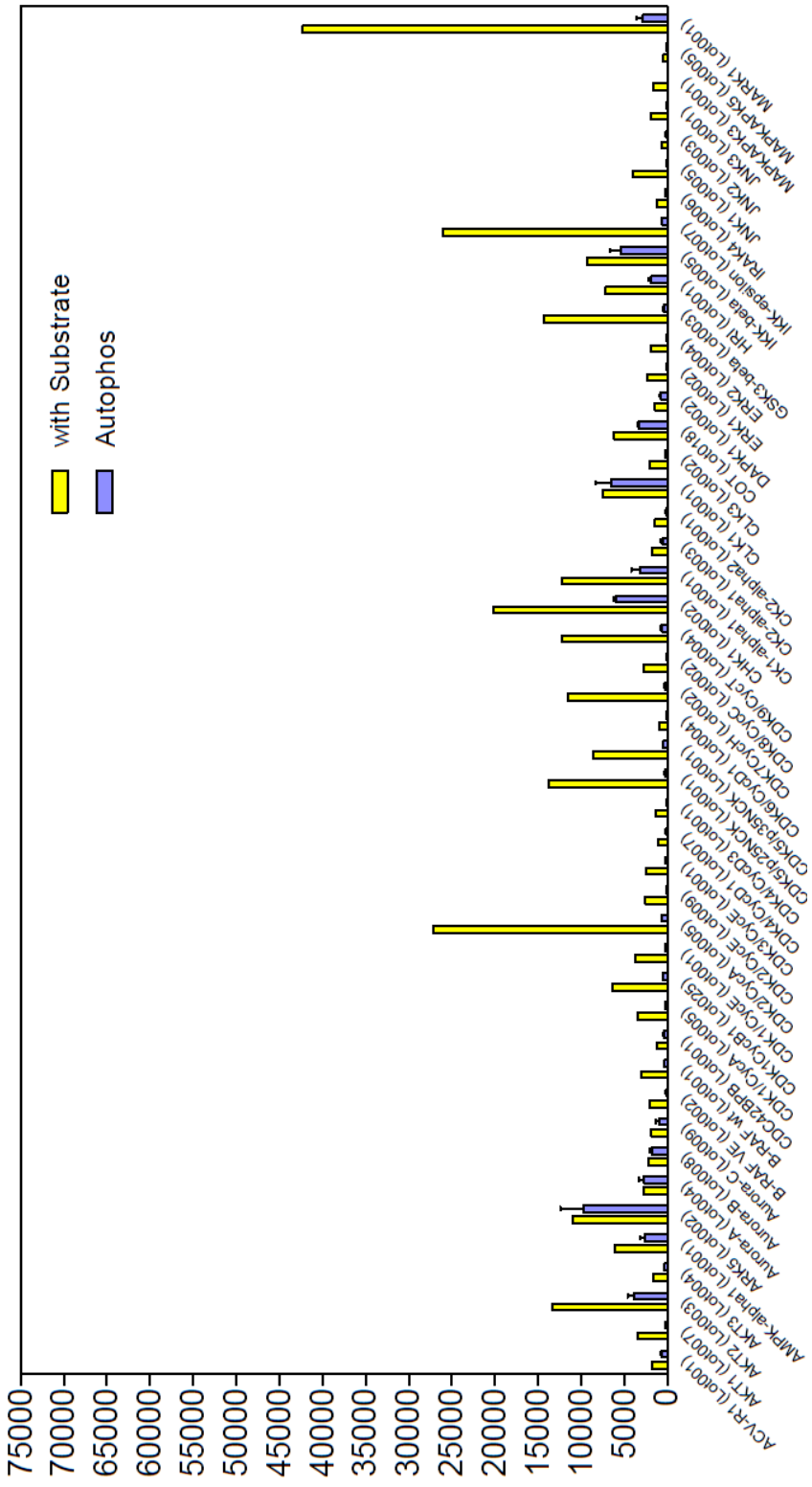
Serine/ Threonine Kinases #1a
with Substrate
Autophos
Kinase activity (cpm)
75000
70000
65000
60000
55000
50000
45000
40000
35000
30000
25000
20000
15000
10000
5000
0
ACV-R1 (Lot001)
AKT1 (Lot001)
AKT2 (Lot007)
AKT3 (Lot003)
AMPK-alpha1 (Lot004)
ARK5 (Lot001)
Aurora-A (Lot002)
Aurora-B (Lot004)
Aurora-C (Lot008)
B-RAF VE (Lot009)
B-RAF wt (Lot002)
CDC42BPB (Lot001)
CDK1/CycA (Lot001)
CDK1/CycB1 (Lot005)
CDK1/CycE (Lot025)
CDK2/CycA (Lot001)
CDK2/CycE (Lot005)
CDK3/CycE (Lot009)
CDK4/CycD1 (Lot001)
CDK4/CycD3 (Lot007)
CDK5/p25NCK (Lot001)
CDK5/p35NCK (Lot001)
CDK6/CycD1 (Lot001)
CDK7/CycH (Lot004)
CDK8/CycC (Lot002)
CDK9/CycT (Lot002)
CHK1 (Lot002)
CK1-alpha1 (Lot001)
CK2-alpha1 (Lot003)
CK2-alpha2 (Lot003)
CLK1 (Lot001)
CLK3 (Lot002)
COT (Lot018)
DAPK1 (Lot002)
ERK1 (Lot002)
ERK2 (Lot004)
GSK3-beta (Lot003)
HPK1 (Lot001)
IKK-beta (Lot005)
IKK-epsilon (Lot007)
IRAK4 (Lot006)
JNK1 (Lot005)
JNK2 (Lot003)
JNK3 (Lot001)
MAPKAPK3 (Lot005)
MARK1 (Lot001)

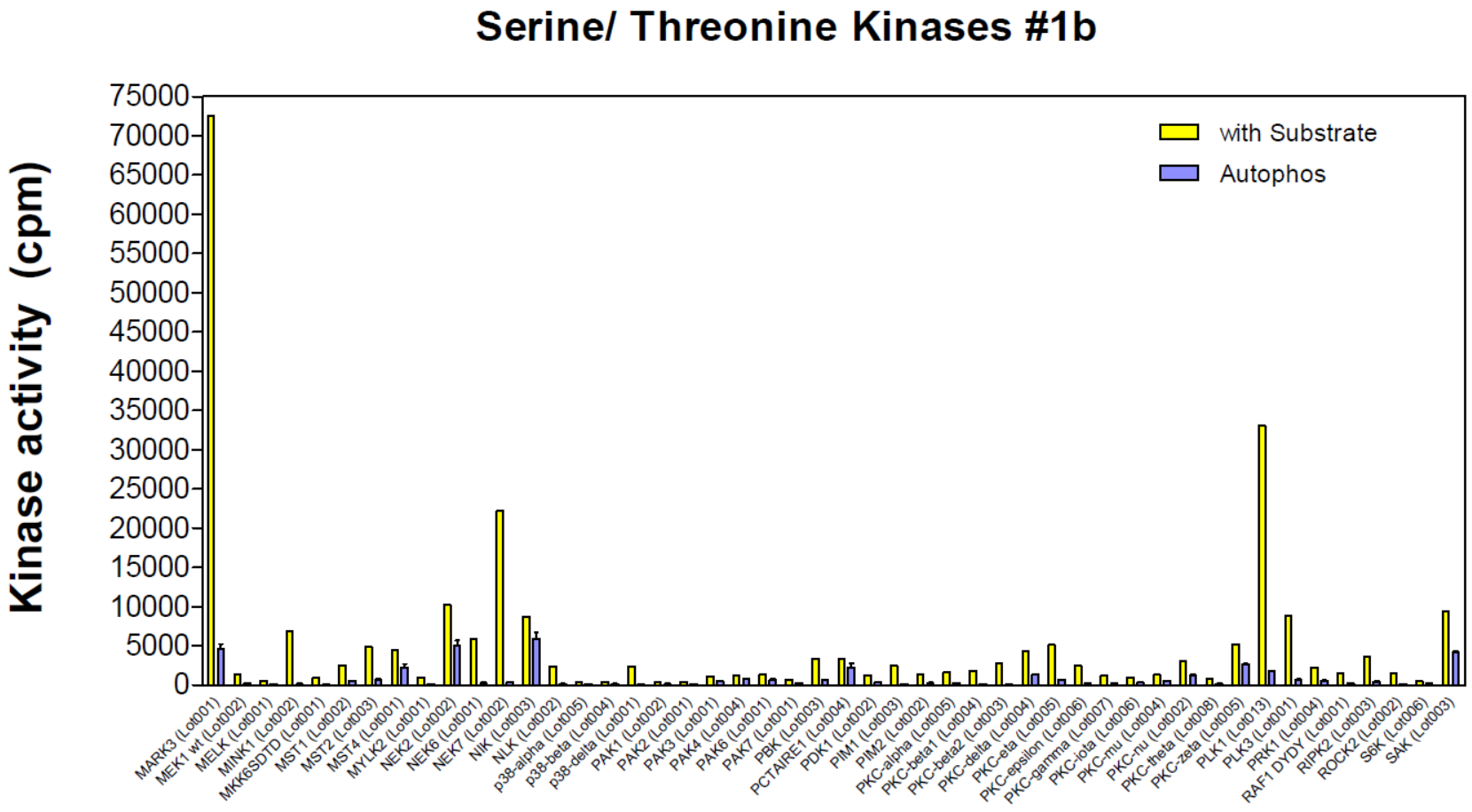
Serine/ Threonine Kinases #1b
Kinase activity (cpm)
75000
70000
65000
60000
55000
50000
45000
40000
35000
30000
25000
20000
15000
10000
5000
0
with Substrate
Autophos
MARK3 (Lot001)
MEK1 wt (Lot002)
MELK (Lot001)
MINK1 (Lot002)
MKK6SDTD (Lot001)
MST1 (Lot002)
MST2 (Lot003)
MST4 (Lot001)
MYLK2 (Lot001)
NEK2 (Lot002)
NEK6 (Lot001)
NEK7 (Lot002)
NIK (Lot003)
NLK (Lot002)
p38-alpha (Lot005)
p38-beta (Lot004)
p38-delta (Lot001)
PAK1 (Lot002)
PAK2 (Lot001)
PAK3 (Lot001)
PAK4 (Lot004)
PAK6 (Lot001)
PAK7 (Lot001)
PBK (Lot003)
PCTAIRE1 (Lot004)
PDK1 (Lot002)
PIM1 (Lot003)
PIM2 (Lot002)
PKC-alpha (Lot005)
PKC-beta1 (Lot004)
PKC-beta2 (Lot003)
PKC-delta (Lot004)
PKC-eta (Lot005)
PKC-epsilon (Lot006)
PKC-gamma (Lot007)
PKC-iota (Lot006)
PKC-mu (Lot004)
PKC-nu (Lot002)
PKC-theta (Lot008)
PKC-zeta (Lot005)
PLK1 (Lot013)
PLK3 (Lot001)
PRK1 (Lot004)
RAF1 DYDY (Lot001)
RIPK2 (Lot003)
ROCK2 (Lot002)
S6K (Lot006)
SAK (Lot003)

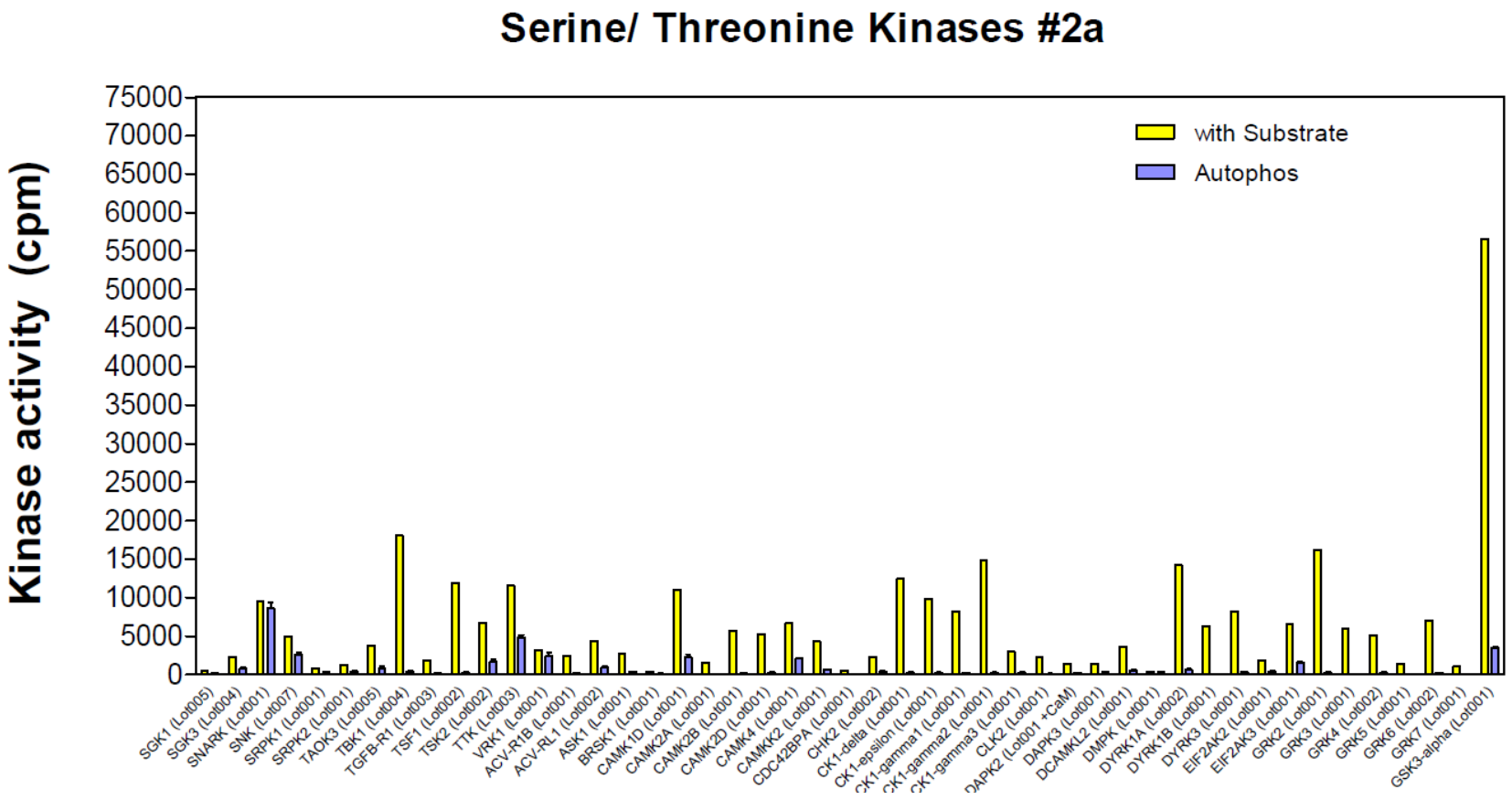
Serine/ Threonine Kinases #2a
Kinase activity (cpm)
75000
70000
65000
60000
55000
50000
45000
40000
35000
30000
25000
20000
15000
10000
5000
0
with Substrate
Autophos
SGK1 (Lot005)
SGK3 (Lot004)
SNARK (Lot001)
SNK (Lot007)
SRPK1 (Lot001)
SRPK2 (Lot001)
TAOK3 (Lot005)
TBK1 (Lot004)
TGFB-R1 (Lot003)
TSF1 (Lot002)
TSK2 (Lot002)
TTK (Lot003)
VRK1 (Lot001)
ACV-R1B (Lot001)
ACV-RL1 (Lot002)
ASK1 (Lot001)
BRSK1 (Lot001)
CAMK1D (Lot001)
CAMK2A (Lot001)
CAMK2B (Lot001)
CAMK2D (Lot001)
CAMK4 (Lot001)
CAMKK2 (Lot001)
CDC42BPA (Lot001)
CHK2 (Lot002)
CK1-delta (Lot001)
CK1-epsilon (Lot001)
CK1-gamma1 (Lot001)
CK1-gamma2 (Lot001)
CK1-gamma3 (Lot001)
CLK2 (Lot001)
DAPK2 (Lot001 +CaM)
DAPK3 (Lot001)
DCAMKL2 (Lot001)
DMPK (Lot001)
DYRK1A (Lot002)
DYRK1B (Lot001)
DYRK3 (Lot001)
EIF2AK2 (Lot001)
EIF2AK3 (Lot001)
GRK2 (Lot001)
GRK3 (Lot001)
GRK4 (Lot002)
GRK5 (Lot001)
GRK6 (Lot002)
GRK7 (Lot001)
GSK3-alpha (Lot001)

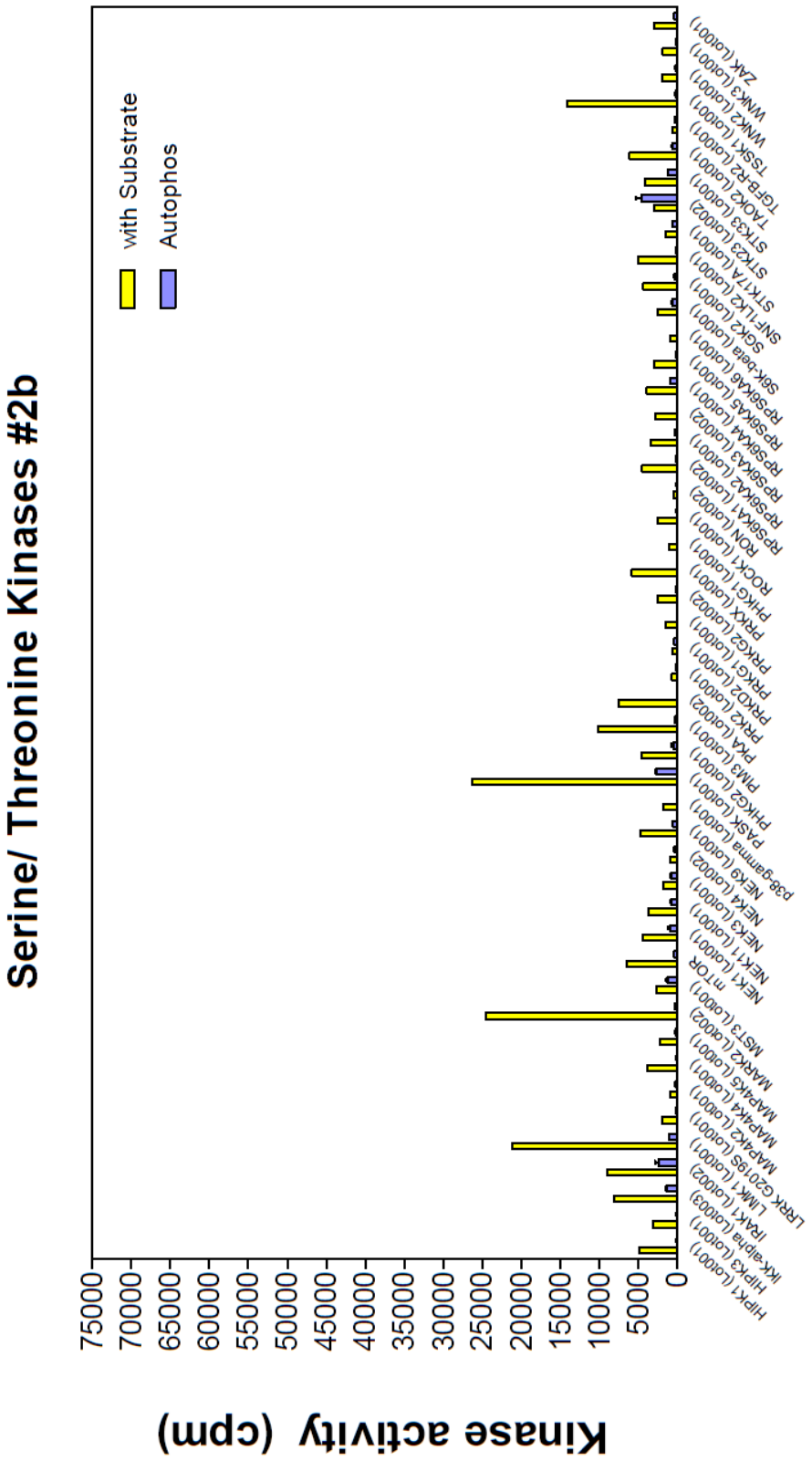

Figure A11. 190 Ser/Thr kinase assays showing activity values (in cpm) with 5µg of paxillin. *Yellow:* Kinase with substrate; *blue*: Kinase autophosphorylation.

Appendix E. List of Publications

1. Tong, L., et al., *Molecular mechanism of transglutaminase-2 in corneal epithelial migration and adhesion.* Biochim Biophys Acta, 2013. **1833**(6): p. 1304-1315.
2. Png, E. and L. Tong, *Transglutaminase-2 in cell adhesion: All roads lead to paxillin?* Cell Adh Migr, 2013. **7**(5): p. 412-417.
3. Png, E., et al., *Hyperosmolarity mediated mitochondrial dysfunction requires transglutaminase-2 in human corneal epithelial cells.* J Cell Physiol, 2010.
4. Png, E., et al., *A new method of high-speed cellular protein separation and insight into subcellular compartmentalization of proteins.* Anal Bioanal Chem, 2011. **400**(3): p. 767-75.
5. L Tong, E.P., W Lan, A Petznick, *Recent Advances: Transglutaminase in Ocular Health and Pathological Processes.* J Clinic Experiment Ophthalmol S, 2011. **2**.